Lista portofoliului de lucrări științifice

Candidat: Coman G. Cristin

1. Ancuța DL, Lovati AB, **Coman C** (2024) - *The clinical significance of inflammatory biomarkers, IL6 cytokine, and systemic immune inflammatory index in rabbit model of acute and chronic Methicillin - resistant Staphylococcus epidermidis - induced osteomyelitis*. PLOS ONE 19(8): e0309145. https://doi.org/10.1371/journal.pone.0309145. IF 2.9, Q1, 2024.

2. Ancuța DL, Alexandru DM, Țucureanu C, **Coman C**. *A Comparative Analysis of the Efficacy of Bacterial Lysate versus Antibiotic Therapy in the Treatment of Experimental Peri-Implantitis in Rats.* Microorganisms. 2024; 12(8):1537. https://doi.org/10.3390/microorganisms12081537, IF-4,1, Q2, 2024.

3. Popescu F, Titorencu I, Albu Kaya M, Miculescu F, Tutuianu R, Coman AE, Danila E, Marin MM, Ancuta D-L, **Coman C**, Barbilian A.. *Development of Innovative Biocomposites with Collagen, Keratin and Hydroxyapatite for Bone Tissue Engineering*. Biomimetics. 2024; 9(7):428. https://doi.org/10.3390/biomimetics9070428, IF-3,4; Q1, 2024.

4. Caracoti, V.-I.; Caracoti, C.-Ș.; Ancuța, D.L.; Ioniță, F.; Muntean, A.-A.; Bhide, M.; Popa, G.L.; Popa, M.I.; **Coman, C**. *Developing a Novel Murine Meningococcal Meningitis Model Using a Capsule-Null Bacterial Strain*. Diagnostics 2024, 14, 1116. ISSN: 2075-4418, https://doi.org/10.3390/diagnostics14111116, IF-3,6; Q1, 2024.

5. Burdusel D, **Coman C**, Ancuta DL, Hermann D, Doeppner T, Gresita A, Popa-Wagner A. *Translatability of life-extending pharmacological treatments between different species*. Aging Cell. 2024 May 26:e14208. https://doi.org/10.1111/acel.14208 . PMID: 38797976. Print ISSN:1474-9718. IF-7,8; Q1, 2024.

6. Ancuța, D.L.; Alexandru, D.M.; Muselin, F.; Cristina, R.T.; **Coman, C**. *Assessment of the Effect on Periodontitis of Antibiotic Therapy and Bacterial Lysate Treatment*. International Journal of Molecular Sciences (IJMS) 25, no. 10: 5432, ISSN:1661-6596, https://doi.org/10.3390/ijms25105432, IF – 5,6, Q1, 2024.

7. Ancuta, D.L.; Alexandru, D.M.; Crivineanu, M.; **Coman, C.** - *Induction of Periodontitis Using Bacterial Strains Isolated from the Human Oral Microbiome in an Experimental Rat Model*. Biomedicines, 2023, 11, 2098, ISSN - 2227-9059 https://doi.org/10.3390/biomedicines11082098 , IF - 4,7, Q2, 2023.

8. A. Bonciu, L. Cremer, A. Calugaru, E. Vlase, **C. Coman**, Alexandra Palla-Papavlu, Dan Alin Cristian, F. Grama - *Laser engineered polymer thin films as drug delivery systems* - Applied Physics A: Materials Science and Processing,129-327, https://doi.org/10.1007/s00339-023-06608-y, 2023, IF – 2,983, Q3, 2023.

9. Doeppner TR, **Coman C**, Burdusel D, Ancuta DL, Brockmeier U, Pirici DN, Yaoyun K, Hermann DM, Popa-Wagner A. *Long-term treatment with chloroquine increases lifespan in middle-aged male mice possibly via autophagy modulation, proteasome inhibition and glycogen metabolism*. Aging (Albany NY). 14, 10: 4195-4210 doi: 10.18632/aging.204069. ISSN – 1945-4589, 2022, IF-5.682, Q2, 2022.

10. Carmen C. Surdu-Bob, Ene Vlase, Florica Barbuceanu, Danut Turcu, Mariana Coman, Marius Badulescu, Mariana Oporanu, **Cristin Coman** - *Copper Bead Therapy in Severe Bone Infection: A Rabbit Tibial Model*, Veterinary and Comparative Orthopaedics and Traumatology. 2019;32:41–50, doi: https://doi.org/10.1055/s-0038-1676292 , FI – 0.877, Q3, 2019.

PLOS ONE

The clinical significance of inflammatory biomarkers, IL6 cytokine, and systemic immune inflammatory index in rabbit model of acute and chronic Methicillin-resistant *Staphylococcus epidermidis*-induced osteomyelitis
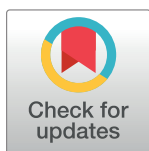
Diana-Larisa Ancuţa[1¤]*, **Arianna Barbara Lovati**[2☯], **Cristin Coman**[1☯]

1 Cantacuzino National Medical Military Institute for Research and Development, Bucharest, Romania,
2 IRCCS Ospedale Galeazzi - Sant'Ambrogio, Milan, Italy

☯ These authors contributed equally to this work.
¤ Current address: Cantacuzino National Medical Military Institute for Research and Development, Preclinical Testing Unit, Bucharest, Romania
* diana.larisa.ancuta@gmail.com

Abstract

Infections are a major complication of open fractures and fracture fixation. In this study, an innovative bioactive medical device was used to experimentally treat MRSE-induced osteomyelitis in rabbit tibia. This paper investigates the clinical significance of inflammatory biomarkers (NLR, PLR, MLR and PMR), SII and IL-6 and assesses their role in the development of osteomyelitis. The main objective is to identify the utility of hematological reports derived from neutrophils, leukocytes, monocytes and platelets in the evolution of implant-related osteomyelitis and the estimation of treatment efficiency. In particular, this study compares the response of these inflammatory markers to different treatments in the presence or absence of bioactive materials and/or topical antibiotics over time. The analysis of the threads showed that NLR, PLR and SII had high values in the acute phase of the disease, so that after chronicization, they decrease. The animals treated with vancomycin nano-functionalized peptide-enriched silk fibroin-coated implants showed lower levels of inflammatory biomarkers compared to the other groups (empty implants and peptide-enriched silk fibroin-coated implants). NLR, PLR and SII, complemented by IL-6 can be used as fairly accurate biomarkers for the diagnosis of osteomyelitis.

Introduction

Osteomyelitis is defined as a bone disease caused by microorganisms characterized by inflammation and bone loss. The classification of osteomyelitis, on a broad scale, includes the acute and the chronic form, the delimitation between the two is the time interval that has elapsed

since the contact of the bone with the pathogens. Thus, acute osteomyelitis appears after a few days or weeks, and early diagnosis and treatment have mostly positive outcomes [1]. The chronic form evolves over a longer period, it is accompanied by bone loss and sequestra due to poor vascularization and necrosis, which makes it difficult to transport antimicrobial agents to the focus of osteomyelitis [2]. Acute and chronic onsets are related not only to the duration of onset but also to the intensity of the cellular response.

The common treatment of these conditions involves debridement combined with systemic antibiotics, but taking into account the cumulative capacity of antibiotics at the level of different organs and their possible toxic potential, an ideal solution to solve osteomyelitis is the creation of biomaterials that release local medication. Consequently, several researchers studied the phenomenon and developed a multitude of local antibiotic deliverers in order to prevent the development and proliferation of bacteria at the implant level [3]. Osteomyelitis depends on the nature of the pathogens and the factors associated with the host. The capacity of bacteria of spreading or forming biofilm or evading the immune system together with an immunodeficient background, comorbidities, or emergency situations (trauma) constitute favorable elements for the development of osteomyelitis. The incidence of osteomyelitis associated with implantable devices varies from 30% in the case of open fractures [4] to 3-8% in the case of arthroplasty [5], despite all measures being used to prevent contamination.

Specific signs of inflammation and infection such as fever, redness, pain, and purulent accumulations allow for an easy diagnosis of acute osteomyelitis. Otherwise, chronic or subclinical forms progress with subtle and non-specific symptoms. This requires the establishment of a heterogeneous protocol, including hematological, biochemical and microbial tests, evaluation of the C-reactive protein, and imaging or histopathological examinations. Currently, the gold standard for the diagnosis of osteomyelitis is the bone biopsy followed by microbiological and histopathological examinations of the sample [6, 7].

With respect to the diagnosis of periprosthetic joint infection, there is no test with absolute accuracy. Therefore, the Society of Musculoskeletal Infections (MSIS) and the Society of Infectious Diseases (IDSA) issued 2018 a globally accepted definition that improved confidence in the diagnosis, and led to an efficient therapeutic approach. This definition includes corroborated analysis of clinical data, peripheral blood laboratory results, microbiological culture, histological evaluation of periprosthetic tissues, and intraoperative findings [8].

Blood tests provide important information about inflammatory markers such as erythrocyte sedimentation rate (ESR) and C-reactive protein (CRP). Sometimes, in the presence of subclinical osteomyelitis, normal ESR and CRP values can be found. A proportion of patients presenting with osteomyelitis have normal inflammatory markers at presentation. The ESR threshold of 60 mm/h demonstrated a sensitivity of 74% (95% confidence interval [CI], 67–80) and a specificity of 56% (95% CI, 48–63) for osteomyelitis, while the CRP threshold of 7.9 mg/dL had a sensitivity of 49% (95% CI, 41–57) and a specificity of 80% (95% CI, 74–86). While ESR is better at ruling out osteomyelitis initially, CRP helps distinguish osteomyelitis from soft tissue infection in patients with elevated ESR.

Further prospective studies addressing the prognostic value of ESR and CRP are needed, and a more comprehensive diagnostic algorithm should be developed that includes other diagnostic tests [9]. However, according to one last meta-analysis, the diagnostic value of these markers is limited [10]. In addition, markers related to coagulation (plasma fibrinogen and D-dimer) were found to be effective in diagnosing inflammation. Platelets and average platelet volume also play an essential role in the inflammatory process [11, 12], as well as the neutrophil/lymphocyte ratio (NLR) in the peripheral blood or the monocyte/lymphocyte ratio (MLR) [13].

The complete hematological examination, routine or performed before surgical intervention, can provide additional information on the patient's state of health, if minimal 100 attention is paid to the ratio of blood elements. It can enhance diagnostic accuracy without additional costs. Data from the literature show that NLR, MLR, PLR (platelet/leukocyte ratio), or PMR (platelet/average platelet volume ratio) are associated with the inflammatory and/or infectious state in the body. In fact, systemic changes in NLR, PLR, and MLR represents primary responses to early inflammation and infection. Thereafter, chronic inflammation is caused by the persistence of the inflammatory inducer, such as microbial/viral invasion or a physical injury. Thus, the report by Djordjevic et al [14] claims that the highest levels of MLR and PLR were found in patients with negative blood culture and the lowest in patients with Gram-positive blood culture, an aspect also supported by Naess et al [15] who claim that higher values of NLR and MLR indicated higher probabilities of bacterial infection and low probabilities of viral infection.

Also, Forget et al [16], through their research, demonstrated that very high levels of NLR are frequently associated with acute and persistent inflammatory states. More importantly, the Systemic Immune Inflammatory Index (SII) has been recently used as a prognostic marker in several clinical fields (cancer, infections, surgeries, etc.) and can be used to diagnose infections in the absence of clear signs. The SII is calculated as (NEU × PLT)/LYM (NEU, PLT, and LYM represent neutrophil counts, platelet counts, and lymphocyte counts, respectively). Compared to NLR, MLR, and PLR biomarkers, the SII describes the host's immune system imbalance and inflammatory condition. Even if various studies have demonstrated the correlation between NLR, PLR, and many diseases such as inflammatory diseases [17] as well as a correlation between high NLR and PLR, which can guide the diagnosis of a bone infection such as osteomyelitis [18], the diagnostic value of NLR, MLR and PLR in anticipating bone infections and their prognosis remains to be explored. This suggests that there is an urgent need for new inflammatory markers to diagnose osteomyelitis. Among inflammatory cytokines, interleukin (IL) -6 has recently been identified as a potential target for inflammatory disease. Some studies revealed that IL-6 is an active player in the immune response and showed that excess of this cytokine and/or its receptor contributes to the pathogenesis of the inflammatory process [19]. Other studies demonstrate that bacterial challenge of osteoblasts during bone diseases, such as osteomyelitis, induces cells to produce inflammatory molecules that can direct appropriate host responses or contribute to progressive inflammatory damage and bone destruction [20–22].

In this scenario, it could be useful to analyze these inflammatory markers in the course of infections, where there is an alteration of the oxidative stress mediators, although an inflammatory status is not clinically evident yet. Since there are no data related to these analyzes in animals, we proposed to evaluate these reports and to determine if there is a modification of the inflammatory markers, IL-6 and SII in a rabbit model of osteomyelitis treated or not with locally delivered antibiotics, as the most frequently used, relevant and reproducible model of orthopedic infections [23]. Thus, special attention is given to experimental laboratory animals, which researchers used to study human osteomyelitis. Indeed, *in vivo* models are the ideal solution for the study of advanced diagnostic and therapeutic approaches to translate into clinical practice.

Materials and methods

Animals, bacterial strains, and medical devices used in the experiments

For each model (acute and chronic), 54 adult New Zealand White rabbits, male and female, with an average weight of 3000 grams were used. The animals were ordered from the CI

animal facility and were housed in individual cages with 12 h light/12h dark cycles. They were acclimatized for five days under the same experimental conditions, at a temperature of 16-21˚C and relative humidity of 45-65%, during which time they received food and water ad libitum.

Methicillin-resistant *Staphylococcus epidermidis* (MRSE, GOI1153754-03-14)—isolated from a knee prosthesis of a human patient—was received from the Istituto Ortopedico Galeazzi of Milan (Italy) [24] and processed in the CI Microbiology Laboratory—the 164 concentration of MRSE used in the study was $5x10^{10}CFU/ml$. Humans are not directly involved in the study. Indeed MRSE, GOI1153754-03-14 strain has been isolated during common diagnostic procedures and the ethical committee approval is not required for diagnostic activities. No human tissue samples are employed but a bacterial strain detached from prosthetic metal implant, and that the bacterial strain is no more attributable to a specific patient.

Medical devices tested: empty titanium metal implants (TMMB10, Zimmer Biomet), titanium implants coated with peptide-enriched silk fibroin, and titanium implants coated with vancomycin nano-functionalized peptide-enriched silk fibroin, as developed elsewhere [25].

Experimental design and procedures

For each study, 54 rabbits, males and females in equal number, were weighed and marked on the ear with an animal marker, assigning an individual ID. Furthermore, depending on weight, sex, clinical status (healthy—acute study, with osteomyelitis—chronic study), 3 uniform groups (9 males and 9 females) were created, depending on the tested implant. The animals were deeply anesthetized by neuroleptanalgesia using a mixture of ketamine (50mg/kg IM, Vetased, Farmavet, Romania) and acepromazine (1mg/kg IM, Sedam, Farmavet, Romania). In the proximal area of the tibia, at approximately 8 mm from the tibio-femoral-patellar joint at the level of the left hind limb, a bone defect was created using progressive diameter drills (ø 1-3.5 mm), under cooling continue with sterile saline solution.

To induce acute osteomyelitis, implants (M, C and T) previously immersed in the bacterial suspension were inserted in the bone defects. Before closing the wound, 0.1 ml of MRSE at the same concentration was dispersed over the implants. The periosteum, muscles, and skin were sutured with absorbable thread 2/0 (Megasorb, Buritis). During the follow-up period (14 days), the rabbits were monitored clinically and hematologically, according to the protocols described elsewhere [26].

To induce the chronic osteomyelitis, in the first stage, a gauze mesh immersed in the bacterial suspension was inserted into the defects created at the level of the tibia, over which an additional 0.1 ml of MRSE at the same concentration was inoculated and the wound was closed. 14 days after the bacterial inocula, further surgery was carried out to remove gauze tampons and to place implants (M, C, and T) at the infected site. This approach was to create a chronic osteomyelitis support, an environment in which the implants could be tested [27].

Post-operatively, the rabbits received analgesic treatment (Ketoprofen—3mg/kg SC, Dopharma, Romania) for 3 days. During the follow-up period (60 days), the rabbits were monitored clinically and hematologically. At the end of the study, the animals were euthanized by an anesthetic overdose, and the tibias were taken for histological analysis.

Blood analyses: Inflammatory markers and systemic inflammatory index

Blood samples were collected in EDTA-preconditioned tubes (Sarstedt, Germany) from the auricular vein on days 0 (basal healthy values), 1, 3, 7, and 14 for acute osteomyelitis and on days 0, 21, 43, and 60 for chronic osteomyelitis. In order to achieve a complete and correct hematological examination, the samples were analyzed at an interval of about one hour after

collection. The hematological examination was carried out with the ProCyte Dx analyzer (IDEXX Laboratories). The reference intervals are represented by the basal values at day 0. Therefore, based on the results obtained at the hematological examination, we calculated the ratios between neutrophil and lymphocyte (NLR = NEU/LYM), monocyte and lymphocyte (MLR = MONO/LYM), platelet and lymphocyte (PLR = PLT/LYM), platelets and the average platelet volume (PMR = PLT/MPV). Moreover, the systemic immune-inflammatory index and the cytokine IL-6 were also analyzed. The interleukin 6 (IL-6) assay was conducted using plasma samples obtained from the blood collected in Lithium-Heparin preconditioned tubes and the measurement of interleukin 6 (IL-6) was performed using an enzyme-linked immuno-sorbent assay (ELISA) method. The specific type and brand of the kit used for measuring IL-6 was R&D Systems™ Rabbit IL-6 DuoSet ELISA (Fisher Scientific, Germany) and the manufac-turer's instructions were followed for the processing of the samples.

Statistical analysis

The sample size was calculated a priori through a two-sample t-test with α error = 0.05% and 80% power (G*Power 3.1 software, Dusseldorf, Germany) [28]. The statistical analysis was per-formed with GraphPad Prism 5 software (GraphPad Software, San Diego, California, USA). The variables taken into account were related to the group of animals (acute and chronic), depending on the medical device tested treated or not (M, C, and T), the days of clinical moni-toring, as well as the laboratory data (white blood cells, neutrophils, lymphocytes, platelets, monocytes, and IL-6).

The inclusion criteria, in the case of the acute study, referred to the uniform formation of groups of animals, in terms of weight and sex. In the case of the chronic study, in addition to the inclusion criteria from the acute study, we also added the criterion of clinical expression of osteomyelitis. In both studies, the exclusion criteria followed the elimination of animals that did not express specific signs of osteomyelitis or that presented fractures of the operated limbs, weight loss greater than 25%, lack of food consumption for more than 48 hours. After checking the normal distribution of the data using the Shapiro-Wilk test, the intergroup comparisons were analyzed with a one-way analysis of variance (ANOVA) and then coupled with Bonferro-ni's post hoc test. All data are reported as means ± standard error (SE). The level of significan-cewas $p < 0.05$.

For each study, 6 different investigators were involved as follows: a first investigator anes-thetized the animals based on the randomization weight table. A second investigator was responsible for the surgical procedure, postoperative treatment and clinical monitoring. This investigator was the only person who knew the treatment group allocation. 2 investigators were responsible for the blind processing of the biological samples collected from the animals and 2 more investigators, who analyzed the raw data and issued the final conclusions.

Results

Various inflammatory factors have been described as prognostic biomarkers, such as the neu-trophil–lymphocyte ratio (NLR), systemic immune-inflammation index (SII) and IL-6 cytokine.

In our experimental setting, we found a time-related variation of all the evaluated parame-ters. In the acute phase (D14), the NLR ratio (Fig 1) is significantly different from that of the baseline (basal healthy values at D0—red dotted line) in all the groups (M $p < 0.001$, C $p < 0.001$, and T $p < 0.01$, respectively).

This trend is also confirmed by the analysis of the SII values (Fig 1), as a more comprehen-sive parameter of whole-body inflammation. Similarly, in M and C groups at D60, both NLR
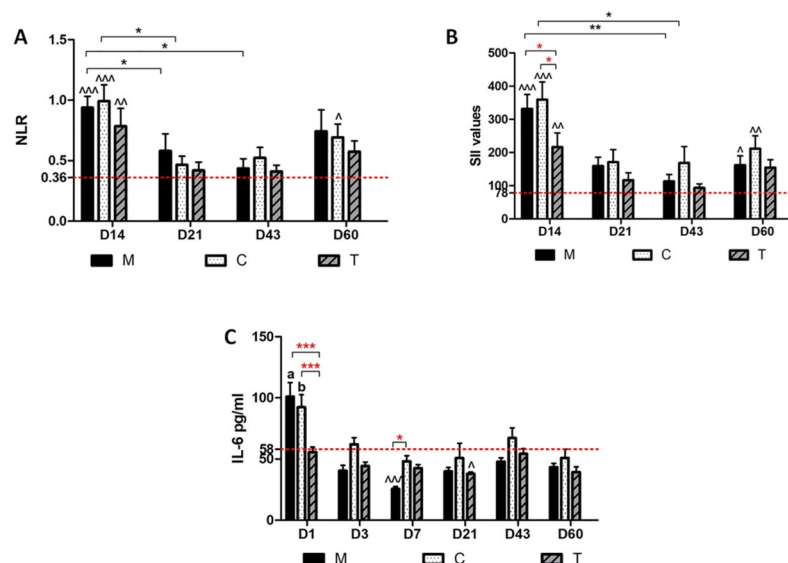
Fig 1. Histograms for NLR, SII and IL-6 cytokine. Histograms reporting (A) the neutrophil–lymphocyte ratio (NLR), (B) the systemic immune-inflammation index (SII) and (C) IL-6 cytokine of the three differently treated groups (M, C, and T) over time. Statistical difference of the group vs healthy values (red dotted lines); (* red) () statistical differences among groups and (*black) time points; (a) $p < 0.001$ between group M at D1 and D3, 7, 21 and 60; (b) $p < 0.01$ between group C at D1 and D3, 7, 21 and 60.

https://doi.org/10.1371/journal.pone.0309145.g001

and SII increased significantly from to the basal values. Moreover, the SII at D14 showed a difference among groups. Indeed, the treated group (T) had significantly lower SII values than M (empty implant) and C (implant coated with silk fibroin w/o antibiotic) for $p < 0.05$.

In the chronic phase, the host's immune response and inflammatory markers are expected to decline. However, at the latter time point (D60), in the presence of a consistent bacterial infection, both the immune response and the inflammatory biomarkers increased again, as demonstrated in our histogram trend, in which this trend was confirmed for the M and C groups but not for the T group. Therefore, this aspect underlines the MRSE characteristic of maintaining the infection at a subclinical level and its reactivation at long intervals after the acute clinical manifestation, in the absence of a long-acting treatment. In the case of our study, this idea proves the effectiveness of the treatment in controlling the inflammatory response through its antimicrobial activity against bacterial proliferation.

Cytokine IL-6 plays a protective role in immune responses to bacterial infections. Our data showed that IL-6 was involved at the very beginning (D1) of the bacterial infection (Fig 1). Indeed, IL-6 is the major inductor of the acute phase proteins and is involved in the control of neutrophil and monocyte responses following infection, thus confirming the increase of NLR and SII at D14. Once again, the IL-6 values showed a difference among groups, where the treated group (T) had significantly lower IL-6 values compared to M (empty implant) and C (implant coated with silk fibroin w/o antibiotic) for $p < 0.001$, thus supporting the SII trend at D14.

During the chronic phase, IL-6 plays a marginal role, in fact, the IL-6 values decreased significantly over time in groups M and C. More importantly, group T did not show any increased difference compared to the basal values at any time point. However, in the case of a chronic bacterial infection, IL-6 can fluctuate and lead to enhanced systemic inflammation associated with the host response. In this series, this phenomenon was found at D43 with an
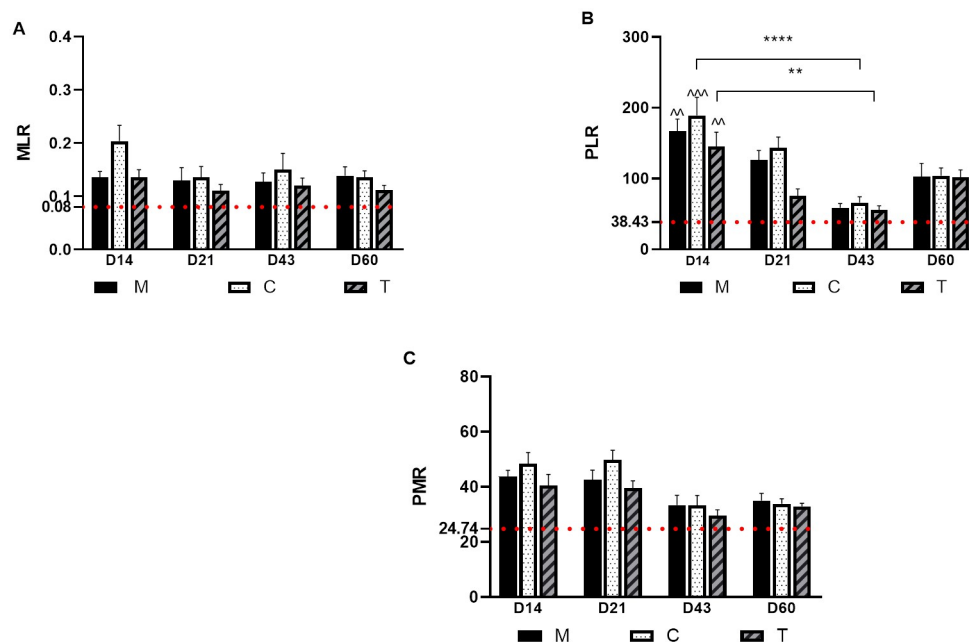
Fig 2. Histograms for MLR, PLR and PMR. Histograms reporting (A) the monocyte-lymphocyte ratio (MLR), (B) the platelet-lymphocyte ratio (PLR), and (C) the platelet-mean platelet volume ratio (PMR) of the three differently treated groups (M, C, and T) over time. (*) statistical difference of the groups (*for $p < 0.05$, ** for $p < 0.001$, and **** for $p < 0.0001$). The red dotted lines are reporting the mean of basal values of the ratios MLR, PLR, and PMR, statistical difference of the healthy values (red dotted lines) vs group^.

increase in IL-6 in all the groups followed by the increase of NLR and SII at D60 in groups M and C.

The MLR histogram (Fig 2) did not show any significant differences over time and groups, only a statistical difference was observed between groups C and T on D14 ($p = 0.04$) and on day 60 ($p = 0.02$). With respect to PLR (Fig 2), there were significant differences at day 14, in the case of all groups compared to the basal values (dotted red line). As in the case of NLR and SII, the PLR ratio tends to decrease as the disease becomes chronic, and with a slight increase observed at D60. The PMR values (Fig 2) remained high on D14 up to D21, and then decreased near to the basal values in the chronic phase of the disease. On D60, the ratio also rose slightly. Significant differences were found in group C on D21 compared to D43 ($p < 0.001$) and compared to groups M and T within the same time interval ($p = 0.05$).

Discussion

The study is the first to investigate the clinical significance of inflammatory biomarkers (NLR, PLR, MLR and PMR), the SII, and IL-6 in a well-established rabbit model of orthopedic infections to evaluate the progression of chronic osteomyelitis development.

The main objective of this study was to assess the utility of hematological data derived from neutrophils, leukocytes, monocytes, and platelet counts in tracking the progression of implant-associated osteomyelitis and evaluating treatment in an experimentally MRSE-induced bone infection. In particular, this study compares the response of these inflammatory markers to various treatments with or without locally deliered bioactive materials and/or antibiotics, over time. To our knowledge, these hematological indices have not been previously studied together for this purpose. The main pathogen responsible for osteomyelitis in humans

is *Staphylococcus aureus* (SA), but other bacteria such as *Staphylococcus epidermidis*, *Staphylococcus lugdunensis*, and *Propionibacterium acnes* [29] can also cause the disease [30]. The biofilm produced by these bacteria can complicate antibiotic treatment. Selecting an appropriate *in vivo* model of osteomyelitis is crucial due to the varying advantages and limitations of different animal models. While rodents are the extensively studied, rabbits are commonly used in musculoskeletal research and were the first documented animal model for osteomyelitis [3]. Rabbits are reliable and reproducible models for orthopedic infections due to their bone structure, immune system, and susceptibility to infections, which closely resemble those of humans [31, 32]. Furthermore, their size allows for the testing of medical devices, such as implants, in the presence of bacterial contaminations [23].

The induction of osteomyelitis in rabbits can be achieved by creating mechanical fractures or bone defects, which may be left untreated or filled with materials that promote bacterial adhesion, [33] or by using contaminated implants [34]. The development of experimental osteomyelitis can be evaluated through clinical examination, radiography, bone biopsy, and bacterial cultures. Studies by Odekerken et al. [35] showed that F-FDG micro-PET is a sensitive tool for early detection of osteomyelitis, and PCR can identify bacteria even at low or metabolically inactive levels [35, 36].

Research on the lagomorph immune system focuses on *Oryctolagus cuniculus*, the reference model for immunology studies. Investigations into diseases such as myxomatosis or rabbit hemorrhagic disease have significantly expanded our understanding of the human oncological field. Advances in understanding innate immunity include the identification of interleukins, chemokines and their receptors, Toll-like receptors, antiviral proteins (RIG-I and Trim5), and genes encoding fucosyltransferases, which rabbit hemorrhagic disease virus uses to invade respiratory and intestinal epithelial cells. Regarding adaptive immunity, the major histocompatibility complex (MHC) and T cells are notable for their genetic diversity in the loci encoding the variable and constant regions of antibodies [37]. Our research suggests that longitudinal analysis of human osteomyelitis can be effectively conducted using cost-efficient methods by focusing on the ratios of white blood cells and inflammatory cytokines. Given the lack of literature on the repetitive analysis of inflammatory markers (NLR, MLR, PLR, PMR), we found it appropriate to track these markers in a study of experimental osteomyelitis in rabbits with MRSE during both the acute and chronic of the disease. Our findings indicate that NLR, PLR, and SII significantly increased during the acute onset of osteomyelitis, as expected. In the chronic phase, the immune response and inflammatory markers typically decline. However, at a later time point (D60), persistent bacterial infection caused both the immune response and inflammatory biomarkers to rise again, resulting in subclinical low-grade inflammation. Specifically, in our series, we demonstrated that animals treated with vancomycin nano-functionalized peptide-enriched silk fibroin-coated implants (group T) exhibited lower NLR, PLR and SII values compared to the other groups during both the acute or chronic phases. Otherwise, MLR and PMR did not show significant values for diagnosing osteomyelitis or evaluating the effectiveness of the treatment.

The systemic inflammatory response triggered by bacterial contamination determines changes in neutrophil, lymphocyte, monocyte and platelet counts. During infections, the immune system induces an inflammatory response to fight pathogens, balancing pathogen clearance with minimizing host tissue damage, ultimately leading to tissue recovery [38]. In fact, neutrophils are the first responders to infection, while lymphocytes generate the adaptive immune response [14, 39, 40]. Consequently, NLR and SII can provide important information about the onset, persistence of infection, and even the occurrence of sepsis. In a cohort study by Salciccioli et al. [41], NLR was significantly higher in patients with sepsis compared to patients without sepsis. Similarly, elevated values are observed in bacteriemia studies, as

described by de Jager et al., where patients with blood cultures contaminated with Gram-negative bacteria had higher NLR than those with Gram-positive pathogens [42]. In contrast, data indicate that lymphocytes and monocytes exhibit higher values in patients with Gram-positive blood cultures compared to those with polymicrobial or negative blood cultures [14]. Emektar et al. observed a elevated PLR levels in patients who had experienced trauma, such as hip fracture or acute appendicitis in children, suggesting that this biomarker is closely related to persistent inflammation [43]. Although recent investigations have proposed PMR ratio as a strong diagnostic marker of sepsis [43], our data do not support this findings. Differently, it has been demonstrated that platelet activation plays a role in the pathogenesis of thrombosis associated with *Staphylococcus aureus* osteomyelitis [44], confirming the importance of platelet increase during both acute and chronic osteomyelitis. Additionally, while inflammatory cytokines like IL-6 are protective in immune responses to bacterial infections, they also promote osteoclast differentiation and inhibit osteoblast formation [45]. Moreover, some studies have demonstrated local production of IL-6 at bacterial infection sites in human osteomyelitis associated with S. aureus [21], as well as in a murine model [46]. In addition, bacterial-stimulated osteoblasts express IL-6 and IL-12, which induce an immune response by attracting leukocytes [22]. Our data indicate that the release of IL-6 occurs primarly at the very acute stage of the disease, but this cytokine levels drop rapidly within 48-72 hours. In summary, the inflammatory biomarkers analyzed currently do not provide conclusive data for validation. However, our study observed increased levels of all ratios, especially in acute osteomyelitis. A possible explanation is that these ratios lose their prognostic capacity once the disease becomes chronic, as reported by Oh et al. [47], where all analyzed biomarkers showed low levels after 48-72 hours [48]. This suggests that the potential value of each inflammatory marker should not be assessed independently but rather evaluated collectively to detect inflammatory markers associated with osteomyelitis.

There were some several limitations in our study. Firstly, the literature lacks reported threshold values for inflammatory markers in animal models, particularly in rabbits, making comparisons difficult. Moreover, unlike human blood counts often performed on hospitalized patients, our measurements were taken at specific, well-defined intervals throughout the experiment. Our findings accentuate the necessity for further research to establish standardized cutoff values for these inflammatory markers in both human and animal models to effectively diagnose and prognose chronic and/or subclinical bacterial infections. Another limitation was the absence of a control group undergoing surgery without bacterial infection, as it is well known that surgery alone can alter inflammatory markers (leukocytes, platelets and cytokines) particularly during the early postoperative period. This may have influenced the data obtained during the acute phase of osteomyelitis. Additionally, our study did not investigate CRP and ESR, which could corroborate the degree of inflammation detected through the analyzed parameters. However, Ustundag and colleagues demonstrated that SII and PLR values might be higher in low-grade inflammation patients with mildly elevated CRP, indicating that CRP did not correlate with SII and PLR [49].

Conclusion

In our study, we found that NLR, PLR, and SII increased significantly during the acute onset of osteomyelitis, as expected. This aspect was also supported by the rapid increase of IL-6 in the first hours of the infection. In the chronic phase, when it was expected that the inflammatory markers would decrease, we observed a slight increase in them (D60) because of the high bacterial load.

The animals treated with vancomycin nano-functionalized peptide-enriched silk fibroin-coated implants had lower NLR, PLR, and SII values compared to the other groups either in the acute or chronic phase. NLR, PLR and SII associated with the clinical context may signal the presence of an osteomyelitis-type infection, especially in the acute phase. However, more long-term studies on the same samples are needed to demonstrate the ability of these inflammatory biomarkers to anticipate the chronic phases of osteomyelitis.

Acknowledgments

Author Contributions

Conceptualization: Cristin Coman.

Formal analysis: Diana-Larisa Ancuţa, Arianna Barbara Lovati, Cristin Coman.

Funding acquisition: Arianna Barbara Lovati.

Investigation: Diana-Larisa Ancuţa, Arianna Barbara Lovati, Cristin Coman.

Methodology: Cristin Coman.

Project administration: Arianna Barbara Lovati, Cristin Coman.

Software: Diana-Larisa Ancuţa.

Supervision: Arianna Barbara Lovati, Cristin Coman.

Validation: Arianna Barbara Lovati, Cristin Coman.

Visualization: Arianna Barbara Lovati, Cristin Coman.

Writing – original draft: Diana-Larisa Ancuţa.

References

1. McNally M, Nagarajah K. Osteomyelitis. Orthop Trauma 2010; 24(6):416–429. https://doi.org/10.1016/j.mporth.2010.09.004

2. Conterno LO, Turchi MD. Antibiotics for treating chronic osteomyelitis in adults. The Cochrane database of systematic reviews (9). 2013; CD004439. https://doi.org/10.1002/14651858.CD004439.pub3 PMID: 24014191

3. Caplin JD, García AJ. Implantable antimicrobial biomaterials for local drug delivery in bone infection models. Acta Biomater. 2019; 93:2–11. https://doi.org/10.1016/j.actbio.2019.01.015 PMID: 30654212

4. Metsemakers WJ, Kuehl R, Moriarty TF, Richards RG, Verhofstad M, Borens O, et al. Infection after fracture fixation: Current surgical and microbiological concepts. Injury. 2018; 49(3), 511–522. https://doi.org/10.1016/j.injury.2016.09.019 PMID: 27639601

5. Seebach E, Kubatzky KF. Chronic Implant-Related Bone Infections-Can Immune 452 Modulation be a Therapeutic Strategy?. Frontiers in immunology. 2019; 10, 1724. https://doi.org/10.3389/fimmu.2019.01724

6. Hatzenbuehler J, Pulling TJ. Diagnosis and management of osteomyelitis. American family physician. 2011; 84(9), 1027–1033. PMID: 22046943

7. Lima AL, Oliveira PR, Carvalho VC, Cimerman S, Savio E, Diretrizes Panamericanas para el Tratamiento de las Osteomielitis e Infecciones de Tejidos Blandos Group. Recommendations for the treatment of osteomyelitis. Braz J Infect Dis. 2014; 18(5):526–34. https://doi.org/10.1016/j.bjid.2013.12.005 PMID: 24698709

8. Parvizi J, Tan TL, Goswami K, Higuera C, Della Valle C, Chen AF, et al. The 2018 Definition of Periprosthetic Hip and Knee Infection: An Evidence-Based and Validated Criteria. The Journal of arthroplasty. 2018; 33(5), 1309–1314. https://doi.org/10.1016/j.arth.2018.02.078 PMID: 29551303

9. Lavery LA, Ahn J, Ryan EC, Bhavan K, Oz OK, La Fontaine J, et al. What are the Optimal Cutoff Values for ESR and CRP to Diagnose Osteomyelitis in Patients with Diabetes-related Foot Infections?. Clinical orthopaedics and related research. 2019; 477(7), 1594–1602. https://doi.org/10.1097/CORR. 0000000000000718 PMID: 31268423

10. van den Kieboom J, Bosch P, Plate JDJ, IJpma FFA, Kuehl R, McNally MA, et al. Diagnostic accuracy of serum inflammatory markers in late fracture-related infection: a systematic review and meta-analysis. Bone Joint J. 2018; 100-B(12):1542–1550. https://doi.org/10.1302/0301-620X.100B12.BJJ-2018-0586.R1 PMID: 30499325

11. Korniluk A, Koper-Lenkiewicz OM, Kamińska J, Kemona H, Dymicka-Piekarska V. Mean Platelet Volume (MPV): New Perspectives for an Old Marker in the Course and Prognosis of Inflammatory Conditions. Mediators of inflammation. 2019; 2019:9213074. https://doi.org/10.1155/2019/9213074 PMID: 31148950

12. Gasparyan AY, Ayvazyan L, Mikhailidis DP, Kitas GD. Mean platelet volume: a link between thrombosis and inflammation?. Current pharmaceutical design. 2011; 17(1), 47–58. https://doi.org/10.2174/138161211795049804 PMID: 21247392

13. Huang Y, Deng W., Zheng S, Feng F, Huang Z, Huang Q, et al. Relationship between monocytes to lymphocytes ratio and axial spondyloarthritis. International immunopharmacology. 2018; 57, 43–46. https://doi.org/10.1016/j.intimp.2018.02.008 PMID: 29471252

14. Djordjevic D, Rondovic G, Surbatovic M, Stanojevic I, Udovicic I, Andjelic T, et al. Neutrophil-to-Lymphocyte Ratio, Monocyte-to-Lymphocyte Ratio, Platelet-to-Lymphocyte Ratio, and Mean Platelet Volume-to-Platelet Count Ratio as Biomarkers in Critically Ill and Injured Patients: Which Ratio to Choose to Predict Outcome and Nature of Bacteremia? Mediators of inflammation. 2018; 3758068. https://doi.org/10.1155/2018/3758068 PMID: 30116146

15. Naess A, Nilssen SS, Mo R, Eide GE, Sjursen H. Role of neutrophil to lymphocyte and monocyte to lymphocyte ratios in the diagnosis of bacterial infection in patients with fever. Infection. 2017; 45(3), 299–307. https://doi.org/10.1007/s15010-016-0972-1 PMID: 27995553

16. Forget P, Dillien P, Engel H, Cornu O, De Kock M, Yombi JC. Use of the neutrophil-to-lymphocyte ratio as a component of a score to predict postoperative mortality after surgery for hip fracture in elderly subjects. BMC research notes. 2016; 9, 284. https://doi.org/10.1186/s13104-016-2089-0 PMID: 27230508

17. Alan S, Tuna S, Turkoglu EB. The relation of neutrophil-to-lymphocyte ratio, platelet-to-lymphocyte ratio, and mean platelet volume with the presence and severity of Behçet's syndrome. The Kaohsiung journal of medical sciences. 2015; 31(12), 626–631. https://doi.org/10.1016/j.kjms.2015.10.010 PMID: 26709224

18. Demirdal T, Sen P. The significance of neutrophil-lymphocyte ratio, platelet-lymphocyte ratio and lymphocyte-monocyte ratio in predicting peripheral arterial disease, peripheral neuropathy, osteomyelitis and amputation in diabetic foot infection. Diabetes Res Clin Pract. 2018; 144:118–125. https://doi.org/10.1016/j.diabres.2018.08.009 PMID: 30176260

19. Rincon M. Interleukin-6: from an inflammatory marker to a target for inflammatory diseases. Trends Immunol. 2012; 33(11):571–7. https://doi.org/10.1016/j.it.2012.07.003 PMID: 22883707

20. Bost KL, Ramp WK, Nicholson N, Bento JL, Marriott I, Hudson MC. Staphylococcus aureus infection of mouse or human osteoblasts induces high levels of IL-6 and IL-12 production. J Infect Dis. 1999; 180:1912–1920. https://doi.org/10.1086/315138 PMID: 10558948

21. Fullilove S, Jellis J, Hughes SP, Remick DG, Friedland JS. Local and systemic concentrations of tumour necrosis factor-a, interleukin-6 and interleukin-8 in bacterial osteomyelitis. Trans R Soc Trop Med Hyg. 2000; 94:221–224. https://doi.org/10.1016/S0035-9203(00)90284-0 PMID: 10897374

22. Marriott I, Gray DL, Tranguch SL, Fowler VG Jr, Stryjewski M, Scott Levin L, et al. Osteoblasts express the inflammatory cytokine interleukin-6 in a murine model of Staphylococcus aureus osteomyelitis and infected human bone tissue. Am J Pathol. 2004; 164(4):1399–406. https://doi.org/10.1016/S0002-9440(10)63226-9 PMID: 15039227

23. Bottagisio M, Coman C, Lovati AB. Animal models of orthopedic infections. A review of rabbit models used to induce long bone bacterial infections. Journal of medical microbiology. 2019; 68(4), 506–537. https://doi.org/10.1099/jmm.0.000952 PMID: 30875284

24. Bottagisio M, Soggiu A, Lovati AB, Toscano M, Piras C, Roman'o CL et al. Draft Genome Sequence of Staphylococcus epidermidis Clinical Strain GOI1153754-03-14 Isolated from an Infected Knee Prosthesis. Genome Announc. 2017; 5(20), e00378–17. https://doi.org/10.1128/genomeA.00378-17 PMID: 28522724

25. Sideratou Z, Biagiotti M, Tsiourvas D, Panagiotaki KN, Zucca MV, Freddi G, et al. Antibiotic-Loaded Hyperbranched Polyester Embedded into Peptide-Enriched Silk Fibroin for the Treatment of Orthopedic or Dental Infections. Nanomaterials. 2022; 12, 3182. https://doi.org/10.3390/nano12183182 PMID: 36144970

26.   Ancuța DL, Soare T, Soare D, Crivineanu M, Coman C. Comparative study of osteomyelitis reproduced on rabbits using human strains of Methicilin—Resistant Staphylococcus aureus (MRSA) and Methicillin—Resistant Staphylococcus epidermidis (MRSE). Veterinary Medicine. 2020; Vol. LXVI (2), 85–92.

27.   Surdu-Bob CC, Vlase E, Barbuceanu F, Turcu D, Coman M, Badulescu M, et al. Copper Bead Therapy in Severe Bone Infection: A Rabbit Tibial Model. Veterinary and comparative orthopaedics and traumatology: V.C.O.T. 2019; 32(1), 41–50. https://doi.org/10.1055/s-0038-1676292 PMID: 30646410

28.   Faul F, Erdfelder E, Lang AG, Buchner. A. G*Power 3: a flexible statistical power analysis program for the social, behavioral, and biomedical sciences. Behav Res Methods. 2007; 39, 175–191. https://doi.org/10.3758/BF03193146 PMID: 17695343

29.   Gahukamble AD, McDowell A, Post V, Salavarrieta Varela J, Rochford ET, Richards RG, et al. Propionibacterium acnes and Staphylococcus lugdunensis cause pyogenic osteomyelitis in an intramedullary nail model in rabbits. J Clin Microbiol. 2014; 52(5):1595–606. https://doi.org/10.1128/JCM.03197-13 PMID: 24599975

30.   Kremers HM, Nwojo ME, Ransom JE, Wood-Wentz CM, Melton LJ, Huddleston PM. Trends in the epidemiology of osteomyelitis: a population-based study, 1969 to 2009. The Journal of bone and joint surgery. American volume. 2015; 97(10), 837–845.

31.   Billings C, Anderson DE. Role of Animal Models to Advance Research of Bacterial Osteomyelitis. Frontiers in veterinary science. 2022; 9, 879630. https://doi.org/10.3389/fvets.2022.879630 PMID: 35558882

32.   Roux KM, Cobb LH, Seitz MA, Priddy LB Innovations in osteomyelitis research: A review of animal models. Animal models and experimental medicine. 2021; 4(1), 59–70. https://doi.org/10.1002/ame2.12149 PMID: 33738438

33.   Odekerken JC, Arts JJ, Surtel DA, Walenkamp GH, Welting TJ. A rabbit osteomyelitis model for the longitudinal assessment of early post-operative implant infections. Journal of orthopedic surgery and research. 2013; 8, 38. https://doi.org/10.1186/1749-799X-8-38 PMID: 24188807

34.   Zhang X, Ma YF, Wang L, Jiang N, Qin CH, Hu YJ, et al. A rabbit model of implant-related osteomyelitis inoculated with biofilm after open femoral fracture. Experimental and therapeutic medicine. 2017; 14 (5), 4995–5001. https://doi.org/10.3892/etm.2017.5138 PMID: 29201204

35.   Odekerken JC, Walenkamp GH, Brans BT, Welting TJ, Arts JJ. The longitudinal assessment of osteomyelitis development by molecular imaging in a rabbit model. BioMed research international. 2014; 424652. https://doi.org/10.1155/2014/424652 PMID: 25295260

36.   Wenter V, Muller JP, Albert NL, Lehner S, Fendler WP, Bartenstein P, et al. The diagnostic value of [(18)F] FDG PET for the detection of chronic osteomyelitis and implant-associated infection. European journal of nuclear medicine and molecular imaging. 2016; 43(4), 749–761. https://doi.org/10.1007/s00259-015-3221-4 PMID: 26547722

37.   Pinheiro A, Neves F, Lemos de Matos A, Abrantes J, van der Loo W, Mage R, et al. An overview of the lagomorph immune system and its genetic diversity. Immunogenetics. 2016; 68(2), 83–107. https://doi.org/10.1007/s00251-015-0868-8 PMID: 26399242

38.   Cicchese JM, Evans S, Hult C, Joslyn LR, Wessler T, Millar JA, et al. Dynamic balance of pro- and anti-inflammatory signals controls disease and limits pathology. Immunological reviews. 2018; 285(1), 147–167. https://doi.org/10.1111/imr.12671 PMID: 30129209

39.   Nauseef WM, Borregaard N. Neutrophils at work. Nature Immunology. 2014; vol. 15, no. 7, pp. 602–611. https://doi.org/10.1038/ni.2921 PMID: 24940954

40.   Zajonc DM, Girardi E. Recognition of microbial glycolipids by natural killer T cells. Frontiers in Immunology. 2015; vol. 6, p. 400. https://doi.org/10.3389/fimmu.2015.00400 PMID: 26300885

41.   Salciccioli JD, Marshall DC, Pimentel MA, Santos MD, Pollard T, Celi LA, et al. The association between the neutrophil-to-lymphocyte ratio and mortality in critical illness: an observational cohort study. Crit Care. 2015; 19(1):13. https://doi.org/10.1186/s13054-014-0731-6 PMID: 25598149

42.   de Jager CP, Wever PC, Gemen EF, Kusters R, van Gageldonk- Lafeber AB, van der Poll T, et al. The neutrophil-lymphocyte count ratio in patients with community-acquired pneumonia. PloS one. 2012; 7 (10), e46561. https://doi.org/10.1371/journal.pone.0046561 PMID: 23049706

43.   Emektar E, Corbacioglu SK, Dagar S, Uzunosmanoglu H, Safak T, Cevik Y. Prognostic value of the neutrophil-lymphocyte and platelet–lymphocyte ratios in predicting one-year mortality in patients with hip fractures and aged over 60 years. Eurasian Journal of Emergency Medicine. 2017; 16(4):165–170. https://doi.org/10.5152/eajem.2017.51523

44.   Niemann S, Bertling A, Brodde MF, et al. Panton-Valentine leucocidin associated with S. aureus osteomyelitis activates platelets via neutrophil secretion products. Scientific Reports. 2018; vol. 8, no. 1, p. 2185. https://doi.org/10.1038/s41598-018-20582-z

45. Josse J, Velard F, Gangloff SC. Staphylococcus aureus vs. osteoblast: relationship and consequences in osteomyelitis. Frontiers in Cellular and Infection Microbiology. 2015; vol.5, p. 85. https://doi.org/10.3389/fcimb.2015.00085 PMID: 26636047

46. Yoshii T, Magara S, Miyai D, Nishimura H, Kuroki E, Furudoi S, et al. Local levels of in-terleukin -1, -4, -6 and tumor necrosis factor in an experimental model of murine osteomyelitis due to staphylococcus aureus. Cytokine. 2002; 19:59–65. https://doi.org/10.1006/cyto.2002.1039 PMID: 12182840

47. Oh GH, Chung SP, Park YS, Hong JH, Lee HS, Chung HS, et al. Mean Platelet Volume to Platelet Count Ratio as a Promising Predictor of Early Mortality in Severe Sepsis. SHOCK. 2017; Volume 47—Issue 3—p 323–330. https://doi.org/10.1097/SHK.0000000000000718 PMID: 27504801

48. Kim CH, Kim SJ, Lee MJ, Kwon YE, Kim YL, Park KS, et al. An increase in mean platelet volume from baseline is associated with mortality in patients with severe sepsis or septic shock. PloS one. 2015; 10 (3), e0119437. https://doi.org/10.1371/journal.pone.0119437 PMID: 25742300

49. Ustundag Y, Kagan H, Sanem KG, Dursun U. Relationship between C-reactive protein, systemic immune-inflammation index, and routine hemogram-related inflammatory markers in low-grade inflam-mation. Int J Med Biochem. 2018; 1(1): 24–28.

A Comparative Analysis of the Efficacy of Bacterial Lysate versus Antibiotic Therapy in the Treatment of Experimental Peri-Implantitis in Rats

Diana Larisa Ancuţa [1,2] , Diana Mihaela Alexandru [2,*] , Cătălin Ţucureanu [1] and Cristin Coman [1,3,*]

1   Cantacuzino National Medical Military Institute for Research and Development, 050096 Bucharest, Romania; diana.larisa.ancuta@gmail.com (D.L.A.); catalintucureanu@gmail.com (C.Ţ.)
2   Faculty of Veterinary Medicine, University of Agronomic Sciences and Veterinary Medicine, 050097 Bucharest, Romania
3   Center of Excellence in Translational Medicine, Fundeni Clinical Institute, 022328 Bucharest, Romania
*   Correspondence: diana.alexandru@fmvb.usamv.ro (D.M.A.); comancristin@yahoo.com (C.C.); Tel.: +40-753830681 (D.M.A.); +40-722320012 (C.C.)

Abstract: Peri-implantitis (PI) is a current concern whose understanding and resolution are ongoing. We aimed to evaluate in vivo a new treatment with antibacterial properties, based on bacterial lysates obtained from the strains of *Aggregatibacter actinomycetemcomitans*, *Streptococcus oralis*, and *Fusobacterium nucleatum.* This research was conducted on 30 rats with PI which were divided into three groups and treated with antibiotic and anti-inflammatory (AAi) drugs, bacterial lysates (BLs), and saline (C), respectively. The monitoring period included the clinical and paraclinical examination where hematological, immunological, imaging, and histopathological analysis were performed. No particular clinical signs were observed, but the radiological examination showed the loss of all implants in group C, in contrast to group BL which had the highest survival rate of devices. White cells showed a decrease from the PI period, as did the immunological analysis. Only IL-6 showed an increase in the AAi and BL groups. Histopathologically, the C group presented a high degree of bone destruction, and in the BL group, many attenuated inflammatory phenomena appeared compared to the AAi animals. Bacterial lysates have similar effects to antibiotic-based therapeutic regimens for PI, and their future use may help to improve the current therapeutic management of the disease.

Keywords: peri-implantitis treatment; bacterial lysate; antibiotic therapy; rodent model; immunological response

1. Introduction

Dental implants have recently become the most convenient solution for replacing lost teeth. They greatly improve the quality of life although they are very prone to bacterial infection [1]. Peri-implantitis starts with the inflammation of the connective tissue around the implant, then progresses rapidly and without following a standard course, until the loss of bone support. Clinical manifestations are varied and often not similar among patients so that signs of inflammation, the formation of pockets of different sizes on probing, bleeding, and/or oozing, and circular bone resorption phenomena may be observed [1].

The etiological factors of peri-implantitis are multiple, and the associated risk factors are closely related to chronic periodontal disease (PD) and include poor oral hygiene, smoking, systemic diseases (diabetes), and genetic factors. Peri-implantitis and periodontal disease share similar pathophysiological aspects although some studies claim significant differences between them [2]. Clinically and radiologically, PI and PD share common features, but the anatomical–histological environment, microbiome, and immune aspects draw a clear demarcation between the two conditions. Thus, the lesions observed in PI are significantly more pronounced than those in PD, as the immune response is generated [3]. In

PI, granulation tissue in the peri-implant site is heavily impregnated with proinflammatory cytokines compared to tissues in periodontal sites [4]. Some findings indicate other factors responsible for PI, and among them, we find residual submucosal cement from restorations, the defective position of implants in the bone, or the lack of peri-implant keratinized membrane [1]. Interestingly, peri-implantitis is not a condition that occurs immediately after fitting but, on average, after about 5 years [3], which is sufficient time for peri-implant plaque accumulation.

One of many threats to the stability of an implant is this bacterial plaque [5] that develops and acts on the implant similar to a periodontal situation [6]. The peri-implant microbiota compared to the periodontal microbiota is worse in terms of quality, but quantitatively, it is higher for some bacterial genera [7]. The adhesion and colonization of bacteria on the surface of an implant ultimately result in the formation of biofilm, and in the process of composition, bacteria contribute gradually, which has led to their classification into early and late colonizers [8]. Biofilm developed on the surface of dental implants is a major problem because in more than 50% of cases, it causes irreversible tissue destruction [9]. The first bacterial strains that adhere to the surface of an implant belong to the genus *Streptococcus* (*Streptococcus oralis, Streptococcus mitis*), and later, anaerobic strains of *Porphyromonas gingivalis* (with black pigment) or *Actinobacillus actinomycetemcomitansitans* adhere and even migrate into the subgingival space [10]. For bacterial species to cooperate in the formation of peri-implant biofilm, Kolenbrander et al. found that the presence of *Fusobacterium nucleatum* (*F. nucleatum*), which can coaggregate both streptococci and *Actinomyces* spp., is required, in addition to *Porphyromonas* spp. or *Prevotella* spp. [11]. *F. nucleatum* appears as an incriminating microbial agent as early as the mucositis stage, and the fact that it is found on the surface of implants in advanced stages of disease makes its major role in the progression of peri-implantitis more than obvious [12]. The bacterial composition of implant-associated biofilms encompasses a wide variety of species, in addition to those mentioned above, including *Treponema denticola*, *Tarnerella forsythia*, *Veionella* spp., etc. [13].

The development of these biofilms must be prevented, especially in areas where effective oral hygiene cannot be ensured. Cases have been detailed in which the migration of biofilm bacteria has endangered the health of implants [14], and the development of effective therapeutic methods and techniques in treating PI is essential to eliminate this risk. The current therapeutic management for peri-implantitis is derived from the strategies used to treat periodontitis, but they often have unpredictable results [15]. Biofilms are usually resistant to the action of the host immune system and even to antibiotic treatments [16], so the only way to resolve peri-implantitis remains the surgical approach complemented using disinfectants and antibiotics [6]. Due to the excessive use of disinfectants and biocides, antibiotic-based therapeutic strategies have suffered, and therefore, immediate alternative solutions are needed to act against the pathogens responsible for peri-implantitis [17]. These refer to materials incorporated into the implant structure or administered preventively or curatively. Three types of adjuvant measures have been found for the non-surgical therapy of PI in recent years: local antimicrobial measures (minocycline microspheres, chlorhexidine chips, or a metronidazole + amoxicillin gel), systemic measures (amoxicillin + metronidazole, either metronidazole alone), and probiotics (*Lactobacillus reuteri* strains) [18–21]. Only local treatment has reduced effects, but systemic treatment significantly improves probing depth reduction and/or bleeding on probing [22].

The complexity of peri-implantitis and its therapy is difficult to understand, so further studies involving animal models are needed. In recent years, several protocols have been tried to induce PI in rodents and test different treatment regimens, allowing researchers to conduct studies much more efficiently, with lower costs and shorter healing time [23].

Rodents have several advantages for assessing microbial and host responses. Studies using these animal models have demonstrated the induction of disease by placing ligatures around implants, resulting in the accumulation of bacterial biofilm [24], but these studies have focused on the etiopathogenesis or therapy of peri-implantitis and less on quantifying biofilm following the application of a novel therapeutic regimen [13]. Potential strategies

to combat peri-implantitis are still being explored, and a remedy that interferes with the adhesion and colonization of bacteria in the implant is needed. In this regard, experimental studies contribute to the progress of novel therapies, even if the results obtained from in vivo tests have been translated into the clinical sphere in only 20% of cases [25]. The purpose of preclinical trials is to test the safety and efficacy of new therapies; before they are tested in humans and until a solution is found that will facilitate the path from the laboratory to marketing to patients, a product must be developed that has outstanding efficacy comparable to current therapies. In this light, in our study, we aimed to evaluate in vivo a new treatment with antibacterial properties, intended for PI, based on bacterial lysates obtained from the strains of *Aggregatibacter actinomycetemcomitans* (*A. actinomycetemcomitans*), *Streptococcus oralis* (*S. oralis*), and *F. nucleatum*. This research was performed on a rat model in which PI was induced by oral contamination with the same bacteria from which the experimental treatment was performed, and the null hypothesis was based on the similar response of the lysates to antibiotic therapy in fighting the bacterial agents involved. Through this hypothesis, the ability of bacterial lysates to act on the bacterial strains involved in the induction of PI by inhibiting their growth and colonization on the implant surface and deep in the peri-implant tissues can be demonstrated. The immune response triggered by the administration of bacterial lysates offers the advantage of avoiding the administration of antibiotics, and the antibiotic-like effects make bacterial lysates a high-potential alternative for the treatment of PI.

2. Materials and Methods

2.1. Ethics Statement

This study was conducted in accordance with Law 43/2014 and Directive 2010/63/EU on the protection of animals used for scientific purposes. All steps of the experiment were approved by the Ethics Committee of the Faculty of Veterinary Medicine Bucharest, Romania (no 25/15 June 2022), and by the Sanitary, Veterinary and Food Safety Directorate Bucharest, Romania, no 27/29 August 2022, with entry number 8224/10 August 2022. This manuscript follows the guidelines provided in "The ARRIVE guidelines 2.0: author checklist—The ARRIVE Essential 10" [26], the animal experiments taking place in the Preclinical Testing Unit of the Cantacuzino National Medical-Military Institute for Research and Development, Bucharest, Romania (CI), a unit authorized for the use of animals for scientific purposes.

2.2. The Cultural Conditions of the Bacterial Strains Used for PI Induction

A. actinomycetemcomitans (ATCC 29522), *S. oralis* (DSM 20627), and *F. nucleatum* (ATCC 25586) from CI's bacterial strain collection in the form of aliquots stored in glycerol were handled and grown under anaerobic conditions (80%N_2, 10%CO_2, and 10%H_2). The culture medium used to grow the three strains was Schaedler Anaerobe Broth (Oxoid, Thermo Scientific, Newton Drive, Carlsbad, CA, USA), and 24 h incubated cultures were used on each day of oral inoculation. As in a previous study [27], the dose used was 0.6 mL inoculum (0.2 mL of each bacterium), 5 days/week, for 6 weeks, and the concentration of each bacterium stable for oral contamination was 10^9 CFU/mL determined by the nephelometric method (Densitometer McFarland Biosan DEN-1, Riga, Lithuania).

2.3. Bacterial Lysate Production Method

The 24 h cultures of *A. actinomycetemcomitans*, *S. oralis*, and *F. nucleatum*, the same cultures that were also used for PI induction, were inactivated in a water bath for 1 h. To verify the efficiency of the inactivation, the resulting suspensions were inoculated onto Brain Heart Infusion (BHI), Sabouraud, and Tyoglycolate (Oxoid, Thermo Scientific, Newton Drive, Carlsbad, CA, USA) culture media and then incubated for 14 days at 37 °C. During this time, the tubes with control media were checked daily for any change in turbidity that might indicate bacterial growth. After inactivation control, the bacterial wall lysis process followed. The method by which this was carried out was a mechanical one involving the

ultrasonication (Ultrasonic CD-4801, Shenzhen, China) of the inactivated suspensions in successive 8 min cycles for 1 h. The effect of the lysates obtained was tested in vitro by cytotoxicity tests (MTT method), the efficacy was verified by contacting different volumes of lysate with live bacteria [28], and we concluded that at least a double dose of lysate inhibited bacterial growth on both solid and liquid culture media. In in vivo testing, we decided to administer rats with PI at a dose of 1.2 mL by oral lavage for 10 days.

2.4. Animals

This study included 30 male, 20-week-old Wistar rats with an average weight of 400 g at the start of the experiment. They were supplied by CI's Specified Pathogen-Free Animal Facility and then housed in CI's Preclinical Testing Unit experimental space. Throughout this study, rats were housed under conventional conditions, including nesting material, with unlimited access to food (Granulated Combined Feed—NCG, produced by CI's Combined Feed Plant) and water ad libitum.

The general health of all animals was checked daily. Implant-specific health status was documented every other day during the experiment, starting after the first surgery, and body weight was monitored every 14 days.

Exclusion criteria were determined prior to the start of the study and included the following conditions: a weight loss of 20% or more at any time during the experiment, which would also result in the immediate euthanasia of the animal or death before the final day.

2.5. Study Design

This study was carried out in 4 major steps, as shown in Figure 1, which involved the extraction of the maxillary first molar, the fixation of the implant on the extracted molar site, and oral contamination with *A. actinomycetemcomitans*, *S. oralis*, and *F. nucleatum*, previously described when creating the PI model [27]. After the completion of the bacterial inoculation period (day 102), we allocated the animals into 3 groups (10 rats/group) to be treated as follows: saline-treated group (C), antibiotic- and anti-inflammatory-treated group (AAi), and bacterial lysate-treated group (BL). As in the case of oral contamination, treatments were also administered by lavage and gavage for 10 days.

2.6. Peri-Implantitis Rat Model Protocol

At the onset of the experiment (day 0), all animals were weighed, and blood samples were taken from the retro-orbital sinus for hematological and immunological analysis. Depending on individual weight, the rats were anesthetized with Medetomidine (0.5 mg/kg, Biotur, Alexandria, Romania) and Ketamine (0.5 mg/kg, Farmavet, Bucharest, Romania) and then underwent the dental extraction procedure as described in a previous article [29]. The period we allowed for the restoration of bone support before implant mounting was 30 days. The appearance of the implant bed was checked by clinical and especially radiological examination, performed on day 30. The implant mounting procedure included the creation of a cavity (using an X-Cube implant motor, Saeshin America, Irvine, CA, USA) with a diameter of 1 mm and 4 mm depth into which the titanium device of the same dimensions was inserted. To protect the implant from masticatory forces, the gingiva was sutured with 4/0 multifilament resorbable thread (Serafit, Serag Weissner, Naila, Germany). Postoperatively, the animals were treated with antibiotics and anti-inflammatories for 3 days (Enrofloxacin 10%, 2.5 mg/kg, Farmavet, Bucharest, Romania, and Ketoprofen, 3 mg/kg, Dopharma, Giroda, Timiș, Romania). The period required for the osseointegration of the implant, as in the previous step, was also 30 days, and the fixation of the implant in the bone was also checked radiologically on day 60.
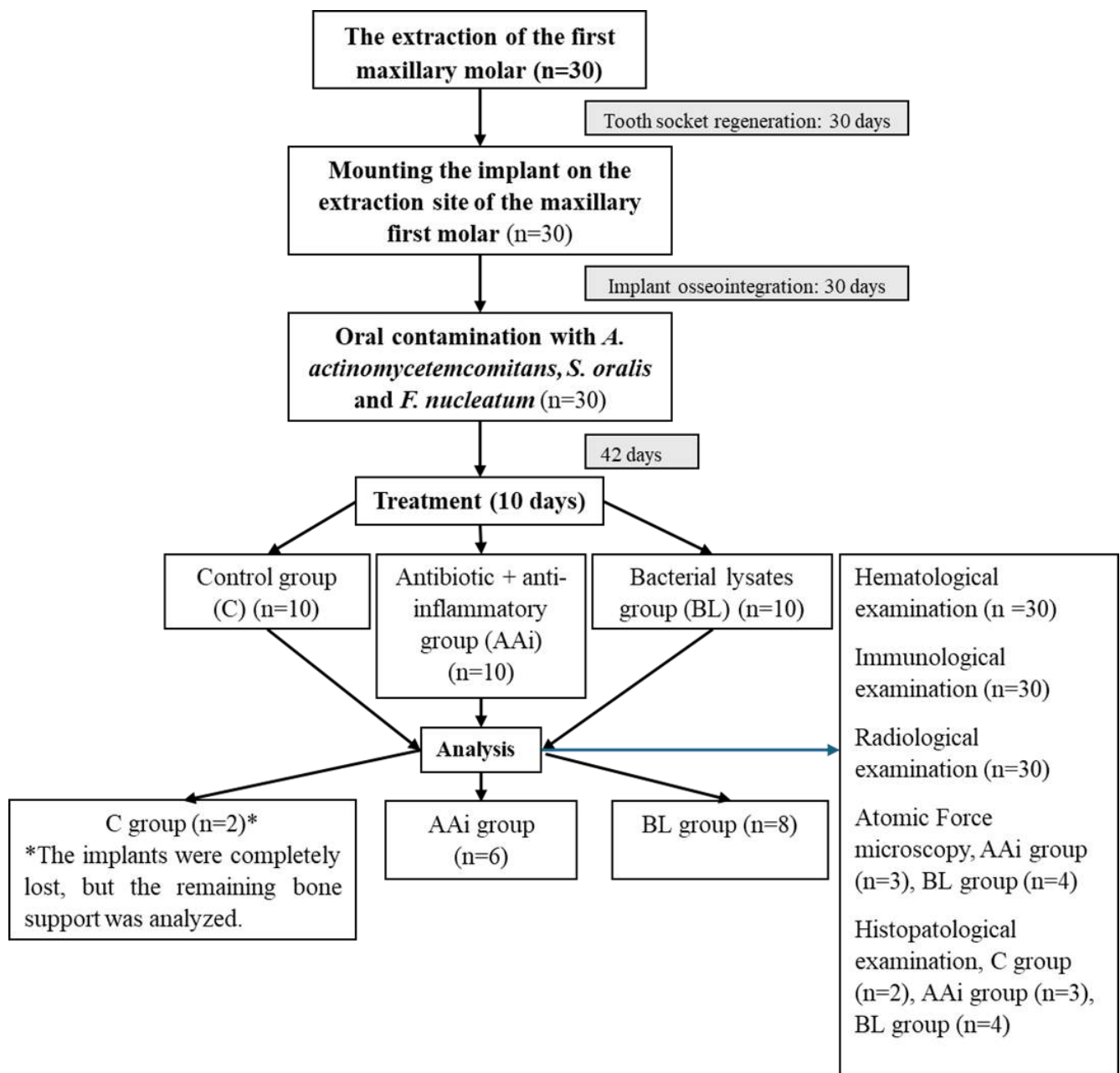
Figure 1. A diagram and consort flow chart of the experimental procedures in this study.

The third phase of this study aimed at enriching the microbiota of rats with bacteria responsible for PI in humans (*A. actinomycetemcomitans*, *S. oralis*, and *F. nucleatum*, whose processing is described in Section 2.2) for 6 weeks; then, after the specific signs of PI were confirmed (day 102), we proceeded to the treatment, as shown in Figure 1, when animals of group AAi received 40 mg/kg amoxicillin with clavulanic acid (Amoksiklav, 600 mg/42.9 mg/5 mL, powder for oral suspension, Sandoz, Bucharest, Romania) and acetaminophen (Tis Paracetamol for children, 120 mg/5 mL, 100 mL, Tis Farmaceutic, Bucharest, Romania). The BL group was treated with 1.2 mL lysate in which 0.4 mL lysate of *A. actinomycetemcomitans*, *S. oralis*, and *F. nucleatum* was present, and the control group was treated with 0.6 mL saline.

At the end of 10 days of treatment, the animals were euthanized by anesthetic overdose, and implant jaw samples were collected for histopathological analysis.

2.7. The Monitoring of Animals and Examinations throughout This Study

The assessment of PI induction was performed by daily clinical examination, monitoring the appearance of the gingiva, bleeding or oozing on implant percussion, device mobility, or loss. Moreover, even after the treatments were instituted, the clinical signs were followed, especially in the BL group, for any signs of intolerance.

The hematological examination performed on day 0, day 60, day 102, and day 112 followed the analysis of the parameters responding to the bacterial infection (lymphocytes, neutrophils, monocytes) and to the treatment applied. For this, we collected retro-orbital blood in EDTA tubes (KIMA Vacutest, Arzergrande, Italy) which we analyzed with the Idexx Procyte 5 diff analyzer.

The immunoassay included an analysis of the proinflammatory cytokines interleukin 1b (IL-1b), interleukin 6 (IL-6), and Tumor Necrosis Factor α (TNF-α). For this, the LXSARM-3 kit (R&D Systems Inc., Minneapolis, MN, USA) was acquired, and duplicate blood samples collected from the Rat Luminex Discovery Assay were run on Lithium Heparin vacutainers.

Radiological examination was performed on days 30, 60, and 102 on the IVIS Lumina XRMS Werner ROEDL (PerkinElmer, Traiskirchen, Austria) to check post-extraction bone regeneration and the integration of the implant into the bone after oral contamination and after the application of treatments.

On the final day of the experiment, parts of the implant jaw samples were collected in containers of 4% formalin, fixed for 1 week, and then further processed for a fluorescent and atomic force microscopy evaluation of potential bacterial biofilms on the surface. Implants were carefully extracted by performing a proximal incision in the bone (around 1 mm from the implant) using a circular saw and then removing the surrounding bone with forceps. Control samples were prepared in parallel by incubating implants for 72 h in culture media and an inoculation of *A. actinomycetemcomitans*, *S. oralis*, and *F. nucleatum*. Implant samples were washed in phosphate buffer saline (PBS) and stained for 30 min with 5 µg/mL DAPI (4′,6-Diamidino-2-phenylindole dihydrochloride) and 1 µg/mL eosin (Sigma-Aldrich, Merck Romania SRL, Bucharest, Romania) in PBS at room temperature. Fluorescent micrographs covering the whole implant were acquired with a 4× objective on a Nikon Ti microscope equipped with a DS-Qi2 monochrome camera, using DAPI and TxRed filters (Nikon BioImaging Labs—Leiden, The Netherlands). Acquisition was controlled with Micro-Manager [30], and individual tiles were fused using the Grid/Collection stitching plugin [31] in Fiji [32].

Implants were washed extensively with water and dried in atmospheric air for 48 h before being mounted in plast support putty (PELCO—Agar Scientific, Stansted, UK) for atomic force microscopy analyses. Atomic force microscopy (AFM) was performed on an alpha300 RAS microscope (WITec GmbH, Ulm, Germany) using 240AC-NG silicone cantilevers (Opus, Sofia, Bulgaria), with a nominal frequency of 70 kHz and a nominal spring constant of 2 N/m. All scans were performed in air, in AC mode, at a scan rate of 0.5–1 Hz. Multiple 10×10 µm scans were randomly acquired on different areas of the implants (more than 20 scans each for the in vivo implants and 5 scans for the in vitro controls). Scans were processed in Gwyddion [33], rows were aligned by median and mean plane subtraction, and topography and amplitude images were exported on fixed Z scales for all samples (0–500 nm for topography and 0–300 mV for amplitude).

Histopathological analysis was performed by fixing the samples in a 10% formaldehyde solution, then decalcifying them by keeping them for 2 weeks in Histo-Decal (Histo-Decal, Pantigliate, Italy). Subsequently, the samples were embedded in paraffin (Histopar—histological paraffin with 5–7% natural wax, Remed ProdImpex, Bucharest, Romania) then sectioned serially (thickness/section: max 5 µm) and finally stained with hematoxylin–eosin. All histological slides thus obtained were examined blindly under a light microscope (DM 4000B, Leica, Wetzlar, Germany) by a specialist histopathologist.

2.8. Statistical Analysis

The sample size was calculated by G*Power 3.1 (Düsseldorf, Germany) where error $\alpha = 0.05\%$, and a power of 80% was set. The number of animals in this study was set to 30, taking into account the complex steps of the experiment, the severity of the applied procedures, and the duration of the study. The normal distribution of data was analyzed using the Shapiro–Wilk test after which we performed a statistical analysis (Version 9.4.1, GraphPad Prism Software Inc., La Jolla, CA, USA) of the data applying a one-way ANOVA test and Bonferroni test with multiple comparisons between group C and group AAi and group C and group BL. Statistical significance was established for $p < 0.05$.

3. Results

Specific clinical signs of PI were observed starting from the second week of oral contamination when the implants appeared above the gingival margin, and later, they were covered with plaque, bleeding appeared on probing, and some of them became mobile (4–5 weeks after bacterial contamination), as shown in Figure 2.
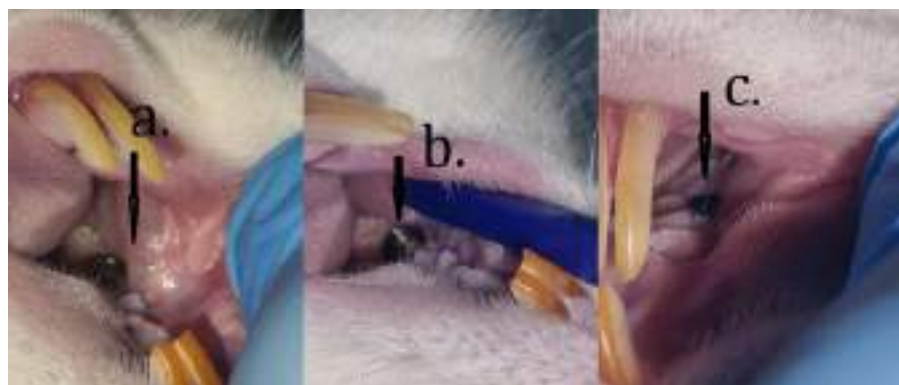

Figure 2. Implant appearance at the end of the contamination period with *A. actinomycetemcomitans*, *S. oralis*, and *F. nucleatum* where the position of the implant above the gingival margin (**a**–**c**), attached dental plaque (**b**), can be seen.

During the treatment period, the animals showed no signs of discomfort. Body weight did not change significantly in any group, and only group AAi showed more pronounced but not statistically significant decreases in body weight compared to groups C or BL (Figure 3). From a clinical point of view, no particular local signs were observed.

The implant survival rate (number of final residual implants) in each group was recorded at the end of the study. The initial number of implants fitted was 10 for each experimental group. The number of implants and survival rates per group are shown in Table 1. The implant survival rate in the control group was 0%, 20% for the AAi group, and 16% for the BL group.

Table 1. Number of implants and implant survival rates/group.

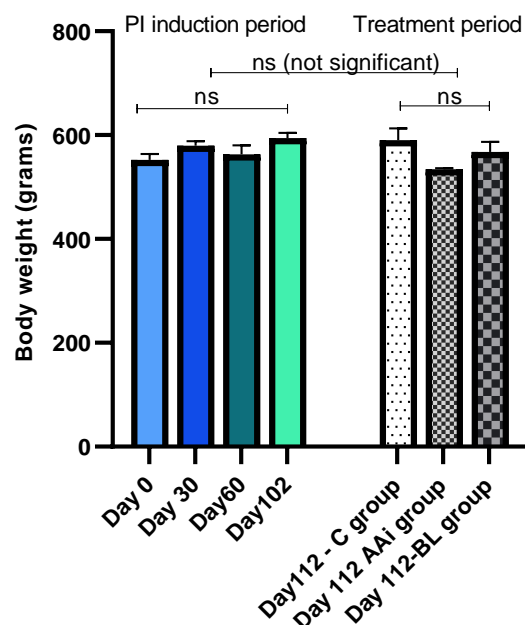|	C Group	AAi Group	BL Group
Number of animals	10	10	10
Number of implants	10	10	10
Final implants	0	6	8
Survival rate of implants	0%	60%	80%

Figure 3. The evolution of body weight during the PI induction period (day 0–day 102) and after treatment/batch administration (day 112).

The hematological examination of all treated groups (regardless of the solution administered) showed low levels of lymphocytes and neutrophils compared to day 102, the day that corresponded to the end of oral contamination, with a *p*-value between 0.001 (lymphocyte levels in the AAi group) and 0.0001 (lymphocytes and neutrophils in the BL group). Monocytes were the only elements whose level remained on an upward trend in group C compared to day 102 ($p < 0.05$); the other two groups did not show statistically significant values. It should be noted that the BL group reacted more markedly in terms of the reduction in the number of monocytes in the circulating blood than the AAi group, as can be seen in Figure 4.

Following the analysis of the main proinflammatory cytokines in PI, we could observe a significant reduction in all groups in terms of IL-1b ($p < 0.01$, AAi group, $p < 0.001$ in BL group) and TNF-α($p < 0.0001$ in BL group) levels compared to day 102. Related to IL-6, the groups that recorded values with strong statistical significance were the AAi- and BL-treated groups where $p < 0.0001$, compared to day 102. In an analysis of cytokines during the treatment period, the AAi and BL groups showed an accelerated increase in IL-6 ($p < 0.0001$) compared to the C group, with IL-1b and TNF-αregistering close values between groups without statistical significance (Figure 5).

Dental X-rays are an integral part of the assessment of peri-implant disease for patients with clinical evidence of tissue destruction around teeth and/or implants. A careful review of the current approach to PI diagnosis shows that radiographs inform only a small proportion of the condition. The area in peri-implant assessment where radiographs play a key role, however, is in treatment planning, making it possible to observe outcomes after curative measures have been instituted. Following radiological examination, in the control groups, where we did not find the implanted devices, we could observe a high level of bone resorption, with a widened aspect of the bone socket (Figure 6, black arrows). In animals treated with antibiotics or bacterial lysate, the implants showed a correct position in the bone and optimal osseointegration (Figure 6).
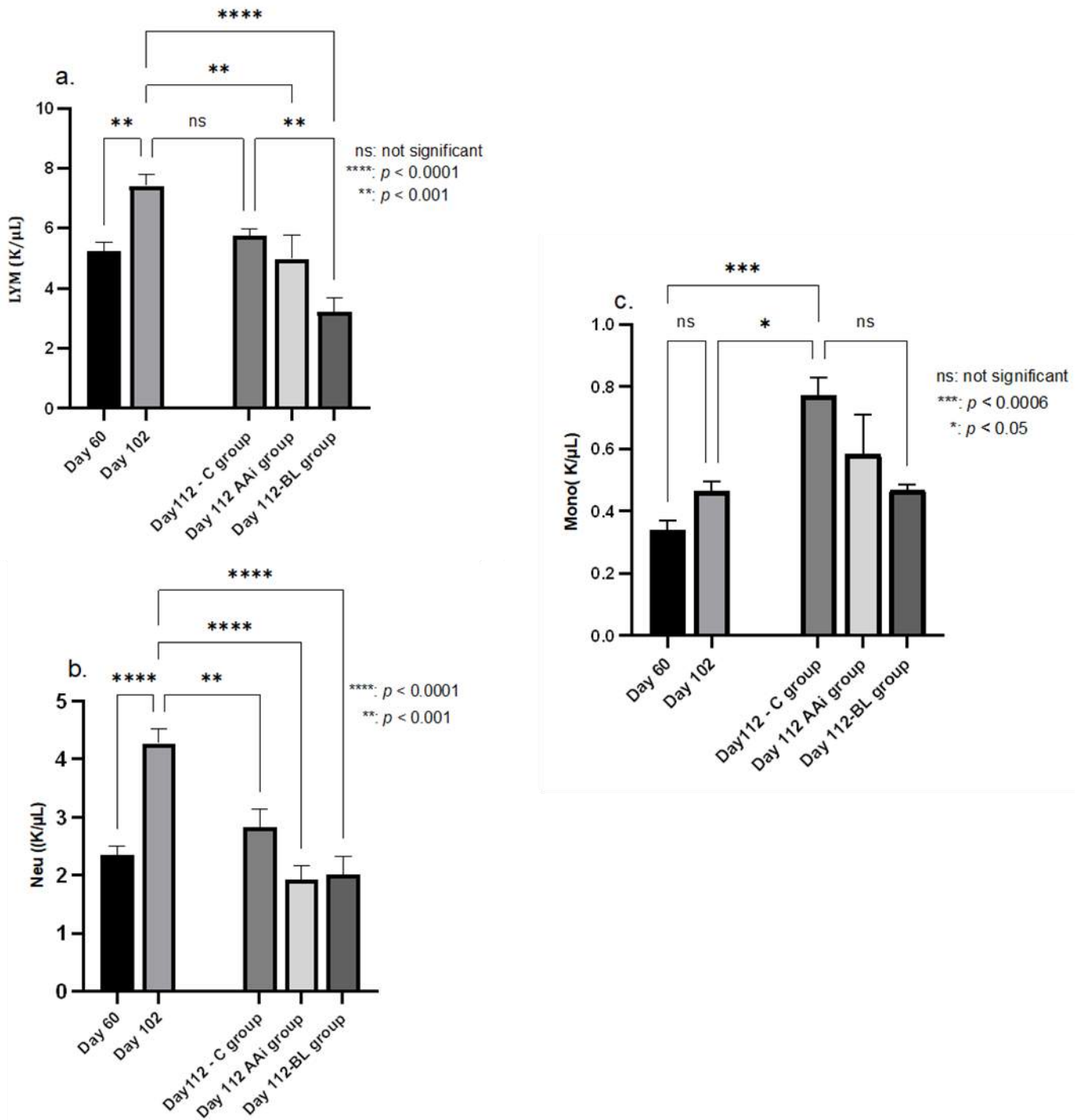
Figure 4. Lymphocyte (L YM—(**a**)), neutrophil (Neu—(**b**)), and monocyte (Mono—(**c**)) levels in response to the treatments administered compared to the onset (day 60) and end of the oral contamination period (day 102) when PI was in full progression. Once treatment was initiated, neutrophils and lymphocytes in the AAi and BL groups were significantly lower ($p < 0.0001$) than on day 102 when PI was clinically active. Monocytes were the only elements whose values continued to increase ($p < 0.05$) in group C, compared to the antibiotic- and bacterial lysate-treated groups whose values remained close to those of the induction phase. Only group BL recorded lower monocyte values compared to day 102 but without statistical significance.
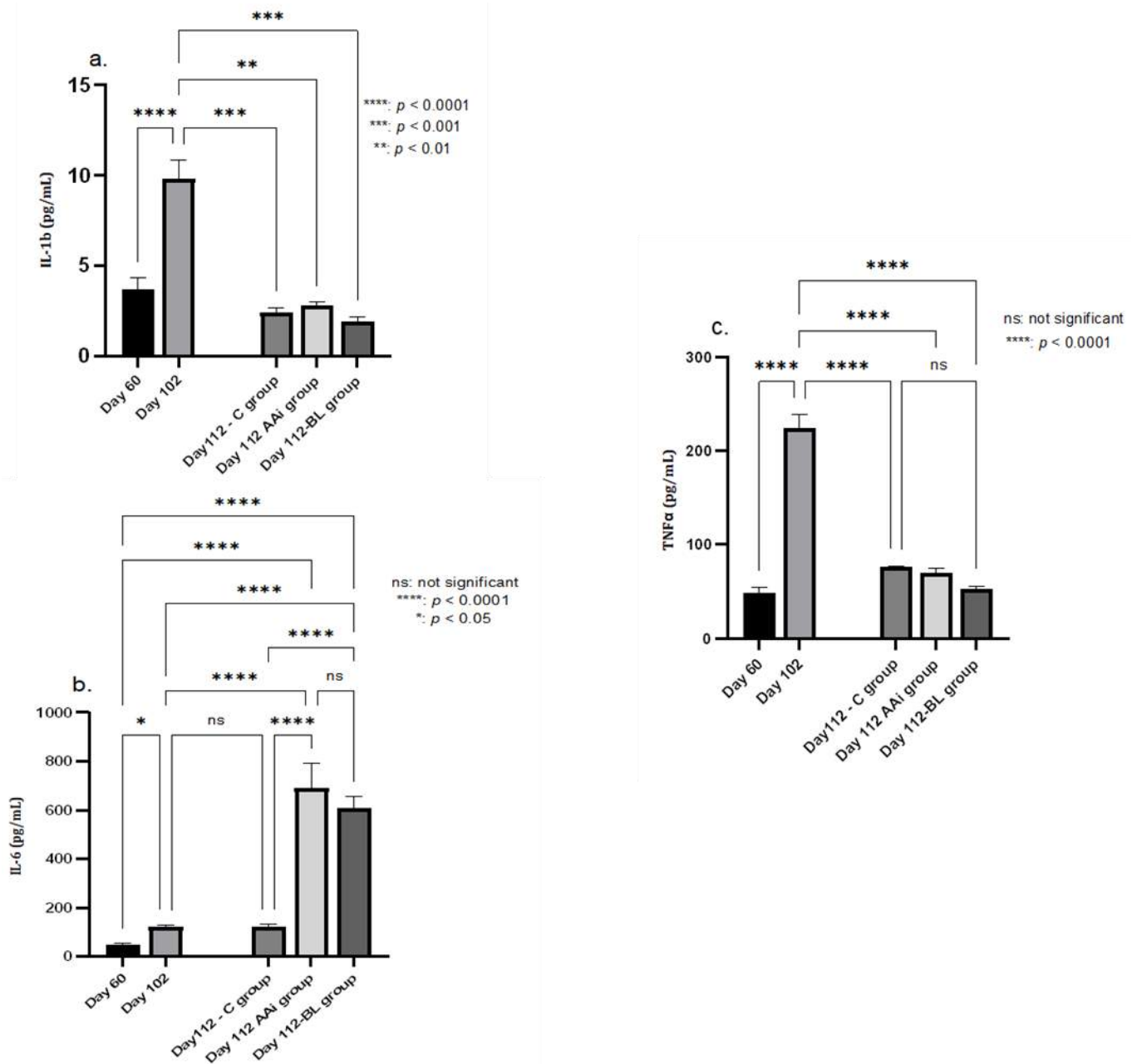
Figure 5. The evolution of proinflammatory cytokines IL-1b (**a**), IL-6 (**b**), and TNF-α(**c**) following treatments compared to day 102. IL-1b levels decreased in all groups upon treatment initiation, with considerable statistical significance in both the AAi ($p < 0.001$) and BL ($p < 0.001$) groups. IL-6 showed a very high level in the AAi and BL groups ($p < 0001$) compared to day 102, and TNF had a similar evolution as IL-1b, with a decrease in all groups ($p < 0001$) compared to the induction phase of the disease.

Figure 6. The radiological appearance of bone support after implant loss where resorbed bone can be seen, with irregular edges (circle and black arrows) in C group and implants in groups AAi and BL at the end of the study.

The histological sections were made from samples of implanted jawbone after implant removal (groups AAi and BL) or samples of bone remaining after implant loss (group C). As in a previous study [34] and adapting the results to the lesion classification system proposed by Bleich et al. [35], we quantified the lesions detected, depending on the treatment of each group by being interested in the host immune response in peri-implant tissues, giving scores ranging from 0 to 4 (no histologically severable detectable elements–severe) which we later summarized and represented in Table 2.

Table 2. Semi-quantitative scoring for histological evaluation in groups of animals undergoing treatment.

Parameter	Score	Occurrence of Injuries	Group
Inflammatory infiltrate in the peri-implant pocket	0	No neutrophils	-
	1	Rare neutrophils	AAi group BL group
	2	Neutrophilia	C group
Fibrosis	0	Absent	-
	1	Mild	-
	2	Moderate	AAi group BL group
	3	Severe	-
Bone–implant interface	0	Completely cured	AAi group BL group
	1	Rare osteoclasts	AAi group BL group
	2	Mild osteoclasts	-
	3	Moderate osteoclast activity	C group
	4	Severe osteoclast activity	-

A histological examination of hematoxylin–eosin-stained slides assessed the presence of inflammation in peri-implant tissue after treatment with bacterial lysates, antibiotics, and anti-inflammatories. The control group showed the presence of a junctional epithelium impregnated with hemorrhagic areas and neutrophils but also rich fibrous tissue (Figure 7). More than half of the samples from the PI groups (regardless of treatment) showed the infiltration of inflammatory cells in the peri-implant tissue, including neutrophils, lymphocytes, and plasma cells, more pronounced in all AAi (Figure 8), moderate in the BL group.

Also, in the latter group (BL), in addition to the migration of inflammatory cells, an increase in the number and thickness of collagen fibers in the surrounding soft tissue was observed (Figure 9).
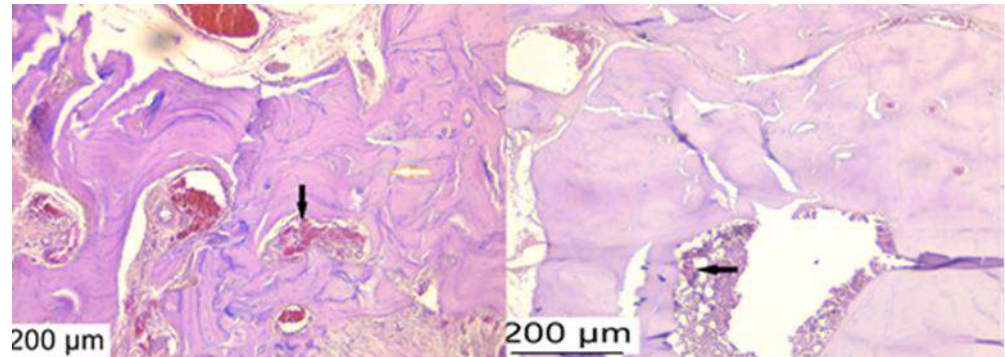

Figure 7. Histological appearance at the level of the implanted bone: the disorganization of the bone plates (yellow arrow) accompanied by hemorrhagic and inflammatory infiltrate (black arrow) observed in the control group. Hematoxylin–eosin staining, ob 10×.
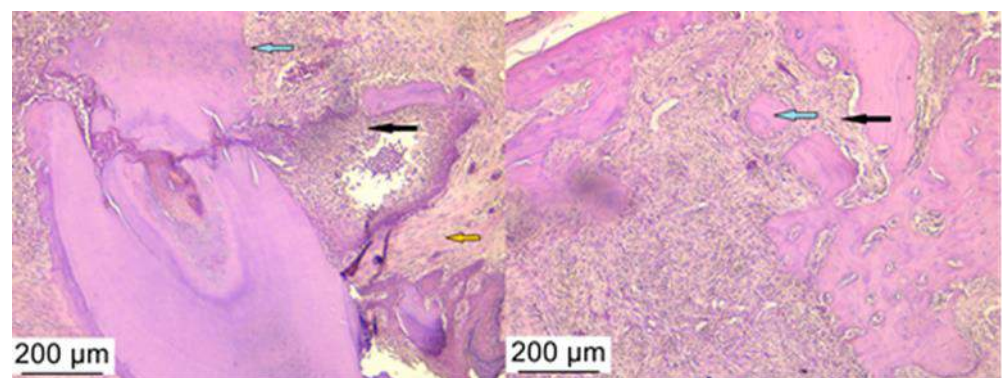

Figure 8. The histological aspect found in the group with PI treated with antibiotic and anti-inflammatory drugs where the persistence of the inflammatory infiltrate rich in lymphocytes and neutrophils (black arrow), fibrous infiltrate (orange arrow), and advanced process of bone destruction (blue arrow) can be observed. Hematoxylin–eosin staining, ob 10×.

Fluorescence microscopy showed that a high amount of tissue and biological fouling was maintained on the implant surface after the fixation and extraction protocol (Figure 10, top). Higher magnification investigations (20×, Supplementary Figure S1) of select areas revealed that most of the fluorescent signal was due to bone tissue autofluorescence, the extracellular matrix (eosin stain), and cell nuclei (DAPI). No structures indicative of bacterial biofilms were identified even at this higher magnification on the ex vivo samples. On the in vitro inoculated control (Figure 10B), a weak network of nucleic acid staining was evident when compared to the culture media-only control (Figure 10MC). Consequently, multiple 10 × 10 μm AFM scans were performed at random locations on different areas of the implants. Representative images for the upper shaft (a–h) and thread area (k,l,o,p) are presented in Figure 10. No scans could be performed in the thread area of in vitro control implants since the high slope, in absence of biological tissue, impeded proper scanning.
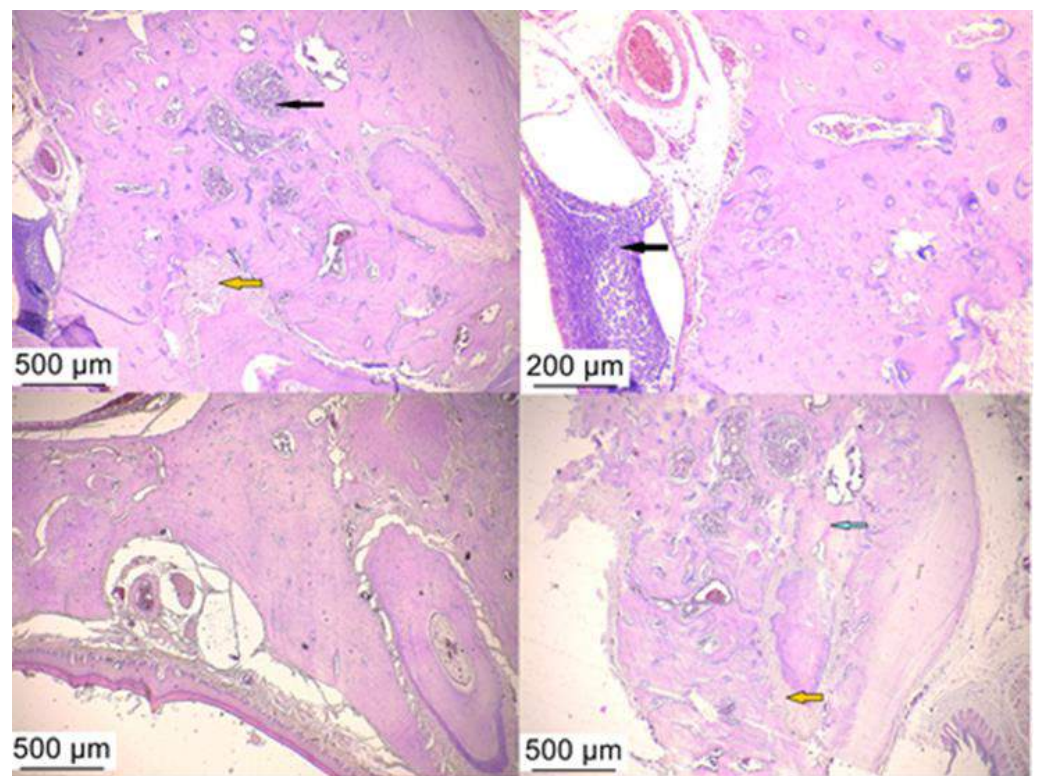
Figure 9. The histological aspect observed in the group with PI treated with bacterial lysate where the inflammatory infiltrate is in a moderate amount (black arrow), the bone destruction (blue arrow) being compensated by fibrous tissue agglomerates (orange arrow). Hematoxylin–eosin staining, ob 4×, and 10×.

Implants retrieved from the AAi and BL groups frequently showed incipient bone-like mineral deposits (Figure 10c,d,g,h), well-developed trabecular bone (l,p), and collagen fibers (triangle in c,g). On a very limited number of scans, all from the AAi group, structures with bacterial morphology could be observed, but these events were too rare to ascertain any difference between samples or support any conclusion of widespread bacterial colonization. Clusters with morphology indicative of *A. actinomycetemcomitans* (asterisk in Figure 10k) were only observed in a single scan of the implant retrieved from the AAi group, embedded in the bone structure adhered to the thread area. On the in vitro colonized control implant, most scans showed bacteria with the characteristic morphology of *F. nucleatum* adhered on the surface.
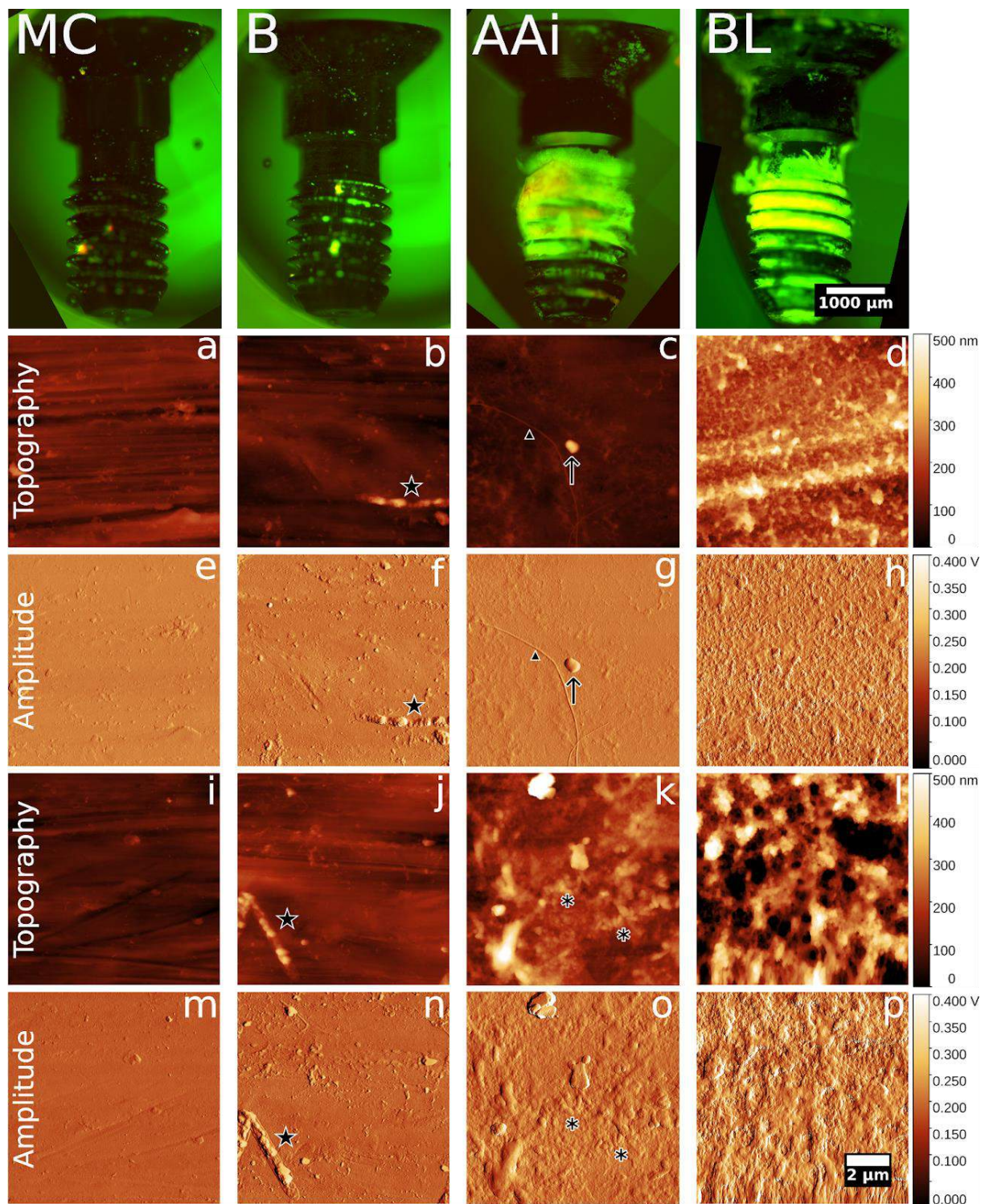
Figure 10. Fluorescence and atomic force microscopy analysis of surviving implants retrieved from the in vivo experiments and in vitro bacteria colonized controls; top—composite fluorescent micrographs of DAPI (green) and EOSIN (red)-stained implants, reconstructed from approximately 35 tiles per implant, (**MC**)—in vitro media control, (**B**)—in vitro bacterial colonization, (**AAi**)—ex vivo from AAi group, (**BL**)—ex vivo from BL group. Bottom—representative AFM scans (2 per condition) corresponding to top panel, (**a**–**d**,**i**–**l**)—topography images false colored from 0 to 500 nm, (**e**–**h**,**m**–**p**) amplitude images false colored from 0.000-0.400 V. Star—*F. nucleatum*, arrow—potential bacteria, asterisk—potential clusters of *A. actinomycetemcomitans*, triangle—collagen fiber.

4. Discussion

In experimental research, rats are often used because of their advantages of size, reproduction rapid growth cycle, maintenance, and easy handling. In terms of bone structure, rats are very similar to humans although bone volume shows variations according to gender, age, weight, and sex [36]. Thus, bone density tends to increase as animals age, and hormonal variations also influenced a study involving the use of bone support [37,38]. Therefore, for this study, rats aged 20 weeks were used, based on these considerations and especially on the fact that after this age, the animals are considered old, thus wishing to simulate a situation similar to humans in which the need for an implant is greater in the second half of life. In the establishment of the PI model, some difficulties were encountered concerning the oral opening or the fragility of the molar roots. Rat first molars have three buccal and two palatal roots, and the instrumentation and technique adapted to the size of the animal allowed for the extraction of the premolars without a great risk of root fracture. Many studies using small animal models for implant insertion have used modified instrumentation to achieve the desired results [39]. The implant site was the extraction site, and the execution of the maneuver was challenging in many ways. The first challenge was the limited space, the second was the increased risk of the perforation of the jawbone, and the third was the stability of the implant. To achieve good stability, it was necessary to reduce movement at the implant–bone interface, thus avoiding the degradation of the newly formed alveolar bone post-extraction. For implant mounting, the palatal alveolus was chosen because of its thickness suitable for the implant size, and by doing so, it was ensured that the bone support is a suitable one that promotes osseointegration, as some authors showed in a meta-analysis [40].

Microbiological diagnosis has been proposed as a possible approach to detecting the most aggressive periodontal pathogens [41]. Since in some patients, there is no clear difference related to the bacterial species involved in peri-implant health and disease, we resorted to oral contamination with common peri-implantitis strains, namely *A. actinomycetemcomitans*, *S. oralis*, and *F. nucleatum*. The bacterial species identified in PI are predominantly anaerobic, Gram-negative, and not related to a uniform microbial profile as found in periodontitis [42]. A significant difference was not observed between the strains isolated from the PD site and PI [43]; therefore, we chose PI-specific bacterial strains. In a healthy organism, the oral bacterial community is in a state of equilibrium with the host, but the intervention of risk factors causes biofilm formation and the implicit occurrence of inflammation. Consequently, the increase in the number of strains adhering to the initial biofilm results in difficult therapeutic management [44]. Thus, PI treatment aims to control infection and reduce bacterial substrate.

Clinically, no differences were observed between the antibiotic-treated and bacterial lysate-treated groups of animals, but after the therapeutic approach, the implant survival rate was higher in the bacterial lysate-treated groups and 0 in group C. For the fact that no device was found in the control group, we can hypothesize that PI still progressed in these animals, speeding up the implant removal process. From a general perspective, out of 30 implants initially fitted, at the end of the study, almost half were still found, which is in line with a recent meta-analysis [45] where out of 213 implants, only 163 survived on the rat model with ligation- or bacterial contamination-induced PI. Recommendations for clinical changes in peri-implant tissues refer to immediate debridement, oral washes with disinfectant substances, and systemic antibiotic therapy, but in animals, the use of antibiotics may influence the healing process and immune response [46]. The results of this study encourage further investigation into the efficacy of bacterial lysates in the healing of PI and their use instead of antibiotics, especially due to the similarity of the response of the animal body to the administered treatments, demonstrated by the reduction in the inflammatory response observed both hematologically and especially histopathologically. In the available literature, bacterial lysates, it appears, may be an option for patients with recurrent respiratory infections, allergies, atopic dermatitis, or asthma [47]. They are antigens obtained from the inactivation of pathogenic bacteria that once had immunogenic

properties. The route of administration of bacterial lysates influences their immunogenic capacity in that they exert their action on dendritic cells whose predominant distribution is in the upper respiratory tract and oral cavity [48]. Bacterial lysate preparations in the form of sublingual tablets or oral solutions have maximum efficacy in the oral cavity without the need for antibiotic pharmacokinetics, and therefore, oral diseases such as PI can be treated with such products.

Based on the current knowledge that PI and PD have similar infectious etiology, the use of systemic antibiotic therapy is considered by some authors to be standard [49], even though in recent years, the increasing antibiotic resistance of pathogenic and opportunistic bacteria has developed. For this reason, it is imperative to develop new therapies that circumvent the unwarranted use of antibiotics. Saline is the most widely used in the care and treatment of oral diseases [50], and the present study compared the effect of antibiotic therapy and bacterial lysate with the effect obtained after saline lavage.

For the assessment of inflammation status, cytokines provided valuable information. The role of IL-1b (a basic cytokine in the inflammatory response) is a major one in the pathogenesis of PI, and an increased level indicates soft tissue inflammation and the degree of bone resorption. IL-1b correlates positively with implant failure [51], even being a predictor of the degree of severity of PI [52]. This cytokine shows higher secretion in the early phases of the disease but not as high as found in peri-implant mucositis [53,54].

In PI, TNFα occurs at a high level in both soft and hard tissues and is directly proportional to the degree of bone destruction and, in turn, may be a predictor of PI severity [51]. Some studies show that this cytokine could be used in the diagnosis of PI which would involve the use of standard antigen swabs with which to collect saliva from patients with suspected disease [55].

IL-6 is excreted by osteocytes and plays a role in osteoclast formation. By some specific mechanisms, IL-6 can block the effects of TNF-alpha. In bacterial-induced PI, IL-6 is secreted by macrophages and has a proinflammatory role, being found in significant amounts in the sulcular fluid [56]. Increased IL-6 indicates the onset and progression of PI, and instituting treatment does not ensure the control of the cytokine [57]. The same aspect could be observed in our experiment where in the AAi and BL groups, IL-6 levels remained elevated compared to the control group. Moreover, some studies claim that a high cytokine concentration could protect the body against IL-1b- and TNF-α-induced osteoclastic re-obstruction [58]. To decrease the average concentration of IL-1b and TNFα, the primary role is played by the correct peri-implant therapy to maintain these cytokines in normal parameters. A study by Gomes et al. showed that instituting peri-implant therapy without proper hygiene maintenance has unfavorable results over time [59]. Even disinfectants (chlorhexidine) are not highly effective in treating oral diseases, and in addition to their action, ozonized gels have proven superior as an alternative treatment [60]. The obtained results in the present study reinforce the theory that the applied treatments have favorable effects by demonstrating the reduction in IL-1b and TNF-α in both the AAi and BL groups; in this situation, bacterial lysates can be considered fundamental components of therapeutic tactics similar to antibiotics. The cytokine response to bacterial lysate action requires further investigation because few studies have addressed this therapeutic method in PI, with no evidence reported in the literature. However, a periodic analysis of cytokine assays facilitates the diagnosis of PI.

It is also required to investigate the osteoimmunological mechanisms involved in alveolar bone shaping. The complex of proteins responding to lesion recognition receptors leads to the secretion and maturation of proinflammatory cytokines along with the activation of the inflammatory response. Inappropriate activity of the protein complex may allow for the persistence of infection and uncontrolled resorption of alveolar bone in PI through the regulatory mechanisms of osteoclasts, osteoblasts, osteocytes, macrophages, monocytes, neutrophils, and adaptive immune cells [61]. Osteoclasts originate from monocytes which are initially involved in implant osseointegration, implant stability, and the long-term maintenance of the marginal bone level. The obtained results on monocyte response confirm this

hypothesis by the fact that they showed increased reactivity, especially in the control group, and by the fact that in the AAi and BL groups, monocyte levels decreased, indicating the efficacy of the treatments in implant stability. The association between PI and the increase in neutrophil count is due to the interaction between the infectious agent and the host immune cells which results in the massive production of leukocytes [62]. In PI induced by *A. actinomycetemcomitans*, *S. oralis*, and *F. nucleatum*, this could be observed as well as their attenuation following the institution of treatments.

The application of both treatments for PI resulted in the compensation of bacterial dysbiosis and peri-implant tissue recovery. The 10-day treatment period was sufficient to evaluate the effects, especially considering the rapid growth rate of these animals and the fact that, at adult age, each day of the animal is approximately equivalent to 34.8 human days [63], so in the case of the translation of the treatment method, it would be recommended that bacterial lysates be administered for longer periods of time. Bacterial lysates can be considered a strong competitor for antibiotic therapy, a fact that was evident from the histologically observed lesional picture, where the inflammatory infiltrate was less pronounced, as was the degree of bone destruction. Histopathologically, the lesions detected confirmed the attenuation of the inflammatory process in the peri-implant sac, regardless of the treatment applied (antibiotic or bacterial lysate). Only in antibiotic-treated animals did the inflammatory infiltrate remains increase in the samples analyzed. As suggested by other authors, experimental PI studies should be continued to establish the mechanisms of tissue development, protection, and recovery under pharmacological correction by bacterial lysate [64,65].

Radiological examination, as an integral part of PI diagnosis, helped establish implant integrity throughout this study. Through it, the level of bone density was compared, and in the control groups, this density was much lower (also revealed by the degree of survival of the implants) than in the antibiotic- and bacterial lysate-treated groups. An analysis of the obtained images revealed optimal osseointegration in the implants and bone densities characteristic of reduced inflammatory processes.

An AFM examination of extracted implants revealed mostly regular bone tissue structures, supporting the rest of the data showing proper osseointegration in both treated groups. AFM imaging is able to readily allow for the assessment of bacterial colonization and measurement of biofilm properties on in vitro colonized implants from different materials [66], as also shown in the current study. While probable planktonic bacteria and bacterial clusters were identified on ex vivo implants from the AAi group alone, these observations were too rare to conclude any difference between samples or the widespread colonization of surviving implants at the assessed timepoint. A major limitation in this respect is the premature loss of all implants in the in vivo control group which might have allowed for a comparison of bacterial biofilm formation at higher levels of bioburden.

However, although the results of this study confirm the null hypothesis which was based on the similar response of the lysates to antibiotic therapy in fighting the bacterial agents involved in PI, there are some limitations to mention. One of them is related to the oral flora of the rats which is quite consistent and could have influenced the results of this study. A well-established and reproducible PI model is extremely important when testing new therapies. The induction time of the disease (6 weeks) is short compared to the clinical situation in which PI evolves in a few years, and the fact that in the control group, there were no implants to be analyzed compared to the treatments applied to the AAi and BL groups may mean that the disease evolves even in the absence of the administration of bacteria (which would be similar to humans) but which may raise doubts about the efficacy of the lysates or even antibiotics on the model created. Given the fact that the treatment of PI induced by three bacterial strains responsible for the disease in humans has been attempted, another limitation relates to the efficacy of the lysates on the microbial complexity of human PI patients, and the translation of the method would be interesting to follow, especially if such lysates were made from the specific pathogenic flora of each patient or a complex bacterial lysate comprising a suite of the most pathogenic oral bacteria.

New therapies can be tested on the PI model created, but further research is needed on the efficacy of bacterial lysates on this disease, both in vitro and in vivo, perhaps using other bacterial strains (to create the bacterial lysate) or other methods of disease induction (without bacterial involvement), as mentioned above. An important criterion in evaluating the efficacy of lysates refers to immunological analysis, and in future studies, the mechanism of action of lysates in triggering the immune response should be further investigated. The bacterial lysate therapy of PI is a new topic, and the results presented are promising for further research and especially for the development of specific PI therapies.

5. Conclusions

The research in this study aimed to evaluate the effect of antibiotic therapy and bacterial lysate treatment on peri-implantitis. By corroborating the results of hematological, immunological, radiological, and histopathological analyses and implant survival rates, we can state that the treatment with bacterial lysate had a similar effect to the standard treatment, based on antibiotics and anti-inflammatory drugs when compared to untreated controls. Furthermore, slightly higher implant survival rates were observed in the bacterial lysate-treated group compared to the group receiving antibiotics. Bacterial lysate administration is a valid treatment option developed for PI because of pathogenic bacteria, and a personalized bacterial lysate-based therapy could reduce unnecessary antibiotic consumption and thus contribute to reducing antibiotic resistance. Furthermore, bacterial lysates, as well as other disinfectants or substances with disinfecting or reparative properties (e.g., ozone-based gels), can be considered valuable alternatives for the treatment of peri-implantitis.

References

1. Schwarz, F.; Derks, J.; Monje, A.; Wang, H.L. Peri-implantitis. *J. Periodontol.* **2018**, *89* (Suppl. S1), S267–S290. [CrossRef] [PubMed]
2. Berglundh, T.; Armitage, G.; Araujo, M.G.; Avila-Ortiz, G.; Blanco, J.; Camargo, P.M.; Chen, S.; Cochran, D.; Derks, J.; Figuero, E.; et al. Peri-implant diseases and conditions: Consensus report of workgroup 4 of the 2017 World Workshop on the Classification of Periodontal and Peri-Implant Diseases and Conditions. *J. Clin. Periodontol.* **2018**, *45* (Suppl. S20), S286–S291. [CrossRef] [PubMed]
3. Dreyer, H.; Grischke, J.; Tiede, C.; Eberhard, J.; Schweitzer, A.; Toikkanen, S.E.; Glöckner, S.; Krause, G.; Stiesch, M. Epidemiology and risk factors of peri-implantitis: A systematic review. *J. Periodontal Res.* **2018**, *53*, 657–681. [CrossRef] [PubMed]

4. Venza, I.; Visalli, M.; Cucinotta, M.; De Grazia, G.; Teti, D.; Venza, M. Proinflammatory gene expression at chronic periodontitis and peri-implantitis sites in patients with or without type 2 diabetes. *J. Periodontol.* **2010**, *81*, 99–108. [CrossRef]

5. Elter, C.; Heuer, W.; Demling, A.; Hannig, M.; Heidenblut, T.; Bach, F.W.; Stiesch-Scholz, M. Supra- and subgingival biofilm formation on implant abutments with different surface characteristics. *Int. J. Oral Maxillofac. Implant.* **2008**, *23*, 327–334.

6. Mombelli, A.; Décaillet, F. The characteristics of biofilms in peri-implant disease. *J. Clin. Periodontol.* **2011**, *38* (Suppl. S11), 203–213. [CrossRef] [PubMed]

7. Butera, A.; Pascadopoli, M.; Pellegrini, M.; Gallo, S.; Zampetti, P.; Scribante, A. Oral microbiota in patients with peri-implant disease: A narrative review. *Appl. Sci.* **2022**, *12*, 3250. [CrossRef]

8. Kolenbrander, P.E.; London, J. Adhere today, here tomorrow: Oral bacterial adherence. *J. Bacteriol.* **1993**, *175*, 3247–3252. [CrossRef] [PubMed]

9. Grischke, J.; Eberhard, J.; Stiesch, M. Antimicrobial dental implant functionalization strategies -A systematic review. *Dent. Mater. J.* **2016**, *35*, 545–558. [CrossRef]

10. Tonon, C.C.; Panariello, B.H.D.; Spolidorio, D.M.P.; Gossweiler, A.G.; Duarte, S. Antibiofilm effect of ozonized physiological saline solution on peri-implant-related biofilm. *J. Periodontol.* **2021**, *92*, 1151–1162. [CrossRef]

11. Kolenbrander, P.E.; Palmer, R.J., Jr.; Rickard, A.H.; Jakubovics, N.S.; Chalmers, N.I.; Diaz, P.I. Bacterial interactions and successions during plaque development. *Periodontology* **2000**, *42*, 47–79. [CrossRef] [PubMed]

12. Ghensi, P.; Manghi, P.; Zolfo, M.; Armanini, F.; Pasolli, E.; Bolzan, M.; Bertelle, A.; Dell'Acqua, F.; Dellasega, E.; Waldner, R.; et al. Strong oral plaque microbiome signatures for dental implant diseases identified by strain-resolution metagenomics. *NPJ Biofilms Microbiomes* **2020**, *6*, 47. [CrossRef] [PubMed]

13. Blank, E.; Grischke, J.; Winkel, A.; Eberhard, J.; Kommerein, N.; Doll, K.; Yang, I.; Stiesch, M. Evaluation of biofilm colonization on multi-part dental implants in a rat model. *BMC Oral Health* **2021**, *21*, 313. [CrossRef] [PubMed]

14. Lauritano, D.; Moreo, G.; Lucchese, A.; Viganoni, C.; Limongelli, L.; Carinci, F. The Impact of Implant-Abutment Connection on Clinical Outcomes and Microbial Colonization: A Narrative Review. *Materials* **2020**, *13*, 1131. [CrossRef] [PubMed]

15. Wong, R.L.; Hiyari, S.; Yaghsezian, A.; Davar, M.; Casarin, M.; Lin, Y.L.; Tetradis, S.; Camargo, P.M.; Pirih, F.Q. Early intervention of peri-implantitis and periodontitis using a mouse model. *J. Periodontol.* **2018**, *89*, 669–679. [CrossRef] [PubMed]

16. Davies, D. Understanding biofilm resistance to antibacterial agents. Nature reviews. *Drug Discov.* **2003**, *2*, 114–122. [CrossRef] [PubMed]

17. Hosseini Hooshiar, M.; Badkoobeh, A.; Kolahdouz, S.; Tadayonfard, A.; Mozaffari, A.; Nasiri, K.; Salari, S.; Safaralizadeh, R.; Yasamineh, S. The potential use of nanozymes as an antibacterial agents in oral infection, periodontitis, and peri-implantitis. *J. Nanobiotechnology* **2024**, *22*, 207. [CrossRef]

18. Estefanía-Fresco, R.; García-de-la-Fuente, A.M.; Egaña-Fernández-Valderrama, A.; Bravo, M.; Aguirre-Zorzano, L.A. One-year results of a nonsurgical treatment protocol for peri-implantitis. A retrospective case series. *Clin. Oral Implant. Res.* **2019**, *30*, 702–712. [CrossRef] [PubMed]

19. Galofré, M.; Palao, D.; Vicario, M.; Nart, J.; Violant, D. Clinical and microbiological evaluation of the effect of Lactobacillus reuteri in the treatment of mucositis and peri-implantitis: A triple-blind randomized clinical trial. *J. Periodontal Res.* **2018**, *53*, 378–390. [CrossRef] [PubMed]

20. Liñares, A.; Pico, A.; Blanco, C.; Blanco, J. Adjunctive Systemic Metronidazole to Nonsurgical Therapy of Peri-implantitis with Intrabony Defects: A Retrospective Case Series Study. *Int. J. Oral Maxillofac. Implant.* **2019**, *34*, 1237–1245. [CrossRef]

21. Mombelli, A.; Feloutzis, A.; Brägger, U.; Lang, N.P. Treatment of peri-implantitis by local delivery of tetracycline. Clinical, microbiological and radiological results. *Clin. Oral Implant. Res.* **2001**, *12*, 287–294. [CrossRef] [PubMed]

22. Liñares, A.; Sanz-Sánchez, I.; Dopico, J.; Molina, A.; Blanco, J.; Montero, E. Efficacy of adjunctive measures in the non-surgical treatment of peri-implantitis: A systematic review. *J. Clin. Periodontol.* **2023**, *50* (Suppl. S26), 224–243. [CrossRef] [PubMed]

23. Graves, D.T.; Fine, D.; Teng, Y.T.; Van Dyke, T.E.; Hajishengallis, G. The use of rodent models to investigate host-bacteria interactions related to periodontal diseases. *J. Clin. Periodontol.* **2008**, *35*, 89–105. [CrossRef] [PubMed]

24. Duarte, P.M.; Tezolin, K.R.; Figueiredo, L.C.; Feres, M.; Bastos, M.F. Microbial profile of ligature-induced periodontitis in rats. *Arch. Oral Biol.* **2010**, *55*, 142–147. [CrossRef] [PubMed]

25. de Avila, E.D.; Nagay, B.E.; Pereira, M.M.A.; Barão, V.A.R.; Pavarina, A.C.; van den Beucken, J.J.J.P. Race for Applicable Antimicrobial Dental Implant Surfaces to Fight Biofilm-Related Disease: Advancing in Laboratorial Studies vs Stagnation in Clinical Application. *ACS Biomater. Sci. Eng.* **2022**, *8*, 3187–3198. [CrossRef]

26. Ancuta, D.L.; Alexandru, D.M.; Crivineanu, M.; Coman, C. Induction of Periodontitis Using Bacterial Strains Isolated from the Human Oral Microbiome in an Experimental Rat Model. *Biomedicines* **2023**, *11*, 2098. [CrossRef]

27. Percie du Sert, N.; Hurst, V.; Ahluwalia, A.; Alam, S.; Avey, M.T.; Baker, M.; Browne, W.J.; Clark, A.; Cuthill, I.C.; Dirnagl, U.; et al. The ARRIVE guidelines 2.0: Updated guidelines for reporting animal research. *PLoS Biol.* **2020**, *18*, e3000410. [CrossRef]

28. Ancuța, D.L.; Vuță, V.; Șalgău, C.; Bărbuceanu, F.; Coman, C. Innovative treatment against human periodontitis and periimplantitis—In vitro study. *Farmacia* **2024**, *72*, 125–131. [CrossRef]

29. Ancuța, D.L.; Alexandru, D.M.; Crivineanu, M.; Coman, C. Induction of Experimental Peri-Implantitis with Strains Selected from the Human Oral Microbiome. *Biomedicines* **2024**, *12*, 715. [CrossRef]

30. Edelstein, A.D.; Tsuchida, M.A.; Amodaj, N.; Pinkard, H.; Vale, R.D.; Stuurman, N. Advanced methods of microscope control using μManager software. *J. Biol. Methods* **2014**, *1*, e10. [CrossRef]

31. Preibisch, S.; Saalfeld, S.; Tomancak, P. Globally optimal stitching of tiled 3D microscopic image acquisitions. *Bioinformatics* **2009**, *25*, 1463–1465. [CrossRef] [PubMed]

32. Schindelin, J.; Arganda-Carreras, I.; Frise, E.; Kaynig, V.; Longair, M.; Pietzsch, T.; Preibisch, S.; Rueden, C.; Saalfeld, S.; Schmid, B.; et al. Fiji: An open-source platform for biological-image analysis. *Nat. Methods* **2012**, *9*, 676–682. [CrossRef] [PubMed]

33. Nečas, D.; Klapetek, P. Gwyddion: An open-source software for SPM data analysis. *Open Phys.* **2012**, *10*, 181–188. [CrossRef]

34. Ancuţa, D.L.; Alexandru, D.M.; Muselin, F.; Cristina, R.T.; Coman, C. Assessment of the Effect on Periodontitis of Antibiotic Therapy and Bacterial Lysate Treatment. *Int. J. Mol. Sci.* **2024**, *25*, 5432. [CrossRef] [PubMed]

35. Bleich, A.; Mähler, M.; Most, C.; Leiter, E.H.; Liebler-Tenorio, E.; Elson, C.O.; Hedrich, H.J.; Schlegelberger, B.; Sundberg, J.P. Refined histopathologic scoring system improves power to detect colitis QTL in mice. *Mamm. Genome Off. J. Int. Mamm. Genome Soc.* **2004**, *15*, 865–871. [CrossRef] [PubMed]

36. Liu, X.; Deng, S.; Li, X.; Liu, H.; Li, Z.; Wu, Y.; Luo, P.; Zhong, X.; Huang, R.; Liu, R.; et al. A Standardized Rat Model to Study Peri-implantitis of Transmucosal Osseointegrated Implants. *Biomater. Res.* **2024**, *28*, 0021. [CrossRef] [PubMed]

37. Kanekawa, M.; Shimizu, N. Age-related changes on bone regeneration in midpalatal suture during maxillary expansion in the rat. *Am. J. Orthod. Dentofac. Orthop.* **1998**, *114*, 646–653. [CrossRef]

38. Novack, D.V. Estrogen and bone: Osteoclasts take center stage. *Cell Metab.* **2007**, *6*, 254–256. [CrossRef]

39. Wang, Y.; Cao, X.; Shen, Y.; Zhong, Q.; Huang, Y.; Zhang, Y.; Wang, S.; Xu, C. Initial Development of an Immediate Implantation Model in Rats and Assessing the Prognostic Impact of Periodontitis on Immediate Implantation. *Bioengineering* **2023**, *10*, 896. [CrossRef]

40. Roca-Millan, E.; González-Navarro, B.; Domínguez-Mínger, J.; Marí-Roig, A.; Jané-Salas, E.; López-López, J. Implant insertion torque and marginal bone loss: A systematic review and meta-analysis. *Int. J. Oral Implantol.* **2020**, *13*, 345–353.

41. Schwarz, F.; Derks, J.; Monje, A.; Wang, H.L. Peri-implantitis. *J. Clin. Periodontol.* **2018**, *45* (Suppl. S20), S246–S266. [CrossRef] [PubMed]

42. De Waal, Y.C.M.; Vangsted, T.E.; Van Winkelhoff, A.J. Systemic antibiotic therapy as an adjunct to non-surgical peri-implantitis treatment: A single-blind RCT. *J. Clin. Periodontol.* **2021**, *48*, 996–1006. [CrossRef] [PubMed]

43. Sahrmann, P.; Gilli, F.; Wiedemeier, D.B.; Attin, T.; Schmidlin, P.R.; Karygianni, L. The Microbiome of Peri-Implantitis: A Systematic Review and Meta-Analysis. *Microorganisms* **2020**, *8*, 661. [CrossRef]

44. Renvert, S.; Roos-Jansåker, A.M.; Claffey, N. Non-surgical treatment of peri-implant mucositis and peri-implantitis: A literature review. *J. Clin. Periodontol.* **2008**, *35* (Suppl. S8), 305–315. [CrossRef]

45. Liu, G.; Sun, H.; Shi, B.; Xia, H.; Wu, T. Rat Peri-implantitis Models: A Systematic Review and Meta-analysis. *Int. J. Oral Maxillofac. Implant.* **2024**, *39*, 65–78. [CrossRef] [PubMed]

46. Qu, Q.; Yang, F.; Zhao, C.; Liu, X.; Yang, P.; Li, Z.; Han, L.; Shi, X. Effects of fermented ginseng on the gut microbiota and immunity of rats with antibiotic-associated diarrhea. *J. Ethnopharmacol.* **2021**, *267*, 113594. [CrossRef] [PubMed]

47. Janeczek, K.; Kaczyńska, A.; Emeryk, A.; Cingi, C. Perspectives for the Use of Bacterial Lysates for the Treatment of Allergic Rhinitis: A Systematic Review. *J. Asthma Allergy* **2022**, *15*, 839–850. [CrossRef]

48. Mellman, I.; Steinman, R.M. Dendritic cells: Specialized and regulated antigen processing machines. *Cell* **2001**, *106*, 255–258. [CrossRef]

49. Deeb, M.A.; Alsahhaf, A.; Mubaraki, S.A.; Alhamoudi, N.; Al-Aali, K.A.; Abduljabbar, T. Clinical and microbiological outcomes of photodynamic and systemic antimicrobial therapy in smokers with peri-implant inflammation. *Photodiagnosis Photodyn. Ther.* **2020**, *29*, 101587. [CrossRef]

50. Manor, Y.; Alkasem, A.; Mardinger, O.; Chaushu, G.; Greenstein, R.B. Levels of bacterial contamination in fresh extraction sites after a saline rinse. *Int. J. Oral Maxillofac. Implant.* **2015**, *30*, 1362–1368. [CrossRef]

51. Corrêa, M.G.; Pimentel, S.P.; Ribeiro, F.V.; Cirano, F.R.; Casati, M.Z. Host response and peri-implantitis. *Braz. Oral Res.* **2019**, *33* (Suppl. S1), e066. [CrossRef] [PubMed]

52. Fernandes, M.H.; Gomes, P.S. Bone Cells Dynamics during Peri-Implantitis: A Theoretical Analysis. *J. Oral Maxillofac. Res.* **2016**, *7*, e6. [CrossRef] [PubMed]

53. Gleiznys, D.; Gleiznys, A.; Abraškevičiūtė, L.; Vitkauskienė, A.; Šaferis, V.; Sakalauskienė, J. Interleukin-10 and Interleukin-1β Cytokines Expression in Leukocytes of Patients with Chronic Peri-Mucositis. *Med. Sci. Monit.* **2019**, *25*, 7471–7479. [CrossRef]

54. Alassy, H.; Parachuru, P.; Wolff, L. Peri-Implantitis Diagnosis and Prognosis Using Biomarkers in Peri-Implant Crevicular Fluid: A Narrative Review. *Diagnostics* **2019**, *9*, 214. [CrossRef] [PubMed]

55. Aleksandrowicz, P.; Brzezińska-Błaszczyk, E.; Kozłowska, E.; Żelechowska, P.; Borgonovo, A.E.; Agier, J. Analysis of IL-1β, CXCL8, and TNF-α levels in the crevicular fluid of patients with periodontitis or healthy implants. *BMC Oral Health* **2021**, *21*, 120. [CrossRef]

56. Ata-Ali, J.; Flichy-Fernández, A.J.; Alegre-Domingo, T.; Ata-Ali, F.; Palacio, J.; Peñarrocha-Diago, M. Clinical, microbiological, and immunological aspects of healthy versus peri-implantitis tissue in full arch reconstruction patients: A prospective cross-sectional study. *BMC Oral Health* **2015**, *15*, 43. [CrossRef] [PubMed]

57. Chmielewski, M.; Pilloni, A. Current Molecular, Cellular and Genetic Aspects of Peri-Implantitis Disease: A Narrative Review. *Dent. J.* **2023**, *11*, 134. [CrossRef] [PubMed]

58. Irwin, C.R.; Myrillas, T.T. The role of IL-6 in the pathogenesis of periodontal disease. *Oral Dis.* **1998**, *4*, 43–47. [CrossRef] [PubMed]

59. Gomes, A.M.; Douglas-de-Oliveira, D.W.; Ferreira, S.D.; Silva, T.A.D.; Cota, L.O.M.; Costa, F.O. Periodontal disease, peri-implant disease and levels of salivary biomarkers IL-1β, IL-10, RANK, OPG, MMP-2, TGF-β and TNF-α: Follow-up over 5 years. *J. Appl. Oral Sci.* **2019**, *27*, e20180316. [CrossRef]
60. Scribante, A.; Gallo, S.; Pascadopoli, M.; Frani, M.; Butera, A. Ozonized gels vs chlorhexidine in non-surgical periodontal treatment: A randomized clinical trial. *Oral Dis.* **2023**, *00*, 1–8. [CrossRef]
61. Li, Y.; Ling, J.; Jiang, Q. Inflammasomes in Alveolar Bone Loss. *Front. Immunol.* **2021**, *12*, 691013. [CrossRef]
62. Belkaid, Y.; Hand, T.W. Role of the microbiota in immunity and inflammation. *Cell* **2014**, *157*, 121–141. [CrossRef] [PubMed]
63. Sengupta, P. The Laboratory Rat: Relating Its Age With Human's. *Int. J. Prev. Med.* **2019**, *4*, 624–630.
64. Ievtushenko, M.; Kosheva, E.; Kryzhna, S. Histological Study of the Effect of Bacterial Lysates on the State of Periodontal Tissue in Experimental Periodontitis in Rats. *Sci. Med. Sci.* **2021**, *5*, 41–47.
65. Ievtushenko, M.; Kosheva, E.; Kryzhna, S. Study of influence of bacterial lysate on cytokine indicators in experimental periodontitis in rats. *EUREKA Health Sci.* **2021**, *4*, 73–80. [CrossRef]
66. van Dun, S.C.J.; Verheul, M.; Pijls, B.G.C.W.; van Prehn, J.; Scheper, H.; Galli, F.; Nibbering, P.H.; de Boer, M.G.J. Influence of surface characteristics of implant materials on MRSA biofilm formation and effects of antimicrobial treatment. *Front. Microbiol.* **2023**, *14*, 1145210. [CrossRef]

Article

Development of Innovative Biocomposites with Collagen, Keratin and Hydroxyapatite for Bone Tissue Engineering

Florin Popescu [1], Irina Titorencu [2], Madalina Albu Kaya [3,*], Florin Miculescu [4], Raluca Tutuianu [2], Alina Elena Coman [3,*], Elena Danila [3], Minodora Maria Marin [5], Diana-Larisa Ancuta [6], Cristin Coman [6] and Adrian Barbilian [1]

[1] Department of Orthopedics and Traumatology, Faculty of Medicine, University of Medicine and Pharmacy "Carol Davila", 8 Eroii Sanitari Bvd., 050474 Bucharest, Romania; popescu_florin_md@yahoo.com (F.P.); adrian.barbilian@yahoo.com (A.B.)

[2] Institute of Cellular Biology and Pathology ''Nicolae Simionescu", 8 B. P. Hasdeu Street, District 5, 050568 Bucharest, Romania; irina.titorencu@gmail.com (I.T.); ralu.tutuianu@gmail.com (R.T.)

[3] INCDTP—Division Leather and Footwear Research Institute, 93 Ion Minulescu Str., 031215 Bucharest, Romania; elena.danila23@yahoo.com

[4] Department of Metallic Materials Science, Physical Metallurgy, National University of Science and Technology Politehnica Bucharest, 313 Independenței Spl., 060042 Bucharest, Romania; f_miculescu@yahoo.com

[5] Advanced Polymer Materials Group, National University of Science and Technology Politehnica Bucharest, 1-7 Polizu Street, 011061 Bucharest, Romania; minodora.marin@ymail.com

[6] "Cantacuzino" National Medical-Military Institute for Research and Development, 103 Independenței Spl., 050096 Bucharest, Romania; diana.larisa.ancuta@gmail.com (D.-L.A.); comancristin@yahoo.com (C.C.)

* Correspondence: albu_mada@yahoo.com (M.A.K.); coman.alina27@yahoo.com (A.E.C.); Tel.: +40-723-395-108 (M.A.K.); +40-742-535-359 (A.E.C.)

Abstract: This study follows the process for the development of an innovative biomimetic composite derived from bovine collagen with keratin, with hydroxyapatite being hybridized into its architecture, and it builds a comprehensive evaluation of the composite's characteristics. The novel biomimetic materials are tailored with special traits to be achieved for the repair of osteochondral defects (OCDs). The purpose of the present research is to create a reliable effective alternative to existing bone graft materials while leveraging the intrinsic properties of the components for enhanced osteoinduction and integration. The composites were characterized based on their morphological properties, including water absorption, through scanning electron microscopy (SEM), and their structural properties were characterized by Fourier-Transform Infrared Spectroscopy (FTIR). Biological performance was assessed in vitro using human bone marrow mesenchymal stem cells (BMSCs), focusing on cytotoxicity, cell viability, and the ability to support cell colonization with forthcoming results. This in vivo study illustrates the real potential that this class of novel composites exhibits in regard to bone and cartilage tissue engineering and encourages further exploration and development for future clinical applications.

Keywords: biomimetic composites; keratin; collagen; hydroxyapatite; biocompatibility; mesenchymal stem cells; regenerative medicine; scaffold biodegradation

1. Introduction

Millions of people worldwide suffer from bone disease each year as a result of trauma, tumors, fractures, or malformations that put a tremendous amount of pressure on all medical systems [1,2]. Sadly, some patients lose their lives because of inappropriate therapy or unsuitable or improper bone substitutes.

Osteochondral defects (OCDs) or lesions (OCLs) are localized injuries of the articular cartilage that also affect the nearby subchondral cancellous bone and subchondral bone plate. Even though OCDs can occur in any joint in the human body, osteochondral abnormalities are most frequently observed in the knee. Chondral refers to cartilage, and osteo

indicates bone [3,4]. A technique to treat OCDs is performing a transplant procedure, bone grafting. Currently, different categories of transplant exist, such as repairing this deficiency with tiny plugs of bone and cartilage from other parts of the knee. The bones can be transplanted from the same patient (autograft) or from other persons (allograft) or a synthetic bone can be used [5]. Thousands of surgical procedures are performed daily to treat OCDs damaged by accidents or diseases. When applying allograft or autograft transplant procedures, the side effects are the possibility of bacterial infection, immunogenic response, and disease transmission from the graft donor for allograft, need of second surgical procedure, limited availability or donor site pain for autografts. In order to eliminate these side effects, synthetic bone materials are used to create scaffolds around which natural bone grows [6].

Biomimetics is a multidisciplinary field that seeks to mimic natural processes and structures to develop innovative materials and technologies. In the realm of tissue engineering, biomimetic materials hold great promise for creating scaffolds that closely resemble the extracellular matrix (ECM), providing an ideal microenvironment for cell growth, tissue regeneration, and integration with host tissues. This study focuses on the development and characterization of a novel biomimetic composite material composed of collagen, keratin, and hydroxyapatite, aiming to harness the structural and biochemical cues of bone and cartilage tissues for enhanced tissue regeneration. Presently, an extensive selection of biomaterials is employed for developing scaffolds for bone grafting. This paper is specifically focused on evaluating the potential of keratin and collagen of animal origin to be used as base ingredients for scaffold manufacturing. Several studies regarding biomaterials have been developed for bone grafting and cartilage tissue engineering, with a wide range of proteins, including collagen, albumin, gelatin, fibroin, and keratin, being explored for the development of naturally derived biomaterials to treat OCDs.

Composites based on collagen and hydroxyapatite are maybe the most used bone biomaterials, having the ability to simulate and substitute skeletal bones [7]. For example, a biomimetic scaffold made of hydroxyapatite and collagen has been properly created using human adipose stem cells, and the scaffold's biophysical characteristics and diverse biological functions were examined. In a mouse model of posterolateral lumbar spinal fusion, this biomimetic microchannel scaffold greatly enhanced new bone formation and blood vessel ingrowth in vivo, and it also showed tremendous potential for osteogenic activities in vitro [8]. In another study, hybrid hydrogels composed of poultry collagen with UV–riboflavin crosslinking revealed low osteo-conductivity, biocompatibility, and biodegradability.

Compared with collagen, collagen–nano-keratin, or collagen–apatite–nano-keratin formulations, the collagen–apatite group exhibited improved functional stability, highlighting potential for development as an osteo-promoting membrane [9]. Because collagen is the primary structural protein present in the extracellular matrix of connective tissues, has exceptional properties, and is biocompatible, it is intensively used in bone reconstruction. In a successful in vivo investigation, the osteo-regenerative potential of collagen/chitosan/hydroxyapatite scaffolds, obtained by two distinct hydroxyapatite manufacturing methods, was examined in defects formed in rats' healthy tibial bone as well as in fragile bone caused by gonadal hormone deficit (ovariectomy) [10].

Keratin is a versatile biopolymer that has been employed for the creation of fibrous composites. It may also be transformed into gels, films, nanoparticles, and microparticles by applying the appropriate technologies of their preparation. Applications in biomedical sciences and regenerative medicine have gained advantages for their resistance against enzymatic degradation and distinct biocompatibility [11]. In the body, keratin affords protection and support. It is composed of a wide variety of proteins, such as enzymes extracted from animal tissues, keratin-associated proteins (KFAPs), and multiple types of keratins. Moreover, isolated keratins can self-assemble into structures that govern the identity and behavior of individual cells. Keratin is extracted from hair, toenails, nails, horns, beaks, claws, and feathers from chickens. Wool is another important source [12]. Keratin-based materials are attractive candidates for revolutionizing the biomaterial market due to

biocompatibility, biodegradability, mechanical durability, and natural abundance [11–13]. Upon research and characterization, an osteo-inductive biocomposite scaffold composed of human hair keratin, jellyfish collagen, and nano-sized spherical hydroxyapatite generated from eggshells was created and has the potential to be implemented in bone tissue engineering [14]. Using a straightforward freeze-drying method, a novel composite scaffold was successfully developed by mixing hydroxypropyl methylcellulose and hydroxyapatite with keratin produced from sheep wool. The produced scaffold's maximal compressive strength was found to be within the range of human trabecular bone, indicating a highly porous and linked network, leading the composite to be an adequate bone substitute [15]. Other authors applied novel approaches to synthesize boron and silicon cryogels with incorporated collagen/hair keratin developed for hard tissue engineering applications [16]. Another study reported an antibacterial wound dressing based on keratin (K)–sodium alginate (A) loaded with green synthesized zinc oxide nanoparticles (ZnO NPs) to be used for skin regeneration [17]. Bone scaffolds based on polymers have many disadvantages such as a low degradation rate, low hydrophilicity, low fragility, and low cell compatibility. Due to the disulfide, hydrogen, and ionic bonds in keratin, biomaterials based on polymers and keratin can have improved tensile strength and elastic moduli. Moreover, research has also demonstrated the antibacterial activity, cell adhesion, and hydrophilicity of keratin as a biomaterial for biomedical applications [18].

Wu et al. showed that keratin had an important role as a crosslinking agent for collagen fiber films inducing highly improved mechanical properties and enhanced thermal stability (a 31.95% increase in elongation at break was achieved for the films prepared by crosslinking collagen fiber with 50% keratin) [19]. Recently a construct for osteogenic induction in bone tissue engineering was built based on keratin, polyhydroxy butyrate, and alumina nanowire with successful results [20]. The keratin–montmorillonite nanocomposite hydrogels enhanced osteogenic differentiation and dramatically stimulated bone regeneration in vivo, being a promising candidate in bone tissue engineering [21].

Biomaterials used for bone grafting are continuously and rapidly developing. In this paper, we propose an innovative biomaterial with bovine collagen, keratin, and hydroxyapatite for bone restoration, combining the properties of each component. As far as we know, these materials have not been used together until now. The composites developed were characterized by water absorption, enzymatic degradation, scanning electron microscopy, biocompatibility with cells, and animal tests. The results proved that the developed biomaterials can be successfully used for bone grafting.

2. Materials and Methods
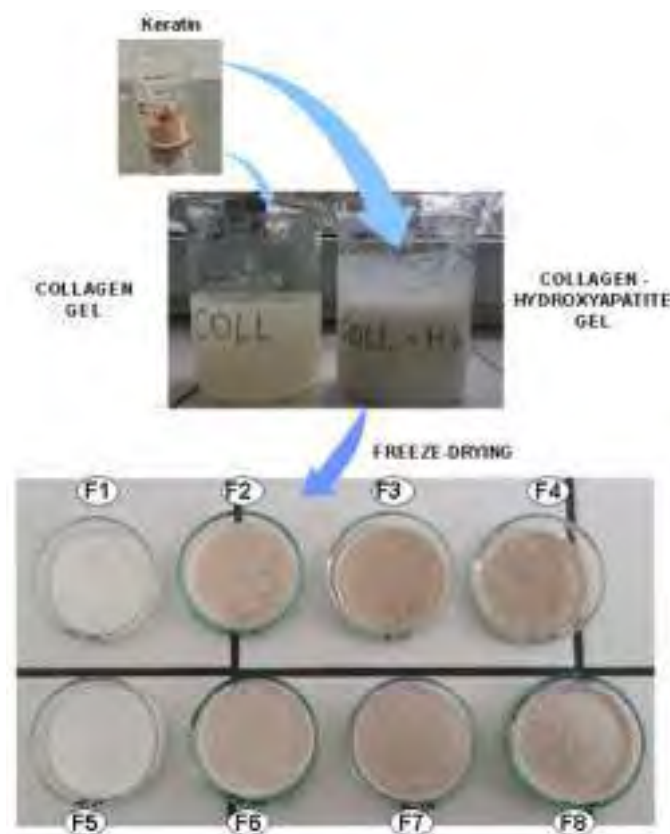
2.1. Preparation of Biocomposites

Type I collagen as fibrillar gel with an initial concentration of 2.39% and acidic pH was obtained from calf skin according to our technology as we previously described [22]. Briefly, collagen derma was treated with organic acid and then the fat was removed; it was washed and treated with alkali to remove the non-collagenous protein and washed and solubilized in acid again. After all the derma was treated, precipitation followed. Composite gels based on collagen gel, keratin from Merck (Darmstadt, Germany), and bovine derived-hydroxyapatite [23] were prepared according to the composition given in Table 1. Hydroxyapatite was obtained by thermally processing deproteinized bovine bone pieces at 1000 °C, followed by milling at ceramic particles sizes of 100–200 μm. Different concentrations (0.5, 1.0 and 1.5%) of keratin were added to samples F2–F4 and F6–F8, and the samples F5–F8 consisted of the same ratio of collagen/hydroxyapatite = 1:1. All the composite gels consisted of a final concentration of collagen of 1%, and they were crosslinked with 0.5% glutaraldehyde from Merck (Hohenbrunn, Germany).

Table 1. Composition of biocomposites.

Biocomposite Codes	Collagen *, %	Keratin *, %	Hydroxyapatite, %
F1	1	0	0
F2	1	0.5	0
F3	1	1.0	0
F4	1	1.5	0
F5	1	0	1
F6	1	0.5	1
F7	1	1.0	1
F8	1	1.5	1

* reported as gel amount.

The composite gels were poured in a glass Petri dish and freeze-dried for 48 h using the Martin Christ 24 Delta LSC freeze-dryer (Martin Christ Gefriertrocknungsanlagen GmbH, Osterode am Harz, Germany) [24] to obtain spongious forms (Figure 1). The gels already poured in Petri dishes were pre-frozen at −40 °C for about 8 h and then the main freeze-drying started at −40 °C and 0.01 bar, reaching 10 °C in 20 h, 20 °C in 8 h, 30 °C in another 8 h, and final freeze-drying for 4 h at 0.001 bar at 30 °C. After 48 h we, obtained the sponge-like samples.

Figure 1. Schematic preparation of collagen biocomposites in form of sponges.

The biocomposite sponges were then gamma irradiated with 25 kgy to be sterile for in vivo tests. The gamma irradiation was done by subcontractor (IRASM Department of IFIN-HH Romania) using a Co-60 gamma irradiator (Institute of isotopes—Budapest, Hungary), an industrial, versatile, panoramic irradiator.

2.2. Water Uptake of Biocomposites

The water uptake capacity of the biocomposite sponges was determined by the weight method [25], by weighing the sponges before and after immersion in water. A piece of

sponge of about 1 cm^3 was weighed at a reference time and then it was placed in 3 mL of water at room temperature (about 23 °C). At predetermined periods of time (1, 2, 4 h and 1, 2, 3, 4 and 7 days), the sponges were weighed and the capacity to retain water was calculated using the following equation (Equation (1)):

$$\text{Water uptake (\%)} = [(W_t - W_d)/W_d] \times 100 \qquad (1)$$

where Wt represents the weight of water retained by sponges at time t and Wd is the weight of dry sponges. Data were presented as mean ± SD of three independent experiments.

2.3. Fourier-Transform Infrared Spectroscopy (FTIR)

FTIR measurements were performed with an attenuated total reflectance (ATR) accessory on a Vertex 70 Bruker FTIR spectrometer (Billerica, MA, USA). The ATR-FTIR mode was used to register the FTIR spectrum for each obtained formulation, with a resolution of 4 cm^{-1} in the 600–4000 cm^{-1} wavenumber range.

2.4. Scanning Electron Microscopy of Biocomposites

The morphology of the biocomposite sponges was observed using the scanning electron microscope Quatro$^{\text{TM}}$ (Thermo Fisher Scientific, Hillsboro, OH, USA).

2.5. Cell Culture of MSCs on Biocomposites

Human mesenchymal stem cells (MSCs) were isolated after informed consent with the approval of the Institutional Ethical Committee (180/27 September 2018), in accordance with the most recent version of the Helsinki declaration of the World Medical Association (Ethical Principles for Medical Research Involving Human Subjects, October 2008).

Patients who were under surgical treatment for osteoarthritis complications were included in this study.

Human bone marrow-derived MSCs were isolated using a modified protocol established and already published by our group [26].

Briefly, BM aspirate (c. 4 mL) was obtained by puncture of the postero-superior spine of the iliac crest.

The cells were collected in cold DMEM containing 4.5 g/L glucose (Sigma Aldrich, St. Louis, MO, USA) supplemented with 40 UI/mL heparin, 300 UI/mL penicillin, 300 µg/mL streptomycin, and 150 µg/mL neomycin (all for Sigma Aldrich, St. Louis, MO, USA), and sedimented by centrifugation at 160 g for 10 min at 4 °C. The nucleated cells were separated on a Histopaque 1077 (Sigma Aldrich, St. Louis, MO, USA). The cells were placed on top of the Histopaque and, after centrifugation at 650 g for 10 min (4 °C), one white band was obtained. The cells from the band were recovered, washed twice with DMEM supplemented with 15% fetal bovine serum (Gibco BRL, Gaithersburg, MD, USA), seeded at a density of 10^5/cm^2, and grown in DMEM 4.5 g/L glucose supplemented with 15% fetal bovine serum (FBS), 1% non-essential amino acids, 300 UI/mL penicillin, 300 mg/mL streptomycin, and 150 mg/ mL neomycin, at 37 °C and 5% CO$_2$. The culture medium was changed after 24 h and then twice a week. All the manipulations were performed according to good manufacturing practice (GMP) criteria and good laboratory practice (GLP). The cells were characterized following the indications of the International Society for Cellular Transplantation.

The cells were characterized as previously described [25]. The cells were plated at 10^4 cell/cm^2 and grown in DMEM 1 g/L glucose supplemented with 1% non-essential amino acids (Sigma Aldrich, St. Louis, MO, USA), 10% fetal bovine serum (FBS), and 1% penicillin, streptomycin, and neomycin, at 37 °C and 5% CO$_2$.

2.6. Viability Assessment

The effect of the Ker:COL:HA scaffolds on the viability of human bone marrow mesenchymal stem cells (BMSCs) was evaluated using the XTT assay. Prior to cell seeding, the scaffolds were sterilized with 70% ethanol overnight at RT and then washed with sterile

water. The sterilized samples were placed in DMEM supplemented with 10% FBS and placed in the incubator at 37 °C in 5% CO_2. Cells at a density of 150,000/cm^2 were cultured on the scaffolds placed in a 96-well plate (37 °C, 5% CO_2) for 7 days. Cell proliferation was evaluated using the XTT assay viability/proliferation kit (Thermo Scientific, Waltham, MA, USA), according to the manufacturer's instructions, and the results were reported as a percentage of the positive control (collagen matrices—F1). Data were presented as the mean ± SD of two independent experiments. Two-group analysis was carried out by Student t test. Probability values (*p*) < 0.05 were considered significant (*, $p < 0.05$, **, $p < 0.01$, ***, $p < 0.001$, ns, not significant).

2.7. Assessment of Biocomposite Capacity to Support Colonization of MSCs

Following the viability tests, the samples that supported MSC growth were selected: F1, F5, and F6. MSCs were seeded at a density of 150,000/cm^2 on top of the scaffolds placed in a 48-well plate. After 4 h, the samples were transferred to new wells to further cultivate only the BMSCs that adhered to the matrix. The medium was changed every two days, and on day seven post-seeding, the scaffolds were fixed in 4% PFA (paraformaldehyde) (Sigma Aldrich, St. Louis, MO, USA), overnight, at 4 °C, followed by inclusion in Shandon Cryomatrix and cryosectioning.

To assess the cell colonization capacity of the scaffolds, we performed an eosin-Hoechst staining as previously described [27]: the sections were washed in PBS, followed by 2 min in eosin and differentiation in 70% ethanol, distilled water for 3 min, and Hoechst solution (1 mg/mL) for 10 min. After a final wash and mounting with glycerol, the samples were visualized using a Zeiss Observer D1 fluorescence microscope.

2.8. Immunofluorescence (IF) Staining

The cryosections were rinsed for 15 min with PBS, blocked in 10% BSA for 15 min, and then incubated for 1 h with primary antibodies directed against vimentin (1:150; mouse monoclonal anti-vimentin (Sigma Alrich, St. Louis, MO, USA)) and fibronectin (1:500, rabbit polyclonal antibody (Thermo Fisher Scientific, Waltham, MA, USA)). In the next step, the cells were incubated for 1 h with secondary antibodies: 1:1000 Alexa-Fluo 568 goat antimouse IgG (Thermo Fisher Scientific, Waltham, MA, USA) and 1:1000 Alexa-Fluo 488 goat antimouse IgG (Thermo Fisher Scientific, Waltham, MA, USA). After three washing steps, the cryosections were mounted with Fluoroshield with DAPI (Sigma Alrich, St. Louis, MO, USA) and visualized using a Zeiss Observer D1 fluorescence microscope. Digital fluorescence images were captured after the optimal exposure time was determined based on control samples to exclude background staining.

2.9. Animal Studies

The animal study protocol was approved by the Ethics Committee of "Cantacuzino" National Medical-Military Institute for Research and Development Bucharest (CI) and by the competent authority (Directorate of Veterinary Health and Food Protection, Bucharest)—Project authorization no. 15 of 17 May 2023.

The sample size was set at 10/group using a simplified calculation formula [28], and to reduce the number of animals, both hind limbs were used for testing, one for the test material and the congener that served as control. Therefore, for this study, thirty 20-week-old male Wistar strain non-specific pathogen (SPF) rats were used. The rats' weight ranged between the 250 and 300 g intervals at baseline. The animals were supplied by the CI, Băneasa Animal Facility (BAF), and maintained in cages (Tecniplast, Italy) with autoclaved bedding. Cage changes were scheduled to be performed once a week. Rats were distributed in study groups of a maximum of five animals per cage and were exposed to a 12 h/12 h (day/night) light/darkness cycle in a ventilated room with a controlled temperature of 20–24 °C and free access to sources of food and filtered water.

The CI's Preclinical Testing Unit and Experimental Medicine and Translational Research Platform, where the animal experiments were set to take place, had an Environmental

Enrichment Programme. Human targets were determined using a clinical examination based on the ARRIVE criteria, with clinical symptoms graded according to severity. Animal health status was evaluated daily by a veterinarian specialist. Animals had a period of acclimatization to the new environment prior to beginning the experiments. In the cage, rats were individually identified by colored permanent marker according to the CI identification procedure.

Surgical Procedure: the surgical intervention that was designed involved preoperative preparation, anesthesia, local infiltrations, incisions, the creation of a cavity in the femur, insertion of the test device, suture, and postoperative care including antibiotics and analgesics.

Prior to surgery, the rats underwent a fasting period to diminish anesthesia risks. The surgical area, at the rats' lower limbs, was shaved and disinfected with a topical solution of Iodine 3%.

For the anesthesia, a combination of Ketamine (Vetased, Farmavet, Romania, 75 mg/kg) and Medetomidine (Dorbene Vet, Altius, Romania, 0.5 mg/kg) was used, thus obtaining the surgical comfort needed and a painless, less stressful procedure for the animals. Anesthesia depth was regularly assessed by reflex testing, and the eyes were covered with an ophthalmic ointment.

An osteochondral bone defect in the shape of a tunnel for the insertion of biomaterials was created through a surgical approach that exposes the trochlear groove, following the study protocol described by Ancuta et al. [29]. Under saline solution cooling in order to minimize thermal damage to the tissue, a drilling machine with 1 mm and 2 mm drill bits was used to allow a gradual enlargement to a desired 2 mm wide tunnel.

The development of the femoral defects involved both limbs. According to the experimental design, the left limb received the test material treatment corresponding to the group it belonged to, while the right limb with the defect remaining untreated was considered the control.

The biomaterial application involved creating a cavity in the femur through a surgical approach that exposed the trochlear groove. The cavity, designed to mimic osteochondral defects, was gradually enlarged using a drilling machine with 1 mm and 2 mm drill bits to achieve a 2 mm wide tunnel. The biomaterial was then inserted into this cavity. The exact size of the biomaterial pieces used in the study was standardized to fit the created defects, ensuring consistency across experiments. The pieces were carefully inserted into the bone defects created in the femurs of the rats. The biomaterials were applied in a hydrated state. Prior to implantation, the materials were sterilized and hydrated with saline solution to mimic physiological conditions and ensure optimal interaction with the surrounding tissue.

At the end of the surgical interventions, the animals were placed in clean cages in the experimental space, protected from noise, and received a substance (Atipamezol 0.25 mg/kg—Alzane, Altius, Romania) to quickly reverse the effect of the anesthetic. Also, postoperatively, all measures were taken to reduce the animals' pain and prevent infections, administering antibiotics (Enrofloxacin 5 mg/kg, Farmavet, Romania) and anti-inflammatory medication (Ketoprofen 5 mg/kg, Dopharma Vet, Giroda, Timis) for five days.

3. Results and Discussion

3.1. Morphology and Structure of Biocomposites

The sponges based on collagen with/without hydroxyapatite and keratin were morphologically characterized by water uptake and SEM, while the structural changes were estimated by FT-IR.

The water uptake was estimated for one week at different intervals of time and showed that all the samples were stable as Figure 2 shows.
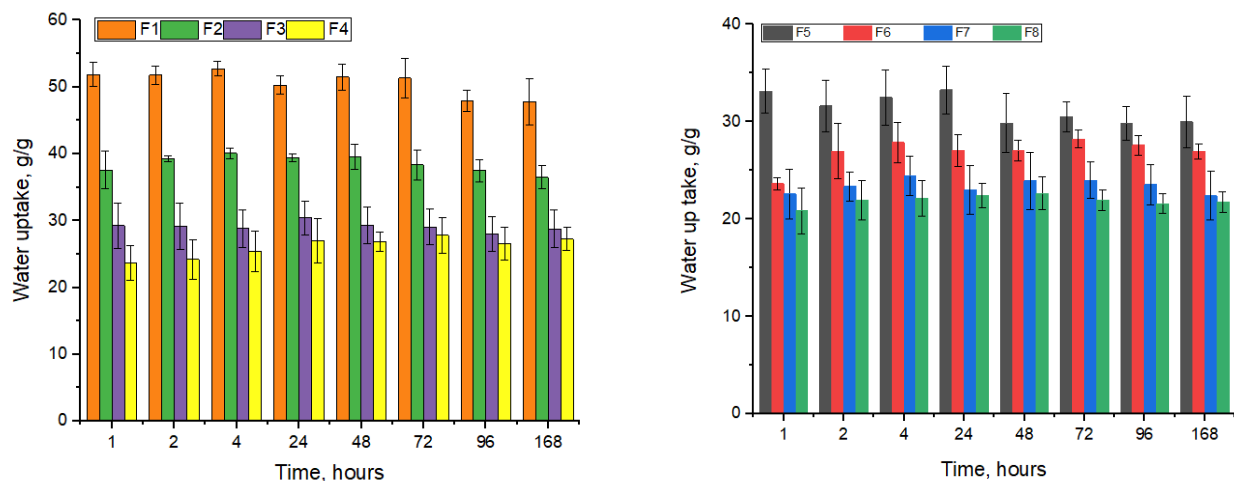
Figure 2. Water uptake of biocomposites.

The samples containing only collagen absorbed about 51 g/g water, and the one with keratin, being denser, absorbed a smaller amount of water. The higher concentration of keratin resulted in a smaller amount of water uptake, as follows: F2, which contains 0.5% keratin, up-took about 38 g/g; F3, which contains 1% keratin, up-took about 29 g/g; and F4, which had the highest amount of keratin (1.5%), absorbed about 23 g/g water. The same trend can be noticed in the samples (F5 ÷ F8) which contain hydroxyapatite (HA), but the values are smaller, with the structure of the samples being denser because of the HA content. Comparing the samples with and without HA, it can be observed that F5 (with HA content) absorbed about 35% water compared with F1 (only crosslinked collagen), which up took about 51 g/g in the first 24 h. Such decreases are visible in all the samples with HA, F6, F7, and F8, which absorbed about 24, 23, and 21 g/g water.

These results are confirmed by the SEM images presented in Figure 3.

All samples presented a spongious structure with pore sizes between 50 and 200 μm, which is ideal for bone scaffolds [30]. The structure of the samples became denser when keratin was added for all the samples, and the HA was attached on collagen fibers in samples F5 ÷ F8. The results are in correlation with those for water absorption and show that the control sample with only collagen (F1) has bigger pores, and their sizes decrease with the amount of keratin, and the smallest ones are for samples which also contain HA (Figure 3e–h). The HA is visible on collagen fibers for all the samples with HA, as you can see, for example, in Figure 3i for sample F8 at ×200 magnification, as well as in Figure 3j.
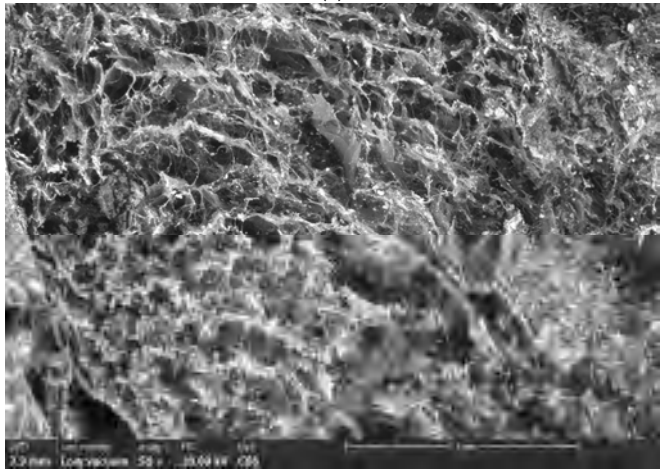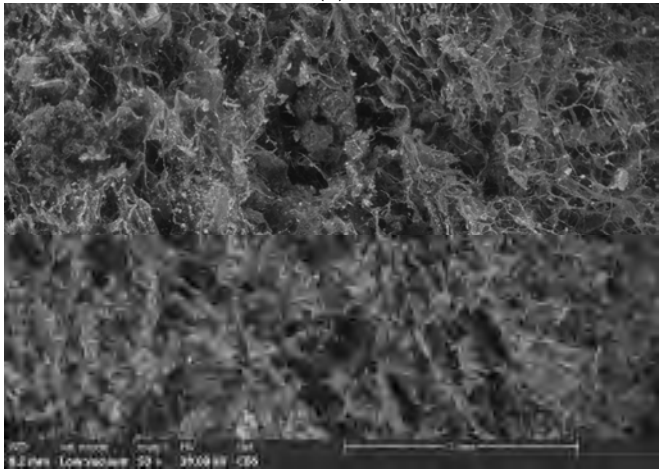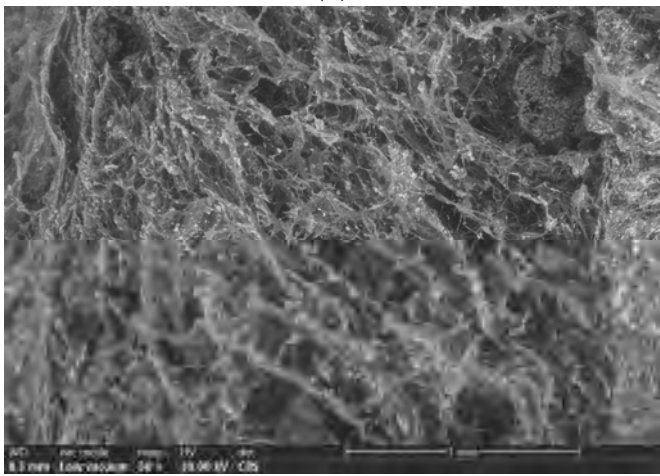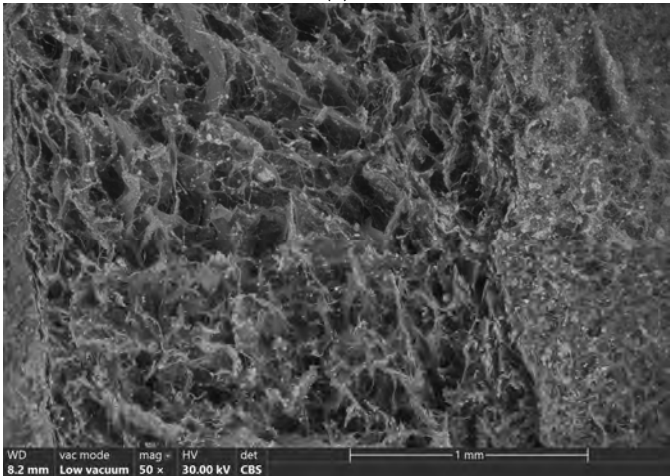

(**a**)

(**b**)

Figure 3. *Cont.*

(**c**)

(**d**)

(**e**)

(**f**)

(**g**)

(**h**)

Figure 3. *Cont.*

(**i**)

(**j**)
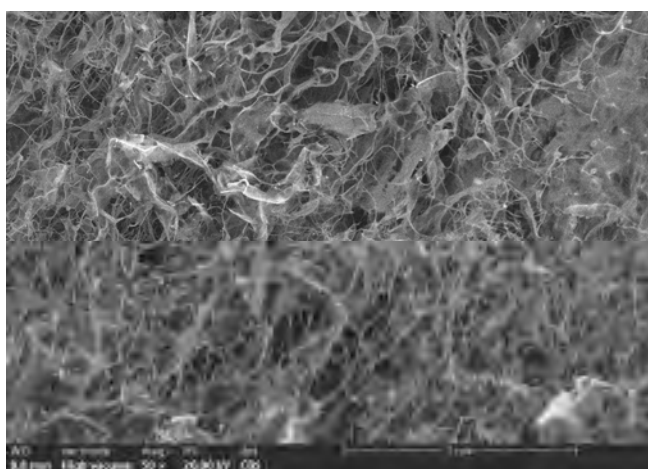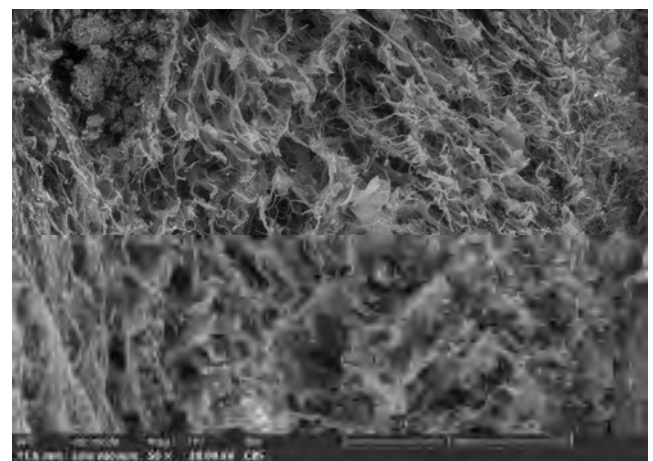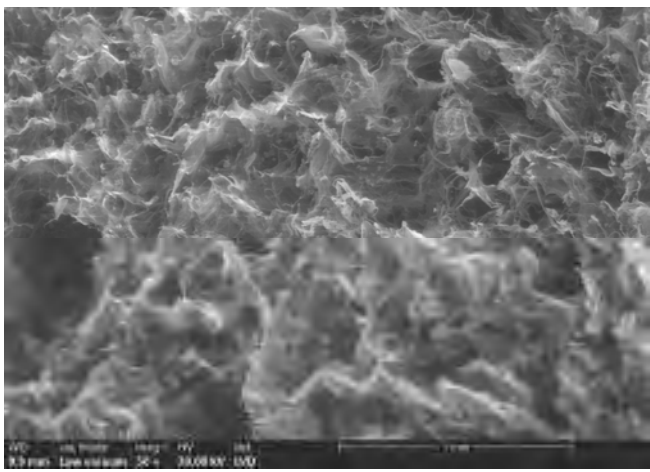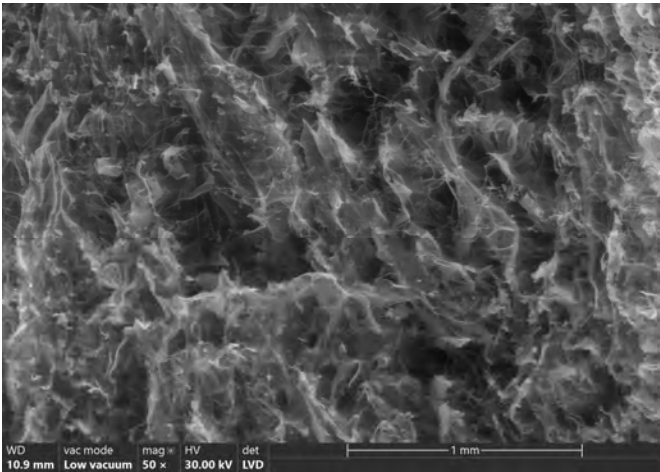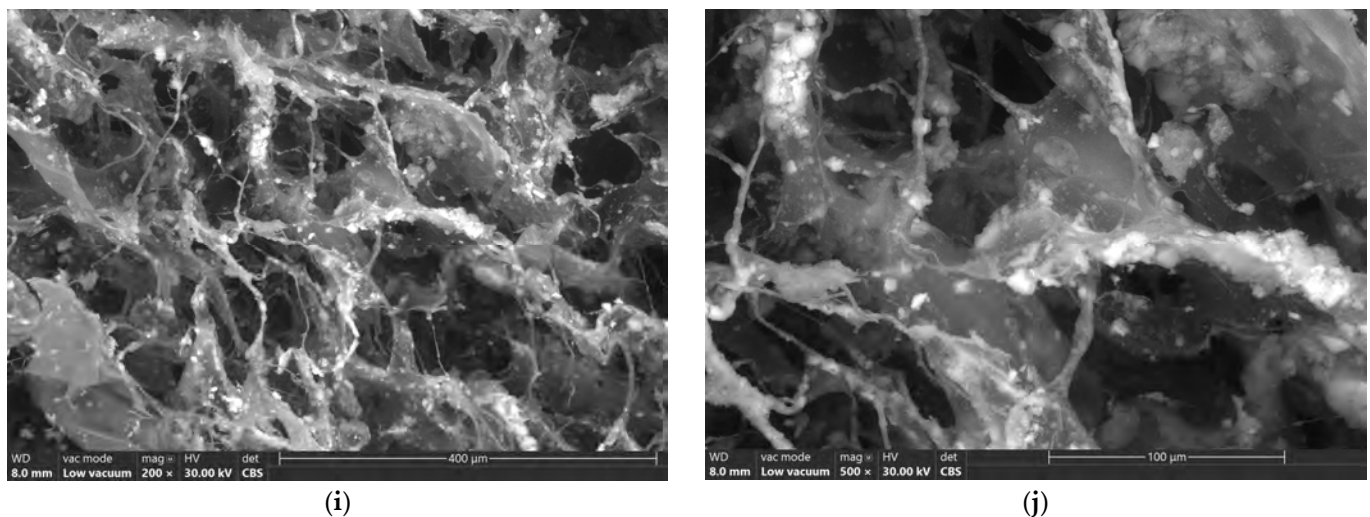
Figure 3. SEM images of biocomposites (×50): (**a**) F1; (**b**) F2; (**c**) F3; (**d**) F4; (**e**) F5; (**f**) F6; (**g**) F7; (**h**) F8; (**i**) F8 (×200); (**j**) F8 (×400).

The samples based on collagen, keratin, and hydroxyapatite were spectrally analyzed by FTIR spectroscopy (Figure 4). The FTIR investigations were performed on the freeze-dried samples.
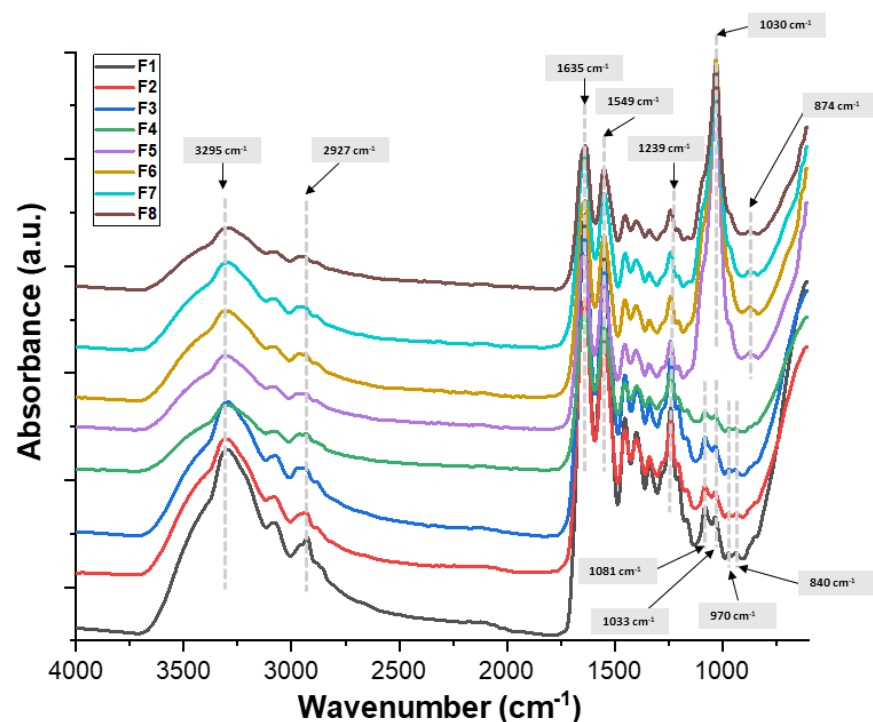
Figure 4. FTIR spectra of biocomposites.

The spectra of composite biomaterials made of collagen, keratin, and hydroxyapatite showed the distinctive infrared bands of each constituent. In the obtained FTIR spectra, the characteristic absorption band for peptide bonds (–CONH–) due to the presence of both proteins, keratin and collagen, can be observed [31]. Also, the amide bands in infrared spectra identify the triple-helix conformation that the collagen macromolecule displays [32]. The amide A and B bands, which are primarily connected to the NH stretching vibrations, OH groups, and CH asymmetric vibration, are responsible for the bands located at around 3295 cm^{-1} and 2927 cm^{-1} [33,34]. The stretching vibrations of the C=O groups

in peptides are responsible for the amide I band at 1635 cm^{-1}. The band at 1549 cm^{-1}, which is attributed to amide II, is caused by CN stretching vibrations. The NH bending vibrations from amide linkages are responsible for the amide III band, which is located at 1239 cm^{-1} [35]. The presence of carbonate at 874 cm^{-1} revealed by the FTIR spectra is attributed to the hydroxyapatite's distinctive absorption bands [35].

3.2. In Vitro Behavior of Biocomposites

The cytotoxicity of the Coll:Ker:HA scaffolds was assessed by means of the XTT test using MSCs. The cells cultured on the collagen matrix had the highest viability, this viability being preserved only in the case of samples F6 and F5. In the cases of F3, F4, and F8, the test indicated an inhibition of cell growth, as seen in Figure 5.
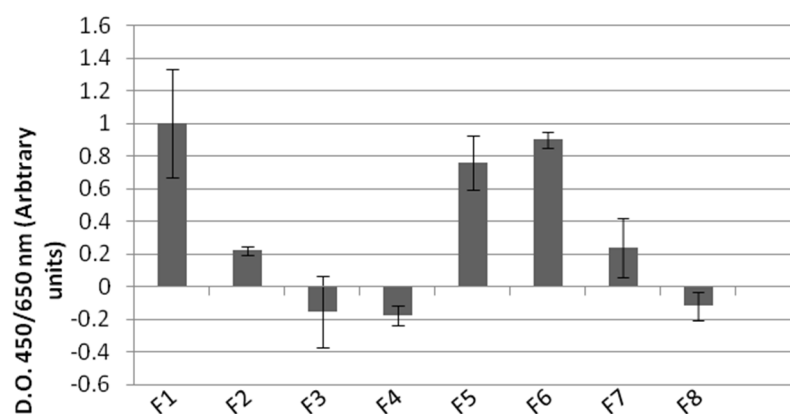

Figure 5. Evaluation of cytotoxic effect of the scaffolds using the XTT assay. The viability of MSCs cultured for 7 days on the specimens was assessed. Data represent mean ± SD of two independent experiments.

The Coll:Ker:HA scaffolds seeded with MSCs were analyzed in respect to the production of the most characteristic ECM components. This analysis was performed after 7 days of cultivation to ensure proper cell adaptation to the 3D environment. Vimentin, a basic mesenchymal cell marker and important participant of cell sprouting and migration [36], was present in MSCs grown on Coll scaffolds and more discreetly distributed in MSCs cultured on F5 and F6—Figure 6. Fibronectin, which acts as a key player for the communication between the intra- and extracellular environment, was observed in MSCs grown on all tested scaffolds [37]—Figure 6.

Regarding the colonization capacity of selected scaffolds, the eosin–Hoechst staining revealed a uniform distribution of MSCs within the F1 sample, while for F5 and F6, the cells mainly grew on the surface and less within the 3D structure—Figure 7. Furthermore, the viability results for these two samples, with F6 supporting a better effect on MSC proliferation, were confirmed by the thickness of the cell layer, which was higher than for F5, as seen in Figure 7.

3.3. In Vivo Behavior of Biocomposites on Animals

The advancement of samples F1, F2, F5, and F6 into further testing is rooted in their distinctive in vitro compositional attributes and their exhibited stability. Sample F1, noted as ctrl, solely comprising collagen, acts as a fundamental control for gauging the impact of the additional components. Sample F2 introduces keratin at a 0.5% concentration without hydroxyapatite, providing insight into keratin's role in the composite matrix. Sample F5 explores the interaction between collagen and hydroxyapatite in a 1:1 ratio, devoid of keratin, aiming to investigate the combined potential of these materials. Sample F6, enriching the biocomposite with both 0.5% keratin and hydroxyapatite, maintains the collagen to hydroxyapatite ratio, thereby exploring the synergistic effects of these components together. These selections highlight the significance of the compositional balance and the ratios of

materials in the development of biocomposites tailored for biomedical use. The progression to animal models aimed to validate the regenerative potential observed during the in vitro testing. As a consequence of the in vitro study, the samples F1, F2, F5, and F6 were found to be the best candidates for the in vivo experimental model.
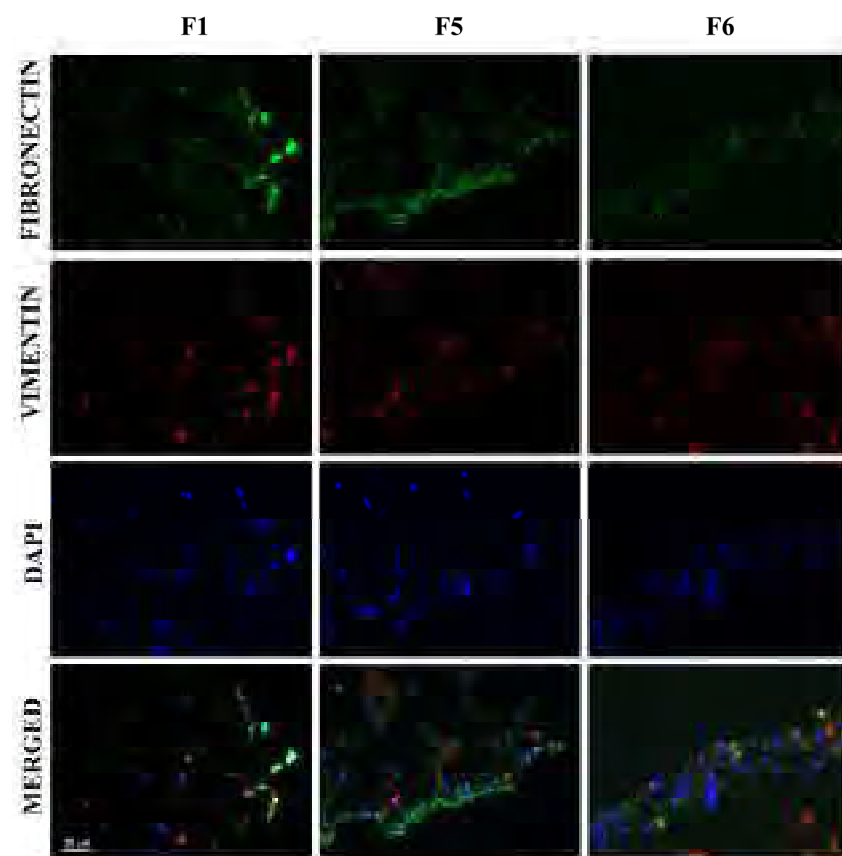

Figure 6. Fibronectin and vimentin expression (mesenchymal markers) by MSCs grown on Coll:Ker:HA scaffolds for 7 days.
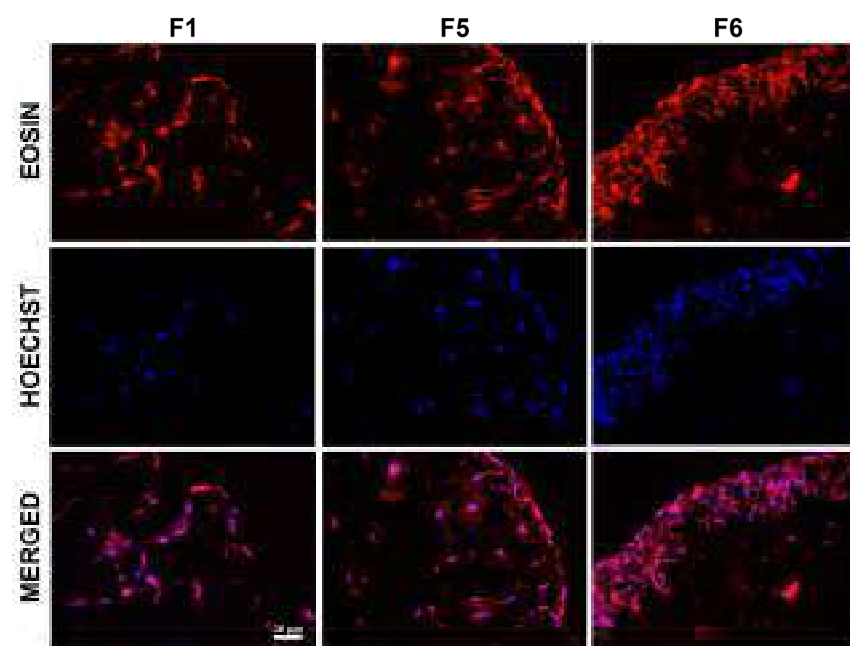

Figure 7. Images of eosin-Hoechst staining for the selected scaffolds seeded with MSCs, 7 days post-cultivation.

Rats underwent the surgical procedure as previously described. Subsequently, from the start of the in vivo experiment, half of the animals were monitored for 30 days and the other half for 60 days. The survey included clinical examinations, weight monitoring, hematologic examinations, and postmortem examinations. Observations of gait, posture, and any signs of distress or discomfort were monitored as early signs of the biomaterials' effect on the experimental organism. The surgical site was observed regularly for signs of infection, dehiscence, or adverse reactions to the materials. From a clinical point of view, the animals responded well, regardless of the substance tested. Thus, upward trends in body weight were observed and no signs of lameness, edema, etc., were observed to indicate any adverse effect of the substances. At the end of the 30 and 60 days, X-ray exams were performed, prior to the animals being humanely euthanized (through an overdose of anesthetic) according to the ethical protocol, as shown in Figure 8.

Figure 8. Postoperative X-ray of test subject with area of analysis highlighted.

Radiological non-invasive imaging techniques to monitor the progression of bone regeneration within and around the biomaterials implanted in the rats were employed. Imaging studies were chosen as non-invasive means to monitor the progression of bone regeneration, resorption, and integration with host tissue. The radiographic analysis aimed to measure and quantify the amount of new bone that formed in the areas where the biomaterials were applied. This quantification was critical for assessing the properties of the materials related to the new bone growth on the inside of the implant and on its surface. Another key aspect of the radiographic analysis was to observe and measure the resorption of the biomaterials over time.

Four parameters related to the pixel intensity distribution in SHG radiological images were monitored and calculated. These parameters were the mean, standard deviation, skewness, and kurtosis (Figure 9). The standard deviation and mean represented frequently used first-order statistical measures, while kurtosis and skewness accounted for the shape of the distribution. The above parameters were assessed in the interest region selected corresponding to the drilled tunnel using the histogram analysis tool comprised in ImageJ. ImageJ is a widely used open-source software with adequate functionalities for performing image processing tasks.
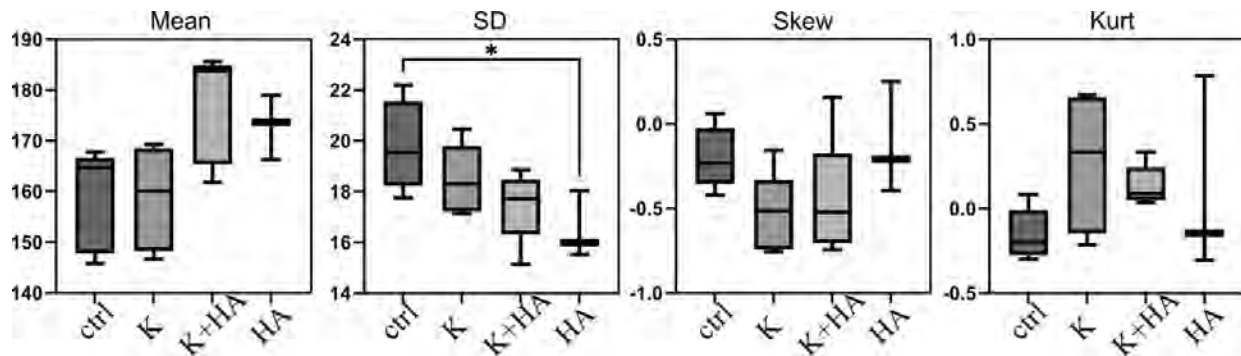
Figure 9. Data for treatment groups were obtained through ImageJ version 1.53 analysis, where the control group (ctrl) is F1, K is F2, HA is F5, and HA + K is F6, as shown in the box plots for Mean, SD, Skew, and Kurt in the provided image. The asterisk (*) specifically in the SD plot signifies a significant difference, highlighting that the variability in the data for the K group (F2) is statistically distinct from the HA group (F5). This finding is important for understanding the consistency and reliability of the results within these groups.

The use of pixel intensity distribution parameters (mean, standard deviation, skewness, and kurtosis) for assessing bone regeneration intensity is well documented. For instance, Kokkinou et al. highlighted the correlation between radiographic texture analysis and biomechanical properties of trabecular bone using these parameters [38]. Similarly, MacKay et al. emphasized the role of higher-order statistics such as skewness and kurtosis in understanding bone texture and regeneration [39].

Data obtained were gathered and processed, cumulated as a single lot. A comparison between different biomaterial groups, treated limb vs. control limb, provided objective data for the research.

The radiological in vivo data obtained suggest that biomaterials may enhance bone density, as indicated by higher mean pixel intensities in the treated groups. This fact is most evident in the case of samples F6 with 0.5% keratin introduced in the Col + HA scaffolds when compared to scaffolds without keratin. A more uniform distribution of pixel intensities, shown in the case of the F6 samples with a decreased standard deviation, hints at a consistent and stable bone structure, likely due to the biomaterials providing a conducive environment for uniform bone growth. Furthermore, the presence of negative skewness and higher positive kurtosis in the treatment groups suggests regions of higher bone density and sharper image features in the group treated with sample F6. These findings imply that the biomaterials not only promote bone growth but also contribute to the formation of precisely defined bone structures, marking effective bone regeneration.

The higher mean pixel intensities for the treatment groups compared to the control group, although not statistically significant, suggest a higher bone density for the F6 group samples.

The standard deviation (SD) of pixel intensities is a measure of the spread or variability within a dataset. Generally, a smaller standard deviation in the pixel intensity distribution might suggest less contrast, indicating a more uniform image. The treatment groups exhibit a decreased standard deviation, indicating a more consistent distribution of pixel values and, consequently, a more uniform bone structure compared to the control group.

Regarding skewness (Skew), all distributions display a negative skew, marked by longer left distribution tails. A decrease in skewness implies a brighter image, indicating regions with higher bone density, as observed in the treatment groups.

All distributions display positive kurtosis (Kurt), nearing zero, with treatment groups showing higher values. This suggests that pixel values are concentrated closer to the mean compared to a normal distribution, with rare extreme deviations contributing minimal variance. The lower standard deviation, linked to higher kurtosis, suggests a tighter spread of pixel values around the mean, indicating sharper features in the image (Figure 9).

Each table below corresponds to a different treatment group and lists parameters including mean, standard deviation (SD), skewness, and kurtosis.

For the exploration of the biomaterial efficacy, image analysis metrics provided critical insights into the tissue responses post-implantation.

The mean pixel intensity within regions of interest (ROIs) quantifies the overall brightness, with higher values typically showing increased bone growth or material deposition. Variability among these pixel intensities, captured by the standard deviation (SD), offers further granularity; a lower SD in treatment groups relative to controls indicates a more uniform response to the biomaterial, potentially signaling consistent bone growth across the treated area.

Furthermore, the skewness and kurtosis of the pixel intensity distribution provide insights into the data's asymmetry and the sharpness of the distribution peaks. Negative skewness values, when reduced in treatment groups, imply a shift toward more symmetrical or even slightly right-skewed distributions, hinting at a denser and more evenly distributed bone or material density. Higher kurtosis values indicate a more pronounced peak in the distribution, pointing to a more localized and intense area of growth or material presence, thus corroborating the effectiveness of the biomaterials under study.

Table 2 represents the collagen base used across all groups, serving as a control for comparison.

Table 2. Control group (ctrl)—collagen sponges (F1).

Parameter	Min Value	1st Quartile	Median	3rd Quartile	Max Value
Mean (30 days)	158	160	161	163	165
SD (30 days)	19	20	21	22	23
Skew (30 days)	−0.3	−0.2	−0.15	−0.1	0.0
Kurt (30 days)	−0.2	−0.1	0.0	0.1	0.2
Mean (60 days)	161	162	163	164	165
SD (60 days)	20	20.5	21	22	23
Skew (60 days)	−0.25	−0.2	−0.15	−0.1	−0.05
Kurt (60 days)	−0.1	0.0	0.05	0.1	0.2

In the control group, utilizing a pure collagen sponge, a slight increase in mean pixel intensity from 161 to 162 was observed over the course from 30 to 60 days, indicating a minor enhancement in bone density or material deposition. The standard deviation remained stable, suggesting consistent variability in bone density across the treated area. Notably, skewness shifted from −0.15 to −0.2, reflecting a trend towards a more symmetrical distribution of pixel intensity, while kurtosis showed a minor increase, suggesting a subtle sharpening of the distribution's peak.

The next table outlines the statistical distribution of image analysis metrics for group K, which features keratin integrated into the collagen sponge.

The keratin-enhanced collagen group demonstrated a significant increase in mean pixel intensity, from a median of 165 to a third quartile of 181, as shown in Table 3, suggesting robust improvements in bone density or material deposition. The standard deviation maintained a steady value around 19, indicating a consistent variability in the treatment response. Additionally, skewness showed substantial improvement, moving towards a less negative value, which demonstrates a more even distribution of bone growth. Moreover, kurtosis increased, indicative of more pronounced and localized peaks of intense growth at the 60-day mark.

Table 4 displays the distribution of image analysis metrics for group K + HA, which combines keratin and hydroxyapatite with the collagen sponge.

For the composite material group of keratin- and hydroxyapatite-enhanced collagen, the mean pixel intensity rose from 172 at 30 days to 176 at 60 days, highlighting an improvement in the effectiveness of the composite material. The standard deviation saw a slight increase, reflecting a mild rise in the variability of material deposition. Improvements in

skewness were noted, moving towards a more balanced material distribution, and kurtosis slightly increased, pointing to more sharply defined peaks in the material's distribution, suggesting concentrated areas of bone growth.

Table 3. Group K—collagen sponges with keratin (F2).

Parameter	Min Value	1st Quartile	Median	3rd Quartile	Max Value
Mean (30 days)	145	149	165	181	190
SD (30 days)	16	18	19	21	22
Skew (30 days)	−0.422	−0.3	−0.231	0.05	0.1
Kurt (30 days)	0.082	0.3	0.4	0.5	0.6
Mean (60 days)	180	182	185	190	194
SD (60 days)	18	19	20	21	22
Skew (60 days)	−0.7	−0.6	−0.55	−0.5	−0.4
Kurt (60 days)	0.4	0.5	0.6	0.7	0.9

Table 4. Group K + HA—collagen sponges with keratin (K) and hydroxyapatite (HA) (F6).

Parameter	Min Value	1st Quartile	Median	3rd Quartile	Max Value
Mean (30 days)	163	167	172	179	186
SD (30 days)	14	15	17	19	21
Skew (30 days)	−0.632	−0.4	−0.1	0.0	0.2
Kurt (30 days)	−0.59	0.3	0.6	0.7	0.9
Mean (60 days)	174	176	178	186	188
SD (60 days)	15	16	17	19	21
Skew (60 days)	−0.6	−0.5	−0.4	−0.3	−0.1
Kurt (60 days)	0.35	0.5	0.65	0.8	1.0

Table 5 summarizes the distribution of image analysis metrics for group HA, which used hydroxyapatite alone.

Table 5. Group HA—hydroxyapatite (F5).

Parameter	Min Value	1st Quartile	Median	3rd Quartile	Max Value
Mean (30 days)	157	167	169	177	188
SD (30 days)	16	17	19	22	24
Skew (30 days)	−0.5	−0.4	−0.3	−0.2	−0.1
Kurt (30 days)	0.1	0.2	0.3	0.4	0.5
Mean (60 days)	177	181	183	187	188
SD (60 days)	12	14	16	18	20
Skew (60 days)	−0.5	−0.4	−0.3	−0.2	−0.1
Kurt (60 days)	0.3	0.4	0.5	0.6	0.7

In the hydroxyapatite-enhanced collagen group, there was a notable increase in mean pixel intensity from 169 to 177 from 30 to 60 days, signaling enhanced material efficacy. The standard deviation decreased, indicating a reduction in variability and a more uniform response across the treatment area. Skewness also improved, becoming less negative, which may reflect a more symmetrical distribution of the material, and a slight increase in kurtosis was observed, suggesting a sharper peak in the distribution and more localized intense growth.

4. Conclusions and Perspectives

The novel biomimetic composites based on collagen, keratin, and hydroxyapatite exhibit desirable morphological and structural properties proved by water absorption, SEM, and FT-IR. The samples have porous structure with pore sizes between 50 and 200 μm, which is ideal for bone scaffolds, and absorbed over 20 g/g water.

Accounting for the biocompatibility and biological performance of the composites, they demonstrated high biocompatibility and promises of good cell viability and proliferation in vitro for samples with maximum 1% keratin. Human bone marrow mesenchymal stem cells (BMSCs) adhered well and thrived on the scaffolds, indicating the material's potential to facilitate cellular activities essential for bone healing and regeneration, akin to ECM characteristics.

The radiological analysis and subsequent image processing outcomes provide insightful data on the osteoconductive capabilities of the biomaterials tested in rat models. Utilizing non-invasive radiological imaging techniques for monitoring bone regeneration highlights the efficacy and interaction of these biomaterials with host tissue, emphasizing their potential in enhancing bone healing processes.

While the current findings show promising results, especially for samples F5 and F6, further studies are needed to scale the biomaterial for clinical trials and to explore the long-term outcomes of its use in larger animal models and eventually in human subject recipients. The potential customization of this type of composite to suit specific patient needs offers a promising avenue for a more personalized approach in orthopedics.

Future research should focus on refining biomaterial compositions to boost osteoconductive properties and resorption, guided by bone density and structure trends. It is essential to pursue longitudinal studies for a deeper understanding of these materials' long-term effectiveness and stability. Additionally, integrating advanced imaging techniques like MRI or CT scans with traditional radiology could yield finer details of bone regeneration and material integration induced by the biomaterials. Biomechanical testing will further illuminate the functional outcomes of regeneration, offering a well-rounded view of material performance.

While the current findings show promising results, further studies are needed to scale the biomaterial for clinical trials and to explore the long-term outcomes of its use in larger animal models and eventually in human subject recipients. The potential customization of this type of composite to suit specific patient needs offers a promising avenue for a more personalized approach in orthopedics.

References

1. World Osteoporosis Day Survey 2023. Available online: https://www.osteoporosis.foundation/wod2023-survey (accessed on 4 March 2024).
2. Wu, A.-M.; Bisignano, C.; James, S.L.; Abady, G.G.; Abedi, A.; Abu-Gharbieh, E.; Alhassan, R.K.; Alipour, V.; Arabloo, J.; Asaad, M.; et al. Global, Regional, and National Burden of Bone Fractures in 204 Countries and Territories, 1990–2019: A Systematic Analysis from the Global Burden of Disease Study 2019. *Lancet Healthy Longev.* **2021**, *2*, e580–e592. [CrossRef]

3. Palmer, W.; Bancroft, L.; Bonar, F.; Choi, J.-A.; Cotten, A.; Griffith, J.F.; Robinson, P.; Pfirrmann, C.W.A. Glossary of Terms for Musculoskeletal Radiology. *Skeletal Radiol.* **2020**, *49*, 1–33. [CrossRef]

4. Gorbachova, T.; Melenevsky, Y.; Cohen, M.; Cerniglia, B.W. Osteochondral Lesions of the Knee: Differentiating the Most Common Entities at MRI. *RadioGraphics* **2018**, *38*, 1478–1495. [CrossRef]

5. Wickramasinghe, M.L.; Dias, G.J.; Premadasa, K.M.G.P. A Novel Classification of Bone Graft Materials. *J. Biomed. Mater. Res.* **2022**, *110*, 1724–1749. [CrossRef]

6. Baldwin, P.; Li, D.J.; Auston, D.A.; Mir, H.S.; Yoon, R.S.; Koval, K.J. Autograft, Allograft, and Bone Graft Substitutes: Clinical Evidence and Indications for Use in the Setting of Orthopaedic Trauma Surgery. *J. Orthop. Trauma* **2019**, *33*, 203–213. [CrossRef]

7. Wahl, D.; Czernuszka, J. Collagen-Hydroxyapatite Composites for Hard Tissue Repair. *Eur. Cells Mater.* **2006**, *11*, 43–56. [CrossRef]

8. Hwangbo, H.; Lee, H.; Roh, E.J.; Kim, W.; Joshi, H.P.; Kwon, S.Y.; Choi, U.Y.; Han, I.-B.; Kim, G.H. Bone Tissue Engineering via Application of a Collagen/Hydroxyapatite 4D-Printed Biomimetic Scaffold for Spinal Fusion. *Appl. Phys. Rev.* **2021**, *8*, 021403. [CrossRef]

9. Souza, F.F.P.D.; Pérez-Guerrero, J.A.; Gomes, M.J.P.; Cavalcante, F.L.; Souza Filho, M.D.S.M.D.; Castro-Silva, I.I. Development and Characterization of Poultry Collagen-Based Hybrid Hydrogels for Bone Regeneration. *Acta Cir. Bras.* **2022**, *37*, e370302. [CrossRef]

10. Chacon, E.L.; Bertolo, M.R.V.; De Guzzi Plepis, A.M.; Da Conceição Amaro Martins, V.; Dos Santos, G.R.; Pinto, C.A.L.; Pelegrine, A.A.; Teixeira, M.L.; Buchaim, D.V.; Nazari, F.M.; et al. Collagen-Chitosan-Hydroxyapatite Composite Scaffolds for Bone Repair in Ovariectomized Rats. *Sci. Rep.* **2023**, *13*, 28. [CrossRef]

11. Chilakamarry, C.R.; Mahmood, S.; Saffe, S.N.B.M.; Arifin, M.A.B.; Gupta, A.; Sikkandar, M.Y.; Begum, S.S.; Narasaiah, B. Extraction and Application of Keratin from Natural Resources: A Review. *3 Biotech.* **2021**, *11*, 220. [CrossRef] [PubMed]

12. Feroz, S.; Muhammad, N.; Ratnayake, J.; Dias, G. Keratin-Based Materials for Biomedical Applications. *Bioact. Mater.* **2020**, *5*, 496–509. [CrossRef]

13. Rouse, J.G.; Van Dyke, M.E. A Review of Keratin-Based Biomaterials for Biomedical Applications. *Materials* **2010**, *3*, 999–1014. [CrossRef]

14. Arslan, Y.E.; Sezgin Arslan, T.; Derkus, B.; Emregul, E.; Emregul, K.C. Fabrication of Human Hair Keratin/Jellyfish Collagen/Eggshell-Derived Hydroxyapatite Osteoinductive Biocomposite Scaffolds for Bone Tissue Engineering: From Waste to Regenerative Medicine Products. *Colloids Surf. B Biointerfaces* **2017**, *154*, 160–170. [CrossRef]

15. Feroz, S.; Dias, G. Hydroxypropylmethyl Cellulose (HPMC) Crosslinked Keratin/Hydroxyapatite (HA) Scaffold Fabrication, Characterization and in Vitro Biocompatibility Assessment as a Bone Graft for Alveolar Bone Regeneration. *Heliyon* **2021**, *7*, e08294. [CrossRef]

16. Cal, F.; Sezgin Arslan, T.; Derkus, B.; Kiran, F.; Cengiz, U.; Arslan, Y.E. Synthesis of Silica-Based Boron-Incorporated Collagen/Human Hair Keratin Hybrid Cryogels with the Potential Bone Formation Capability. *ACS Appl. Bio Mater.* **2021**, *4*, 7266–7279. [CrossRef]

17. Sellappan, L.K.; Manoharan, S. Fabrication of Bioinspired Keratin/Sodium Alginate Based Biopolymeric Mat Loaded with Herbal Drug and Green Synthesized Zinc Oxide Nanoparticles as a Dual Drug Antimicrobial Wound Dressing. *Int. J. Biol. Macromol.* **2024**, *259*, 129162. [CrossRef]

18. Wang, L.; Shang, Y.; Zhang, J.; Yuan, J.; Shen, J. Recent Advances in Keratin for Biomedical Applications. *Adv. Colloid. Interface Sci.* **2023**, *321*, 103012. [CrossRef]

19. Wu, X.; Liu, A.; Wang, W.; Ye, R. Improved Mechanical Properties and Thermal-Stability of Collagen Fiber Based Film by Crosslinking with Casein, Keratin or SPI: Effect of Crosslinking Process and Concentrations of Proteins. *Int. J. Biol. Macromol.* **2018**, *109*, 1319–1328. [CrossRef]

20. Ghafari, F.; Karbasi, S.; Eslaminejad, M.B.; Sayahpour, F.A.; Kalantari, N. Biological Evaluation and Osteogenic Potential of Polyhydroxybutyrate-Keratin/Al2O3 Electrospun Nanocomposite Scaffold: A Novel Bone Regeneration Construct. *Int. J. Biol. Macromol.* **2023**, *242*, 124602. [CrossRef]

21. Ke, Y.; Wu, J.; Zhang, X.; Gu, T.; Wang, Y.; Jiang, F.; Yu, J. Feather Keratin-Montmorillonite Nanocomposite Hydrogel Promotes Bone Regeneration by Stimulating the Osteogenic Differentiation of Endogenous Stem Cells. *Int. J. Biol. Macromol.* **2023**, *243*, 125330. [CrossRef]

22. Albu, M.G. *Collagen Gels and Matrices for Biomedical Applications: The Obtaining and Characterization of Collagen-Based Biomaterials as Support for Local Release*; LAP LAMBERT Academic Publishing: Saarbrücken, Germany, 2011; pp. 9–12.

23. Maidaniuc, A.; Miculescu, F.; Mocanu, A.C.; Voicu, S.I.; Miculescu, M.; Purcaru, A.; Muhuleţ, A.; Pop, C.; Rada, M.E. Sinterability study of bovine-derived hydroxyapatite and silver microcomposites. *Sci. Bull. Ser. B* **2017**, *79*, 145–154.

24. Albu, M.G.; Ficai, A.; Lungu, A. Preparation and characterization of collagen matrices obtained at different freezing temperatures. *Rev. Piel. Incaltaminte* **2010**, *10*, 39–50.

25. Albu Kaya, M.G.; Ferdes, M.; Kaya, D.A.; Ghica, M.V.; Titorencu, I.; Popa, L.; Albu, L. Collagen wound dressings with anti-inflamatory activity. *Mol. Cryst. Liq. Cryst.* **2012**, *555*, 271–279. [CrossRef]

26. Titorencu, I.; Jinga, V.V.; Constantinescu, E.; Gafencu, A.V.; Ciohodaru, C.; Manolescu, I.; Zaharia, C.; Simionescu, M. Proliferation, differentiation and characterization of osteoblasts from human BM mesenchymal cells. *Cytotherapy* **2007**, *9*, 682–696. [CrossRef]

27. Tutuianu, R.; Rosca, A.M.; Albu Kaya, M.G.; Pruna, V.; Neagu, T.P.; Lascar, I.; Simionescu, M.; Titorencu, I. Mesenchymal stromal cell-derived factors promote the colonization of collagen 3D scaffolds with human skin cells. *J. Cell Mol. Med.* **2020**, *24*, 9692–9704. [CrossRef]

28. Arifin, W.N.; Zahiruddin, W.M. Sample Size Calculation in Animal Studies Using Resource Equation Approach. *Malays. J. Med. Sci. MJMS* **2017**, *24*, 101–105.

29. Ancuța, D.L.; Crivineanu, M.; Soare, T.; Coman, C. In vivo effects of titanium implants treated with biomaterials in the bone regeneration process. *Sci. Works. Ser. C Vet. Med.* **2021**, *LXVII*, 155–160.

30. Li, S.-T. *Biomaterials. Chapter 6: Biologic Biomaterials: Tissue-Derived Biomaterials (Collagen)*, 1st ed.; Wong, J.Y., Bronzino, J.D., Eds.; CRC Press: Boca Raton, FL, USA, 2007; p. 131.

31. Balaji, S.; Kumar, R.; Sripriya, R.; Rao, U.; Mandal, A.; Kakkar, P.; Reddy, P.N.; Sehgal, P.K. Characterization of keratin–collagen 3D scaffold for biomedical applications. *Polym. Adv. Technol.* **2012**, *23*, 500–507. [CrossRef]

32. Su, D.; Wang, C.; Cai, S.; Mu, C.; Li, D.; Lin, W. Influence of palygorskite on the structure and thermal stability of collagen. *Appl. Clay Sci.* **2012**, *62*, 41–46. [CrossRef]

33. Marin, M.M.; Albu Kaya, M.G.; Vlasceanu, G.M.; Ghitman, J.; Radu, I.C.; Iovu, H. The effect of crosslinking agents on the properties of type II collagen biomaterials. *Mater. Plast.* **2020**, *57*, 166–180. [CrossRef]

34. Nistor, M.T.; Vasile, C.; Chiriac, A.P. Hybrid collagen-based hydrogels with embedded montmorillonite nanoparticles. *Mater. Sci. Eng. C* **2015**, *53*, 212–221. [CrossRef]

35. Odusote, J.K.; Danyuo, Y.; Baruwa, A.D.; Azeez, A.A. Synthesis and characterization of hydroxyapatite from bovine bone for production of dental implants. *J. Appl. Biomater. Funct. Mater.* **2019**, *17*, 228080001983682. [CrossRef]

36. Bradshaw, A.D. *The Extracellular Matrix, Encyclopedia of Cell Biology*; Bradshaw, R.A., Stahl, P.D., Eds.; Academic Press: Cambridge, MA, USA, 2016; pp. 694–703.

37. Parisi, L.; Toffoli, A.; Ghezzi, B.; Mozzoni, B.; Lumetti, S.; Macaluso, G.M. A glance on the role of fibronectin in controlling cell response at biomaterial interface. *Jpn. Dent. Sci. Review* **2020**, *56*, 50–55. [CrossRef]

38. Kokkinou, E.; Boniatis, I.; Costaridou, L.; Saridis, A.; Panagiotopoulos, E.; Panayiotakis, G. Monitoring of bone regeneration process by means of texture analysis. *J. Instrum.* **2009**, *4*, P09007. [CrossRef]

39. MacKay, J.W.; Murray, P.J.; Low, S.B.L.; Kasmai, B.; Johnson, G.; Donell, S.T.; Toms, A.P. Quantitative analysis of tibial subchondral bone: Texture analysis outperforms conventional trabecular microarchitecture analysis. *J. Magn. Reson. Imaging* **2016**, *43*, 1159–1170. [CrossRef]

Developing a Novel Murine Meningococcal Meningitis Model Using a Capsule-Null Bacterial Strain

Viorela-I. Caracoti [1], Costin-Ș. Caracoti [1,2], Diana L. Ancuța [2,3], Fabiola Ioniță [2,3], Andrei-A. Muntean [1,2], Mangesh Bhide [4,5], Gabriela L. Popa [1], Mircea I. Popa [1,2,*] and Cristin Coman [2,3,6]

[1] Faculty of Medicine, Microbiology Discipline II, Carol Davila University of Medicine and Pharmacy, 020021 Bucharest, Romania; viorela-ioana.nicolae@drd.umfcd.ro (V.-I.C.); costin-stefan.caracoti@drd.umfcd.ro (C.-Ș.C.); alexandru.muntean@umfcd.ro (A.-A.M.); gabriela.popa@umfcd.ro (G.L.P.)

[2] Cantacuzino National Military Medical Institute for Research and Development, Preclinical Testing Unit, 050096 Bucharest, Romania; ancuta.diana@cantacuzino.ro (D.L.A.); ionita.fabiola@cantacuzino.ro (F.I.); coman.cristin@cantacuzino.ro (C.C.)

[3] Faculty of Veterinary Medicine, University of Agronomic Sciences and Veterinary Medicine, 050097 Bucharest, Romania

[4] Faculty of Veterinary Medicine, University of Veterinary Medicine and Pharmacy in Kosice, Komenskeho 73, 04181 Kosice, Slovakia; mangesh.bhide@uvlf.sk

[5] Institute of Neuroimmunology of Slovak Academy of Sciences, Dubravska Cesta 9, 84510 Bratislava, Slovakia

[6] Fundeni Clinical Institute Translational Medicine Centre of Excellence, 022328 Bucharest, Romania

* Correspondence: mircea.ioan.popa@umfcd.ro; Tel.: +40-744386245

Abstract: Background: *Neisseria meningitidis* (meningococcus) is a Gram-negative bacterium that colonises the nasopharynx of about 10% of the healthy human population. Under certain conditions, it spreads into the body, causing infections with high morbidity and mortality rates. Although the capsule is the key virulence factor, unencapsulated strains have proved to possess significant clinical implications as well. Meningococcal meningitis is a primarily human infection, with limited animal models that are dependent on a variety of parameters such as bacterial virulence and mouse strain. In this study, we aimed to develop a murine *Neisseria meningitidis* meningitis model to be used in the study of various antimicrobial compounds. Method: We used a capsule-deficient *Neisseria meningitidis* strain that was thoroughly analysed through various methods. The bacterial strain was incubated for 48 h in brain–heart infusion (BHI) broth before being concentrated and injected intracisternally to bypass the blood–brain barrier in CD-1 mice. This prolonged incubation time was a key factor in increasing the virulence of the bacterial strain. A total of three more differently prepared inoculums were tested to further solidify the importance of the protocol (a 24-h incubated inoculum, a diluted inoculum, and an inactivated inoculum). Antibiotic treatment groups were also established. The clinical parameters and number of deaths were recorded over a period of 5 days, and comatose mice with no chance of recovery were euthanised. Results: The bacterial strain was confirmed to have no capsule but was found to harbour a total of 56 genes coding virulence factors, and its antibiotic susceptibility was established. Meningitis was confirmed through positive tissue culture and histological evaluation, where specific lesions were observed, such as perivascular sheaths with inflammatory infiltrate. In the treatment groups, survival rates were significantly higher (up to 81.25% in one of the treatment groups compared to 18.75% in the control group). Conclusion: We managed to successfully develop a cost-efficient murine (using simple CD-1 mice instead of expensive transgenic mice) meningococcal meningitis model using an unencapsulated strain with a novel method of preparation.

Keywords: meningococcal meningitis; murine model; *Neisseria meningitidis*; capsule deficient meningococcus; capsule null locus

1. Introduction

Neisseria meningitidis is a human-specific Gram-negative bacterium that is frequently responsible for severe cases of bacterial meningitis and is one of the few species that can cause large epidemics of such a disease [1]. It relies on several virulence factors, the capsule being one of the most important, as it prevents host phagocytosis and assists in the evasion of the host immune response [2]. Based on the capsular polysaccharide, multiple serogroups have been described as having A, B, C, Y, and W-135 major epidemiological importance [3]. However, unencapsulated strains exist, and they have been documented to have significant clinical implications, being capable of causing meningitis, bacteraemia, and other kinds of infections in humans worldwide [4].

Meningococcal vaccination may protect against the most common serogroups that cause meningococcal disease; however, the antibodies against A, C, Y, and W-135 *Neisseria* strains do not protect against unencapsulated strains because, in these cases, the vaccinal component is a group-specific polysaccharide [5,6]. Serogroup B meningococcal vaccines target other bacterial components, such as factor H-binding protein. Although these components may be present in other *N. meningitidis* strains, studies on protection against unencapsulated meningococci provided by serogroup-B vaccines are scarce to date [7].

Despite vaccine availability, vaccination is not universal, and based on the latest reports, *Neisseria meningitidis* remains one of the four main causes of bacterial meningitis worldwide [8]. It is a rapidly progressing infection that requires immediate diagnosis and efficient antibiotic treatment [9,10]. However, even when adequate care is provided, up to 15% of cases are still fatal [11]. Therefore, there is a great interest in the development of specific fast-acting anti-neisserial treatment molecules that can cross the blood–brain barrier. However, all new medications aimed at treating confirmed cases of meningococcal meningitis have to go through rigorous in vivo testing phases, which require animal infection models.

After going through the literature in our review [12], we have concluded that the existing meningococcal meningitis mouse models are scarce and rely on different factors, such as transgenic mice and hypervirulent encapsulated strains of *Neisseria meningitidis*. The most promising meningococcal meningitis animal model we found [13] was developed on the CD-1 mouse using a hypervirulent serotype C *Neisseria meningitidis* and a capsule-deficient variant of the same bacterial strain from Novartis.

Our aim was to develop an animal model using a widely available mouse strain and a clinically isolated capsule-deficient ST-823 strain of *Neisseria meningitidis*. The model's veracity is strengthened by incorporating two antibiotic treatment groups meant to save the inoculated animals, by performing bacterial counts in sampled target organs, and by having all the necessary control groups to eliminate other possible causes of death. However, certain variables must be considered, including the broth inoculum incubation duration, which has proven to be a critical and novel feature of the model.

2. Materials and Methods

2.1. Animals

For this study, we have used 88 females aged 8–10 weeks, specific pathogen-free (SPF) CD-1 strain mice. Animals were provided by the Cantacuzino National Military Medical Institute for Research and Development (CI), Băneasa Animal Facility (BAF), and maintained in individually ventilated cages (Tecniplast, Buguggiate, Italy) with autoclaved bedding. Mice were allocated to groups with a maximum of six animals per cage, maintained under a 12 h/12 h (day/night) light cycle in a ventilated room with a controlled temperature of 20–24 °C and unrestricted access to food and filtered water. The CI experimental medicine and translational research platform where the animal experiments took place has an Environmental Enrichment Program. The humane endpoints were determined using a clinical examination based on the ARRIVE criteria [14], with clinical symptoms ranked according to severity. A veterinarian assessed the animal's health. The animals were left to settle in the new environment for 1 week before conducting the experiments.

Ethics Statement: The animal experiment was approved by the Ethics Committee of the Cantacuzino National Military Medical Institute for Research and Development, Bucharest, and authorised by the Romanian Competent Authority. It was conducted in accordance with the national legislation 43/2014 and the EU Directive 63/2010 on the care, use, and protection of animals used for scientific purposes.

2.2. Bacterial Strain

We used a clinical strain of *Neisseria meningitidis* isolated from the cerebrospinal fluid of a hospitalised patient. This strain was later confirmed through whole-genome sequencing analysis to belong to an ST-823 strain from the ST-198 complex.

The bacterial strain was thoroughly characterised before the development of the animal model [14–17].

Agglutination tests for serogroup identification were performed using the Pastorex kit [18] for bacterial meningitis (Bio-Rad Laboratories, Inc., Hercules, CA, USA).

Antibiotic susceptibility testing was performed using the EUCAST guidelines for the standardised disc-diffusion antibiogram [19].

Whole-genome sequencing was performed on the strain using Illumina sequencing (Novaseq 6000). Annotation of the bacterial genome was performed using the Prokka annotation tool [20] embedded in Proksee [21] for the list of identified genes. Genes coding for virulence factors were identified by similarity searches across the hierarchical pre-build datasets performed using the VFanalyzer tool from the Virulence Factors of Pathogenic Bacteria Data Base (VFDB) [22]. Serotyping was also performed using the data from a Multi-Locus Sequence Typing (MLST) analysis [23] from the Centre for Genomic Epidemiology (CGE) based on the 7 gene signatures [24,25].

2.3. Bacterial Culture and 48-h Inoculum Preparation

Cryotube stocks of the meningococcus stored at $-80\ °C$ were thawed, and one 10 μL microbiological loop was inoculated on chocolate agar plates. The plates were then incubated at $36 \pm 1\ °C$ in an atmosphere containing 5–10% CO_2 in order to obtain a pure culture. From the resulting 24-h culture, one isolated colony was inoculated on another chocolate agar plate and incubated under the same conditions.

From the resulting culture, a full 10 μL loop of bacterial growth was inoculated in 400 mL of brain–heart infusion (BHI) broth media supplemented with 5 mg/L iron dextran and incubated in aerobic conditions at $36 \pm 1\ °C$ for 24 h in the initial stages of our model's development and for 48 h in the second stage.

After 24 h of incubation, 3 samples of the liquid culture were inoculated on chocolate agar plates and incubated for 24 h at $36 \pm 1\ °C$ in an atmosphere containing 5–10% CO_2 to verify the purity of our culture. The broth was introduced back into the incubator for another 24 h. The purity of the broth culture was confirmed after 24 h by observing the growth aspect of the colonies and was certified by identification using the bacterial identification application of the matrix-assisted laser-desorption/ionisation time of flight (MALDI-TOF) mass spectrometry assay performed on a Bruker AutoFlex Speed using the MBT Compass (HT) IVD software (version 2023).

After another 24 h of incubation, the BHI broth culture was centrifuged at $2602 \times g$ for 10 min at room temperature.

The bacterial pellet obtained was transferred into an Eppendorf tube and resuspended in a small amount of BHI broth media with a 5 mg/L iron dextran supplement. Using a Tecan Sunrise Microplate Spectrophotometer, we adjusted the bacterial concentrate to an optical density of 3 measured at a wavelength of 630 nm. We have used the BHI broth supplemented with iron dextran as the baseline reading. This value was measured using the colony-forming unit (CFU) plate count method to correspond to an average of 1.5×10^{10} CFU/mL. To accomplish this, two 10^{-6} and 10^{-7} dilutions of the concentrate were obtained, and 10 μL from each dilution were inoculated on 3 chocolate agar plates and spread evenly with a sterile loop. The plates were incubated for 24 h at $36 \pm 1\ °C$ in

an atmosphere containing 5–10% CO_2. The resulting colonies were counted, and a mean bacterial concentration was calculated.

To obtain the inoculum used in the experiment, the bacterial concentrate was diluted to 1.5×10^9 CFU/mL in BHI broth media. Considering the inoculum volume was 10 μL, this would correspond to 1.5×10^7 CFU/mouse. Before intracisternal delivery, the concentration of the bacterial inoculum was verified one last time using the CFU plate count method in triplicate.

2.4. Inoculation Procedure

Before inoculation, all the animals were weighed, and their corporal temperature was measured using an intrarectal thermometer.

Two hours before intracisternal bacterial inoculation, the mice received a single intraperitoneal dose of 250 mg/kg of a pharmaceutical iron dextran supplement for veterinary use (FierDextran 20% from Farmavet Group).

The mice were anaesthetised intraperitoneally, according to individual weight, with a mixture of ketamine (50 mg/kg) and xylazine (3 mg/kg).

An ophthalmic lubricant was used to prevent eye drying.

Their cervical fur was shaved, and the exposed skin was cleaned with an antiseptic containing a 70% ethanol solution and 3% betadine.

The depth of anaesthesia was assessed by observing their reaction to touch and to the pain response when pinched.

The inoculation procedure was performed in a laminar airflow work cabinet.

The animal's head was held with the left hand in a ventral flexed position. The craniocervical junction, which appears as a diamond-shaped indentation, is the inoculation area for the *cisterna magna* administration site. After being gently homogenised, the bacterial inoculum was delivered using a 30 G needle syringe.

The total volume of inoculum was 10 μL, corresponding to approximately 1.5×10^7 CFU/mouse.

Following anaesthesia and inoculation, the mice were kept warm for an hour post-anaesthesia and then placed in cages until fully awakened.

2.5. Inactive Inoculum Control

An inactive bacterial inoculum control group was established to rule out any deaths induced by possible endotoxic shock or organic lesions caused by the inoculation procedure.

The inoculum was prepared as described above and inactivated with wet heat for one hour at 100 °C. To confirm the inactivation, two samples of inoculum were plated on chocolate agar and incubated for up to 48 h at 36 ± 1 °C in an atmosphere containing 5–10% CO_2, and no bacterial growth was observed.

2.6. Diluted Inoculum Group

A 10^{-2} dilution of the bacterial concentrate was obtained and used, corresponding to 1.5×10^6 CFU/mouse.

2.7. 24-h Incubated Inoculum

A neisserial broth culture was obtained using the same protocol as stated in [2,3], which was allowed to grow for only 24 h before being prepared for inoculation. The purpose of this inoculum was to compare it to the 48-h inoculum that proved successful in our study.

2.8. Antibiotic Treatment

Two different antibiotics were used based on the strain's susceptibility and clinical indication.

We have agreed upon ceftriaxone as the drug of choice for the treatment of most bacterial meningitis, including meningococcal meningitis [26,27]. The animals received an initial intravenous (IV) dose of 50 mg/kg ceftriaxone (corresponding to an average

volume of 10 μL/mouse, depending on the animal weight) 3 h after the intracisternal inoculation. Antibiotic treatment was administered every 12 h for the next 5 days (a total of 10 additional doses).

To further solidify the usefulness of the model, a second treatment group using ciprofloxacin chlorhydrate was established. This antibiotic was chosen since it is used in the prophylaxis of meningococcal meningitis after a possible exposure event. The animals received an initial IV dose of 25 mg/kg ciprofloxacin (corresponding to an average volume of 200 μL/mouse, depending on the animal weight) 3 h after the bacterial inoculation and thereafter a single identical dose daily for the next 5 days.

The control groups received 100 μL of phosphate-buffered saline (PBS) intravenously for each inoculation. The administration procedure was the same as with the antibiotic groups.

Before every administration, the animals' tails were kept in warm water for a few minutes to induce tail vein dilation and then disinfected with 70% alcohol before injecting the needle. The treatment solution and PBS were administered slowly to avoid vascular injury. After the needle was removed, gentle pressure with a sterile compress was applied to stop the bleeding.

2.9. Infection Monitoring

All mice were evaluated once daily for the next five days, and any changes in temperature and weight, clinical illness signs, comatose state, or death were noted.

Weak individuals who were unable to sustain themselves were kept hydrated with saline solutions administered subcutaneously and orally.

We assessed the mice using the following scale: 1 = coma; 2 = the animal does not return to the quadrupedal position after being positioned on its back; 3 = the animal returns to the quadrupedal position after 30 s of being positioned on its back; 4 = the animal stands up after 5 s of being positioned on its back, showing minimal motor activity; 5 = normal behaviour [13,28]. Mice assessed as a 1 or 2 on the scale, with no chance of recovery, were humanely euthanised and sampled. Euthanasia was performed using a high dose of anaesthetic.

On the last day, any surviving animals were culled and sampled.

2.10. Tissue Sampling and Processing

The animal bodies were processed right after death or euthanasia.

The entire mouse was antiseptised with a 70% ethanol solution and 3% betadine in a sterile laminar airflow work cabinet. Using sterile surgical equipment, a horizontal incision was made at the base of the skull. The skin covering the scalp was pulled over to expose the cranium. The calvaria was detached by cutting the occipital and interparietal bones and then cutting carefully between the frontal and parietal bone junctions with the tip of the scissors to avoid damaging the brain. The calvaria was removed, and the brain was exposed. Using a scalpel, the peduncles and nerves connected with the brain were cut, and the two hemispheres were separated. Half of the brain matter (one hemisphere) was collected into a 2 mL Eppendorf tube for microbiological analysis. The other hemisphere was collected in a histological cassette, submerged in 37% formaldehyde, and sent for histopathological examination to a third-party laboratory.

To reach the spleen, the abdomen was cut open, exposing it on the left side, under the ribcage. Using forceps and scissors, the entire spleen was collected into a 2 mL Eppendorf tube for microbiological analysis.

The samples collected for microbiological analysis were weighed, ground up, and mixed with 1 mL of BHI broth using sterile steel balls and a shaker. From each mix, a 10^{-2} dilution was obtained, and 10 μL of all 4 tubes were inoculated in duplicate on chocolate agar plates supplemented with 10 μg/L vancomycin and 25 μg/L trimethoprim-sulfamethoxazole. The supplement was added to prevent the growth of potential bacterial contaminants, and the neisserial strain was verified to be resistant to the 2 antibiotics at

the concentrations mentioned before the experiment. The agar plates were incubated as previously described. After 24 and 48 h, grown colonies were evaluated via MALDI-TOF analysis assay and counted. The results were expressed in CFU/g of brain matter.

The other half of the brain was collected in 37% formaldehyde and sent for histopathological examination to a third-party laboratory.

3. Results

3.1. Extensive Characterisation of the Neisserial Strain

Our bacterial strain was proven to be susceptible to most antibiotics, as interpreted using the most recent EUCAST guide [19].

The strain was classified as (inhibition diameter shown after the antibiotic and reference diameter for susceptibility shown in brackets) susceptible to the following antibiotics:

Ciprofloxacin 36 mm ($\geq$35 mm), cefotaxim 35 mm ($\geq$34 mm), meropenem 38 mm ($\geq$30 mm), rifampicin 32 mm ($\geq$25 mm), azithromycin 28 mm ($\geq$20), chloramphenicol 26 mm ($\geq$26), and minocycline 28 mm ($\geq$26).

Resistant to trimethoprim-sulfamethoxazole 9 mm ($\geq$30 mm)

During the latex agglutination test, the strain was agglutinated with both serogroup A and serogroup C antibody reagents from the kit. No agglutination has been observed with the serogroup B antibody reagent. The kit's quality control was performed and revealed no malfunctions (Figure 1). Agglutination for group Y/W-135 was not performed as the manufacturer's indications do not recommend testing *Neisseria meningitidis* colonies isolated on agar media for Y/W-135 serogroups.
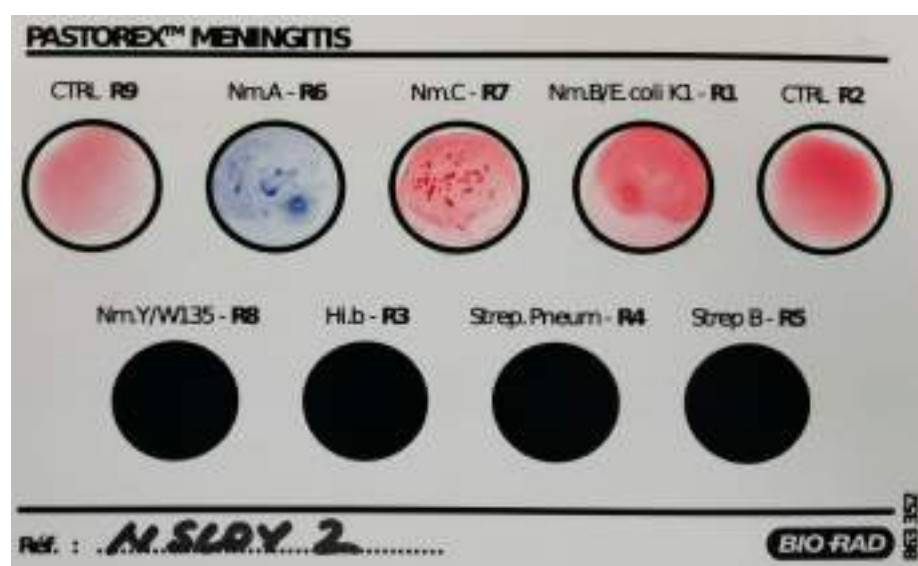
Figure 1. Latex agglutination results of the *Neisseria meningitidis* strain showed non-specific positivity for both serogroups A and C and negative results for serogroup B. Testing for serogroup Y/W135 was not performed as the manufacturer does not recommend using bacterial isolates from agar media. No testing was performed for Hi.b-R3, Strep.Pneum-R4, and Strep B-R5, as these are designated for other bacterial species. (CTRL R9: negative polyvalent control, Nm.A-R6: serogroup A *Neisseria meningitidis*, Nm.C-R7: serogroup C *Neisseria meningitidis*, Nm.B/E.coli K1-R1: serogroup B *Neisseria meningitidis/Escherichia coli* K1 antigen, CTRL R2: negative control for serogroup B *Neisseria meningitidis/Escherichia coli* K1 antigen, Nm.Y/W135-R8: serogroup Y/serogroup W135 *Neisseria meningitidis*, Hi.b-R3: *Haemophilus influenzae* serotype b, Strep. Pneum-R4: *Streptococcus pneumoniae*, Strep B-R5: group B *Streptococcus*).

The whole genome sequencing proved that the strain harboured a "capsule null locus" gene instead of any other serogroup capsule-encoding genes (Table 1). It was characterised as a sequence-type (ST) 823 strain from the ST-198 complex [29].

Table 1. Results of serotyping by MLST based on seven genes [25].

Locus	Identity	Coverage	Alignment Length	Allele Length	Gaps	Allele
abcZ	100	100	433	433	0	abcZ_5
adk	100	100	465	465	0	adk_4
aroE	100	100	490	490	0	aroE_17
fumC	100	100	465	465	0	fumC_15
gdh	100	100	501	501	0	gdh_30
pdhC	100	100	480	480	0	pdhC_7
pgm	100	100	450	450	0	pgm_12

Despite the lack of a capsule, we have identified 56 genes involved in different virulence mechanisms, i.e., 33 genes for adherence, 2 genes for immune modulation, 3 genes for invasion, 11 genes for iron uptake, 1 protease gene, and 6 genes related to stress adaptation (Table 2).

Table 2. Virulence genes identified using the VFanalyzer tool from the Virulence Factors of Pathogenic Bacteria Data Base (VFDB) [22].

VFclass	Virulence Factor	Gene	Start	Stop	Contig and Orientation
Adherence	Adhesion and penetration protein	app	163	4539	92−
	LOS sialylation	lst	7320	7982	22+
	LOS synthesis	kdtA/waaA	7985	8419	22+
	LOS synthesis	lgtA	3884	5038	51−
	LOS synthesis	lgtB	2334	3860	51−
	LOS synthesis	lgtE	161	1156	27+
	LOS synthesis	lgtF	1212	2741	27+
	LOS synthesis	lgtG	2762	3820	27+
	LOS synthesis	rfaC	88	2229	142−
	LOS synthesis	rfaF	9003	9827	42−
	LOS synthesis	rfaK	230	1156	96+
	Neisseria adhesion A	nadA	1187	3613	96+
	Phosphoethanolamine modification	lptA	10,777	16,284	39−
	Type IV pili	pilC	256	1770	138−
	Type IV pili	pilD	22,475	23,746	19−
	Type IV pili	pilF	244	3081	104−
	Type IV pili	pilG	3078	5291	104−
	Type IV pili	pilH	4889	5977	23−
	Type IV pili	pilI	4050	4889	23−
	Type IV pili	pilJ	3059	3901	23−
	Type IV pili	pilK	3861	4619	101+
	Type IV pili	pilM	2718	3770	43−
	Type IV pili	pilN	14,645	16,279	35+

Table 2. *Cont.*

VFclass	Virulence Factor	Gene	Start	Stop	Contig and Orientation
Adherence	Type IV pili	pilO	4323	5459	83+
	Type IV pili	pilP	23,691	24,446	18+
	Type IV pili	pilQ	24,470	25,345	18+
	Type IV pili	pilT	25,422	26,348	18+
	Type IV pili	pilT2	5708	7276	49+
	Type IV pili	pilU	4741	5979	99−
	Type IV pili	pilV	1526	4729	99−
	Type IV pili	pilW	68	1471	99−
	Type IV pili	pilX	5198	6286	9+
	Type IV pili	pilZ	435	959	105+
Immune modulator	Factor H binding protein	fHbp	2729	3397	130−
	Neisserial surface protein A	nspA	2085	2732	130−
Invasion	Class 5 outer membrane protein	opc	1147	2088	130−
	PorA	porA	572	1168	130−
	PorB	porB	11,222	12,337	40+
Iron uptake	ABC transporter	fbpA	12,340	12,939	40+
	ABC transporter	fbpB	12,940	13,587	40+
	ABC transporter	fbpC	13,605	14,150	40+
	Ferric enterobactin transport protein A/ ferric-repressed protein B	fetA/frpB	14,169	16,454	40+
	Heme uptake	hpuA	3959	5002	86−
	Heme uptake	hpuB	5462	6592	34+
	Lactoferrin-binding protein	lbpA	2570	3796	86−
	Lactoferrin-binding protein	lbpB	8035	8424	12+
	Ton system	exbB	3049	3810	4+
	Ton system	exbD	94	567	130−
	Ton system	tonB	7607	7957	34+
Protease	IgA protease	iga	458	1627	151−
Stress adaptation	Catalase	katA	375	1370	160+
	Manganese transport system	mntA	8226	9899	66+
	Manganese transport system	mntB	5061	6041	19−
	Manganese transport system	mntC	17,713	18,723	28−
	Methionine sulphoxide reductase	msrA/B (pilB)	4620	5684	101+
	Recombinational repair protein	recN	6412	7254	22+

3.2. Establishing the Model

The meningococcal meningitis mouse model was established after testing and verifying key variables. In Table 3, the tested variables of each mouse group, as well as survival rate and deaths per day, are presented. The experiments' succession and results will be presented below in Sections 3.2.1 and 3.2.2.

Table 3. Mice groups survival throughout the experiment.

| Stage | Mouse Group | Mice no. | Inoculum | | Deaths | | | | | | Survival Rate (%) |
			Incubation Period	CFU/ Mouse	D0	D1	D2	D3	D4	D5	
Stage 1	24-h incubated inoculum group	8	24 h	1.5×10^7	0	0	0	0	0	0	100.00
	48-h incubated inoculum group	8	48 h	1.5×10^7	0	2	4	1	0	0	12.50
Stage 2	Inactivated inoculum group	8	48 h	1.5×10^7	0	0	0	0	0	0	100.00
	Diluted inoculum control group	8	48 h	1.5×10^6	0	2	2	0	0	0	50.00
	48-h incubated control group	8	48 h	1.5×10^7	0	1	4	1	0	0	25.00
	Ceftriaxone treatment group	16	48 h	1.5×10^7	0	1	1	0	2	0	75.00
	Ciprofloxacin treatment group	16	48 h	1.5×10^7	0	1	0	2	0	0	81.25
	Summed 48-h incubated control group *	16	48 h	1.5×10^7	0	3	8	2	0	0	18.75

* The 16 mice from this group were comprised of the pooled results of the 48-h incubated inoculum group and the 48-h incubated control group.

3.2.1. Stage 1: Establishing the Required Incubation Time

In the first part of the experiment, we used the protocol described above but with a 24-h incubation time for our BHI broth culture. However, no animals succumbed to the disease.

We decided to increase the incubation time of the culture to 48 h, as this might allow the strain to better express its virulence factors [30]. This time, seven out of eight mice succumbed to the disease. The results can be observed in Figure 2.
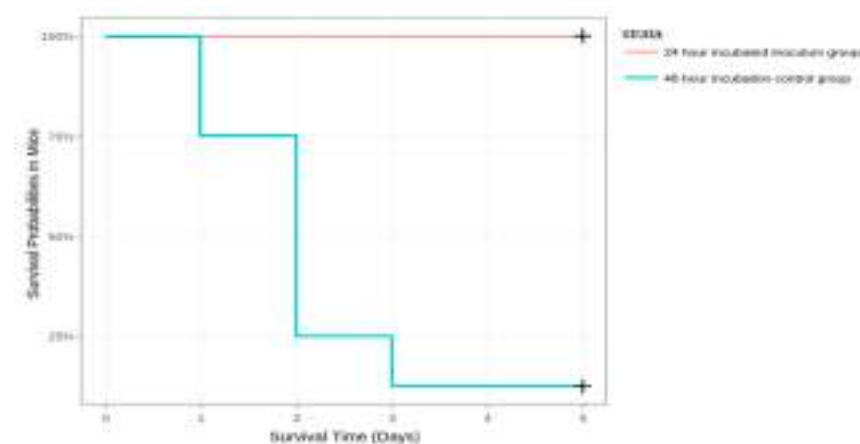

Figure 2. Survival of mice inoculated with the 24-h and 48-h incubated inoculums.

3.2.2. Stage 2: Excluding Endotoxic Shock Death, Establishing the Lethal Dose for Half the Inoculated Mice (LD50), and Rising the Survivability Rate through Treatment

All mice from the inactivated inoculum group survived and showed no signs of illness during the six-day period. LD50 was established using a 10^{-2} dilution of the bacterial concentrate (Figure 3).
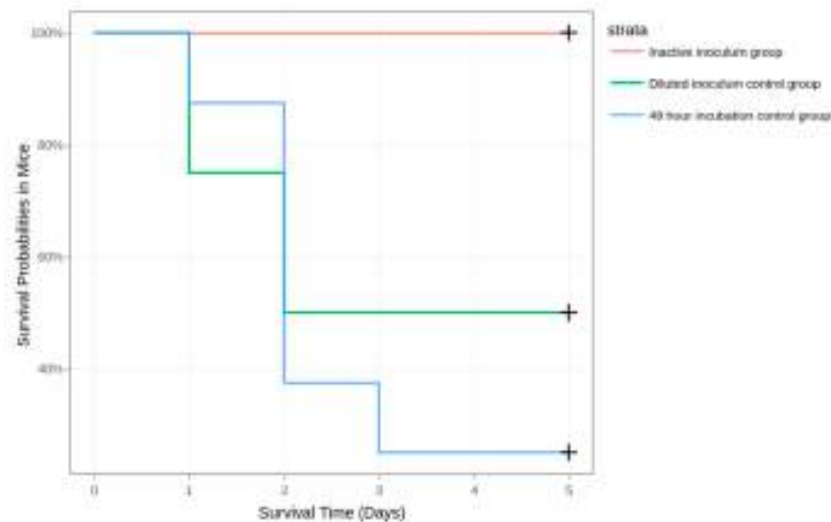

Figure 3. Survival of mice in the inactive inoculum, diluted inoculum (10^{-2}), and 48-h incubation group.

The survival of mice was significantly different between the 48-h incubated inoculum group and treatment groups. A total of 13 mice succumbed to the disease in the control group, 3 in the ciprofloxacin treatment group, and 4 in the ceftriaxone treatment group (Figure 4). Therefore, the survival rates were 18.75% in the control group, 81.25% in the ciprofloxacin treatment group, and 75% in the ceftriaxone treatment group.
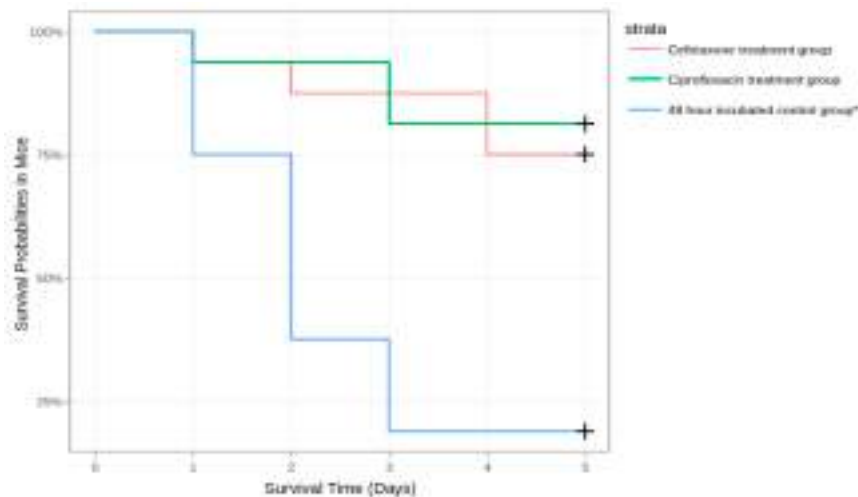

Figure 4. Survival of mice in the two antibiotic treatment groups compared to the 48-h incubated control group* (data pooled from 16 mice from the two 48-h incubated inoculum groups).

3.3. Clinical Parameters and Mortality

At the start of the experiment, the animals weighed an average of 23.7 g and had an average temperature of 36 °C. In all groups where some of the mice succumbed to the disease, the subjects' clinical parameters deteriorated during the course of the experiment. The temperature and weight seemed to be directly correlated to the health of the animal, decreasing as the animal was going through the onset stages of the disease and gradually

increasing in animals that had survived the first 3 days after inoculation. More details regarding the clinical parameters and mortality can be found in the Supplementary Material (Table S1).

3.4. CFU Count in Tissue Samples

Spleen samples never yielded any bacterial growth throughout the experiment.

In the ceftriaxone treatment group and in the ciprofloxacin treatment group, brain samples never yielded any bacterial growth.

In the summed 48-h incubated control group, mice that either died or were euthanised in the first four days of the experiment presented variable bacterial growth. There was a two-tenfold variation in CFU/g in the brain samples, with the average being 10^3 CFU/g of brain tissue (Figure 5).
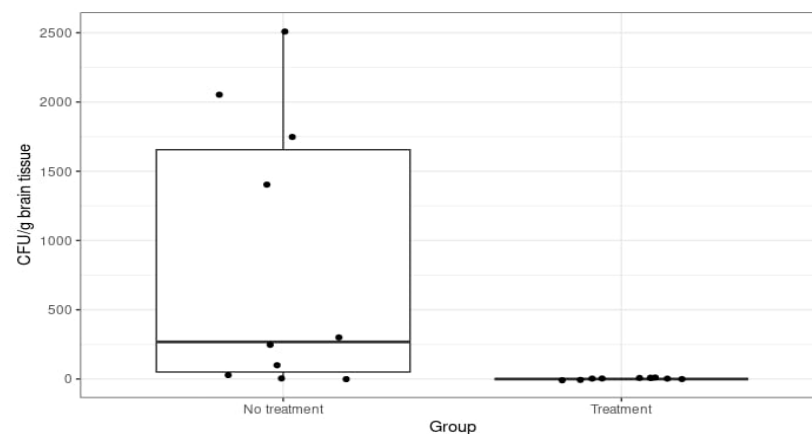

Figure 5. Colony-forming units per gramme of brain tissue in the 48-h incubated control group (No treatment) and the ciprofloxacin and ceftriaxone groups (Treatment).

Mice that survived until the 6th day of the experiment never yielded any bacterial growth.

3.5. Histologic Examination

Histological analysis of the brain tissue samples with haematoxylin-eosin staining revealed signs of meningitis with leukocytic and haemorrhagic infiltrates (Figures 6 and 7).
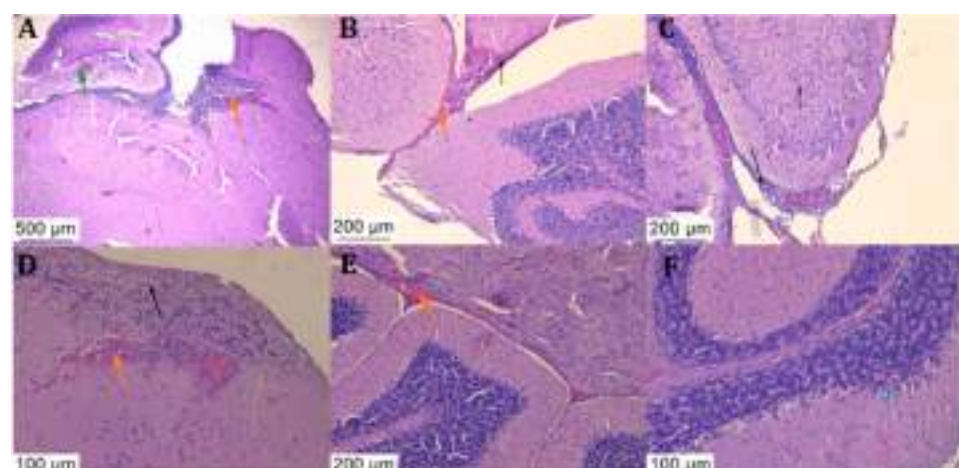
Figure 6. Histological sections of the brains of the animals treated with PBS, stained with haematoxylin and eosin stain: Severe inflammation in the brain parenchyma is characterised by neutrophilic and lymphocytic infiltrate ((**A**–**D**), black arrow) along with haemorrhagic foci both in the brain parenchyma and at its border and at the border with the cerebellum ((**A**–**E**), orange arrow), with perivascular inflammation. Abscess formation is accompanied by inflammation of the vascular endothelium ((**A**), green arrow) and phagocytosis of neutrophils ((**F**), blue arrow).

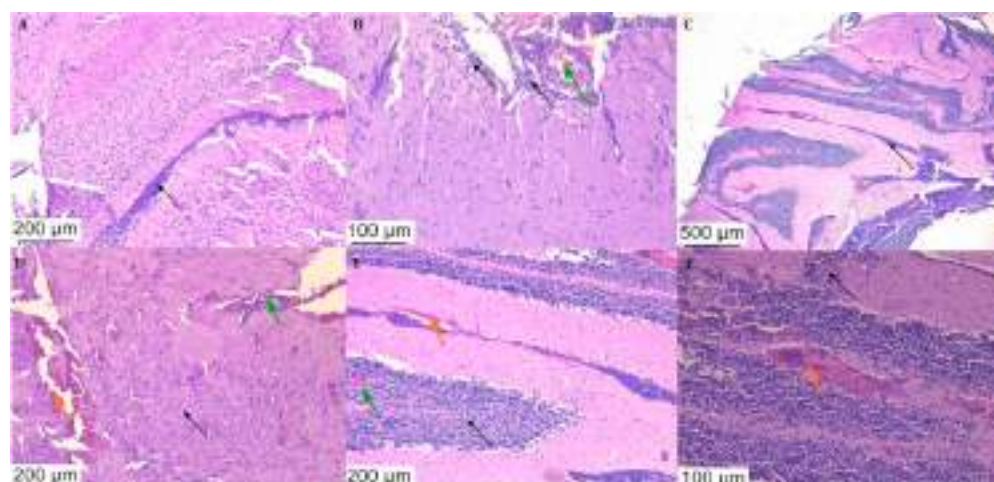**Figure 7.** Histological sections of the brains of the ceftriaxone-treated (**A**–**C**) and ciprofloxacin-treated (**D**–**F**) animals that succumbed to the disease, stained with haematoxylin and eosin stain: maintenance of neutrophilic and lymphocytic inflammatory infiltrate ((**A,C**), black arrow) or diffuse (black arrow), inflammation of vascular tissues and abscesses delimited by inflammatory reaction ((**B,D**), green arrow) together with haemorrhagic foci ((**D**–**F**), orange arrow).

Typical meningitis lesions were observed, which were consistent with histological analysis from other mouse models [12], such as abscesses, multiple zones of neutrophilic and lymphocytic infiltrate, and many other signs of inflammation. All of the observed lesions in the PBS-treated mice that succumbed to the disease were also found in the ceftriaxone and ciprofloxacin-treated mice.

4. Discussion

We wanted to create an easy-to-replicate meningococcal meningitis mouse model without using expensive mouse strains or hypervirulent *Neisseria meningitidis* strains.

We chose the iron dextran supplement because it was found to be less toxic than other iron compounds, even at higher concentrations [31,32], and it appeared to have a role in the severity of the infection [13,33].

Identical lesions were found in both PBS and antibiotic-treated mouse groups that succumbed to the disease. The histological analysis revealed inflammatory infiltrates and haemorrhages in both the brain parenchyma and the cerebellum, similar to other murine meningitis models [33].

The lack of bacterial growth in all brain tissue samples from the ceftriaxone and ciprofloxacin treatment groups can be explained by the antibiotics still persisting in the tissue samples but failing to save the animal.

The spleen samples never yielded any neisserial growth, despite being one of the main organs that act as antigen filters [34]. This proves that the infection never disseminated throughout the body and was strictly localised in the cerebrum. This further underlines the meningitis aspect of the model rather than septic multi-organ infection.

The model is highly dependent on the bacterial dose inoculum. In the initial phases, while working with the bacterial concentrate (1.5×10^{10} CFU/mL), we concluded it was too viscous to administer efficiently with the fine needle syringe. Thus, we used a 10^{-1} dilution, which corresponded to 1.5×10^7 CFU/mouse. This inoculum appeared to be the equivalent of the lethal dose of 90% (LD90) for this strain, as seven out of eight mice died.

A 10^{-2} dilution, which corresponded to 1.5×10^6 CFU/mouse, was obtained and used. In this group, only half of the mice succumbed to the infection (LD50), which was deemed unsatisfactory for the testing of antibiotic compounds for this type of model. However, it is interesting to compare this result with the model developed by Pagliuca et al. [13] using the capsule gene knock-out strain, since they have obtained the LD50 at a value of

10^9 CFU/mouse. A smaller LD50 could be explained by the fact that our ST-823 strain was naturally capsule-deficient and capable of inducing meningitis in humans and not a knock-out variant of an encapsulated strain. We do not believe this difference is due to the capsule gene knock-out strain lacking virulence factors because the serogroup C strain from which it was obtained was characterised as hypervirulent [13].

After using the 1.5×10^7 CFU/mouse inoculum, six out of eight mice died, and we established the LD80 of the strain by adding in the results from the first group. To lower the number of animals used, the two groups were pooled to create a control group with an identical number of animals as the antibiotic treatment groups.

A peculiarity of the model became apparent in the early stages of development when none of the four inoculated animals succumbed to the infection. The inoculum was prepared using a BHI broth with a 5 mg/L iron dextran culture of our meningococcal strain, which was incubated for 24 h. However, the inoculum optical density and bacterial concentration were the same as in the established protocol. We repeated this 24-h incubation protocol with four more animals, and yet again, all of the animals survived the infection with no signs of illness. The data from these two 24-h incubated inoculum groups were pooled together into a single group and presented in the results section. We obtained the mortality needed in our model only after switching to the 48-h incubation period. This proves, in our opinion, the importance of a longer incubation time for the bacterial inoculum. Most likely, this is attributed to a phenotypic switch in the bacteria, which increased its virulence in the mice.

Another novel part of the model was using the ST-823 capsule-deficient strain. This is a rather rare type of *Neisseria meningitidis* that is not commonly associated with human pathology. However, this was a clinical isolate from a patient who suffered from meningococcal meningitis, and other such cases have been reported [7,35–38].

Regarding the limitations of the study, we mention the use of only one Neisseria meningitidis strain when developing the model. The LD 50% and LD 80% may vary when using other neisserial strains with different levels of virulence, and concentrations of the bacterial inoculum will have to be adjusted accordingly. Another limitation could be considered the lack of bacterial recovery from mice that succumbed to the disease in the antibiotic treatment groups. Showing that bacteria are still alive in the mice and being able to measure their concentration might prove relevant for certain in-vivo future studies.

The survival rate of treated mice can also be considered a limitation. Both antibiotics did not achieve a 100% survival rate. However, the results of the histological analysis and the clinical outcome are in concordance with human meningococcal meningitis [39,40].

5. Conclusions

Our meningococcal meningitis mouse model is not limited to an expensive mouse strain, hypervirulent or encapsulated *Neisseria meningitidis* strain, or antibiotic (as long as the bacterial isolate is susceptible to the antibiotic used and it can penetrate the blood-brain barrier).

The model is inexpensive, simple, and efficient to replicate and implement whenever new antibiotic compounds are to be tested for such a disease.

A novel feature of the model was the use of a BHI broth medium for the bacterial inoculum, a 48-h incubation period of the bacterial inoculum, and the use of an unencapsulated neisserial ST-823 strain from the ST-198 complex.

Another distinguishing feature of the model was that we not only determined the strain's LD50 and LD80 but also successfully treated and saved mice inoculated with the latter with two clinically used antibiotics (ceftriaxone and ciprofloxacin), demonstrating its utility and flexibility in concordance with other meningococcal murine models used to test new antibacterial compounds [41].

References

1. Meningococcus—PAHO/WHO|Pan American Health Organization. Available online: https://www.paho.org/en/topics/meningococcus (accessed on 10 March 2024).
2. Joshi, R.; Saroj, S.D. Survival and Evasion of *Neisseria meningitidis* from Macrophages. *Med. Microecol.* **2023**, *17*, 100087. [CrossRef]
3. Harrison, L.H.; Trotter, C.L.; Ramsay, M.E. Global Epidemiology of Meningococcal Disease. *Vaccine* **2009**, *27*, B51–B63. [CrossRef]
4. Johswich, K.O.; Zhou, J.; Law, D.K.S.; St. Michael, F.; McCaw, S.E.; Jamieson, F.B.; Cox, A.D.; Tsang, R.S.W.; Gray-Owen, S.D. Invasive Potential of Nonencapsulated Disease Isolates of *Neisseria meningitidis*. *Infect. Immun.* **2012**, *80*, 2346–2353. [CrossRef]
5. Vogel, U.; Claus, H. Vaccine Development against *Neisseria meningitidis*. *Microb. Biotechnol.* **2011**, *4*, 20–31. [CrossRef]
6. Tzeng, Y.-L.; Thomas, J.; Stephens, D.S. Regulation of Capsule in *Neisseria meningitidis*. *Crit. Rev. Microbiol.* **2016**, *42*, 759–772. [CrossRef]
7. Claus, H.; Jördens, M.S.; Kriz, P.; Musilek, M.; Jarva, H.; Pawlik, M.-C.; Meri, S.; Vogel, U. Capsule Null Locus Meningococci: Typing of Antigens Used in an Investigational Multicomponent Meningococcus Serogroup B Vaccine. *Vaccine* **2012**, *30*, 155–160. [CrossRef]
8. Bacterial Meningitis|CDC. Available online: https://www.cdc.gov/meningitis/index.html (accessed on 24 April 2024).
9. Yadav, S.; Rammohan, G. Meningococcal Meningitis. In *StatPearls*; StatPearls Publishing: Treasure Island, FL, USA, 2024.
10. Meningococcal Disease|CDC. Available online: https://www.cdc.gov/meningococcal/index.html (accessed on 5 November 2023).
11. UHS Health Topic—Meningitis. Available online: https://healthyhorns.utexas.edu/HT/HT_meningitis.html (accessed on 10 March 2024).
12. Caracoti, V.I.; Caracoti, C.S.; Muntean, A.A.; Coman, C.; Popa, M.I. Proposing a murine meningococcal meningitis animal model based on extensive review of literature. *ROAMI* **2023**, *1*, 35–41.
13. Pagliuca, C.; Scaglione, E.; Carraturo, F.; Mantova, G.; Marino, M.M.; Pishbin, M.V.; Pagliarulo, C.; Colicchio, R.; Salvatore, P. Inducing Meningococcal Meningitis Serogroup C in Mice via Intracisternal Delivery. *J. Vis. Exp. JoVE* **2019**, *153*, e60047. [CrossRef]
14. Kánová, E.; Pulzová, L.; Kováč, A.; Bhide, M. Deciphering the Interactome of *Neisseria meningitidis* With Human Brain Microvascular Endothelial Cells. *Front. Microbiol.* **2018**, *9*, 2294. [CrossRef]
15. Káňová, E.; Tkáčová, Z.; Bhide, K.; Kulkarni, A.; Jiménez-Munguía, I.; Mertinková, P.; Drážovská, M.; Tyagi, P.; Bhide, M. Transcriptome Analysis of Human Brain Microvascular Endothelial Cells Response to *Neisseria meningitidis* and Its Antigen MafA Using RNA-Seq. *Sci. Rep.* **2019**, *9*, 18763. [CrossRef]
16. Kulkarni, A.; Mochnáčová, E.; Majerova, P.; Čurlík, J.; Bhide, K.; Mertinková, P.; Bhide, M. Single Domain Antibodies Targeting Receptor Binding Pockets of NadA Restrain Adhesion of *Neisseria meningitidis* to Human Brain Microvascular Endothelial Cells. *Front. Mol. Biosci.* **2020**, *7*, 573281. [CrossRef]

17. Kulkarni, A.; Jozefiaková, J.; Bhide, K.; Mochnáčová, E.; Bhide, M. Differential Transcriptome Response of Blood Brain Barrier Spheroids to Neuroinvasive Neisseria and Borrelia. *Front. Cell. Infect. Microbiol.* **2023**, *13*, 1326578. [CrossRef]

18. Uadiale, K.; Bestman, A.; Kamau, C.; Caugant, D.A.; Greig, J. Evaluation of Pastorex Meningitis Kit Performance for the Rapid Identification of *Neisseria meningitidis* Serogroup C in Nigeria. *Trans. R. Soc. Trop. Med. Hyg.* **2016**, *110*, 381–385. [CrossRef]

19. Eucast: AST of Bacteria. Available online: https://www.eucast.org/ast_of_bacteria (accessed on 10 March 2024).

20. Seemann, T. Prokka: Rapid Prokaryotic Genome Annotation. *Bioinformatics* **2014**, *30*, 2068–2069. [CrossRef]

21. Grant, J.R.; Enns, E.; Marinier, E.; Mandal, A.; Herman, E.K.; Chen, C.; Graham, M.; Van Domselaar, G.; Stothard, P. Proksee: In-Depth Characterization and Visualization of Bacterial Genomes. *Nucleic Acids Res.* **2023**, *51*, W484–W492. [CrossRef]

22. Liu, B.; Zheng, D.; Zhou, S.; Chen, L.; Yang, J. VFDB 2022: A General Classification Scheme for Bacterial Virulence Factors. *Nucleic Acids Res.* **2022**, *50*, D912–D917. [CrossRef]

23. Larsen, M.V.; Cosentino, S.; Rasmussen, S.; Friis, C.; Hasman, H.; Marvig, R.L.; Jelsbak, L.; Sicheritz-Pontén, T.; Ussery, D.W.; Aarestrup, F.M.; et al. Multilocus Sequence Typing of Total-Genome-Sequenced Bacteria. *J. Clin. Microbiol.* **2020**, *50*, 1355–1361. [CrossRef]

24. Maiden, M.C.; Bygraves, J.A.; Feil, E.; Morelli, G.; Russell, J.E.; Urwin, R.; Zhang, Q.; Zhou, J.; Zurth, K.; Caugant, D.A.; et al. Multilocus Sequence Typing: A Portable Approach to the Identification of Clones within Populations of Pathogenic Microorganisms. *Proc. Natl. Acad. Sci. USA* **1998**, *95*, 3140–3145. [CrossRef]

25. Bennett, J.S.; Jolley, K.A.; Sparling, P.F.; Saunders, N.J.; Hart, C.A.; Feavers, I.M.; Maiden, M.C. Species Status of Neisseria Gonorrhoeae: Evolutionary and Epidemiological Inferences from Multilocus Sequence Typing. *BMC Biol.* **2007**, *5*, 35. [CrossRef]

26. Theilen, U.; Wilson, L.; Wilson, G.; Beattie, J.O.; Qureshi, S.; Simpson, D. Management of Invasive Meningococcal Disease in Children and Young People: Summary of SIGN Guidelines. *BMJ* **2008**, *336*, 1367–1370. [CrossRef]

27. Hoffman, O.; Weber, R.J. Pathophysiology and Treatment of Bacterial Meningitis. *Ther. Adv. Neurol. Disord.* **2009**, *2*, 401–412. [CrossRef]

28. Coman, C.; Ancuta, D.L.; Ionita, F.; Muntean, A.A.; Caracoti, C.S.; Caracoti, I.V.; Dragomirescu, C.; Popa, M.I. Preliminary results in inducing meningitis in balb/c mice using a human strain of *Neisseria meningitidis*. *Sci. Work. Ser. C Vet. Med.* **2022**, *1*, 199–205.

29. Schork, S.; Schlüter, A.; Blom, J.; Schneiker-Bekel, S.; Pühler, A.; Goesmann, A.; Frosch, M.; Schoen, C. Genome Sequence of a *Neisseria meningitidis* Capsule Null Locus Strain from the Clonal Complex of Sequence Type 198. *J. Bacteriol.* **2012**, *194*, 5144–5145. [CrossRef]

30. Rouphael, N.G.; Stephens, D.S. Neisseria meningitidis: Biology, Microbiology, and Epidemiology. In *Neisseria meningitidis: Advanced Methods and Protocols*; Christodoulides, M., Ed.; Humana Press: Totowa, NJ, USA, 2012; pp. 1–20, ISBN 978-1-61779-346-2.

31. Holbein, B.E. Iron-Controlled Infection with *Neisseria meningitidis* in Mice. *Infect. Immun.* **1980**, *29*, 886–891. [CrossRef]

32. Holbein, B.E.; Jericho, K.W.; Likes, G.C. *Neisseria meningitidis* Infection in Mice: Influence of Iron, Variations in Virulence among Strains, and Pathology. *Infect. Immun.* **1979**, *24*, 545–551. [CrossRef]

33. Colicchio, R.; Ricci, S.; Lamberti, F.; Pagliarulo, C.; Pagliuca, C.; Braione, V.; Braccini, T.; Talà, A.; Montanaro, D.; Tripodi, S.; et al. The Meningococcal ABC-Type L-Glutamate Transporter GltT Is Necessary for the Development of Experimental Meningitis in Mice. *Infect. Immun.* **2009**, *77*, 3578–3587. [CrossRef] [PubMed]

34. Bronte, V.; Pittet, M.J. The Spleen in Local and Systemic Regulation of Immunity. *Immunity* **2013**, *39*, 806–818. [CrossRef]

35. Hoang, L.M.N.; Thomas, E.; Tyler, S.; Pollard, A.J.; Stephens, G.; Gustafson, L.; McNabb, A.; Pocock, I.; Tsang, R.; Tan, R. Rapid and Fatal Meningococcal Disease Due to a Strain of *Neisseria meningitidis* Containing the Capsule Null Locus. *Clin. Infect. Dis.* **2005**, *40*, e38–e42. [CrossRef]

36. Ganesh, K.; Allam, M.; Wolter, N.; Bratcher, H.B.; Harrison, O.B.; Lucidarme, J.; Borrow, R.; de Gouveia, L.; Meiring, S.; Birkhead, M.; et al. Molecular Characterization of Invasive Capsule Null *Neisseria meningitidis* in South Africa. *BMC Microbiol.* **2017**, *17*, 40. [CrossRef]

37. Xu, Z.; Zhu, B.; Xu, L.; Gao, Y.; Shao, Z. First Case of *Neisseria meningitidis* Capsule Null Locus Infection in China. *Infect. Dis.* **2015**, *47*, 591–592. [CrossRef]

38. Sorhouet-Pereira, C.; Efron, A.; Gagetti, P.; Faccone, D.; Regueira, M.; Corso, A.; Group, A.S.I.W.; Gabastou, J.-M.; Ibarz-Pavón, A.B. Phenotypic and Genotypic Characteristics of *Neisseria meningitidis* Disease-Causing Strains in Argentina, 2010. *PLoS ONE* **2013**, *8*, e58065. [CrossRef] [PubMed]

39. Sadarangani, M.; Scheifele, D.W.; Halperin, S.A.; Vaudry, W.; Le Saux, N.; Tsang, R.; Bettinger, J.A.; Bridger, N.; Morris, R.; Top, K.; et al. Outcomes of Invasive Meningococcal Disease in Adults and Children in Canada Between 2002 and 2011: A Prospective Cohort Study. *Clin. Infect. Dis.* **2015**, *60*, e27–e35. [CrossRef] [PubMed]

40. Miller, F.; Lécuyer, H.; Join-Lambert, O.; Bourdoulous, S.; Marullo, S.; Nassif, X.; Coureuil, M. *Neisseria meningitidis* Colonization of the Brain Endothelium and Cerebrospinal Fluid Invasion. *Cell. Microbiol.* **2013**, *15*, 512–519. [CrossRef] [PubMed]

41. Barman, T.K.; Kumar, M.; Chaira, T.; Gangadharan, R.; Singhal, S.; Rao, M.; Mathur, T.; Bhateja, P.; Pandya, M.; Ramadass, V.; et al. Potential of the Fluoroketolide RBx 14255 against *Streptococcus pneumoniae*, *Neisseria meningitidis* and *Haemophilus influenzae* in an Experimental Murine Meningitis Model. *J. Antimicrob. Chemother.* **2019**, *74*, 1962–1970. [CrossRef]

REVIEW ARTICLE

Aging Cell

WILEY

Translatability of life-extending pharmacological treatments between different species

Daiana Burdusel[1,2] | Cristin Coman[3] | Diana–Larisa Ancuta[3] | Dirk Hermann[2] | Thorsten Doeppner[4,5] | Andrei Gresita[6] | Aurel Popa-Wagner[1,2]

[1]Doctoral School, University of Medicine and Pharmacy of Craiova, Craiova, Romania

[2]Chair of Vascular Neurology and Dementia, Department of Neurology, University Hospital Essen, Essen, Germany

[3]Cantacuzino National Medical Military Institute for Research and Development, Bucharest, Romania

[4]Department of Neurology, University Medical Center Göttingen, Göttingen, Germany

[5]Department of Neurology, University of Giessen Medical School, Giessen, Germany

[6]Department of Biomedical Sciences, New York Institute of Technology, College of Osteopathic Medicine, Old Westbury, New York, USA

Correspondence
Aurel Popa-Wagner, Doctoral School, University of Medicine and Pharmacy of Craiova, Craiova 200349, Romania.
Email: aurel.popa-wagner@geriatricshealthyageing.com

Abstract

Anti-aging research has made significant strides in identifying treatments capable of extending lifespan across a range of organisms, from simple invertebrates to mammals. This review showcases the current state of anti-aging interventions, highlighting the lifespan extensions observed in animal models through various treatments and the challenges encountered in translating these findings to humans. Despite promising results in lower organisms, the translation of anti-aging treatments to human applications presents a considerable challenge. This discrepancy can be attributed to the increasing complexity of biological systems, species-specific metabolic and genetic differences, and the redundancy of metabolic pathways linked to longevity. Our review focuses on analyzing these challenges, offering insights into the efficacy of anti-aging mechanisms across species and identifying key barriers to their translation into human treatments. By synthesizing current knowledge and identifying gaps in translatability, this review aims to underscore the importance of advancing these therapies for human benefit. Bridging this gap is essential to assess the potential of such treatments in extending the human healthspan.

KEYWORDS
aging, drug treatments, humans, invertebrates, lifespan, translatability, vertebrates

1 | INTRODUCTION

Aging is a complex biological process influenced by many factors, including genetics, lifestyle, and environmental conditions (Mak et al., 2022; Mather, 2022). Understanding the underlying mechanisms interventions to extend lifespan in aging organisms has been the focus of many studies being of interest to both scientists and the general public.

The rapid increase in life expectancy since the 20th century suggests that aging is not solely driven by genetics. Long-lived individuals without health problems are clustered in certain populations in Greece and Japan, indicating that environment and lifestyle play a significant role. Factors such as diet, education, physical activity, and early life experience all influence mortality (Amorim et al., 2022).

The hallmarks of mammalian aging include genetic instability, telomere shortening, epigenetic alterations, and metabolic disruptions. These disruptions encompass deregulated proteostasis, altered nutrient signaling, and energy shortages due to mitochondrial dysfunction. Together, they reveal a strong connection between aging, age-related diseases, and the balance of cellular energy. Indeed, accumulating data shows that aging and diseases associated with aging are closely linked to an imbalance between energy supply and demand (Amorim et al., 2022). This suggests that interventions such as exercise, dietary adjustments, and molecules targeting longevity pathways could address these factors (Amorim et al., 2022; Johnson et al., 2013; López-Otín et al., 2013). Thus, exercise is widely recognized as a crucial lifestyle change that wards off metabolic issues, including obesity and type 2 diabetes mellitus, while a lack of physical activity and a sedentary lifestyle plays a significant role in their development.

Limiting calorie intake is also a well-established method for preventing metabolic problems associated with aging across various species. When calories are restricted, there is an increase in oxidative phosphorylation (OXPHOS) and antioxidant defenses, as well as the creation of new mitochondria. Furthermore, reducing caloric intake enhances the renewal of mitochondria by promoting the formation of new mitochondria and the removal of damaged ones through the process of mitophagy (Amorim et al., 2022).

Various treatments including rapamycin, resveratrol, spermidine, and others have been proposed as potential lifespan-extending treatments (Doeppner et al., 2022). However, despite the promising results obtained in organism models such as yeast, worms, and flies, the translatability of these interventions across species of increasing complexity and to humans is still uncertain. Furthermore, the results of lifespan studies in different species and dosages are frequently inconsistent (Hector et al., 2012). Of note, many studies take into account how different types of diets can influence the aging process in distinct ways depending on the organism model (Fontana et al., 2010), adding to the complexity of the field. In addition, the testing of life-extending treatments in humans raises questions about safety, efficacy, and optimal dosage, making it challenging to identify the most promising candidates for further development.

Among the biological theories of aging, mitochondrial dysfunction, and metabolic dysregulation are key factors, impacting cellular energy management and susceptibility to oxidative stress (López-Otín et al., 2013). Treatments like rapamycin and resveratrol target these processes; rapamycin modulates the mTOR pathway, enhancing autophagy and mitochondrial health, while resveratrol activates sirtuins to improve mitochondrial function and stress resistance (Johnson et al., 2013). These interventions suggest a pathway to lifespan extension by directly addressing the cellular underpinnings of aging.

This review aims to identify the current state of knowledge on treatments and interventions that have been shown to impact the lifespan of different species. We will compare and contrast the results of different studies, such as dosage and species, to learn more about how these findings can be applied to other species and how they could be utilized in future studies involving humans.

2 | METHODOLOGY

In this study, our main focus was on exploring the existing literature concerning the translatability of life-extending treatments across various species. Specifically, we examined the effects of metformin, resveratrol, rapamycin, spermidine, and chloroquine treatments on the lifespan of *Saccharomyces cerevisiae*, *Drosophila melanogaster*, *Caenorhabditis elegans*, mice, rats, and humans. To achieve this objective, we conducted a comprehensive search of pertinent scientific literature using two major databases: PubMed and Web of Science. The search terms we employed included "metformin," "resveratrol," "rapamycin," "spermidine," "chloroquine," "lifespan," "longevity," "species comparison," "translational research," and "aging interventions." To ensure a comprehensive approach, we considered a wide array of both qualitative and quantitative studies, including primary research articles and review papers.

In selecting the drugs for our analysis, we applied stringent criteria based on their widespread study across multiple species and their documented impact on lifespan and aging-related processes. These five drugs were chosen because they have been extensively tested and reported in the literature for their effects on longevity in at least five of the six species we selected. This selection allows for a comprehensive cross-species comparison, facilitating a deeper understanding of the translatability of anti-aging interventions from model organisms to humans. The inclusion of these specific drugs in our study was also predicated on their diverse mechanisms of action, which target key pathways implicated in aging, such as mTOR signaling, sirtuin activation, autophagy, and metabolic regulation. This diversity ensures a broad examination of potential anti-aging interventions across the evolutionary spectrum, from simple unicellular organisms to complex mammals, providing insights into the fundamental processes of aging and the potential for these interventions to impact human health and longevity.

Additionally, we included governmental and non-governmental reports, statistical databases, and regulatory frameworks related to longevity research and aging interventions. Our literature search covered studies published up to the date of this review, ensuring the inclusion of the most recent research findings in the field. Given the flexibility that a review article provides, we employed a thematic analysis to synthesize the findings, identifying patterns and common themes across the selected literature.

3 | RESULTS

3.1 | Metformin

Metformin (MTF), an indirect mTOR kinase inhibitor, is a widely recognized oral medication commonly used to manage type 2 diabetes by improving insulin sensitivity and reducing blood sugar levels. It belongs to a class of medications known as biguanides. Beyond its primary role in diabetes management, there has been growing interest in exploring metformin's potential effects on lifespan and aging. Some research suggests that metformin might influence cellular and molecular pathways associated with aging, such as reducing inflammation and enhancing mitochondrial function (Du et al., 2022). These effects have led to investigations into whether metformin could have a positive impact on extending lifespan and promoting healthy aging in various organisms, including model organisms like mice (Martin-Montalvo et al., 2013). While further studies are needed to fully understand metformin's role in longevity and aging in humans (Stevenson-Hoare et al., 2023), its potential as a tool for promoting healthy aging continues to be an area of active scientific inquiry.

3.1.1 | Effects of metformin on the lifespan of *Saccharomyces*

A comprehensive study examining the impact of 25 mM metformin exposure on *Schizosaccharomyces pombe* revealed a notable extension of chronological lifespan when the compound was administered from the outset. Specifically, the inclusion of metformin in a medium containing 3% glucose led to an approximate 50% increase in chronological lifespan compared to the control group. Furthermore, the investigation analyzed the effects of glucose on lifespan. Intriguingly, it was observed that metformin exhibited an even more pronounced impact on chronological lifespan when the yeast cells were cultivated in a glucose-free environment, resulting in a remarkable 33% increase in lifespan compared to the counterparts cultured in the presence of 3% glucose (Şeylan & Tarhan, 2023).

In another study, the authors used the budding yeast's, *S. cerevisiae*, as a model for studying aging and age-related diseases. Previous studies lacked quantitative precision in identifying aging factors, prompting the authors to introduce a refined method. They

applied this method to study gene deletions' effects on lifespan, ultimately revealing a connection between protein glycosylation and metformin's ability to extend lifespan. This research highlights the power of competitive-aging and advanced modeling in understanding the mechanisms of drugs like metformin in extending lifespan from 10.7 to 15.5 days (Avelar-Rivas et al., 2020).

3.1.2 | Effects of metformin on the lifespan of *Drosophila melanogaster*

One study showed that metformin has a dose-dependent effect on the larvae's development when provided on a 4% amylose starch diet. Diets with metformin concentrations ranging from 0.1 to 25 mM did not significantly affect the larval pupariation time compared to diets without metformin. However, when flies' food was supplemented with the highest concentration of metformin (50 mM), half-pupariation time was extended by 17%.

Previous research suggests that, within the context of a sucrose diet, increasing the concentration of metformin above 10 mM leads to a dose-dependent reduction in lifespan (Slack et al., 2012). They also tried an experimental medium with 10 mM metformin. They found that at this concentration, metformin prolonged developmental time by 8% on a low-starch diet (0.25%) and accelerated pupariation by 11% on a high-starch diet (20%). This indicates that metformin partially counteracted the negative effects of high-starch concentrations on fly development. The 10 mM metformin supplementation failed to prevent the negative consequences of a starch diet and decreased the lifespan of both male and female flies (Abrat et al., 2018).

To evaluate the impact of metformin on the lifespan of *D. melanogaster* (*DM*) under different conditions, a study was conducted using wild-type flies (*Canton S*) and *Trap1*-deficient flies. *Trap1* (tumor necrosis factor receptor-associated protein 1) encodes a mitochondrial Hsp90 chaperone. The flies were also subjected to severe hypoxia in a specially designed chamber, followed by a reperfusion period of 120 h. *Trap1* deficiency resulted in significantly shorter lifespans under both normoxic and hypoxic conditions and negatively affected activity and negative geotaxis. However, the introduction of metformin appeared to mitigate the negative effects of *Trap1* deficiency on mortality rates after hypoxia, leading to decreased post-hypoxic mortality rates of 28.57% (Kokott-Vuong et al., 2021).

Another study investigated the effects of metformin on the lifespan on *DM* when administered at different concentrations (1–100 mM). For both genders, there were no significant differences in survival between flies maintained on 0, 1, 2.5, and 5 mM metformin. However, males maintained on 100 mM metformin had significantly shorter lifespans than flies maintained on 0–50 mM metformin. On the other hand, females maintained on 25, 50, and 100 mM metformin had significantly shorter lifespans than non-treated controls and flies fed with 0–10 mM metformin (Slack et al., 2012).

3.1.3 | Effects of metformin on the lifespan of *Caenorhabditis elegans*

The effect of metformin on lifespan was also tested on *C. elegans* cocultured with *Escherichia coli*. The study found that metformin increases lifespan by altering microbial folate and methionine metabolism. The percentage of median lifespan increase and maximum lifespan varied depending on the *E. coli* strain metformin sensitivity and glucose concentration. They reported an increment of lifespan with 18%, 36%, and 3% for 25, 50, and 100 mM of metformin, respectively (Cabreiro et al., 2013).

Another report showed that the lifespan of *C. elegans* was extended by 15 days compared with 12 days control group, when treated with metformin at young ages (3 days old). However, when treatment was initiated at old age (10 days old), metformin was found to be toxic at all tested doses (10, 25, and 50 mM), and shortened the lifespan, that is, 11 versus 15 days. This indicates an age-dependent decrease in metformin tolerance, which culminated in late-life toxicity of all metformin doses tested, indicating possible safety risks of late-life metformin administration (Espada et al., 2020).

3.1.4 | Effects of metformin on the lifespan of mice

In a study conducted on male mice, supplementation with 0.1% (w/w) metformin led to a significant extension of mean lifespan by 5.83% and 4.15% in two different strains of mice, C57BL/6 and B6C3F1. Higher concentrations of metformin (1% w/w) were toxic and significantly shortened mean lifespan by 14.4% in C57BL/6 mice, likely due to renal failure. Male mice treated with 0.1% metformin did not show any major differences in pathologies or obvious causes of death compared to control mice (Martin-Montalvo et al., 2013).

Another study reported that metformin given in drinking water at a concentration of 0.13 μg/mL significantly increased the medium and maximum lifespan of SHR mice by 37.8% and 10.3%, respectively. Indeed, fibroblasts obtained from the skin of metformin-treated mice showed a significant delay in the accumulation of markers of cellular senescence compared to control animals (Arkadieva et al., 2011).

3.1.5 | Effects of metformin on human health

A 20-year clinical study assessing the impact of metformin on longevity in individuals with type 2 diabetes and matched non-diabetic peers revealed that metformin initially conferred better survival within the first 3 years but later led to shorter survival times than controls after 5 years of treatment. The survival time ratio (STR) for metformin-treated patients was 0.819, indicating 81.9% of the control's survival. Sulphonylurea-treated patients exhibited even worse survival outcomes (STR of 0.799), while patients on both medications showed decreased survival for metformin patients (STR of 0.693). The hazard ratio (HR) indicated that metformin and sulphonylurea patients had a 69% and 59% higher likelihood of death, respectively, than non-diabetic controls. To conclude, while metformin demonstrated initial benefits, the study suggests that these were overshadowed by the long-term effects of type 2 diabetes over two decades (Stevenson-Hoare et al., 2023).

A comprehensive meta-analysis, involving 20 studies and 13,008 participants investigated the relationship between metformin and overall survival (OS) as well as cancer-specific survival (CSS) among individuals with both cancer and type 2 diabetes. The findings illuminated a notable survival advantage associated with metformin usage when compared to alternative glucose-lowering treatments, evident in both OS and CSS outcomes. Importantly, this favorable survival trend extended across various cancer types and countries.

The study's implications underscored metformin's potential as the preferred therapeutic option for individuals dealing with concurrent type 2 diabetes and cancer, as it exhibited enhanced OS (HR = 0.66) and CSS (HR = 0.62) compared to alternative diabetic medications (Yin et al., 2013).

3.2 | Resveratrol

Resveratrol (3, 5, and 4′-trihydroxy-trans-stilbene) is a bioflavonoid that is found in a variety of foods, including grapes, berries, and peanuts. It has been the subject of numerous studies examining its potential health benefits, including its effect on lifespan (Bass et al., 2007; Bhullar & Hubbard, 2015). Some studies have shown that resveratrol (RES) can extend the lifespan of certain species, such as yeast, worms, flies, and mice, by activating a group of enzymes called sirtuins. Sirtuins are a family of enzymes that are involved in a variety of biological processes, including metabolism, DNA repair, and regulation of gene expression. One member of this family, SIRT1, has been extensively studied in the context of aging and lifespan extension (Lee et al., 2016; Wang et al., 2013).

3.2.1 | Effects of resveratrol on the lifespan of *Saccharomyces cerevisiae*

In yeast, resveratrol exhibits a remarkable ability to replicate the positive effects of calorie restriction on lifespan extension. This is achieved through its capacity to stimulate Sir2, a crucial protein involved in maintaining DNA stability and repair processes within the cell. This activation leads to an extension of the yeast's lifespan, often by as much as 70% (Howitz et al., 2003).

Pannakal et al. demonstrated a dose-dependent capacity to increase chronological lifespan of *S. cerevisiae*, with the most pronounced effect seen at 1 μg/mL. This concentration significantly extended mean lifespan from 5.61 ± 0.10 days (for the vehicle control) to 7.48 ± 0.07 days (at 10 μg/mL) and 8.44 ± 0.04 days (at 1 μg/mL). At the optimal 1 μg/mL concentration, the yeast extract leads to a substantial 34% increase in mean lifespan and an impressive 41% extension of overall lifespan. While the TORC1

signaling pathway plays a role in this extension, it is noteworthy that the *Gcn5*, *Sir2*, and *Snf1* pathways are not required, suggesting a pathway-independent mechanism for this lifespan enhancement (Pannakal et al., 2017).

3.2.2 | Effects of resveratrol on the lifespan of *Drosophila melanogaster*

In a representative study on *DM*, resveratrol was added to five different diets (CR calorie restriction diet, HS-LP high sugar–low protein diet, LS-HP low sugar–high protein diet) at concentrations of 100, 200, or 400 μM, 48 h after hatching, to male and female groups of wild-type Canton S and sodRNA1 knockdown flies, respectively. Thus, for the Canton S flies kept on the base diet or the calorie-restricted base diet, no effect on the lifespan was reported for either 100 or 200 μM RES. Male *Sod1* knockdown (sodRNAi) worms kept on a base diet supplemented with 400 μM RES experienced a lifespan *decrease* of 9.6%. However, 200 μM RES increased the lifespan of female *Sod1* knockdown worms (sodRNAi) kept on a standard diet by 8.7%. The change in the survival percentage decreased to 7% at 400 μM RES. The highest significant increase in lifespan, approximately 15%, was observed in association with an LS-HP diet and 200 μM RES in Canton S females. In this study, 100 μM RES did not influence the lifespan. In contrast, Canton S males kept on the LS-HP diet experienced a small lifespan increase (7.8%) at 100 μM that decreased to 3% at the 200 μM dose. For the Canton S flies kept on the base diet or the calorie-restricted base diet, no effect on the lifespan was reported for either 100 or 200 μM RES. Resveratrol had no significant effect on LS when they were kept on an HS-LP diet. On the contrary, RES had a significant effect on PS females, with an increase of 11.4% in sodRNAi worms kept on the HS-LP diet (Wang et al., 2013). The different results observed between the wild-type and *Sod1* knockdowns suggest the potential involvement of the enzyme superoxide dismutase 1 in resveratrol's mechanism of action. This could be due to lower levels of this enzyme in *Sod1* knockdown flies (Denu, 2005; Martin et al., 2009).

Another study examined the effect of RES on *DM*, utilizing male and female flies of the ORR and Harwich strains. The treatment started 48 h after eclosion, and the flies were kept either on corn-meal (control) or corneal supplemented with 31.54 μg/L RES. When compared to the control group, the findings revealed that both male and female flies who received RES had a longer lifespan, with an increase of up to 40.7% in the ORR strain and 41.4% in the Harwich strain with similar results for both genders (Islam et al., 2019).

In a study conducted by Khan et al., the researchers examined the effects of resveratrol-enriched rice callus (at a concentration of 5.7 mg/L) on 48-h-old male and female ORR and Harwich flies, under similar experimental conditions to ensure comparability. The results showed that the resveratrol rice DJ526 callus had a significant impact on the median lifespan of all the wild-type flies tested—ORR males and females, Harwich males and females. Specifically, it extended their median lifespans by 30%, 20%, 50%, and 36%,

respectively, when compared to the control group. Interestingly, notable differences were observed in the extent of the lifespan extension between males and females (Khan et al., 2019).

Another experiment compared the effect of resveratrol supplementation on DTT (DJ651-driven tetanus toxin) and wild-type Canton S flies. Significant results were observed at a concentration of 200 μM RES, which increased the lifespan in DTT males by 9% and in females by 8%. In Canton S flies, the lifespan increased by 10% in males and 17% in females (Bauer et al., 2004).

3.2.3 | Effects of resveratrol on the lifespan of *Caenorhabditis elegans*

Next, we examined the effect of resveratrol and oxyresveratrol on the lifespan of *C. elegans*. Both RESI and oxyresveratrol (ORES) increased the mean lifespan (MLS) of the wild-type worms compared to the control group. The MLS of worms treated with RES at concentrations of 100, 500, and 1000 μM increased by 22.2%, 23.7%, and 30.4%, respectively. The MLS of worms treated with ORES at concentrations of 100, 500, and 1000 μM increased by 7.4%, 17.8%, and 31.1%, respectively. These results suggest that both RES and ORES can extend the lifespan of *C. elegans*, with RES having a more substantial effect. However, the sir-2.1 mutants did not exhibit a lifespan increase. Sir-2.1 is a member of the Sir-2 family of NAD+-dependent protein deacetylases, has been shown to regulate nematode aging via the insulin/IGF pathway transcription factor *daf-16*. However, the mechanisms behind this lifespan extension and whether it is dependent on the Sir-2.1 gene were not examined in this study (Lee et al., 2016).

The effects of the antioxidant and radical scavenging activity of resveratrol have been mostly tested in *C. elegans* treated with free radical-producing chemicals, such as juglone and paraquat. Thus, under stressful conditions, *C. elegans* wild-type N2 var. Bristol strain pretreated with RES at concentrations of 50, 100, and 200 μM for 72 h at 18°C experienced an expansion of lifespan by 53.1%, 30.1%, and 15.6%, respectively. The lethal stressor used was 10 μg/mL juglone (Rea et al., 2005).

Two-day-old *C. elegans* wild-type strain nematodes were treated with 50 μM of RES to assess its effect on lifespan. The results showed an enhancement of medium lifespan (mLS) and maximum lifespan (MLS) by 64% and 30%, respectively. Additionally, when exposed to highly toxic paraquat, the treated group had a higher average survival time (Gruber et al., 2007).

3.2.4 | Effects of resveratrol on the lifespan of mice

In a study focused on understanding the impact of dietary and resveratrol interventions on longevity, cohorts of middle-aged male C57BL/6NIA mice were strategically divided. These groups were exposed to distinct dietary regimens: a standard diet (SD) and a high-calorie (HC) diet composed of 60% fat calories. To

explore the potential of resveratrol, two varying concentrations were incorporated into both diet categories—approximately 5.2 and 22.4 mg/kg/day. The results revealed among mice on the HC diet, those treated with resveratrol (HCR group) exhibited a distinct survival advantage, a phenomenon that became apparent at around 60 weeks. By the time the study reached 114 weeks, the disparity in survival rates became more pronounced: 58% of mice kept on HC diet had succumbed, whereas a substantially lower 42% mortality rate was observed among both HCR mice and those on the SD (Baur et al., 2006). Additionally, combining the effects of alternate-day fasting with the lower dose of resveratrol extended both mean and maximum lifespans by 15% in comparison to SD controls. However, applying a higher dose of resveratrol from the age of 12 months (SDHR) did not significantly influence longevity. Notably, under an SD regimen, resveratrol failed to enhance OS or maximum lifespan (Miller et al., 2011; Pearson et al., 2008).

In humans, resveratrol has been tested in an open-label, single-arm, phase IIa trial to determine if it provides therapeutic benefits to patients with Duchenne, Becker, or Fukuyama muscular dystrophies. The results suggest that resveratrol offers benefits in terms of quantitative muscle testing and serum creatine kinase levels for these patients (Kawamura et al., 2020).

3.3 | Rapamycin

Rapamycin (RAPA) is a drug originally discovered in a soil sample from Easter Island. It has been shown to have anti-aging properties in various organisms including yeast, worms, flies, and mice. The mechanisms by which rapamycin extends lifespan are not yet fully understood, but it is believed to work by inhibiting the target of the rapamycin (TOR) signaling pathway, which plays a role in growth, proliferation, and aging (Villa-Cuesta et al., 2014). Rapamycin has also been found to improve healthspan, which refers to the period of life during which an organism is healthy and able to function well.

3.3.1 | Effects of rapamycin on the lifespan of *Saccharomyces*

A study that investigated the effect of rapamycin on the lifespan of yeast at various concentrations, ranging from 0.1 to 40 nM, revealed that rapamycin extends MLS in yeast strains, except for atg1Δ and atg7Δ strains, which are deficient in autophagy-related genes. The most significant extension of lifespan occurs at 10, 20, and 40 nM concentrations. Interestingly, lower concentrations of rapamycin (0.1 and 1 nM) do not impact CLS. Notably, the extension of lifespan correlates with rapamycin-induced upregulation of macroautophagy during chronological aging. These findings emphasize the role of autophagy in rapamycin's ability to extend yeast lifespan, suggesting that autophagy modulation may hold promise for enhancing longevity and healthspan (Alvers et al., 2009).

In another research study that examined the impact of caffeine and rapamycin on chronological lifespan in yeast maintained on two different types of medium, namely, YES media (with 3% glucose) and EMM (with 2% glucose), it was revealed that in the nutrient-rich medium, rapamycin exerted a notable increase in lifespan compared to caffeine and the control group. When compared to the control group, rapamycin treatment resulted in a 57% increase in lifespan (Rallis et al., 2013).

3.3.2 | Effects of rapamycin on the lifespan of *Drosophila melanogaster*

The idea that rapamycin treatment during early developmental stages contributes to longevity control was assessed experimentally using the *wiso31 Drosophila* strain for both males and females. Thus, the treatment was initiated during the third larval stage, employing varied rapamycin concentrations (1, 50, or 200 μM) from 72 h post-egg laying until either the pupal stage or days 0 to 10, and days 10 to 20. The findings revealed distinct effects of different rapamycin concentrations on lifespan. For concentrations of 1 and 50 μM rapamycin, there was no significant change in median lifespan observed in either males or females, irrespective of the treatment window. In contrast, administering 200 μM rapamycin extended the median lifespan when examining both genders collectively. Specifically, treatment of males during days 0–10 resulted in a significant increase in median lifespan, rising from 61 days (control) to 66 days (rapamycin-treated). Interestingly, female flies did not show a significant increase in median lifespan during this treatment period. To confirm that the time frame of treatment is more important than the duration of treatment, the researchers additionally administered 200 μM rapamycin from day 10 to 20, yet this had no impact on lifespan. These findings highlight the gender-specific impact of early-stage rapamycin treatment on *DM* longevity, reinforcing the importance of precise timing for achieving significant effects (Aiello et al., 2022).

Another study investigated the effect of rapamycin treatment on the lifespan of various strains of *D. melanogaster*, including wild-type, null mutants, and strains with manipulated gene expression. The results showed that a concentration of 200 μM resulted in a 13% increase in lifespan for female wild-type flies, while male flies showed a 6% increase. Female flies exposed to lower (50 μM) and higher (400 μM) concentrations exhibited a 9% and 10% increase in lifespan, respectively. Additionally, the study examined the impact of rapamycin treatment under paraquat treatment conditions. The findings revealed that the flies experienced a 70% increase under oxidative stress conditions induced by paraquat injection, suggesting that the effect of rapamycin on lifespan involves more factors than just targeting the nutrient-sensing TOR pathway, as the enhancement of the stress resistance of the cell through upregulation of antioxidant defense systems or enhancement of DNA repair, mechanisms autophagy activation that can also help the reduction of the reactive oxygen species (ROS) and a metabolic shift toward enhance mitochondrial efficiency or alter energy production

pathways to reduce ROS production and reduce oxidative damage (Bjedov et al., 2010; Shaposhnikov et al., 2022).

DM's lifespan is largely determined by amino acid imbalances, and food restriction is typically performed by diluting yeast as a protein source (Grandison et al., 2009). The effect of rapamycin on the lifespan of Drosophila, when fed various yeast diets known to extend longevity, was investigated. The researchers also included a starvation diet consisting of 0.8% w/v agar in water without additional nutrients. Rapamycin was added to the diets at various concentrations (5, 50, 100, 200, and 400 μM) to examine its dose-dependent effects and the presence-absence effects on the survival of Drosophila strains wDha and OreR. The study found that rapamycin's impact on *D. melanogaster* (DM) lifespan varied depending on the diet, with some diets showing a significant increase in lifespan and others showing no effect. The most promising results were observed at rapamycin concentrations ranging from 50 to 200 μM, which significantly extended the MLS of flies fed a 2% yeast diet. The maximum extension was achieved at 200 μM rapamycin with a lifespan increment of 9% (Villa-Cuesta et al., 2014).

3.3.3 | Effects of rapamycin on the lifespan of *Caenorhabditis elegans*

Transcriptomic studies were conducted using *C. elegans* (CL2070) to explore the impact of rapamycin treatment on lifespan and the accumulation of insoluble proteins as organisms age. To ensure age synchronization in the study, a germline-deficient strain (JK1107) was utilized to generate cohorts of worms. At 72 h of life, the worms were administered either 100 μM rapamycin or a control vehicle. The findings revealed that the rapamycin treatment led to a mere 9% increase in lifespan. Furthermore, compared to the control group, the animals receiving rapamycin only achieved this level of extension on day 8 of life (Yee et al., 2021).

Another study showed that treatment of *C. elegans* WT with rapamycin had a maximum lifespan of 31.35 days, which is a 29% increase compared to the control group (Robida-Stubbs et al., 2012).

3.3.4 | Effects of rapamycin on the lifespan of mice

The National Institute on Aging's Intervention Testing Program (ITP) conducted a pioneering study across three locations: The Jackson Laboratory, the University of Michigan (UM), and the University of Texas Health Science Center (UT). The research identified rapamycin as the first drug able to extend the maximum lifespan of mice. In this study, mice were provided with food containing 14 parts per million (ppm) of rapamycin. The investigation involved both male and female mice and initiated treatment either after 270 days or after 600 days of age. The study found that both treatment timelines effectively extended the maximum lifespan of UM-HET3 mice by 14% for females and 9% for males

(Harrison et al., 2009). Furthermore, researchers observed that the combination of rapamycin and acarbose, a drug used for managing type 2 diabetes, substantially extended the median lifespan of 9-month-old UM-HET3 mice. The study revealed an average lifespan increase of 28% for female mice and 34% for male mice. When the same treatment regimen was applied to 16-month-old mice, an overall 13% lifespan extension was observed for both genders. A closer look at the data revealed that the treatment consistently improved longevity for females across all labs, while for males, only the UT lab showed a significant 32% lifespan increase (Miller et al., 2011). In a subsequent investigation at the ITP location, it was found that the oral administration of 4.7, 14.4, or 42 ppm of rapamycin to UM-HET3 mice, initiated at 9 months, had a significant positive effect on the maximum and median lifespan of female mice. Furthermore, the two higher doses (14 and 42 ppm) significantly increased the lifespan of male mice, including both maximum and median lifespan extension (Miller et al., 2014).

The impact of administering rapamycin to male and female mice after birth was also reported. Specifically, rapamycin at a dosage of 10 mg/kg was given to the mice from postnatal day 4 to day 30 (P4–P30) or from day 30 to day 60 (P30–P60). In the P4–P30 group, both genders exhibited an approximate 9.6% increase in maximum lifespan, whereas no notable alterations were observed in the P30–P60 group (Aiello et al., 2022).

3.3.5 | Effects of rapamycin on human health

While its beneficial effects on lifespan extension are well-documented in model organisms, the application to human aging remains exploratory. Notably, a recent study on the mTOR inhibitor RAD001 offers promising insights, showing improved immune function in elderly humans, as evidenced by enhanced responses to influenza vaccination. This finding opens the door to further investigations into whether mTOR inhibition can positively impact a broader range of aging-related conditions in humans (Mannick et al., 2014, 2018).

In humans, it is worth nothing that although people on an "every other day" diet with resveratrol seemed to live longer, this difference was not statistically significant (Pearson et al., 2008). Another study conducted in overweight and slightly obese patients for 4 weeks did not confirm any significant differences in the cardiovascular and metabolic risk markers between groups, after daily resveratrol intake. Presently, several clinical trials are being conducted to assess the safety and effectiveness of resveratrol in humans, and initial findings have shown promise (Berman et al., 2017; de Cabo et al., 2014; Kawamura et al., 2020; Longo et al., 2015; Ramírez-Garza et al., 2018).

Increased oxidative stress has been associated with muscular dystrophy. Resveratrol, an activator of the protein deacetylase SIRT1 and an antioxidant, decreases muscular and cardiac oxidative damage and improves pathophysiological conditions in animal models of muscular dystrophy (MD). This suggests that resveratrol may offer therapeutic benefits to patients with muscular dystrophies (Kawamura et al., 2020).

Other phase I, II, and III clinical trials have utilized rapamycin to inhibit the signal transduction induced by most cytokines, offering a unique method to both disengage the immune response and inhibit injuries not dependent on antigens (Taner et al., 2005).

Unfortunately, all studies involving humans were conducted on patients suffering from various diseases.

3.4 | Spermidine

Spermidine is a naturally occurring polyamine that is present in a variety of foods and is gaining recognition for its potential health benefits (Kiechl et al., 2018). Spermidine is involved in several cellular processes, including DNA synthesis, cell growth, and autophagy. Spermidine has been shown to possess anti-inflammatory and antioxidant properties and has been the subject of several studies for its potential role in the aging process and age-related diseases. While the full extent of its benefits has yet to be understood, spermidine is gaining attention as a promising agent for promoting health and wellness, especially as it relates to aging. With ongoing research, we may discover more about the potential benefits of spermidine and how it can be used to improve health and longevity.

3.4.1 | Effects of spermidine on the lifespan of *Saccharomyces cerevisiae*

The anti-aging effects of spermidine have been initially tested on yeast cells as a model system. Chronological aging experiments revealed that yeast cells lacking ornithine decarboxylase experienced increased mortality and a shortened lifespan. However, supplementation with spermidine, particularly at low doses of 0.1 mM, led to a remarkable increase in lifespan, up to fourfold compared to untreated cells. Additionally, higher concentrations of spermidine were found to extend the lifespan of wild-type yeast cells with various genetic backgrounds. The specific doses of spermidine used in this study demonstrated its significant impact on longevity in yeast. Furthermore, spermidine treatment not only slowed down chronological aging but also rejuvenated replicative old yeast cells. These long-lived yeast cells also exhibited improved stress resistance. These findings underscore the potential of spermidine in promoting cellular longevity, with low doses showing substantial benefits in terms of lifespan extension (Eisenberg et al., 2009). A more recent study confirmed previous results, although the median survival was extended only by 33% (Su et al., 2021).

3.4.2 | Effects of spermidine on the lifespan of *Drosophila melanogaster*

A study conducted by Eisenberg et al. explored the extension of longevity through the stimulation of autophagy and examined the mechanisms involved. The study found that supplementing the *DM* W1118 strain with varying concentrations of spermidine (0.01, 0.1, 1, 4, and 10 mM) for both male and female flies resulted in an increased lifespan of up to 30%, particularly at the concentration of 1 mM (Eisenberg et al., 2009).

3.4.3 | Effect of spermidine on the lifespan of *Caenorhabditis elegans*

One study found that treating *C. elegans* with 0.2 mM spermidine upon reaching adulthood led to an increased lifespan of up to 15%. Next, the investigators tested the hypothesis that spermidine extends the lifespan by modulating autophagy. They compared the lifespan of wild-type nematodes with that of the autophagy-deficient *bec-1* (*RNAi*) strain and found that the MLS of the wild-type strain was about 25% higher than that of the *bec-1* (*RNAi*) strain (Eisenberg et al., 2009).

The experiments conducted in the same study provided support for the positive effects of spermidine on the lifespan of *C. elegans*. Both the wrn-1 (gk99) and N2 wild-type strains were treated with varying concentrations of spermidine (1, 5, 10, and 20 mM). The most effective dose was found to be 5 mM, which resulted in a lifespan extension of approximately 36%.

3.4.4 | Effects of spermidine on the lifespan of mice

A study was conducted to examine the effect of polyamine administration on cardiovascular diseases in both male and female C57BL6 mice. The study divided the mice into two groups: one receiving lifelong treatment (starting at 4 months) and the other receiving late-in-life treatment (starting at 18 months). The results showed that the lifespan of the mice increased by approximately 10% under polyamine administration. However, it was observed that the group receiving lifelong treatment had a higher likelihood of experiencing toxic effects compared to the group receiving late-in-life treatment (Eisenberg et al., 2016).

Finally, administration of spermidine enhanced cardiac autophagy, mitophagy, and mitochondrial respiration. Additionally, it improved the mechanical and elastic properties of cardiomyocytes in vivo, accompanied by elevated titin phosphorylation and the suppression of subclinical inflammation. However, in mice deficient in the autophagy-related protein Atg5 specifically within cardiomyocytes, spermidine supplementation did not convincingly confer cardioprotective effects. This suggests that the primary beneficial effect of spermidine is to enhance autophagy in cardiomyocytes (Eisenberg et al., 2016).

Despite numerous studies demonstrating an increase in lifespan in lower and higher organisms such as mice, our research team did not observe any statistically significant outcomes in a study involving Sprague–Dawley male rats treated with a daily dosage of 25 mg/kg of spermidine, starting from 18 months of age. However, we did observe notable enhancements in behavioral tests assessing motor function, anxiety, and memory. Additionally, when examining brain

tissue, we observed an improvement in brain autophagy and a reduction in neuroinflammation (Filfan et al., 2020).

3.4.5 | Effects of spermidine on human health

A recent study examined the effect of spermidine on peripheral blood mononuclear cells isolated from young and healthy individuals (under 35 years old). The cells were treated in vitro with different concentrations of spermidine (0 nM, 0.2 nM, 2 nM, 20 nM, and 2 μM) for 12 days. The authors investigated the effects of spermidine supplementation by comparing the survival rates of cells treated at 1 and 7 days after extraction. The results showed that the control group had a survival rate of approximately 15%. In contrast, the cells supplemented with spermidine at a 20 nM dose demonstrated a survival rate of up to 50% (Eisenberg et al., 2009).

Recently, a small population-based study has shown that nutrition rich in spermidine, divided into three groups (<62.2 μmol/day; 62.2–79.8 μmol/day; >79.8 μmol/day) based on quinquennial food-frequency questionnaires is linked to increased survival in humans. The survival advantage was driven by a reduced risk of death from all major causes (Kiechl et al., 2018).

In a preclinical research study, a 28-day toxicity test was conducted on a group of mice using the highest dose of 60 mg/kg of spermidine. Post-mortem histological data revealed no significant organ damage, except for a 12% increase in kidney weight compared to the control group. Subsequently, the authors performed a translational study to examine the impact of spermidine supplementation using a spermidine-rich plant extract equivalent to 41 mg/kg on cognitive function, mental status, and laboratory parameters in humans. The reported results showed no significant differences in weight, vital signs, clinical chemistry, and hematological parameters of safety. Additionally, there were no discernible differences in self-reported physical and mental health between the spermidine and placebo-treated groups at the end of the 3-month intervention. The spermidine treatment was deemed safe and well-tolerated (Schwarz et al., 2018).

3.5 | Chloroquine

Chloroquine (CQ), known for its effectiveness in treating malaria and reducing inflammation, has been employed for various medical conditions including systemic lupus erythematosus and rheumatoid arthritis. Recently, CQ has also shown potential in the treatment of cancers and viral infections (Zhou et al., 2020).

3.5.1 | Effects of chloroquine on the lifespan of mice

The role of CQ as an autophagy inhibitor has garnered recent attention, with investigations focusing on its potential opposing effect to spermidine on lifespan in model organisms (Doeppner et al., 2022). Against all odds, male NMRI mice treated with chloroquine at a dose of 50 mg/kg/day, starting at 500 days old and continuing for 286 days, significantly outlived the control group, with an average lifespan of 786 days compared to 689 days in the controls. Furthermore, the median lifespan and the maximum lifespan were also significantly different between the two groups. Chloroquine treatment at a dose of 50 mg/kg extended the median lifespan of middle-aged NMRI male mice by 11.8% and the maximum lifespan by 11.4% (Doeppner et al., 2022).

3.5.2 | Effect of chloroquine on the lifespan of rats

Another study treated 24-month-old Sprague–Dawley rats with a low dose of chloroquine (0.1 mg/kg) twice a week for 5 months. The study demonstrated an extended lifespan in aged rodents, with a 6% increase in median lifespan and a 13% increase in maximum lifespan. This effect was attributed to the reduction of tissue fibrosis and chronic inflammation (Li et al., 2022).

4 | DISCUSSION

In this narrative review, we explored the translatability of findings from longevity studies utilizing diverse drug treatments across various species and their potential applications to humans. It is important to note that our study specifically excluded nutritional approaches, such as caloric restriction and intermittent fasting. The results are summarized in Tables S1–S5.

While our study primarily focuses on the effects of non-genetic (pharmacological) interventions on lifespan across various species, it is important to acknowledge the significant contributions of genetic studies to our understanding of aging. Notably, a wide-scale comparative analysis of longevity genes and interventions has revealed that manipulations of orthologous longevity genes often result in concordant effects on lifespan across different model organisms, despite their significant evolutionary distance. This underscores the potential universality of certain aging mechanisms and highlights the importance of both genetic and pharmacological approaches in unraveling the complexities of aging. Such findings complement our pharmacological intervention data by suggesting that targeting fundamental biological pathways, whether through genetic or pharmacological means, holds promise for influencing lifespan and healthspan across species (Yanai et al., 2017).

The pursuit of increasing healthy lifespan is of interest to many academic disciplines, including biogerontology, medicine, and biochemistry (Harrison et al., 2009). In recent years, numerous studies have investigated the potential of diverse treatments in prolonging life and delaying age-related illnesses in animal models. Well-documented treatments across species of increasing complexity include drugs such as rapamycin, resveratrol, spermidine, chloroquine, and even medications historically employed for treating

different diseases, like metformin, which is used in the management of type 2 diabetes (Cabreiro et al., 2013; Martin-Montalvo et al., 2013).

The decreasing magnitude of the positive effect with increasing complexity in anti-aging treatments is obvious (Figure 1). Thus, we noted the positive effects of metformin decreased from 50% in *S. cerevisiae* to negligible (if any) effects in humans. Similarly, the effects of resveratrol decreased almost linearly from 70% in *S. cerevisiae* to 41% in *DM*, to 30% in *C. elegans*, to 26% in rodents.

The impact of rapamycin on lifespan across species decreased progressively, from 57% in *S. cerevisiae* to approximately 29% in *DM*, further declining to 25% in *C. elegans*, and ultimately reaching 13% in rodents (Figure 1).

Among the interventions explored, rapamycin, through its inhibition of the mTOR pathway, has been documented to extend lifespan and delay aging-associated diseases across numerous species, signifying its role in regulating aging processes (Johnson et al., 2013). Various mechanisms have been proposed to explain the effect of rapamycin on longevity. Specifically, the regulation of the mTORC1 component raptor (*daf-15*) by rapamycin has been demonstrated to extend lifespan in the nematode *C. elegans*. Further studies conducted on the fruit fly *D. melanogaster* have shown that mutations in mTOR and various other components of the mTORC1 pathway can also prolong lifespan in these organisms (Johnson et al., 2013; Kaeberlein et al., 2015; Sharp & Strong, 2023). Decreased signaling via the insulin/IGF-1 pathway (IIS) has been linked to increased lifespan in species such as nematodes, fruit flies, and mice. The activity of mTOR is stimulated by IIS through the action of AKT, and mTORC1 has the ability to downregulate IIS via S6K, which in turn suppresses the insulin receptor substrate 1 (IRS-1). Further research has shown that in mammalian cells, FOXO3A can control the expression of tuberous sclerosis protein 1 (TSC1), a regulatory factor that inhibits mTORC1. Additionally, it has been found that 4E-BP1, a target of mTORC1, is also regulated by FOXO in fruit flies (Johnson et al., 2013; Mannick & Lamming, 2023).

It has been proposed that aging and age-associated illnesses are influenced by nutrient detection. Thus, it is hypothesized that the overall nutritional status within multicellular organisms is monitored via both overarching and cellular-level nutrient detection mechanisms. The overarching system governs the release of hormonal signals into the bloodstream, such as GH, IGF-1, and insulin. These hormones interact with cell surface receptors, triggering pathways inside the cell related to nutrient signaling. On a cellular level, indicators like ATP/ADP ratios, NADH/NAD+ levels, amino acid concentrations, and the status of ribosome assembly directly influence cellular pathways, thereby altering how cells respond to hormones in the bloodstream. The way in which the various tissues and cell types of multicellular organisms respond is intricately managed through the unique expression of cellular factors and receptors, the specific nature of systemic factors, and the presence of tissue-specific and circulating elements that adjust biological activity. These complex networks of signals are designed to prioritize growth and reproduction over cellular repair and maintenance. Persistent activation of these nutrient-sensing signals is a key factor in the process of aging and the development of various chronic conditions that often accompany older age (Johnson, 2018).

Thus, now we know that if any anti-aging rapamycin treatment is to be effective, it should commence after growth is completed. This timing is crucial to directly inhibit aging without affecting developmental growth. Of note, in post-development, mTOR is hyperfunctional and, therefore, a suitable anti-aging target for inhibition (Blagosklonny, 2022).
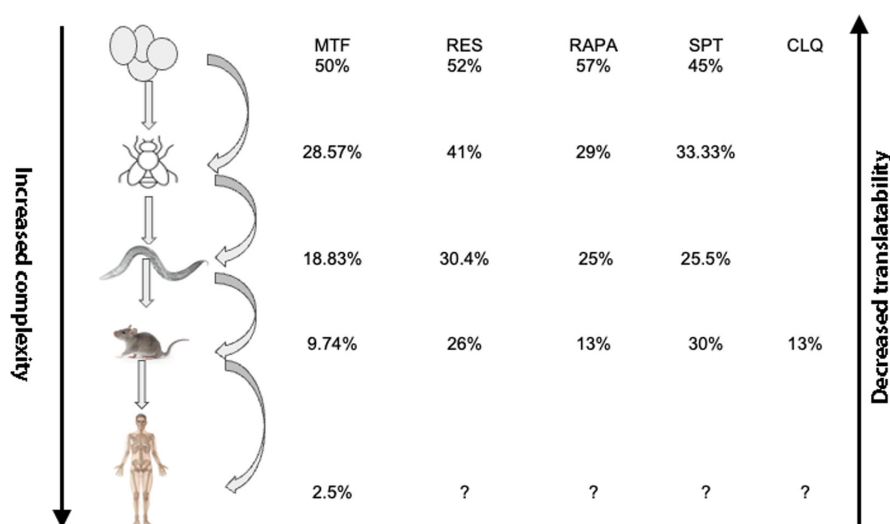
FIGURE 1 The decreasing magnitude of the positive effect with increasing complexity in anti-aging treatments is obvious. For example, we noted that the positive effects of metformin decreased from 50% in *Saccharomyces cerevisiae* to negligible (if any) effects in humans. Similarly, the effects of resveratrol decreased almost linearly from 70% in *S. cerevisiae* to 41% in *DM*, to 30% in *Caenorhabditis elegans*, to 26% in rodents. In humans, it is worth noting that although people on an "every other day" diet with resveratrol seemed to live longer, this difference was not statistically significant. For details, see Tables S1–S5.

The anti-aging drug spermidine is relatively new. The autophagy-inducing agent, spermidine, has become available, which may mirror the effects of caloric restriction. Autophagy plays a vital role in cellular balance, and its dysregulation can lead to various issues including impaired stress responses. Although it did show positive results for lifespan extension in lower organisms, a recent study on aged rats showed that spermidine, when given in drinking water, did not extend either the median or the maximum lifespan of middle-aged male Sprague–Dawley rats. However, spermidine treatment had a beneficial effect on body weight and was associated with a reduction in anxiety and an increase in curiosity, as assessed by exploratory behavior.

Other positive effects of spermidine treatment were recently reported on mice fertility. Mice give birth to litters, and their litter size is affected by aging. Young mice often give birth to 14 pups at a time, while older mice normally give birth to only three. However, older mice given spermidine gave birth to an average of six (Zhang et al., 2023).

In humans, longer-term spermidine supplementation in participants with subjective cognitive decline did not modify memory and biomarkers compared to the placebo. However, exploratory analyses indicated possible beneficial effects on verbal memory and inflammation, which need validation in future studies at higher dosages (Schwarz et al., 2022).

Notably, antidepressants influence autophagy pathways. Spermidine supplementation might offer benefits for psychiatric conditions, presenting a safe, affordable, and easy adjunct to current treatments. The project's goal is to study the clinical effects of spermidine, correlated with molecular profiling (ClinicalTrials.gov ID NCT04823806).

A new anti-aging agent is chloroquine, the effect of which was discovered on mice longevity during the COVID pandemic (Doeppner et al., 2022). Several studies are underway in our laboratory to investigate the effect of chloroquine on lifespan and health of mice and rats.

5 | CONCLUSIONS

Although animal studies offer valuable insights into biological mechanisms and potential interventions, their applicability to species of varying complexity, including humans, has been limited. Despite of these difficulties, there is an increasing curiosity in investigating the possibilities of longevity interventions in the human population.

The translatability of longevity treatments to humans can be influenced by various factors, including the dosage or schedule employed in animal studies. There are instances where the dosages utilized in animal studies may not be practical or safe for human use, necessitating adjustments to achieve the intended outcome. Furthermore, variances in diet, gender, and strain among animal models can also impact the efficacy of treatments, posing difficulties in extrapolating the findings to humans (Schwarz et al., 2018; van der Made et al., 2015).

The limited translatability between species of increasing complexity can be explained by a number of factors:

1. The effectiveness or significance of the targeted molecule from a pathway might differ in various metabolic scenarios. For example, the anti-aging mechanisms of resveratrol primarily involve ameliorating oxidative stress by scavenging ROS. However, ROS play a more significant role in flying species like Drosophila than in mammals, which may possess additional mechanisms to counteract ROS. Indeed, recent research has revealed a more complex and beneficial role of ROS in regulating metabolism, development, and lifespan (Popa-Wagner et al., 2013; Santos et al., 2018).

2. Second, the weight of targeted signaling pathways differs for a species' general metabolism. Therefore, single mutations that reduce insulin/IGF-1 signaling can significantly increase the lifespan of simple organisms such as *C. elegans* and *D. melanogaster*. However, the increased complexity of the pathway, attributed to additional regulators like insulin and growth hormone, has made it challenging to distinguish the roles of each key component in mammalian longevity.

3. Third, redundancy in pathways is a widespread phenomenon in species of increasing complexity, observed across all forms of life. It has developed as a safeguard against disturbances that might otherwise interfere with essential processes, such as mutations or shifts in the environment. Thus, blocking one pathway does not necessarily impede the cellular or organismal process.

4. Forth, as we make progress into research on anti-aging therapies, the challenges posed by the increasing complexity of species remind us that, much like many aspects of biology and medicine, there exists a law of diminishing returns. While the initial interventions may yield significant and noticeable impacts, the subsequent benefits might be less pronounced with the addition of more layers of complexity and control.

Additional research is necessary to assess the safety and efficacy of these findings within human populations. Various factors, such as genetic variations, metabolic disparities, the age at which treatment begins, duration of treatment, dosage, and environmental influences, can all affect the effectiveness of treatments across different species. For instance, certain treatments that extend lifespan in rodents may not yield identical outcomes in humans due to differences in drug metabolism or pharmacokinetics. We believe that mice genetics, enabling to pinpoint crucial pathways involved in longevity and medical genetics offering drugs developed using gene technologies on are the key for future studies on aging.

The future of aging research, especially in mouse and medical genetics for drug development using gene technologies, is very promising. Mouse genetics provides deep insights into aging mechanisms, potentially leading to human aging process breakthroughs. Medical genetics offers prospects for targeted therapies that could slow aging or lessen its negative effects, with gene technology enabling personalized medicine for more effective treatments

with fewer side effects. Additionally, combining computational models, bioinformatics, and systems biology could fast-track the identification of genes and pathways related to longevity, improving our grasp of factors that influence lifespan and healthspan. In the future, prospects for targeted therapies could benefit from two comprehensive databases on anti-aging drugs and interventions, DrugAge (Barardo et al., 2017) and Geroprotectors (Moskalev et al., 2015).

Finally, with the increasing complexity of organisms, targeting only one pathway is unlikely to consistently extend lifespan. Healthy aging might be a more realistic aim of anti-aging research.

AUTHOR CONTRIBUTIONS

Conceptualization, A.P.-W. and C.C.; methodology and investigation, D.B; writing—original draft preparation, A.P.-W. and D.B.; review and editing, D.H., T.D. and A.G.; funding acquisition, A.P.-W. and D.H.

ACKNOWLEDGMENTS

FUNDING INFORMATION

CONFLICT OF INTEREST STATEMENT

No conflicts of statement to declare.

DATA AVAILABILITY STATEMENT

The data that support the findings of this study are available from the corresponding author upon reasonable request.

ORCID

Aurel Popa-Wagner https://orcid.org/0000-0003-4574-8605

REFERENCES

Abrat, O. B., Storey, J. M., Storey, K. B., & Lushchak, V. I. (2018). High amylose starch consumption induces obesity in *Drosophila melanogaster* and metformin partially prevents accumulation of storage lipids and shortens lifespan of the insects. *Comparative Biochemistry and Physiology Part A: Molecular & Integrative Physiology*, *215*, 55–62. https://doi.org/10.1016/j.cbpa.2017.10.011

Aiello, G., Sabino, C., Pernici, D., Audano, M., Antonica, F., Gianesello, M., Ballabio, C., Quattrone, A., Mitro, N., Romanel, A., Soldano, A., & Tiberi, L. (2022). Transient rapamycin treatment during developmental stage extends lifespan in *Mus musculus* and *Drosophila melanogaster*. *EMBO Reports*, *23*(9), e55299. https://doi.org/10.15252/embr.202255299

Alvers, A. L., Wood, M. S., Hu, D., Kaywell, A. C., Dunn, W. A., Jr., & Aris, J. P. (2009). Autophagy is required for extension of yeast chronological life span by rapamycin. *Autophagy*, *5*(6), 847–849. https://doi.org/10.4161/auto.8824

Amorim, J. A., Coppotelli, G., Rolo, A. P., Palmeira, C. M., Ross, J. M., & Sinclair, D. A. (2022). Mitochondrial and metabolic dysfunction in ageing and age-related diseases. *Nature Reviews Endocrinology*, *18*(4), 243–258. https://doi.org/10.1038/s41574-021-00626-7

Arkadieva, A. V., Mamonov, A. A., Popovich, I. G., Anisimov, V. N., Mikhelson, V. M., & Spivak, I. M. (2011). Metformin slows down ageing processes at the cellular level in SHR mice. *Cell and Tissue Biology*, *5*(2), 151–159. https://doi.org/10.1134/s1990519x11020027

Avelar-Rivas, J. A., Munguía-Figueroa, M., Juárez-Reyes, A., Garay, E., Campos, S. E., Shoresh, N., & DeLuna, A. (2020). An optimized competitive-aging method reveals gene-drug interactions underlying the chronological lifespan of *Saccharomyces cerevisiae*. *Frontiers in Genetics*, *11*, 468. https://doi.org/10.3389/fgene.2020.00468

Barardo, D., Thornton, D., Thoppil, H., Walsh, M., Sharifi, S., Ferreira, S., Anžič, A., Fernandes, M., Monteiro, P., Grum, T., Cordeiro, R., DeSouza, E. A., Budovsky, A., Araujo, N., Gruber, J., Petrascheck, M., Fraifeld, V. E., Zhavoronkov, A., Moskalev, A., & de Magalhães, J. P. (2017). The DrugAge database of aging-related drugs. *Aging Cell*, *16*(3), 594–597. https://doi.org/10.1111/acel.12585

Bass, T. M., Weinkove, D., Houthoofd, K., Gems, D., & Partridge, L. (2007). Effects of resveratrol on lifespan in *Drosophila melanogaster* and *Caenorhabditis elegans*. *Mechanisms of Ageing and Development*, *128*(10), 546–552. https://doi.org/10.1016/j.mad.2007.07.007

Bauer, J. H., Goupil, S., Garber, G. B., & Helfand, S. L. (2004). An accelerated assay for the identification of lifespan-extending interventions in *Drosophila melanogaster*. *Proceedings of the National Academy of Sciences of the United States of America*, *101*(35), 12980–12985. https://doi.org/10.1073/pnas.0403493101

Baur, J. A., Pearson, K. J., Price, N. L., Jamieson, H. A., Lerin, C., Kalra, A., Prabhu, V. V., Allard, J. S., Lopez-Lluch, G., Lewis, K., Pistell, P. J., Poosala, S., Becker, K. G., Boss, O., Gwinn, D., Wang, M., Ramaswamy, S., Fishbein, K. W., Spencer, R. G., … Sinclair, D. A. (2006). Resveratrol improves health and survival of mice on a high-calorie diet. *Nature*, *444*(7117), 337–342. https://doi.org/10.1038/nature05354

Berman, A. Y., Motechin, R. A., Wiesenfeld, M. Y., & Holz, M. K. (2017). The therapeutic potential of resveratrol: A review of clinical trials. *NPJ Precision Oncology*, *1*, 35. https://doi.org/10.1038/s41698-017-0038-6

Bhullar, K. S., & Hubbard, B. P. (2015). Lifespan and healthspan extension by resveratrol. *Biochimica et Biophysica Acta (BBA) – Molecular Basis of Disease*, *1852*(6), 1209–1218. https://doi.org/10.1016/j.bbadis.2015.01.012

Bjedov, I., Toivonen, J. M., Kerr, F., Slack, C., Jacobson, J., Foley, A., & Partridge, L. (2010). Mechanisms of life span extension by rapamycin in the fruit fly *Drosophila melanogaster*. *Cell Metabolism*, *11*(1), 35–46. https://doi.org/10.1016/j.cmet.2009.11.010

Blagosklonny, M. V. (2022). Rapamycin treatment early in life reprograms aging: Hyperfunction theory and clinical practice. *Aging*, *14*(20), 8140–8149. https://doi.org/10.18632/aging.20435

Cabreiro, F., Au, C., Leung, K. Y., Vergara-Irigaray, N., Cochemé, H., Noori, T., Weinkove, D., Schuster, E., Greene, N. D., & Gems, D. (2013). Metformin retards aging in *C. elegans* by altering microbial folate and methionine metabolism. *Cell*, *153*(1), 228–239. https://doi.org/10.1016/j.cell.2013.02.035

de Cabo, R., Carmona-Gutierrez, D., Bernier, M., Hall, M., & Madeo, F. (2014). The search for antiaging interventions: From elixirs to fasting regimens. *Cell*, *157*(7), 1515–1526. https://doi.org/10.1016/j.cell.2014.05.031

Denu, J. M. (2005). The Sir2 family of protein deacetylases. *Current Opinion in Chemical Biology*, *9*(5), 431–440. https://doi.org/10.1016/j.cbpa.2005.08.010

Doeppner, T. R., Coman, C., Burdusel, D., Ancuta, D. L., Brockmeier, U., Pirici, D. N., Yaoyun, K., Hermann, D. M., & Popa-Wagner, A. (2022). Long-term treatment with chloroquine increases lifespan in middle-aged male mice possibly via autophagy modulation, proteasome inhibition and glycogen metabolism. *Aging*, *14*(10), 4195–4210. https://doi.org/10.18632/aging.204069

Du, M. R., Gao, Q. Y., Liu, C. L., Bai, L. Y., Li, T., & Wei, F. L. (2022). Exploring the pharmacological potential of metformin for neurodegenerative diseases. *Frontiers in Aging Neuroscience*, *14*, 838173. https://doi.org/10.3389/fnagi.2022.838173

Eisenberg, T., Abdellatif, M., Schroeder, S., Primessnig, U., Stekovic, S., Pendl, T., Harger, A., Schipke, J., Zimmermann, A., Schmidt, A., Tong, M., Ruckenstuhl, C., Dammbrueck, C., Gross, A. S., Herbst, V., Magnes, C., Trausinger, G., Narath, S., Meinitzer, A., … Madeo, F. (2016). Cardioprotection and lifespan extension by the natural polyamine spermidine. *Nature Medicine*, *22*(12), 1428–1438. https://doi.org/10.1038/nm.4222

Eisenberg, T., Knauer, H., Schauer, A., Büttner, S., Ruckenstuhl, C., Carmona-Gutierrez, D., Ring, J., Schroeder, S., Magnes, C., Antonacci, L., Fussi, H., Deszcz, L., Hartl, R., Schraml, E., Criollo, A., Megalou, E., Weiskopf, D., Laun, P., Heeren, G., … Madeo, F. (2009). Induction of autophagy by spermidine promotes longevity. *Nature Cell Biology*, *11*(11), 1305–1314. https://doi.org/10.1038/ncb1975

Espada, L., Dakhovnik, A., Chaudhari, P., Martirosyan, A., Miek, L., Poliezhaieva, T., Schaub, Y., Nair, A., Döring, N., Rahnis, N., Werz, O., Koeberle, A., Kirkpatrick, J., Ori, A., & Ermolaeva, M. A. (2020). Loss of metabolic plasticity underlies metformin toxicity in aged *Caenorhabditis elegans*. *Nature Metabolism*, *2*(11), 1316–1331. https://doi.org/10.1038/s42255-020-00307-1

Filfan, M., Olaru, A., Udristoiu, I., Margaritescu, C., Petcu, E., Hermann, D. M., & Popa-Wagner, A. (2020). Long-term treatment with spermidine increases health span of middle-aged Sprague-Dawley male rats. *GeroScience*, *42*(3), 937–949. https://doi.org/10.1007/s11357-020-00173-5

Fontana, L., Partridge, L., & Longo, V. D. (2010). Extending healthy life span—From yeast to humans. *Science*, *328*(5976), 321–326. https://doi.org/10.1126/science.1172539

Grandison, R. C., Piper, M. D. W., & Partridge, L. (2009). Amino-acid imbalance explains extension of lifespan by dietary restriction in Drosophila. *Nature*, *462*(7276), 1061–1064. https://doi.org/10.1038/nature08619

Gruber, J., Tand, S. Y., & Halliwell, B. (2007). Evidence for a trade-off between survival and fitness caused by resveratrol treatment of *Caenorhabditis elegans*. *Annals of the New York Academy of Sciences*, *1100*(1), 530–542. https://doi.org/10.1196/annals.1395.059

Harrison, D. E., Strong, R., Sharp, Z. D., Nelson, J. F., Astle, C. M., Flurkey, K., Nadon, N. L., Wilkinson, J. E., Frenkel, K., Carter, C. S., Pahor, M., Javors, M. A., Fernandez, E., & Miller, R. A. (2009). Rapamycin fed late in life extends lifespan in genetically heterogeneous mice. *Nature*, *460*(7253), 392–395. https://doi.org/10.1038/nature08221

Hector, K. L., Lagisz, M., & Nakagawa, S. (2012). The effect of resveratrol on longevity across species: A meta-analysis. *Biology Letters*, *8*(5), 790–793. https://doi.org/10.1098/rsbl.2012.0316

Howitz, K. T., Bitterman, K. J., Cohen, H. Y., Lamming, D. W., Lavu, S., Wood, J. G., Zipkin, R. E., Chung, P., Kisielewski, A., Zhang, L. L., Scherer, B., & Sinclair, D. A. (2003). Small molecule activators of sirtuins extend *Saccharomyces cerevisiae* lifespan. *Nature*, *425*(6954), 191–196. https://doi.org/10.1038/nature01960

Islam, M. S., Jin, Y. Y., Chung, H. J., Kim, H. J., Baek, S. H., & Hong, S. T. (2019). Effect of the resveratrol rice DJ526 on longevity. *Nutrients*, *11*(8), 1804. https://doi.org/10.3390/nu11081804

Johnson, S. C. (2018). Nutrient sensing, signaling and ageing: The role of IGF-1 and mTOR in ageing and age-related disease. *Subcellular Biochemistry*, *90*, 49–97. https://doi.org/10.1007/978-981-13-2835-0_3

Johnson, S. C., Rabinovitch, P. S., & Kaeberlein, M. (2013). mTOR is a key modulator of ageing and age-related disease. *Nature*, *493*(7432), 338–345. https://doi.org/10.1038/nature11861

Kaeberlein, M., Rabinovitch, P. S., & Martin, G. M. (2015). Healthy aging: The ultimate preventative medicine. *Science*, *350*(6265), 1191–1193. https://doi.org/10.1126/science.aad3267

Kawamura, K., Fukumura, S., Nikaido, K., Tachi, N., Kozuka, N., Seino, T., Hatakeyama, K., Mori, M., Ito, Y. M., Takami, A., Hinotsu, S., Kuno, A., Kawasaki, Y., Horio, Y., & Tsutsumi, H. (2020). Resveratrol improves motor function in patients with muscular dystrophies: An open-label, single-arm, phase IIa study. *Scientific Reports*, *10*, 20585. https://doi.org/10.1038/s41598-020-77197-6

Khan, M., Park, S., Kim, H. J., Lee, K. J., Kim, D. H., Baek, S. H., & Hong, S. T. (2019). The resveratrol rice DJ526 callus significantly increases the lifespan of Drosophila (resveratrol rice DJ526 callus for longevity). *Nutrients*, *11*(5), 983. https://doi.org/10.3390/nu11050983

Kiechl, S., Pechlaner, R., Willeit, P., Notdurfter, M., Paulweber, B., Willeit, K., Werner, P., Ruckenstuhl, C., Iglseder, B., Weger, S., Mairhofer, B., Gartner, M., Kedenko, L., Chmelikova, M., Stekovic, S., Stuppner, H., Oberhollenzer, F., Kroemer, G., Mayr, M., … Willeit, J. (2018). Higher spermidine intake is linked to lower mortality: A prospective population-based study. *The American Journal of Clinical Nutrition*, *108*(2), 371–380. https://doi.org/10.1093/ajcn/nqy102

Kokott-Vuong, A., Jung, J., Fehr, A. T., Kirschfink, N., Noristani, R., Voigt, A., Reich, A., Schulz, J. B., Huber, M., & Habib, P. (2021). Increased post-hypoxic oxidative stress and activation of the PERK branch of the UPR in Trap1-deficient *Drosophila melanogaster* is abrogated by metformin. *International Journal of Molecular Sciences*, *22*(21), 11586. https://doi.org/10.3390/ijms222111586

Lee, J., Kwon, G., Park, J., Kim, J. K., & Lim, Y. H. (2016). Brief communication: SIR-2.1-dependent lifespan extension of *Caenorhabditis elegans* by oxyresveratrol and resveratrol. *Experimental Biology and Medicine*, *241*(16), 1757–1763. https://doi.org/10.1177/1535370216650054

Li, W., Zou, Z., Cai, Y., Yang, K., Wang, S., Liu, Z., Geng, L., Chu, Q., Ji, Z., Chan, P., Liu, G. H., Song, M., Qu, J., & Zhang, W. (2022). Low-dose chloroquine treatment extends the lifespan of aged rats. *Protein & Cell*, *13*(6), 454–461. https://doi.org/10.1007/s13238-021-00903-1

Longo, V. D., Antebi, A., Bartke, A., Barzilai, N., Brown-Borg, H. M., Caruso, C., Curiel, T. J., de Cabo, R., Franceschi, C., Gems, D., Ingram, D. K., Johnson, T. E., Kennedy, B. K., Kenyon, C., Klein, S., Kopchick, J. J., Lepperdinger, G., Madeo, F., Mirisola, M. G., … Fontana, L. (2015). Interventions to slow aging in humans: Are we ready? *Aging Cell*, *14*(4), 497–510. https://doi.org/10.1111/acel.12338

López-Otín, C., Blasco, M. A., Partridge, L., Serrano, M., & Kroemer, G. (2013). The hallmarks of aging. *Cell*, *153*(6), 1194–1217. https://doi.org/10.1016/j.cell.2013.05.039

Mak, J. K. L., Kuja-Halkola, R., Bai, G., Hassing, L. B., Pedersen, N. L., Hägg, S., Jylhävä, J., & Reynolds, C. A. (2022). Genetic and environmental influences on longitudinal frailty trajectories from adulthood into old age. *The Journals of Gerontology: Series A*, *78*(2), 333–341. https://doi.org/10.1093/gerona/glac197

Mannick, J. B., Del Giudice, G., Lattanzi, M., Valiante, N. M., Praestgaard, J., Huang, B., Lonetto, M. A., Maecker, H. T., Kovarik, J., Carson, S., Glass, D. J., & Klickstein, L. B. (2014). mTOR inhibition improves immune function in the elderly. *Science Translational Medicine*, *6*(268), 268ra179. https://doi.org/10.1126/scitranslmed.3009892

Mannick, J. B., & Lamming, D. W. (2023). Targeting the biology of aging with mTOR inhibitors. *Nature Aging*, *3*(6), 642–660. https://doi.org/10.1038/s43587-023-00416-y

Mannick, J. B., Morris, M., Hockey, H. U. P., Roma, G., Beibel, M., Kulmatycki, K., Watkins, M., Shavlakadze, T., Zhou, W., Quinn, D., Glass, D. J., & Klickstein, L. B. (2018). TORC1 inhibition enhances immune function and reduces infections in the elderly. *Science*

Translational Medicine, *10*(449), eaaq1564. https://doi.org/10.1126/scitranslmed.aaq1564

Martin, I., Jones, M. A., & Grotewiel, M. (2009). Manipulation of Sod1expression ubiquitously, but not in the nervous system or muscle, impacts age-related parameters in Drosophila. *FEBS Letters*, *583*(13), 2308–2314. https://doi.org/10.1016/j.febslet.2009.06.023

Martin-Montalvo, A., Mercken, E. M., Mitchell, S. J., Palacios, H. H., Mote, P. L., Scheibye-Knudsen, M., Gomes, A. P., Ward, T. M., Minor, R. K., Blouin, M. J., Schwab, M., Pollak, M., Zhang, Y., Yu, Y., Becker, K. G., Bohr, V. A., Ingram, D. K., Sinclair, D. A., Wolf, N. S., … de Cabo, R. (2013). Metformin improves healthspan and lifespan in mice. *Nature Communications*, *4*(1), 1–9. https://doi.org/10.1038/ncomms3192

Mather, K. A. (2022). Genetic and environmental factors in ageing and age-related disease. *Genes*, *13*(3), 396. https://doi.org/10.3390/genes13030396

Miller, R. A., Harrison, D. E., Astle, C. M., Baur, J. A., Boyd, A. R., de Cabo, R., Fernandez, E., Flurkey, K., Javors, M. A., Nelson, J. F., Orihuela, C. J., Pletcher, S., & Strong, R. (2011). Rapamycin, but not resveratrol or simvastatin, extends life span of genetically heterogeneous mice. *The Journals of Gerontology: Series A*, *66A*(2), 191–201. https://doi.org/10.1093/gerona/glq178

Miller, R. A., Harrison, D. E., Astle, C. M., Fernandez, E., Flurkey, K., Han, M., Javors, M. A., Li, X., Nadon, N. L., Nelson, J. F., Pletcher, S., Salmon, A. B., Sharp, Z. D., Van Roekel, S., Winkleman, L., & Strong, R. (2014). Rapamycin-mediated lifespan increase in mice is dose and sex dependent and metabolically distinct from dietary restriction. *Aging Cell*, *13*(3), 468–477. https://doi.org/10.1111/acel.12194

Moskalev, A., Chernyagina, E., de Magalhães, J. P., Barardo, D., Thoppil, H., Shaposhnikov, M., Budovsky, A., Fraifeld, V. E., Garazha, A., Tsvetkov, V., Bronovitsky, E., Bogomolov, V., Scerbacov, A., Kuryan, O., Gurinovich, R., Jellen, L. C., Kennedy, B., Mamoshina, P., Dobrovolskaya, E., … Zhavoronkov, A. (2015). Geroprotectors.org: A new, structured and curated database of current therapeutic interventions in aging and age-related disease. *Aging*, *7*(9), 616–628. https://doi.org/10.18632/aging.100799

Pannakal, S. T., Jäger, S., Duranton, A., Tewari, A., Saha, S., Radhakrishnan, A., Roy, N., Kuntz, J. F., Fermas, S., James, D., Mellor, J., Misra, N., & Breton, L. (2017). Longevity effect of a polysaccharide from *Chlorophytum borivilianum* on *Caenorhabditis elegans* and *Saccharomyces cerevisiae*. *PLoS One*, *12*(7), e0179813. https://doi.org/10.1371/journal.pone.0179813

Pearson, K. J., Baur, J. A., Lewis, K. N., Peshkin, L., Price, N. L., Labinskyy, N., Swindell, W. R., Kamara, D., Minor, R. K., Perez, E., Jamieson, H. A., Zhang, Y., Dunn, S. R., Sharma, K., Pleshko, N., Woollett, L. A., Csiszar, A., Ikeno, Y., Le Couteur, D., … de Cabo, R. (2008). Resveratrol delays age-related deterioration and mimics transcriptional aspects of dietary restriction without extending life span. *Cell Metabolism*, *8*(2), 157–168. https://doi.org/10.1016/j.cmet.2008.06.011

Popa-Wagner, A., Mitran, S., Sivanesan, S., Chang, E., & Buga, A. M. (2013). ROS and brain diseases: The good, the bad, and the ugly. *Oxidative Medicine and Cellular Longevity*, *2013*, 963520. https://doi.org/10.1155/2013/963520

Rallis, C., Codlin, S., & Bähler, J. (2013). TORC1 signaling inhibition by rapamycin and caffeine affect lifespan, global gene expression, and cell proliferation of fission yeast. *Aging Cell*, *12*(4), 563–573. https://doi.org/10.1111/acel.12080

Ramírez-Garza, S. L., Laveriano-Santos, E. P., Marhuenda-Muñoz, M., Storniolo, C. E., Tresserra-Rimbau, A., Vallverdú-Queralt, A., & Lamuela-Raventós, R. M. (2018). Health effects of resveratrol: Results from human intervention trials. *Nutrients*, *10*(12), 1892. https://doi.org/10.3390/nu10121892

Rea, S. L., Wu, D., Cypser, J. R., Vaupel, J. W., & Johnson, T. E. (2005). A stress-sensitive reporter predicts longevity in isogenic populations of *Caenorhabditis elegans*. *Nature Genetics*, *37*(8), 894–898. https://doi.org/10.1038/ng1608

Robida-Stubbs, S., Glover-Cutter, K., Lamming, D., Mizunuma, M., Narasimhan, S., Neumann-Haefelin, E., Sabatini, D. M., & Blackwell, T. (2012). TOR signaling and rapamycin influence longevity by regulating SKN-1/Nrf and DAF-16/FoxO. *Cell Metabolism*, *15*(5), 713–724. https://doi.org/10.1016/j.cmet.2012.04.007

Santos, A. L., Sinha, S., & Lindner, A. B. (2018). The good, the bad, and the ugly of ROS: New insights on aging and aging-related diseases from eukaryotic and prokaryotic model organisms. *Oxidative Medicine and Cellular Longevity*, *2018*, 1941285. https://doi.org/10.1155/2018/1941285

Schwarz, C., Benson, G. S., Horn, N., Wurdack, K., Grittner, U., Schilling, R., Märschenz, S., Köbe, T., Hofer, S. J., Magnes, C., Stekovic, S., Eisenberg, T., Sigrist, S. J., Schmitz, D., Wirth, M., Madeo, F., & Flöel, A. (2022). Effects of spermidine supplementation on cognition and biomarkers in older adults with subjective cognitive decline: A randomized clinical trial. *JAMA Network Open*, *5*(5), e2213875. https://doi.org/10.1001/jamanetworkopen.2022.13875

Schwarz, C., Stekovic, S., Wirth, M., Benson, G., Royer, P., Sigrist, S. J., Pieber, T., Dammbrueck, C., Magnes, C., Eisenberg, T., Pendl, T., Bohlken, J., Köbe, T., Madeo, F., & Flöel, A. (2018). Safety and tolerability of spermidine supplementation in mice and older adults with subjective cognitive decline. *Aging*, *10*(1), 19–33. https://doi.org/10.18632/aging.101354

Şeylan, C., & Tarhan, A. (2023). Metformin extends the chronological lifespan of fission yeast by altering energy metabolism and stress resistance capacity. *FEMS Yeast Research*, *23*, foad018. https://doi.org/10.1093/femsyr/foad018

Shaposhnikov, M. V., Guvatova, Z. G., Zemskaya, N. V., Koval, L. A., Schegoleva, E. V., Gorbunova, A. A., Golubev, D. A., Pakshina, N. R., Ulyasheva, N. S., Solovev, I. A., Bobrovskikh, M. A., Gruntenko, N. E., Menshanov, P. N., Krasnov, G. S., Kudryavtseva, A. V., & Moskalev, A. A. (2022). Molecular mechanisms of exceptional lifespan increase of *Drosophila melanogaster* with different genotypes after combinations of pro-longevity interventions. *Communications Biology*, *5*, 566. https://doi.org/10.1038/s42003-022-03524-4

Sharp, Z. D., & Strong, R. (2023). Rapamycin, the only drug that has been consistently demonstrated to increase mammalian longevity. An update. *Experimental Gerontology*, *176*, 112166. https://doi.org/10.1016/j.exger.2023.112166

Slack, C., Foley, A., & Partridge, L. (2012). Activation of AMPK by the putative dietary restriction mimetic metformin is insufficient to extend lifespan in Drosophila. *PLoS One*, *7*(10), e47699. https://doi.org/10.1371/journal.pone.0047699

Stevenson-Hoare, J., Leonenko, G., & Escott-Price, V. (2023). Comparison of long-term effects of metformin on longevity between people with type 2 diabetes and matched non-diabetic controls. *BMC Public Health*, *23*(1), 804. https://doi.org/10.1186/s12889-023-15764-y

Su, W. H., Chan, C. E., Lian, T., Biju, M., Miura, A., Alkhafaji, S. A., Do, K. K., Latifi, B., Nguyen, T. T., & Schriner, S. E. (2021). Protection of nuclear DNA by lifespan-extending compounds in the yeast *Saccharomyces cerevisiae*. *Mutation Research/Fundamental and Molecular Mechanisms of Mutagenesis*, *822*, 111738. https://doi.org/10.1016/j.mrfmmm.2021.111738

Taner, T., Hackstein, H., Wang, Z., Morelli, A. E., & Thomson, A. W. (2005). Rapamycin-treated, alloantigen-pulsed host dendritic cells induce ag-specific T cell regulation and prolong graft survival. *American Journal of Transplantation*, *5*(2), 228–236. https://doi.org/10.1046/j.1600-6143.2004.00673.x

van der Made, S. M., Plat, J., & Mensink, R. P. (2015). Resveratrol does not influence metabolic risk markers related to cardiovascular health in overweight and slightly obese subjects: A randomized, placebo-controlled crossover trial. *PLoS One*, *10*(3), e0118393. https://doi.org/10.1371/journal.pone.0118393

Villa-Cuesta, E., Holmbeck, M. A., & Rand, D. M. (2014). Rapamycin increases mitochondrial efficiency by mtDNA-dependent reprogramming of mitochondrial metabolism in Drosophila. *Journal of Cell Science*, *127*, 2282–2290. https://doi.org/10.1242/jcs.142026

Wang, C., Wheeler, C. T., Alberico, T., Sun, X., Seeberger, J., Laslo, M., Spangler, E., Kern, B., de Cabo, R., & Zou, S. (2013). The effect of resveratrol on lifespan depends on both gender and dietary nutrient composition in *Drosophila melanogaster*. *Age*, *35*(1), 69–81. https://doi.org/10.1007/s11357-011-9332-3

Yanai, H., Budovsky, A., Barzilay, T., Tacutu, R., & Fraifeld, V. E. (2017). Wide-scale comparative analysis of longevity genes and interventions. *Aging Cell*, *16*(6), 1267–1275. https://doi.org/10.1111/acel.12659

Yee, Z., Lim, S. H. Y., Ng, L. F., & Gruber, J. (2021). Inhibition of mTOR decreases insoluble proteins burden by reducing translation in *C. elegans*. *Biogerontology*, *22*(1), 101–118. https://doi.org/10.1007/s10522-020-09906-7

Yin, M., Zhou, J., Gorak, E. J., & Quddus, F. (2013). Metformin is associated with survival benefit in cancer patients with concurrent type 2 diabetes: A systematic review and meta-analysis. *The Oncologist*, *18*(12), 1248–1255. https://doi.org/10.1634/theoncologist.2013-0111

Zhang, Y., Bai, J., Cui, Z., Li, Y., Gao, Q., Miao, Y., & Xiong, B. (2023). Polyamine metabolite spermidine rejuvenates oocyte quality by enhancing mitophagy during female reproductive aging. *Nature Aging*, *3*, 1372–1386. https://doi.org/10.1038/s43587-023-00498-8

Zhou, W., Wang, H., Yang, Y., Chen, Z. S., Zou, C., & Zhang, J. (2020). Chloroquine against malaria, cancers and viral diseases. *Drug Discovery Today*, *25*(11), 2012–2022. https://doi.org/10.1016/j.drudis.2020.09.010

SUPPORTING INFORMATION

Additional supporting information can be found online in the Supporting Information section at the end of this article.

How to cite this article: Burdusel, D., Coman, C., Ancuta, D., Hermann, D., Doeppner, T., Gresita, A., & Popa-Wagner, A. (2024). Translatability of life-extending pharmacological treatments between different species. *Aging Cell*, *00*, e14208. https://doi.org/10.1111/acel.14208

Article

Assessment of the Effect on Periodontitis of Antibiotic Therapy and Bacterial Lysate Treatment

Diana Larisa Ancuţa [1] , Diana Mihaela Alexandru [2,*] , Florin Muselin [3,*] , Romeo Teodor Cristina [3]
and Cristin Coman [1,4]

1   Cantacuzino National Medical Military Institute for Research and Development, 050096 Bucharest, Romania;
    diana.larisa.ancuta@gmail.com (D.L.A.); comancristin@yahoo.com (C.C.)
2   Faculty of Veterinary Medicine, University of Agronomic Sciences and Veterinary Medicine,
    050097 Bucharest, Romania
3   Faculty of Veterinary Medicine, University of Life Sciences "King Mihai I" from Timisoara,
    300645 Timisoara, Romania; rtcristina@yahoo.com
4   Center of Excellence in Translational Medicine, Fundeni Clinical Institute, 022328 Bucharest, Romania
*   Correspondence: diana.alexandru@fmvb.usamv.ro (D.M.A.); florinmuselin@usvt.com (F.M.);
    Tel.: +40-753830681 (D.M.A.); +40-23626908 (F.M.)

Abstract: Periodontitis is an inflammatory process that starts with soft tissue inflammation caused by the intervention of oral bacteria. By modulating local immunity, it is possible to supplement or replace current therapeutic methods. The aim of this study was to compare the effects of an immunostimulatory treatment with the antibiotherapy usually applied to periodontitis patients. On a model of periodontitis induced in 30 rats (divided into three equal groups) with bacterial strains selected from the human oral microbiome (*Aggregatibacter actinomycetemcomitans*, *Fusobacterium nucleatum* and *Streptococcus oralis*), we administered antibiotics, bacterial lysates and saline for 10 days. Clinically, no significant lesions were observed between the groups, but hematologically, we detected a decrease in lymphocyte and neutrophil counts in both the antibiotic and lysate-treated groups. Immunologically, IL-6 remained elevated compared to the saline group, denoting the body's effort to compensate for bone loss due to bacterial action. Histopathologically, the results show more pronounced oral tissue regeneration in the antibiotic group and a reduced inflammatory reaction in the lysate group. We can conclude that the proposed bacterial lysate has similar effects to antibiotic therapy and can be considered an option in treating periodontitis, thus eliminating the unnecessary use of antibiotics.

Keywords: periodontitis; bacterial lysate; antibiotic therapy; oral microbiome; rat

1. Introduction

Periodontitis is an immune-mediated inflammatory disorder, which can affect up to 45% of the population [1]; globally, it is considered the most common cause of tooth loss [2]. Periodontitis, also called periodontal disease (PD), is caused by biofilms developed subgingivally, destroying oral soft tissue, followed by the progression of infection to the bone, where resorption occurs, resulting in tooth loss [3]. The continuous action of oral microbial agents causes uncontrolled bone metabolism, leading to the release of proinflammatory cytokines, growth factors and cellular messengers [4].

The etiological factors of periodontitis are multiple, similar to periimplantitis, and the common thread is the interaction between bacterial biofilm and the host protector immune response. Risk factors deregulate the microbiome at this level [5], resulting in gingival inflammation and dental biofilm formation [6]. In dental plaque, we find bacteria such as *Streptococcus* spp., which, through expressed adhesins, provide support for the colonization of other bacterial species. Moreover, among the main bacterial agents that trigger periodontitis are *Porphyromonas gingivalis* (P.g), *Tannerella forsythia* (T.f), *Treponema*

denticola (T.d), *Aggregatibacter actinomycetemcomitans* (A.a) and *Fusobacterium nucleatum* (F.n) [7,8].

Animal experiments in periodontology are still necessary, and the obtained information is of solid scientific relevance. Animal models are superior to in vitro tests or clinical trials when addressing questions in the area of mechanisms of action and serve as a bridge between hypotheses and the real clinical situation. There is no single animal model that mimics all the characteristics of human periodontitis and its tissue architecture or healing. However, human studies do not allow for the complete evaluation associated with tissue harvesting necessary for microscopic analyses, the importance of which lies in defining the biological impact of regenerative methods and materials. Therefore, research on animal models is necessary to establish cause–effect relationships and, equally important, to test new regenerative devices and advanced therapies [9]. In rats, periodontal disease is an infectious process caused by periodontal pathogens resulting in specific lesions [10]. Thus, rodents are suitable for research targeting teeth or investigating the dynamics of oral inflammatory diseases, and the information gained in this way allows for the translation of basic science into applied research.

In rats, there are several methods to induce periodontitis, starting from tying a cotton or silk thread around the teeth (the most commonly used method), applying acute trauma to the gums or even accelerated induction models that involve placing ligatures contaminated with dental plaque from PD patients [11]. The ligature alone causes, in a very short time, loss of periodontal tissue, biofilm accumulation, ulceration in the sulcular epithelium and eventually infiltration of surrounding tissues. Even if PD is induced by the ligation method without bacterial involvement, bone loss is still dependent on the presence of microorganisms [12]. As a result, in periodontal studies, when rodents are chosen, oral infection with selected human pathogens is used in an attempt to document the virulence of these species [11]. The bacterial composition of periodontitis-associated biofilms comprises a wide diversity of species, an important role of which is played by Streptococcus species that initiate the biofilm and form the basis to which the late colonizers of the red complex (P.g, T.d and T.f) subsequently attach [13].

The development of periodontitis depends on several etiological factors or risk factors, but the relationship between the imbalance of the oral microbiome and the consequent inflammation remains essential in the progression of the disease [14]. The microorganisms responsible for inducing PD trigger the immediate immune response to remedy the dysbiosis and regenerate the damaged periodontal tissue [15]. Thus, the leukocyte lineage is the main pawn controlling the pathogenicity of periodontitis generated by bacterial imbalances, activation of the adaptive immune response and inflammation of surrounding tissues [16].

Treatment of periodontitis, with or without antimicrobial administration, complemented by mechanical plaque removal, is today the gold standard [17]. In early forms of PD, non-surgical therapy and antibiotics may be sufficient, but severe forms require a surgical approach to reduce the periodontal pocket [18]. However, if the focus is only on the involvement of bacteria in the development of PD, current treatments may not always be successful; therefore, current therapies need to be complemented by therapeutic strategies that target the re-enhancement of the immune response capable of remedying the inflammatory and osteolytic process [19].

Drugs targeting the immune system have shown favorable effects in periodontitis [20,21]. Therefore, this study aimed to test a new therapy for periodontitis based on bacterial lysates obtained from strains of A.a, *Streptococcus oralis* (S.o) and F.n, thus evaluating in vivo a new antibacterial treatment for periodontal disease. The experimental model of periodontal disease was created by oral contamination of rats with the same bacteria from which the experimental treatment was obtained.

Null hypothesis: all animals with periodontitis included in this study will heal as a result of bacterial lysate treatment, similar to the effects of antibiotic therapy.

2. Results

The results regarding the induction of PD were similar to those obtained in a previous study [4], the evaluation methods being based on the microbiological examination, especially the clinical one, where we followed the gingival bleeding, the color of the periodontal tissue, the measurement of the periodontal pocket (using periodontal probes model CP 15, KOHLER Medizintechnik Gmbh, Stockach, Germany) and also the observation of any sign of discomfort in mastication expressed by reduced feed consumption and implicitly the reduction in body weight (unpublished data for this study). However, we closely followed the specific signs of periodontitis and as can be seen in Figure 1, compared to the first day, when we fixed the ligatures and started the oral contamination (a), at 2 weeks (b), the appearance of the gums had changed both in terms of color and structure; it became grayish pink, crumbly. At 4 weeks (c), the ligature wire was heavily impregnated with plaque, and bleeding appeared upon probing the periodontal gingival tissue. At the end of the 6 weeks of oral contamination with the selected bacteria, we can observe a visible periodontal pocket (d). All these elements in conjunction with the results of the study we performed previously [4] were sufficient to consider the disease as installed and thus the model to be suitable for treatment testing.
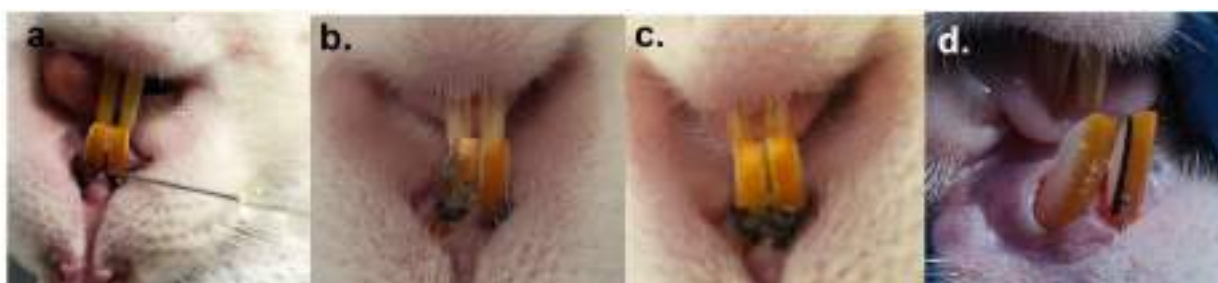

Figure 1. Appearance of periodontal tissue during periodontitis induction period: (**a**). insertion of the ligature wire and its impregnation with bacterial suspension, (**b**). appearance of the gingiva (grayish pink, friable) at 2 weeks after the onset of oral contamination, (**c**). ligature wire with attached dental plaque, observed at 4 weeks of oral contamination, (**d**). appearance of the periodontal pocket at the end of 6 weeks of oral contamination.

During the treatment, the animals showed no signs of discomfort. They were responsive to the doses of the substance established for each group, depending on the weight of the animals (in the case of the antibiotic and anti-inflammatory treated groups) or on the results obtained from the in vitro evaluation when the dose of bacterial lysate was established (in the case of the bacterial lysate-treated group), and no adverse effects were observed. Body weight did not change significantly, and no lesions of particular significance were identified locally. Upon macroscopic examination, the gingiva was similar in color or consistency, regardless of the group (Figure 2). However, bleeding was observed in moderate amounts (similar in antibiotic-treated and lysate-treated groups) when pressure was applied to the periodontal soft tissue.
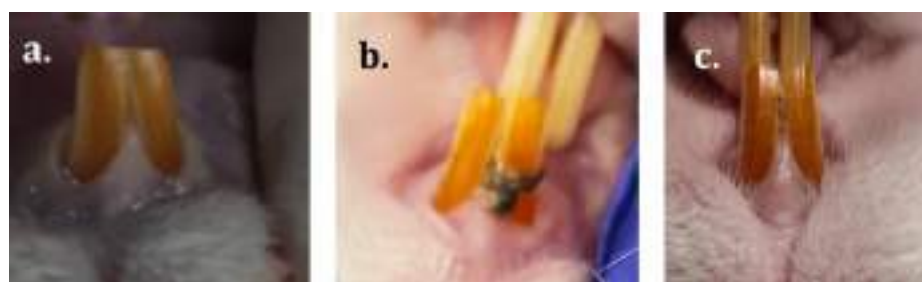

Figure 2. The appearance of the gingival mucosa at the end of the study—(**a**). control group, (**b**). antibiotic and anti-inflammatory group, (**c**). group with bacterial lysate.

2.1. Hematological Examination Results

We compared antibiotic therapy and bacterial lysate therapy in periodontitis by analyzing neutrophil, lymphocyte, WBC, platelet, hemoglobin, MCH, MCHC and RBC levels. Neutrophils were decreased in both treated groups, in the group receiving bacterial lysate, with a decrease ($p < 0.001$) in circulating blood neutrophil concentration compared to the control group. Lymphocytes decreased irrespective of the therapy applied but without statistically significant relevance. After the application of the treatment, a clear decrease in WBC, RBC and MCHC, moderate reductions in HGB and MCH concentrations and a significant increase in blood platelets could be observed, especially in the bacterial lysate-treated group (Table 1).

Table 1. Level of blood parameters before and after application of therapeutic protocols.

Hematological Parameter (Mean ± SD)	Control Group		Antibiotic and Anti-Inflammatory Group		Bacterial Lysates Group	
	Day 0	Final Day	Day 0	Final Day	Day 0	Final Day
WBC, K/µL	12.25 ± 2.83	6.72 ± 1.70	14.00 ± 2.85	10.92 ± 0.30	12.34 ± 4.84	4.0 1 ± 2.29
	$p < 0.001$		$p < 0.05$		$p < 0.001$	
HGB, g/dL	16.76 ± 1.31	16.07 ± 1.09	16.34 ± 0.91	15.1 ± 1.57	15.85 ± 0.77	14.05 ± 3.32
	ns (not significant)		ns		ns	
RBC, M/µL	9.45 ± 0.75	9.32 ± 0.45	9.01 ± 0.73	7.91 ± 0.91	8.73 ± 0.51	8.05 ± 1.81
	ns		ns		ns	
MCH, pg	17.75 ± 0.77	17.22 ± 0.92	18.18 ± 0.98	19.1 ± 0.95	18.15 ± 0.21	17.45 ± 0.21
	ns		ns		ns	
MCHC, g/dL	35.65 ± 0.64	34.5 ± 0.60	36.12 ± 0.63	35 ± 0.45	35.9 ± 0.70	34.8 ± 0.42
	ns		ns		ns	
PLT, K/µL	743.83 ± 169.64	964.75 ± 94.10	616.85 ± 69.27	701.66 ± 512.24	530 ± 11.31	918.5 ± 229.80
	$p < 0.05$		ns		$p < 0.05$	

However, by calculating the SII, we observed the maintenance of the inflammatory process even though the statistical analysis did not provide results of significance. The graphically represented SII was higher in the group of animals treated with antibiotic and anti-inflammatory treatment, and by comparison with the group of animals that received bacterial lysate, we can say that this therapeutic approach also provides a considerable reduction in inflammation in the oral tissues (Figure 3).
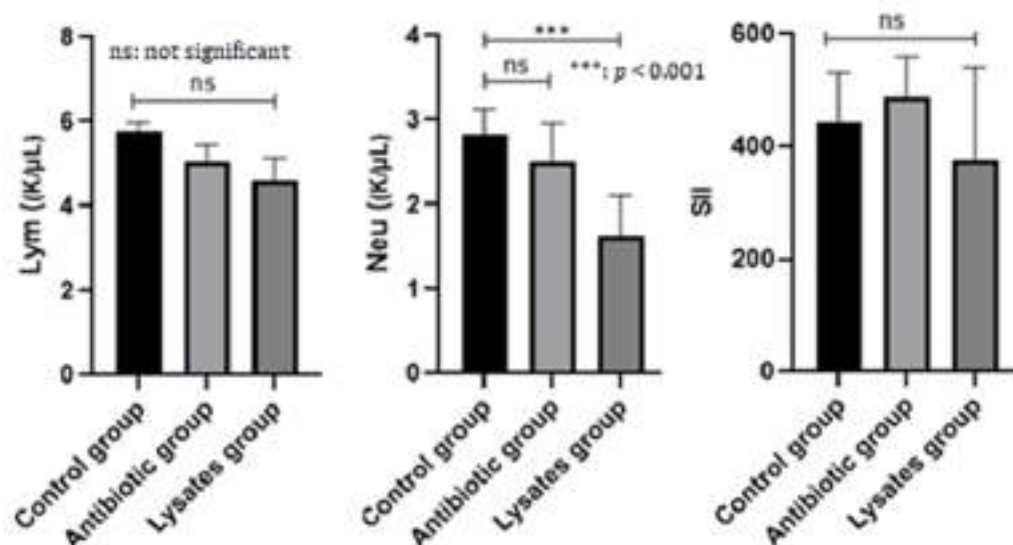

Figure 3. Neutrophils, lymphocytes and SII at the end of the study.

2.2. Immunological Examination Results

The immunological examination consisted of an analysis of IL-1, IL-6 and TNFα levels. Related to IL-6, several studies have focused on the potential role of this cytokine in directing the destructive processes in periodontal disease. Reported results have suggested a proinflammatory role for IL-6 alongside IL-1 and TNFα; thus, the biological function of IL-6 related to tissue destruction at the periodontal site differs from that of IL-1 and TNFα and may, in part, play a protective role [22]. This hypothesis applies to our research, where IL-6 levels remained increased ($p < 0.01$) in the antibiotic-treated group, but especially in the group that received bacterial lysate, where $p < 0.001$. The results indicate the organism's response to the treatment received and indicate similar efficacy for the two therapies. The expressed values of TNFα were close to those of IL-1b, as both the antibiotic and the bacterial lysate caused decreases in TNFα, but without statistical significance (Figure 4).
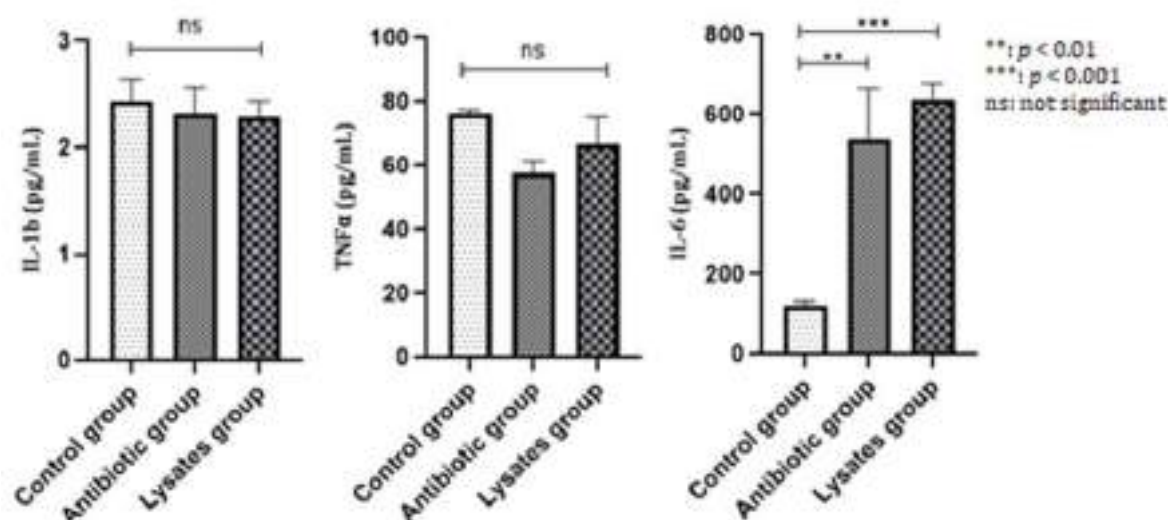

Figure 4. IL-1b, TNFα, and IL-6 at the end of the study.

2.3. Microbiological Examination Results

After the oral decontamination step, we found that the bacterial flora was not completely eliminated, which was expected, the residual microorganisms being staphylococcus species (*Staphylococcus xylosus*, *Staphylococcus sciuri*) and micrococci (*Micrococcus luteus*). We thus created a bacterial panel at the onset of the introduction of A.a, F.n and S.o into the mouths of rats. At the end of the 6 weeks of contamination with the selected strains, our concern was to verify the presence of bacteria in the oral cavity.

We selected the strains commonly identified with MaldiTof from the various results. In the control group, it was possible to recover A.a and S.o, but the confidence interval was low, unlike the antibiotic and lysate groups where the oral flora was dominated by commensal bacteria, resistant to the therapeutic means approach, the same as the one we identified after antibiotic therapy with kanamycin and ampicillin (Table 2).

2.4. Histopathological Examination Results

Histological sections were blindly evaluated by a histopathologist, and after generating the results, we conducted a semi-quantitative histological assessment to ascertain the host inflammatory reaction, depending on the treatment of each group. The used scoring scheme was adapted from a lesional grade grading system described in mice [23]. The grading methodology was adjusted to account for the host immune reaction observed in rat periodontal tissues, and the total score for each group was calculated by summing the individual scores (Table 3).

Table 2. The main microorganisms identified with MaldiTof at the end of the study.

ID	Microorganisms Identification	Score
Control 1	*Staphylococcus sciuri*	1.93
Control 2	*Micrococcus luteus*	1.76
Control 3	*Aggregatibacter actinomycemcomitans*	0.57
Control 4	*Streptococcus oralis*	1.45
Control 5	*Staphylococcus xylosus*	2.87
Antibiotic and anti-inflammatory group 1	Unidentified organism	1.45
Antibiotic and anti-inflammatory group 2	*Corynebacterium minutissimum*	1.63
Antibiotic and anti-inflammatory group 3	Unidentified organism	0.22
Bacterial lysates group 4	Unidentified organism	1.19
Bacterial lysates group 5	*Staphylococcus epidermidis*	1.84
Highly reliable identification		2.00–3.00
Low confidence identification		1.70–1.99
Not possible to identify organism		0.00–0.69

Table 3. Semi-quantitative scoring for histological evaluation in groups of treated animals.

Parameter	Score	Incidence of Lesions	Group
Inflammatory infiltrate in periodontal connective tissue	0	No neutrophils/macrophages in the microscopic field	Antibiotic and anti-inflammatory group Bacterial lysates group
	1	Reduced neutrophil/macrophage	Antibiotic and anti-inflammatory group Bacterial lysates group
	2	Moderated neutrophil/macrophage	-
	3	Neutrophil/macrophage marked	Control group
Fibrosis	0	Absent	-
	1	Mild	-
	2	Moderate	Antibiotic and anti-inflammatory group Bacterial lysates group
	3	Severe	-

The control group revealed the junctional epithelium impregnated with neutrophils but also with a rich fibrous tissue (Figure 5). In the antibiotic and anti-inflammatory treated group, we observed an advanced tissue regeneration process, with minimal inflammatory processes (Figure 6) and minimal inflammation in the periodontal tissue after treatment with bacterial lysates (Figure 7).
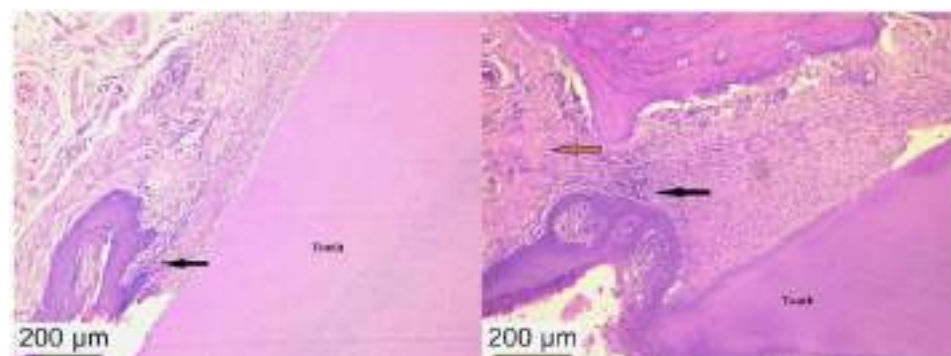

Figure 5. Histological appearance of the periodontal tissues in the control group where inflammatory infiltration can be observed in the periodontal ligament (black arrow) and fibrous tissue (brown arrow). Hematoxylin–eosin staining, ob. 10×.
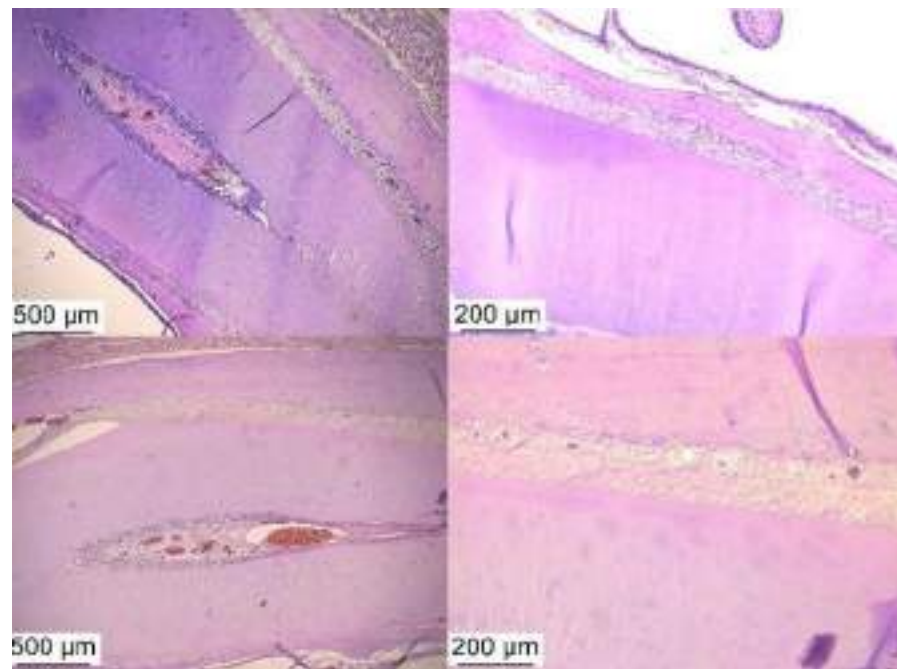
Figure 6. Normal-appearing periodontal tissues were found in groups of animals with antibiotic and anti-inflammatory-treated PD. Hematoxylin–eosin staining, ob. 4× and 10×.
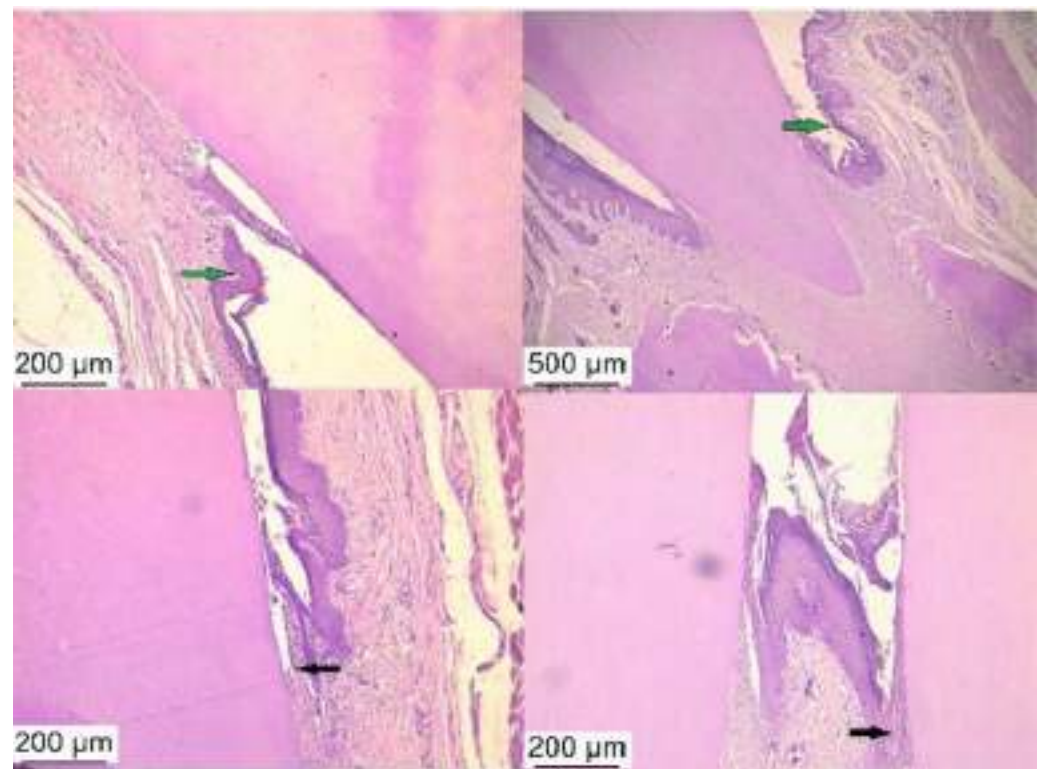

Figure 7. Histological aspect of periodontal tests showing reduced inflammatory infiltrate (black arrow) and periodontal sac free of cellular detritus (green arrow)—group with PD treated with bacterial lysate. Hematoxylin–eosin staining, ob. 4× and 10×.

3. Discussion

The use of rats in experimental research brings many benefits, including in the dental field, as the anatomy and physiology of the oral cavity in these animals are similar to those of humans.

In this study, microbiological diagnosis was suggested as a potential method for identifying the most virulent periodontal pathogens [24]. The bacterial species identified in periodontitis are predominantly anaerobic and Gram-negative without being related to a uniform microbial profile [25]. In a healthy organism, the oral bacterial community is in a balanced state with the host, but the intervention of predisposing factors causes bacterial film development and the implicit occurrence of inflammation. Consequently, the increase in the number of strains adhering to the initial biofilm makes therapeutic management difficult [26]. Thus, periodontitis treatment aims to control infection and reduce bacterial substrate. Currently, the standard therapy in PD is the use of systemic antibiotics, which is why we believe that it is necessary to research and develop new therapies to replace antimicrobials, especially in the context of antibiotic resistance, representing an increasingly pressing global problem. Adjuvant therapy for periodontitis is a safe therapy that could also reduce antibiotic consumption. Many studies [27,28] have shown that the use of probiotics shows favorable results, especially when administered preventively, with probiotic strains having the ability to adhere to the periodontium and counteract the activity of oral pathogenic microorganisms. This approach reduces the inflammatory process in the short term [29], which requires more frequent administration [30]. On the other hand, to improve the action of probiotics, knowledge of the individual oral microbiome is necessary so that personalized treatments can be developed [31]. Treatment with antibacterial substances providing immunity against the bacteria responsible for inducing periodontitis should be in the form of vaccines targeting the main virulence factors of microorganisms; so far, vaccination against PD has only been reported in mice [32]. Therapies such as photodynamic, gene and mesenchymal stem cell therapies can slow the progression of periodontal disease by their action on the immune system [33–35]. Bacterial lysates act to non-specifically increase the body's systemic immunity by acting on non-specific defense mechanisms through increased type A antibodies in mucous membranes, phagocytic activity and INF-γ production. They may also stimulate the production of specific antibodies against bacterial antigens that compose the bacterial lysate [36]. Based on this consideration, we considered that bacterial lysate therapy can reduce the oral inflammatory process specific to periodontitis.

In this experimental study, clinically, no differences were observed between the antibiotic-treated and bacterial lysate-treated groups. Locally, the gingiva showed slight signs of inflammation, both in the antibiotic-treated and in the bacterial lysate-treated groups, mainly expressed by moderate bleeding upon palpation. Hematologically, we found a decrease in white blood cells in the two treated groups, more pronounced in the animals treated with bacterial lysate. Some observational studies have shown that chronic or aggressive periodontitis is associated with increased white cell counts (mainly neutrophils) and a decrease in red cell counts, and non-surgical periodontal treatments have been associated with decreased white cell counts [37,38]. The results of the present study are consistent with other research which reports that bacterial lysates act similarly to antibiotics to reduce inflammation in the oral cavity [39]. These data reflect the body's inflammatory response to a periodontium-localized infection, which supports the involvement of periodontitis as a promoter of inflammation. A multitude of mechanisms could explain the association between periodontitis and the increase in leukocytes (neutrophils); more specifically, the inflammatory response of gingival tissue characterized by a leukocyte-dominated infiltrate that can pass into the systemic circulation [40]. Another mechanism addresses the host interaction with pathogenic bacterial flora that determines the chronic production of white matter in the bone marrow [41]. Furthermore, oral bacteria can graft onto existing periodontal lesions, triggering a systemic response to eliminate pathogens. Thus, chemotaxis or phagocytosis are mechanisms that support the destruction of periodontal tissues [42]. The main result of PD is tooth loss, as this disease is characterized by local inflammation that can generate a distant inflammatory process [43]. SII is a relatively new, stable and reliable biomarker that encompasses both localized and systemic immune responses [44]. SII, in recent studies, has been linked to an increased risk of periodontitis [45–47], although it was initially correlated with tumor diseases [48]. Chronic inflammatory diseases such as

PD, in the case of our study, express a lower SII following treatment with bacterial lysate, without statistical significance compared to antibiotic treatment which denotes that SII can be considered when specific treatments for PD are followed.

Immunologically, potential immunological markers indicating the onset and progression of periodontitis are matrix metalloproteinase (MMP)-8, IL-1, IL-6, TNFα and PGE 2 [49]. The immunological examination performed in this study paid close attention to the biological function of IL-6 and examined its link to periodontal tissue destruction compared to IL-1 and TNFα. In the literature, there are data supporting the gene expression of IL-1 and IL-6 in gingival tissues and relevant protein levels in gingival crevicular fluid, thus confirming an increase in both markers during inflammation [50]. IL-6 is produced by activated T cells or B cells, macrophages, dendritic cells or endothelial cells and fibroblasts [51]. The role of IL-6 has been demonstrated in several diseases, including periodontitis, where it contributes to the development of chondral inflammation, periodontal ligament damage and destruction of bone support [52]. IL-6 is not only a cytokine that responds in the active phase of PD but it is also a potent modulator from the acute to the chronic phase of the inflammatory process [53]. Persistence of IL-6 at high levels may indicate the presence of periodontal pathogenic microorganisms and osteoclastic activity in the dental alveolus. [54,55], IL-6 being directly involved in the pathogenesis of periodontitis [56]. This cytokine reacts to bacterial infections by directing neutrophils and monocytes to the infectious process. Along with IL-6, other proinflammatory cytokines (IL-1, IL-8 or TNF-α) are also associated with osteoclast generation, leading to the development of periodontitis symptoms and/or associated diseases [57,58]. Bone resorption phenomena are initiated by IL-6-mediated factors [56,58], and in the case of treatments applied to periodontitis patients, cytokine levels decrease [59]. In our case, IL-6, following the application of the treatments, remained elevated in the treated groups, demonstrating a similar efficacy of the two treatments. IL1-b and TNF-alpha in attenuated concentrations along with an increased level of IL-6 indicate, however, the body's effort to ameliorate bone resorption phenomena, providing a protective role against the progression of PD following the applied treatments.

The microbiological examination also showed the positive effect of bacterial lysate so that, at the final identification of oral microorganisms, the strains of A.a, F.n and S.o were no longer isolated. Even though these three bacterial strains were able to induce periodontitis in rats, following antibiotic and lysate treatments, they were not detected. Taking into account that F.n was also not detected in the control group, and that the titer of A.a. and S.o was low, we could think that the bacterial remanence is limited (which should be investigated in future studies) or that the existence of other microorganisms could cover or inhibit the growth of the selected strains on the liquid media.

The methods that can be used to assess the loss of bone support or, in our case, its regeneration, refer to micro-CT, X-rays, photography, densitometry and histology [60]. The degree of destruction of gingival tissue can be easily detected by photographing tissue stained with methylene blue, but with this method, we can obtain a picture based on the influence of external factors. Micro-CT is most often used for multidimensional bone assessment, and other indicators such as bone volume, bone mineral density and trabecular bone parameters can be analyzed without breaking the bone [61,62]. Histological assessment, although laborious, is an effective means of determining the level of internal substances in gingival tissue [63]. In our study, through histological analysis, the detected lesions confirmed the attenuation of the inflammatory process in the periodontal tissues, similarly for both groups that received treatment.

In periodontal research, rats are frequently used as animal models mainly because they have well-characterized biological mechanisms. Specific periodontitis lesions in these animals occur in a short time frame, so researchers can have the necessary support to study new treatment regimens. Over the years, several therapeutic schemes ideal for the treatment of PD have been tested. This topic remains open, and with the results presented in this study, we want to contribute to the improvement in the therapeutic management of one of the most common conditions encountered among patients. Of course, we agree that

our proposed product is a new one for use in oral cavity diseases, but the favorable effects obtained in other diseases, such as recurrent respiratory infections [36] and the results obtained in the experiment (concerning antibiotherapy), which support the null hypothesis, encourage us to further investigate bacterial lysates and their effects on oral diseases. In our study, the periodontitis model developed in rats proved to be optimal for analyzing the effects of applied therapy, with the results providing a perspective on the use of bacterial lysates to develop personalized therapy.

4. Materials and Methods

4.1. Ethics Statement

This study was conducted at the Baneasa Animal Facility (BAF) within the Bucharest Cantacuzino National Medical-Military Institute for Research and Development (INCD-MMC). Approval for this study was granted by the Ethics Committee of the Faculty of Veterinary Medicine Bucharest (no 25/15 June 2022), as well as by the veterinary health authority, following EU Directive 63/2010 concerning the care, use and safeguarding of animals utilized for scientific objectives.

4.2. Bacterial Cultures and Their Processing

To develop periodontal disease, we selected three bacterial strains (A.a, S.o and F.n), which can form oral biofilm. These came from the bacterial strain bank of the National Institute for Medical and Military Research and Development "Cantacuzino" (CI). Two were authenticated bacteria (A.a—ATCC 29522 and F.n—ATCC 25586), and the third belonged to the German collection of microorganisms and cell cultures (S. o—DSM 20627). All microorganisms used were checked for authenticity, viability, purity and special characteristics to ensure that the experiment was performed to the highest quality.

Bacteria were processed and a cryotube with 1 mL of A.a serogroup b (ATCC 29522) was revived by inoculation into a tube containing Schadler broth medium, left to incubate for a period of one day at 37 °C under anaerobic conditions (80% Nitrogen, 10% Carbon dioxide, and 10% Hydrogen). The suspension density in a tube of unseeded medium was measured with a densitometer (Densitometer McFarland Biosan DEN-1, Riga, Lithuania). The difference determined the A.a strain concentration, amounting to 10^9 CFU/mL. The rejuvenated A.a culture was preserved in cryotubes at -80 °C, from which daily inoculations were performed throughout the oral contamination period. Specifically, one cryotube of A.a from the primary culture was utilized for each inoculation.

F.n (ATCC 25586) and S.o (DSM 20627) inocula were prepared following the same steps as for A.a, utilizing identical culture media, culture conditions and procedures to establish the density of the inoculum.

The final concentration of each tested strain was 10^9 CFU/mL, determined by the nephelometric method. The dose to be administered to each animal was 0.6 mL, which included 0.2 mL suspension of A.a, F.n and S.o, and the period over which they were administered was 6 weeks, 5 days/week.

4.3. Bacterial Lysate

The method of producing the lysates, as well as the methods of verifying efficacy, have already been described in another manuscript [21]. Briefly, we used the same bacterial strains used to induce periodontitis in the same concentration. Thus, 24 h cultures of A.a, F.n and S.o, at a concentration of 10^9 CFU/mL, were inactivated on a water bath (56 °C, 60 min). After the inactivation control (when we put 1 mL bacterial lysate belonging to each strain in contact with 9 mL liquid medium of Brain Heart Infusion, Thioglycolate, and Sabouraud which we incubated and daily monitored for possible growth of aerobic or anaerobic bacteria and fungi), which lasted 14 days, the inactivated microorganisms were subjected to the process of mechanical breakage of the bacterial wall by ultrasonication at 70 °C for one hour. The effects of the lysates were tested in vitro by cytotoxicity tests

(MTT method) and by contacting lysates (in different concentrations) with live bacteria, the results showing that a double dose of lysate inhibited bacterial growth after 24–48 h.

4.4. Animal Selection

Induction of periodontitis was performed on 30 adult male Wistar rats, aged 5 months and weighing an average of 400 g at the start of the study, from the CI's Specific Pathogen Free (SPF) Animal Facility. Throughout the study, rats were housed under conventional conditions, including nesting material, with unlimited access to food (standard diet produced by the CI's Combined Feed Mill) and water ad libitum. The animals were housed in groups of five per cage, identified by a tag on which data on species, line, age, sex and cage number were specified, according to the CI's internal procedures. The general health status of all yearlings was constantly monitored during the experiment.

4.5. Periodontitis Rat Model Protocol

Rats were administered kanamycin and ampicillin (20 mg/mL each) in drinking water for 5 days to depress the indigenous microbiota. After the treatment period, saliva samples were collected using cotton swabs from the animals' mouths to assess the effectiveness of decontamination and to identify any flora that remained unaffected by the treatment. Samples were seeded on liquid culture media (Schadler) and incubated for 24 h at 37 °C under anaerobic conditions. Schadler agar plates were grown from this culture and followed the same thermostat conditions. After the 24 h required for the growth of bacterial colonies, their identification was carried out with the MaldiTof apparatus.

For the induction of PD, we opted to apply ligatures on the upper incisors, employing a gingival retraction thread (UltraPack, Ultradent, Bucharest, Romania), as in a preliminary study [4].

4.6. Therapeutic Scheme Applied to Rats with Periodontitis

After completion of the 6 weeks of oral contamination with A.a, F.n and S.o, the rats were divided into three groups of 10, according to the treatment received: control group, treated with saline solution; antibiotic group, treated with amoxicillin + clavulanic acid (40 mg/kg) and acetaminophen (50 mg/kg) and lysate group, which received 1.2 mL bacterial lysate consisting of the three bacterial species, in equal volumes. In all groups, treatment was applied by oral gavage for 10 days.

4.7. Animal Monitoring and Analysis

The animals were carefully and clinically monitored throughout the study period for local gingival tissue aspirations or periodontal sac formation. Blood samples were taken from the retro orbital sinus for hematological and immunological examination, and after the study, we euthanized the animals via anesthetic suppression, and samples were collected for microbiological and histopathological examination.

The complete hematological examination was performed on the Idexx Procyte 5diff analyzer on venous blood collected from the retro orbital plexus in vacutainers with EDTA (KIMA Vaccutest, Arzergrande, Italy) at the beginning of the experiment, after 3 weeks of oral contamination and at the end of this procedure. Hematological analysis aimed to follow polymorphonuclear cells (PMN), white blood cells (WBCs), hemoglobin (Hb), red blood cells (RBCs), mean corpuscular hemoglobin (MCH), mean hemoglobin concentration (MCHC), platelet count (PLT) as well as the systemic immune–inflammatory index (SII), calculated with the following formula: $SII = NEU \times PLT/LYM$, which is the product of the number of neutrophils (NEU) and the number of blood platelets (PLT) in relation to the number of lymphocytes (LYM). We preferred to examine this index because it is an easy way (using the results of the blood count) to check for inflammation in the system.

Immunological examination was performed by determining the concentrations of cytokines IL-1b, IL-6 and TNFα in plasma samples collected on day 0 and on the final day of the experiment. This was achieved using the Rat Luminex Discovery Assay, a

pre-customized 3-cytokine multiplex assay (LXSARM-3; R&D Systems Inc., Minneapolis, MN, USA). All samples were tested in duplicate. The technique followed the manufacturer's guidelines.

The MaldiTof bacterial strain identification technique was used for microbiological examination. Rats received ampicillin and kanamycin at the start of the experiment for 5 days to decontaminate the oral cavity and to check for residual bacterial strain types; samples were taken and analyzed in the MaldiTof for identification. Also, at the end of the oral contamination period, we checked for the presence of microorganisms taken in the study using the same method. After, the samples collected from the rats, both at the beginning and at the end of the experiment, were seeded on Schadler culture medium (liquid and solid); then, from the 24 h colonies, the identification of the antibiotic-resistant oral flora and that developed during the experiment was made to follow the presence of A.a, F.n and S.o, along with the commensal microorganisms.

For histopathological examination, the samples collected were fixed in 10% formaldehyde and then decalcified in a decalcifying solution (Histo-Decal, Pantigliate, Italy) for 14 days. After the decalcification period, the samples were processed for paraffin embedding by re-sectioning 5 μm serial sections, followed by staining with hematoxylin–eosin for light microscopic analysis (DM 4000B, Leica, Wetzlar, Germany).

4.8. Statistical Analysis

The sample size was calculated a priori using the simplified calculation formula proposed by Arifin et al. supplemented by data entry in the software G*Power 3.1 (Düsseldorf, Germany) where an error $\alpha = 0.05\%$ and power of 80% were set [64,65]. Finally, it was decided that the number of animals per group should be 10, considering the complexity of the study related to the induction of periodontal disease, the types of treatments tested, the interval of clinical monitoring of the animals as well as the intervention points for the collection of biological samples (hematological examination).

The normal distribution of the data was analyzed using the Shapiro–Wilk test, after which we performed a statistical analysis of the data by applying one-way ANOVA, Bonferroni test with multiple comparisons between the control and antibiotic group, control and bacterial lysate group. The statistical significance level was set at $p < 0.05$, and GraphPad Prism software (Version 9.4.1, GraphPad Prism Software Inc., La Jolla, CA, USA, released on 26 July 2022) was used.

5. Conclusions

This experimental study aimed to compare the effects of antibiotic therapy and bacterial lysate-based therapy in periodontitis induced by oral contamination with A.a, F.n and S.o. For this, we conducted more clinical and paraclinical investigations and the results show that bacterial lysates can be considered strong competitors for antibiotics. By corroborating the results, we can conclude that treatment with bacterial lysates had a similar effect to the standard antibiotic-based periodontitis-specific treatment. Thus, in a situation wherein antibiotic resistance is an increasing problem, the use of bacterial lysates as an alternative is a useful solution worldwide. We recommend further research, development and use of bacterial lysate-based therapies to reduce excessive and unnecessary antibiotic consumption.

Author Contributions: Conceptualization, D.L.A. and C.C.; methodology, D.L.A. and F.M.; software, D.L.A., D.M.A. and F.M.; validation, R.T.C. and C.C.; formal analysis, D.L.A., D.M.A. and F.M.; investigation, D.L.A., D.M.A. and F.M.; resources, F.M., R.T.C. and C.C.; data curation, D.L.A. and D.M.A.; writing—original draft preparation, D.M.A. and D.L.A.; writing—review and editing, R.T.C. and C.C.; visualization, F.M. and C.C.; supervision, R.T.C. and C.C.; project administration, D.L.A. and D.M.A.; funding acquisition, F.M. and R.T.C. All authors have read and agreed to the published version of the manuscript.

References

1. Nazir, M.; Al-Ansari, A.; Al-Khalifa, K.; Alhareky, M.; Gaffar, B.; Almas, K. Global Prevalence of Periodontal Disease and Lack of Its Surveillance. *Sci. World J.* **2020**, *2020*, 2146160. [CrossRef]
2. GBD 2016 Disease and Injury Incidence and Prevalence Collaborators. Global, regional, and national incidence, prevalence, and years lived with disability for 328 diseases and injuries for 195 countries, 1990–2016: A systematic analysis for the Global Burden of Disease Study 2016. *Lancet* **2017**, *390*, 1211–1259. [CrossRef] [PubMed]
3. Bhattarai, G.; Poudel, S.B.; Kook, S.H.; Lee, J.C. Resveratrol prevents alveolar bone loss in an experimental rat model of periodontitis. *Acta Biomater.* **2016**, *29*, 398–408. [CrossRef] [PubMed]
4. Ancuta, D.L.; Alexandru, D.M.; Crivineanu, M.; Coman, C. Induction of Periodontitis Using Bacterial Strains Isolated from the Human Oral Microbiome in an Experimental Rat Model. *Biomedicines* **2023**, *11*, 2098. [CrossRef]
5. Eke, P.I.; Dye, B.A.; Wei, L.; Slade, G.D.; Thornton-Evans, G.O.; Borgnakke, W.S.; Taylor, G.W.; Page, R.C.; Beck, J.D.; Genco, R.J. Update on Prevalence of Periodontitis in Adults in the United States: NHANES 2009 to 2012. *J. Periodontol.* **2015**, *86*, 611–622. [CrossRef] [PubMed]
6. Okuda, K.; Kato, T.; Ishihara, K. Involvement of periodontopathic biofilm in vascular diseases. *Oral Dis.* **2004**, *10*, 5–12. [CrossRef] [PubMed]
7. Brennan, C.A.; Garrett, W.S. Fusobacterium nucleatum—Symbiont, opportunist and oncobacterium. *Nat. Rev. Microbiol.* **2019**, *17*, 156–166. [CrossRef]
8. Leonov, G.E.; Varaeva, Y.R.; Livantsova, E.N.; Starodubova, A.V. The Complicated Relationship of Short-Chain Fatty Acids and Oral Microbiome: A Narrative Review. *Biomedicines* **2023**, *11*, 2749. [CrossRef] [PubMed]
9. Kantarci, A.; Hasturk, H.; Van Dyke, T.E. Animal models for periodontal regeneration and peri-implant responses. *Periodontology 2000* **2015**, *68*, 66–82. [CrossRef]
10. Proff, P.; Schröder, A.; Seyler, L.; Wolf, F.; Korkmaz, Y.; Bäuerle, T.; Gölz, L.; Kirschneck, C. Local Vascularization during Orthodontic Tooth Movement in a Split Mouth Rat Model—A MRI Study. *Biomedicines* **2020**, *8*, 632. [CrossRef]
11. Moiseev, D.; Donskov, S.; Dubrovin, I.; Kulyukina, M.; Vasil'ev, Y.; Volel, B.; Shadieva, S.; Babaev, A.; Shevelyuk, J.; Utyuzh, A.; et al. A New Way to Model Periodontitis in Laboratory Animals. *Dent. J.* **2023**, *11*, 219. [CrossRef]
12. Graves, D.T.; Kang, J.; Andriankaja, O.; Wada, K.; Rossa, C., Jr. Animal models to study host-bacteria interactions involved in periodontitis. *Front. Oral Biol.* **2012**, *15*, 117–132. [CrossRef] [PubMed]
13. Blank, E.; Grischke, J.; Winkel, A.; Eberhard, J.; Kommerein, N.; Doll, K.; Yang, I.; Stiesch, M. Evaluation of biofilm colonization on multi-part dental implants in a rat model. *BMC Oral Health* **2021**, *21*, 313. [CrossRef] [PubMed]
14. Hajishengallis, G.; Kajikawa, T.; Hajishengallis, E.; Maekawa, T.; Reis, E.S.; Mastellos, D.C.; Yancopoulou, D.; Hasturk, H.; Lambris, J.D. Complement-Dependent Mechanisms and Interventions in Periodontal Disease. *Front. Immunol.* **2019**, *10*, 406. [CrossRef] [PubMed]
15. Alvarez, C.; Rojas, C.; Rojas, L.; Cafferata, E.A.; Monasterio, G.; Vernal, R. Regulatory T Lymphocytes in Periodontitis: A Translational View. *Mediat. Inflamm.* **2018**, *2018*, 7806912. [CrossRef] [PubMed]
16. Sima, C.; Viniegra, A.; Glogauer, M. Macrophage immunomodulation in chronic osteolytic diseases-the case of periodontitis. *J. Leukoc. Biol.* **2019**, *105*, 473–487. [CrossRef] [PubMed]
17. Balta, M.G.; Papathanasiou, E.; Blix, I.J.; Van Dyke, T.E. Host Modulation and Treatment of Periodontal Disease. *J. Dent. Res.* **2021**, *100*, 798–809. [CrossRef]
18. Slots, J. Low-cost periodontal therapy. *Periodontology 2000* **2012**, *60*, 110–137. [CrossRef] [PubMed]
19. Heitz-Mayfield, L.J. How effective is surgical therapy compared with nonsurgical debridement? *Periodontology 2000* **2005**, *37*, 72–87. [CrossRef]

20. Zou, J.; Zeng, Z.; Xie, W.; Zeng, Z. Immunotherapy with regulatory T and B cells in periodontitis. *Int. Immunopharmacol.* **2022**, *109*, 108797. [CrossRef]

21. Ancuța, D.L.; Vuță, V.; Șalgău, C.; Bărbuceanu, F.; Coman, C. Innovative treatment against human periodontitis and periimplantitis—In vitro study. *Farmacia* **2024**, *72*, 125–131. [CrossRef]

22. Irwin, C.R.; Myrillas, T.T. The role of IL-6 in the pathogenesis of periodontal disease. *Oral Dis.* **1998**, *4*, 43–47. [CrossRef] [PubMed]

23. Bleich, A.; Mähler, M.; Most, C.; Leiter, E.H.; Liebler-Tenorio, E.; Elson, C.O.; Hedrich, H.J.; Schlegelberger, B.; Sundberg, J.P. Refined histopathologic scoring system improves power to detect colitis QTL in mice. *Mamm. Genome* **2004**, *15*, 865–871. [CrossRef] [PubMed]

24. Schwarz, F.; Derks, J.; Monje, A.; Wang, H.-L. Peri-Implantitis. *J. Clin. Periodontol.* **2018**, *45*, S246–S266. [CrossRef]

25. De Waal, Y.C.M.; Vangsted, T.E.; Van Winkelhoff, A.J. Systemic Antibiotic Therapy as an Adjunct to Non-Surgical Peri-Implantitis Treatment: A Single-Blind RCT. *J. Clin. Periodontol.* **2021**, *48*, 996–1006. [CrossRef] [PubMed]

26. Renvert, S.; Roos-Jansåker, A.-M.; Claffey, N. Non-Surgical Treatment of Peri-Implant Mucositis and Peri-Implantitis: A Literature Review. *J. Clin. Periodontol.* **2008**, *35*, 305–315. [CrossRef] [PubMed]

27. Doğan, B.; Kemer Doğan, E.S.; Özmen, Ö.; Fentoğlu, Ö.; Kırzıoğlu, F.Y.; Calapoğlu, M. Synergistic Effect of Omega-3 and Probiotic Supplementation on Preventing Ligature-Induced Periodontitis. *Probiotics Antimicrob. Proteins* **2022**, *14*, 114–120. [CrossRef] [PubMed]

28. Martin-Cabezas, R.; Davideau, J.L.; Tenenbaum, H.; Huck, O. Clinical efficacy of probiotics as an adjunctive therapy to non-surgical periodontal treatment of chronic periodontitis: A systematic review and meta-analysis. *J. Clin. Periodontol.* **2016**, *43*, 520–530. [CrossRef]

29. İnce, G.; Gürsoy, H.; İpçi, Ş.D.; Cakar, G.; Emekli-Alturfan, E.; Yılmaz, S. Clinical and Biochemical Evaluation of Lozenges Containing *Lactobacillus reuteri* as an Adjunct to Non-Surgical Periodontal Therapy in Chronic Periodontitis. *J. Periodontol.* **2015**, *86*, 746–754. [CrossRef]

30. Horz, H.P.; Meinelt, A.; Houben, B.; Conrads, G. Distribution and persistence of probiotic *Streptococcus salivarius* K12 in the human oral cavity as determined by real-time quantitative polymerase chain reaction. *Oral Microbiol. Immunol.* **2007**, *22*, 126–130. [CrossRef]

31. Zidar, A.; Kristl, J.; Kocbek, P.; Zupančič, Š. Treatment challenges and delivery systems in immunomodulation and probiotic therapies for periodontitis. *Expert Opin. Drug Deliv.* **2021**, *18*, 1229–1244. [CrossRef]

32. Wang, L.; Guan, N.; Jin, Y.; Lin, X.; Gao, H. Subcutaneous vaccination with *Porphyromonas gingivalis* ameliorates periodontitis by modulating Th17/Treg imbalance in a murine model. *Int. Immunopharmacol.* **2015**, *25*, 65–73. [CrossRef]

33. Nuñez, J.; Vignoletti, F.; Caffesse, R.G.; Sanz, M. Cellular therapy in periodontal regeneration. *Periodontology 2000* **2019**, *79*, 107–116. [CrossRef]

34. Brodzikowska, A.; Górska, R.; Kowalski, J. Interleukin-1 Genotype in Periodontitis. *Arch. Immunol. Ther. Exp.* **2019**, *67*, 367–373. [CrossRef]

35. Murakami-Malaquias-da-Silva, F.; Rosa, E.P.; Oliveira, J.G.; Avelar, I.S.; Palma-Cruz, M.; Silva, J.G.; Rigonato-Oliveira, N.C.; Bussadori, S.K.; Negreiros, R.M.; Ligeiro-de-Oliveira, A.P.; et al. The role of periodontal treatment associated with photodynamic therapy on the modulation of systemic inflammation in the experimental model of asthma and periodontitis. *Photodiagnosis Photodyn. Ther.* **2020**, *29*, 101619. [CrossRef]

36. Jurkiewicz, D.; Zielnik-Jurkiewicz, B. Bacterial lysates in the prevention of respiratory tract infections. *Pol. J. Otolaryngol.* **2018**, *72*, 1–8. [CrossRef]

37. Bhattacharya, H.S.; Srivastava, R.; Gummaluri, S.S.; Agarwal, M.C.; Bhattacharya, P.; Astekar, M.S. Comparison of blood parameters between periodontitis patients and healthy participants: A cross-sectional hematological study. *J. Oral Maxillofac. Pathol.* **2022**, *26*, 77–81. [CrossRef] [PubMed] [PubMed Central]

38. Ryder, M.I. Comparison of neutrophil functions in aggressive and chronic periodontitis. *Periodontology 2000* **2010**, *53*, 124–137. [CrossRef]

39. Ievtushenko, M.; Koshova, A.; Kryzhna, S.; Tyupka, T. Study of the influence of bacterial lysate on oxidative stress indicators in experimental periodontis in rats. *Likarska Sprav.* **2020**, *7–8*, 50–55. [CrossRef]

40. Hirschfeld, J. Dynamic interactions of neutrophils and biofilms. *J. Oral Microbiol.* **2014**, *6*, 26102. [CrossRef]

41. Belkaid, Y.; Hand, T.W. Role of the microbiota in immunity and inflammation. *Cell* **2014**, *157*, 121–141. [CrossRef]

42. Ryder, M.I.; Couch, E.T.; Chaffee, B.W. Personalized periodontal treatment for the tobacco- and alcohol-using patient. *Periodontology 2000* **2018**, *78*, 30–46. [CrossRef]

43. Suh, J.S.; Kim, S.; Boström, K.I.; Wang, C.Y.; Kim, R.H.; Park, N.H. Periodontitis-induced systemic inflammation exacerbates atherosclerosis partly via endothelial-mesenchymal transition in mice. *Int. J. Oral Sci.* **2019**, *11*, 21. [CrossRef]

44. Meng, L.; Yang, Y.; Hu, X.; Zhang, R.; Li, X. Prognostic value of the pretreatment systemic immune-inflammation index in patients with prostate cancer: A systematic review and meta-analysis. *J. Transl. Med.* **2023**, *21*, 79. [CrossRef]

45. Cao, R.; Li, C.; Geng, F.; Pan, Y. J-shaped association between systemic immune-inflammation index and periodontitis: Results from NHANES 2009–2014. *J. Periodontol.* **2023**; *Advance online publication*. [CrossRef]

46. Mishra, S.; Johnson, L.; Gazala, M.P.; Dahiya, S.; Rahman, W.; Sreeraj, V.S. Systemic immune-inflammation index in patients with generalized stage III grade C periodontitis. *Oral Dis.* **2023**, *29*, 3599–3609. [CrossRef]

47. Hao, Y.; Li, S.; Dong, S.; Niu, L. The Association between Tooth Loss and Insulin Resistance Mediated by Diet Quality and Systemic Immunoinflammatory Index. *Nutrients* **2023**, *15*, 5008. [CrossRef]

48. Hu, B.; Yang, X.R.; Xu, Y.; Sun, Y.F.; Sun, C.; Guo, W.; Zhang, X.; Wang, W.M.; Qiu, S.J.; Zhou, J.; et al. Systemic immune-inflammation index predicts prognosis of patients after curative resection for hepatocellular carcinoma. *Clin. Cancer Res.* **2014**, *20*, 6212–6222. [CrossRef]

49. Isola, G. Advances in biomarkers and diagnostics in periodontitis and oral diseases. *Int. J. Environ. Res. Public Health* **2021**, *18*, 1886. [CrossRef]

50. Kowalski, J.; Nowak, M.; Górski, B.; Górska, R. What Has Immunology Brought to Periodontal Disease in Recent Years? *Arch. Immunol. Ther. Exp.* **2022**, *70*, 26. [CrossRef]

51. Kang, S.; Narazaki, M.; Metwally, H.; Kishimoto, T. Historical overview of the interleukin-6 family cytokine. *J. Exp. Med.* **2020**, *4*, 217, Erratum in *J. Exp. Med.* **2020**, *217*, e20190347. [CrossRef]

52. Nibali, L.; Fedele, S.; D'Aiuto, F.; Donos, N. Interleukin-6 in oral diseases: A review. *Oral Dis.* **2012**, *18*, 236–243. [CrossRef]

53. Kaur, S.; Bansal, Y.; Kumar, R.; Bansal, G. A panoramic review of IL-6: Structure, pathophysiological roles and inhibitors. *Bioorg. Med. Chem.* **2020**, *28*, 115327. [CrossRef]

54. Ptasiewicz, M.; Grywalska, E.; Mertowska, P.; Korona-Głowniak, I.; Poniewierska-Baran, A.; Niedźwiedzka-Rystwej, P.; Chałas, R. Armed to the Teeth-The Oral Mucosa Immunity System and Microbiota. *Int. J. Mol. Sci.* **2022**, *23*, 882. [CrossRef]

55. Ptasiewicz, M.; Bębnowska, D.; Małkowska, P.; Sierawska, O.; Poniewierska-Baran, A.; Hrynkiewicz, R.; Niedźwiedzka-Rystwej, P.; Grywalska, E.; Chałas, R. Immunoglobulin Disorders and the Oral Cavity: A Narrative Review. *J. Clin. Med.* **2022**, *11*, 4873. [CrossRef]

56. Kudo, O.; Sabokbar, A.; Pocock, A.; Itonaga, I.; Fujikawa, Y.; Athanasou, N.A. Interleukin-6 and interleukin-11 support human osteoclast formation by a RANKL-independent mechanism. *Bone* **2003**, *32*, 1–7. [CrossRef]

57. Shyu, K.G.; Choy, C.S.; Wang, D.C.; Huang, W.C.; Chen, S.Y.; Chen, C.H.; Lin, C.T.; Chang, C.C.; Huang, Y.K. Change of scaling-induced proinflammatory cytokine on the clinical efficacy of periodontitis treatment. *Sci. World J.* **2015**, *2015*, 289647. [CrossRef]

58. Wu, K.J.; Tu, C.C.; Hu, J.X.; Chu, P.H.; Ma, K.S.; Chiu, H.Y.; Kuo, M.Y.; Tsai, T.F.; Chen, Y.W. Severity of periodontitis and salivary interleukin-1β are associated with psoriasis involvement. *J. Formos. Med. Assoc.* **2022**, *121*, 1908–1916. [CrossRef]

59. Rudick, C.P.; Lang, M.S.; Miyamoto, T. Understanding the pathophysiology behind chairside diagnostics and genetic testing for IL-1 and IL-6. *Oral Dis.* **2019**, *25*, 1879–1885. [CrossRef]

60. Kim, J.H.; Goo, B.H.; Nam, S.S.; Park, Y.C. A review of rat models of periodontitis treated with natural extracts. *J. Tradit. Chin. Med. Sci.* **2020**, *7*, 95–103. [CrossRef]

61. Irie, M.S.; Rabelo, G.D.; Spin-Neto, R.; Dechichi, P.; Borges, J.S.; Soares, P.B.F. Use of micro-computed tomography for bone evaluation in dentistry. *Braz. Dent. J.* **2018**, *29*, 227–238. [CrossRef]

62. Shim, J.; Iwaya, C.; Ambrose, C.G.; Suzuki, A.; Iwata, J. Micro-computed tomography assessment of bone structure in aging mice. *Sci. Rep.* **2022**, *12*, 8117. [CrossRef]

63. Boca, C.; Truyen, B.; Henin, L.; Schulte, A.G.; Stachniss, V.; De Clerck, N.; Bottenberg, P. Comparison of micro-CT imaging and histology for approximal caries detection. *Sci. Rep.* **2017**, *7*, 6680. [CrossRef]

64. Arifin, W.N.; Zahiruddin, W.M. Sample Size Calculation in Animal Studies Using Resource Equation Approach. *MJMS* **2017**, *24*, 101–105. [CrossRef]

65. Serdar, C.C.; Cihan, M.; Yücel, D.; Serdar, M.A. Sample size, power and effect size revisited: Simplified and practical approaches in pre-clinical, clinical and laboratory studies. *Biochem. Medica* **2021**, *31*, 010502. [CrossRef]

Article

Induction of Periodontitis Using Bacterial Strains Isolated from the Human Oral Microbiome in an Experimental Rat Model

Diana Larisa Ancuta [1,2,*], Diana Mihaela Alexandru [1], Maria Crivineanu [1] and Cristin Coman [1,2,3]

1 Faculty of Veterinary Medicine, University of Agronomic Sciences and Veterinary Medicine, 050097 Bucharest, Romania; albu.dm@gmail.com (D.M.A.); maria_crivineanu@yahoo.com (M.C.); comancristin@yahoo.com (C.C.)
2 Cantacuzino National Medical Military Institute for Research and Development, 050096 Bucharest, Romania
3 Center of Excellence in Translational Medicine, Fundeni Clinical Institute, 022328 Bucharest, Romania
* Correspondence: diana.larisa.ancuta@gmail.com; Tel.: +40-726257409

Abstract: Periodontal disease is that condition resulting in the destruction of periodontal tissues, bone resorption, and tooth loss, the etiology of which is linked to immunological and microbiological factors. The aim of this study was to evaluate the potential trigger of periodontal disease in a rat model using bacterial species incriminated in the pathology of human periodontitis and to establish their optimal concentrations capable of reproducing the disease, with the idea of subsequently developing innovative treatments for the condition. In this study, we included 15 male Wistar rats, aged 20 weeks, which we divided into three groups. In each group, we applied ligatures with gingival retraction wire on the maxillary incisors. The ligature and the gingival sac were contaminated by oral gavage with a mixture of fresh cultures of *Aggregatibacter actinomycetemcomitans* (A.a), *Fusobacterium nucleatum* (F.n) and *Streptococcus oralis* (S.o) in concentrations of 10^8, 10^9, and 10^{10} CFU/mL each for 5 days a week for 4 weeks. During the clinical monitoring period of 28 days, overlapped with the period of oral contamination, we followed the expression of clinical signs specific to periodontitis. We also monitored the evolution of body weight and took weekly samples from the oral cavity for the microbiological identification of the tested bacteria and blood samples for hematological examination. At the end of the study, the animals were euthanized, and the ligated incisors were taken for histopathological analysis. The characteristic symptomatology of periodontal disease was expressed from the first week of the study and was maintained until the end, and we were able to identify the bacteria during each examination. Hematologically, the number of neutrophils decreased dramatically ($p < 0.0001$) in the case of the 10^9 group, unlike the other groups, as did the number of lymphocytes. Histopathologically, we identified neutrophilic infiltrate in all groups, as well as the presence of coccobacilli, periodontal tissue hyperplasia, and periodontal lysis. In the 10^9 group, we also observed pulpal tissue with necrotic bone fragments and pyogranulomatous inflammatory reaction. By corroborating the data, we can conclude that for the development of periodontal disease using A.a, F.n, and S.o, a concentration of 10^9 or 10^{10} CFU/mL is required, which must necessarily contaminate a ligature thread applied to the level of the rat's dental pack.

Keywords: periodontitis; rat; ligature; *Aggregatibacter actinomycetemcomitans*; *Fusobacterium nucleatum*; *Streptococcus oralis*

1. Introduction

Periodontitis, or periodontal disease (PD), is an inflammatory immune condition caused by bacterial biofilms developed in the subgingival space that causes the destruction of the connective tissue, destruction of the alveolar ligament, and, ultimately, bone resorption, resulting in the loss of teeth [1]. Therefore, the persistence of oral micro-organisms at the level of dental structures causes an imbalance in bone metabolism, resulting in the release of proinflammatory mediators, growth mediators, and signaling molecules. Periodontitis is the most common cause of tooth loss in the human population and is associated

with atherosclerosis, carotid stenosis, premature birth, and low-birth-weight fetuses if from mothers with periodontitis [2,3]. Subsequently, periodontal bacterial colonization in children increases with age, and the bacterial flora in children is similar to that of their mothers [4].

Among the frequent causes associated with periodontitis, we find smoking, diabetes, stress, age, social status, and genetic factors [5], all of which affect the homeostasis of the oral cavity, ultimately leading to disturbances in the oral microbiome [6]. As a result, inflammation and biofilm formation occur on the tooth surface, as well as invasion of the gingival tissues [2]. In dental plaque, bacteria such as *Streptococcus* spp., which are frequently found in the mouth of all people and express adhesins, provide the necessary support for other bacterial colonizers.

Since the pathogenesis of PD has been studied for a long time, today, data are available to characterize the microbial flora both in healthy and affected patients [7]. *Porphyromonas gingivalis* (P.g), *Tannerella forsythia* (T.f), *Treponema denticola* (T.d), and A.a are the most incriminated pathogens that trigger periodontitis. F.n is also involved in periodontal health [8,9] as demonstrated by its frequent detection in subgingival plaque samples, with an important role in the organization of biofilms as a result of the expression of multiple adhesins [10]. PD symptomatology varies according to the patient's age; thus, in the case of young people, it is mainly triggered by A.a, whereas in adults, the triggering agents of PD are P.g, T.d, and spirochetes. In an anaerobic environment, as we find in the subgingival space, periodontal pockets are formed, where pathogens and pathobionts that express virulence factors grow, leading to imbalances in the host's inflammatory response [11].

A.a is a non-motile Gram($-$) facultative anaerobe belonging to the *Pasteurellaceae* family [12] that contributes to the occurrence of PD due to several virulence factors that it expresses, such as cytolethal distention toxin, leucotoxin A, and collagenase [13]. In the case of juvenile periodontitis, leukotoxin A is the most studied virulence factor because it kills the polymorphonuclear cells (PMNs) and macrophages, important components of host defense [14], through a proinflammatory process called pyroptosis [15,16]. Under conditions of oral existence of commensals such as F.n and S.o, A.a has a devastating action because in the early stages of periodontitis, A.a uses the lactic acid produced by *Streptococcus* spp. as a nutrient to increase its number [17]. The production of H_2O_2 by *Streptococcus* spp. causes A.a to migrate deeper into the gingival pocket, where the bacterial cells are exposed to the host's immune response [14]. A.a activates the transcriptional regulator of oxygen resistance, which regulates the expression of the Outer membrane protein 100 (Omp100—produced by A.a in response to H_2O_2) and catalase [18]. The latter contributes to the degradation of H_2O_2 produced by neutrophils and streptococci, protecting A.a from oxidative damage [19]. The release of cytolethal distension toxin in this environment inhibits phagocytosis, and the release of leukotoxin by A.a promotes neutrophil degranulation or death, which leads to the promotion of bone resorption [20].

The purpose of our research was to study the potential trigger of PD in a rat model using the bacterial species incriminated in the pathology of human periodontitis and to establish their optimal concentration capable of reproducing the disease, with the idea of subsequently developing innovative treatments for the condition. To achieve our objectives, we chose S.o, F.n, and A.a as bacterial species. The selection was based on the characteristic of streptococci with respect to its involvement in the early formation of bacterial plaque [21], as well as the fact that F.n is a predominant bacterium that contributes to the formation of biofilm [22] and because A.a is the major pathogenic agent of PD and inflammation [23].

2. Materials and Methods

2.1. Ethics Statement

The animal experiments were carried out at the Baneasa Animal Facility (BAF) of the Cantacuzino National Medical Military Institute for Research and Development, Bucharest, Romania (CI). The study was approved by the Ethics Committee of the Faculty of Veterinary Medicine, Bucharest, (no. 25/15.06.2022) and by the Romanian competence authority, in

accordance with EU Directive 63/2010 on the care, use, and protection of animals used for scientific purposes.

2.2. Processing of Bacterial Strains Selected for Study

A.a (ATCC 29522), serogroup b, isolated from a mandibular abscess, was provided by the CI bacterial strain bank. Thus, a cryotube with 1 mL of A.a was revitalized by inoculating a tube with Schadler broth medium, which was incubated for 24 h at 37 °C under anaerobic conditions (95% O_2 and 5% CO_2). The density of the 24 h suspension was measured using a densitometer (Densitometer McFarland Biosan DEN-1, Riga, Lithuania), like that of a tube with unseeded medium. The difference determined the concentration of the A.a strain, which corresponded to a concentration of 10^9 CFU/mL. A concentration of 10^8 CFU/mL was produced decimal dilution and centrifugation ($\times$4000 rpm, 10 min); with removal of the supernatant, the concentration of 10^{10} CFU/mL was also established. The revitalized A.a culture was stored in cryotubes at -80 °C, which were used to make the daily inoculum throughout oral contamination, that is, for each inoculation, one tube with A.a from the "mother" culture was used.

F.n (ATCC 25586), was isolated from a cervicofacial lesion, and S.o (DSM 20627) was isolated from the mouth of a human patient. A.a came from the CI bacterial strain bank. The inocula were prepared by following the same steps as in the case of A.a, using the same culture media, cultivation conditions, and steps to establish the inoculum density.

For oral contamination, we established 3 concentrations of each strain, namely 10^8, 10^9, and 10^{10} CFU/mL, with the inoculum dose established as 0.6 mL (thus, the concentrations per animal were 10^7 CFU/animal, 10^8 CFU/animal, and 10^9 CFU/animal, respectively). The dose at which the 3 bacteria were found in equal volumes (0.2 mL of each bacteria and each concentration) were administered by gavage 5 days/week for 4 weeks.

2.3. Periodontitis Rat Model Protocol

The procedures developed to create the animal model for PD were performed on 15 Wistar rats, aged 20 weeks, from the CI Specific Pathogen Free (SPF) animal facility. Throughout the experiment, the animals were housed in groups of 5 under conventional conditions at a temperature of 20–22 °C and under a 12H:12H light–dark cycle and received water and feed ad libitum. Rats were provided with 20 mg/mL kanamycin and 20 mg/mL ampicillin in their drinking water for five days to suppress the resident flora. At the end of the treatment, cotton swabs with saliva were taken from the mouths of the animals to determine the effectiveness of the decontamination and of the flora left unaffected by the treatment. In order to induce periodontitis, we resorted to the application of ligatures on the upper incisors, using a gingival retraction thread (Ultrapak, UltraDent, Bucharest, Romania). Thus, the rats were deeply anesthetized with ketamine (0.5 mg/kg, Pasteur Institute, Bucharest, Romania) and medetomidine (0.5 mg/kg, Biotur, Bucharest, Romania) in a weight-dependent dose. The animals were positioned in ventrodorsal recumbency on the operating table. By applying a mouth spacer, the incisors were isolated. With a dental curette, the gum was detached, and a ligature was applied around each incisor in the bag thus created. The animals were divided into 3 groups depending on the bacterial concentration used (10^8, 10^9, and 10^{10} groups). At the end of the procedure, the fresh 24 h inoculum consisting of the three bacteria was used to impregnate the thread and to wash the gingival pocket (Figure 1). Then, the animals received atipamezole (0.02 mg/kg, Biotur, Romania) to reverse the effect of anesthesia.

At the time of each intervention, the body weight and the periodontal pocket were monitored, and blood samples were taken from the retro-orbital sinus to perform a hematological examination. At the end of the study, the animals were euthanized by an overdose of anesthetic, and samples were collected for microbiological examination, as well as the incisors for histopathological analysis.
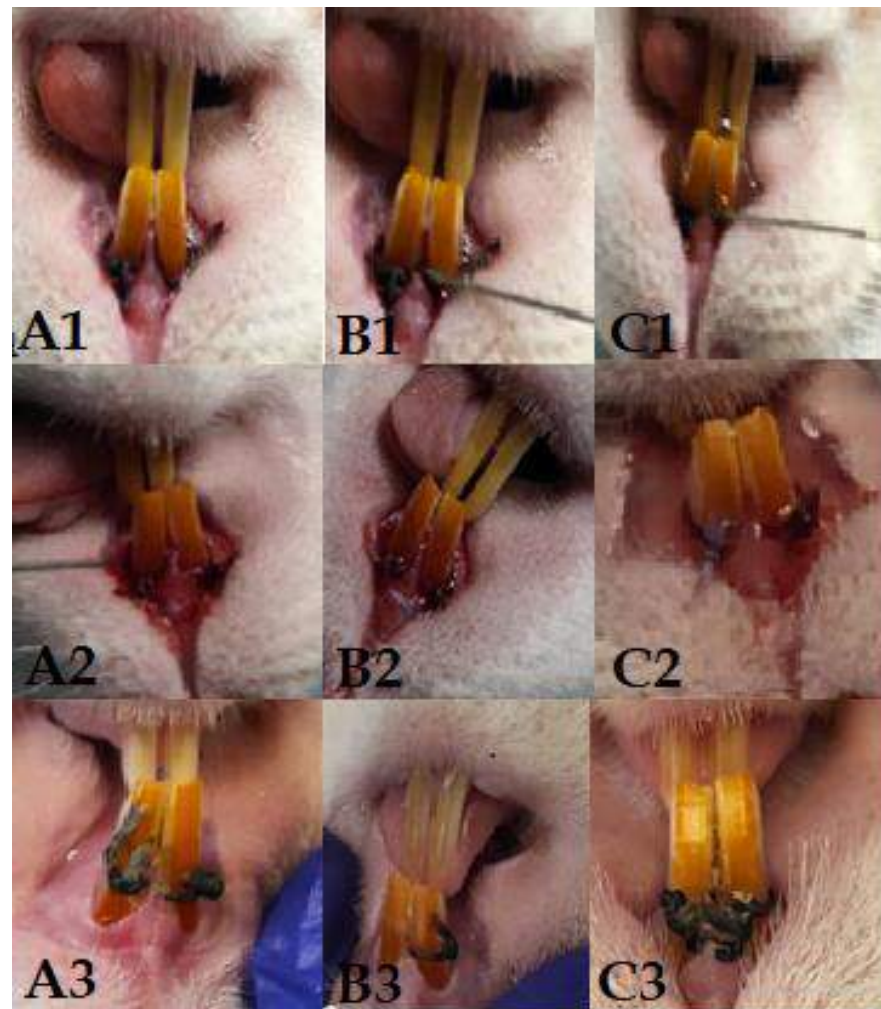
Figure 1. Columns (**A1**–**A3**) represent the 10^8 group, with clinical aspect at the time of application of the first ligature (**A1**), after 14 days of contamination (**A2**), and on day 28 (**A3**). Columns (**B1**–**B3**) represent the 10^9 group, with clinical aspect at the time of application of the first ligature (**B1**), after 14 days of contamination (**B2**), and on day 28 (**B3**). Columns (**C1**–**C3**) represent the 10^{10} group, with clinical aspect at the time of application of the first ligature (**C1**), after 14 days of contamination (**C2**), and on day 28 (**C3**).

2.4. Statistical Analysis

Analyses were performed using Prism 9 software for Windows (GraphPad LLC, Chicago, IL, USA). To compare the data, the one-way ANOVA function was used, and a value of $p < 0.05$ was considered statistically significant. Regarding the analysis of the data obtained after the hematological examination, we compared the results obtained from each group (10^8, 10^9, and 10^{10}), comparing them with day 0 using the one-way ANOVA function and multiple comparisons and comparing the data from days 7, 24, and 28 with those from day 0 using Dunnet's test.

3. Results

From a clinical point of view, the animals did not present discomfort during mastication, and through the weekly monitoring of body weight, we observed a relatively upward trend in the first three weeks, with a slight weight decrease recorded in the last week (Figure 2). Gingival bleeding and periodontal pocket formation were clinically visible starting in the second week after contamination.
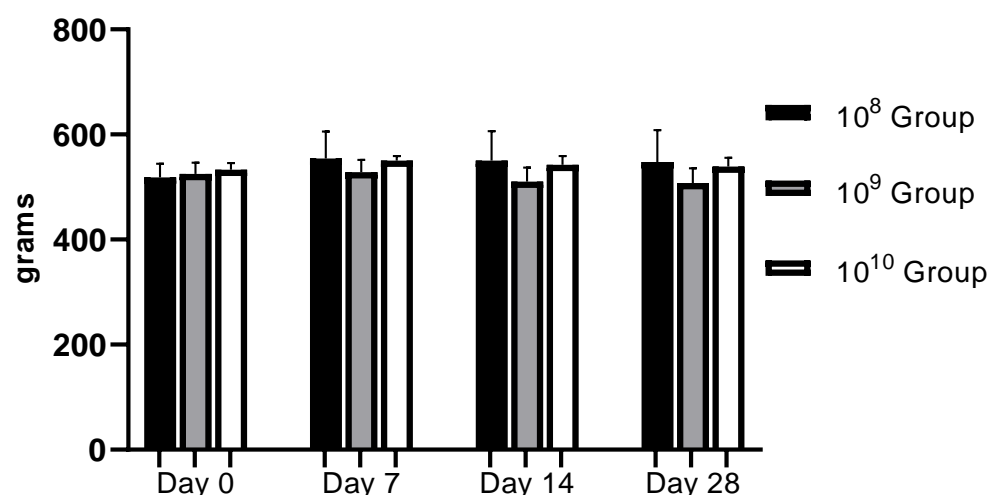
Figure 2. Evolution of body weight during the study (regardless of the bacterial concentration used, no statistically significant changes were recorded).

The hematological examination was performed on an Idexx Procyte 5diff analyzer using blood collected in EDTA vacutainers (KIMA Vacutest, Arzergrande, Italy). We followed the PMNs, since in PD, they are the cells responsible for the annihilation of pathogens. Regarding the number of neutrophils, which represent 50–70% of the total PMN, a decrease in their number was observed as periodontitis was installed in the case of all groups, but a strongly statistically significant relevance was recorded in the 10^9 group ($p < 0.0001$; Figure 3) in the last 2 weeks of the study. The values expressed on day 0 can be explained by the fact that the blood was collected after finishing the application of ligatures to all animals. Thus, after we finished applying the ligature to the last animal, the blood collection started from animal number 1. Therefore, the time elapsed from the application of the ligatures to the time of blood collection influenced the entry of and the number of neutrophils as the body's response to the trauma and to the presence of bacteria. The initial response to acute periodontal inflammation is the physiological response to the oral microbial challenge to recruit leukocytes to sites of infection [24]. Regarding the expression of and the number of neutrophils, our analysis focused on the body's response within the group. In the case of group 10^9, an increase in the number of neutrophils can be observed from the first blood collection (approximately 3 h after the application of the ligature and contamination with the bacterial inoculum). This is a hyperactive response that occurred as a result of the body's interaction with micro-organisms, which most likely led to the release of proinflammatory cytokines from the tissues. The same observation was made by Matthews et al. (2007) in a comparative study showing hyperfunctionality of blood PMNs in PD patients compared to healthy controls [25].

Lymphocytes, the elements involved in the immune response of the host, did not provide statistically significant results between day 0 and the final day of the study ($p < 0.05$) except in the case of group 10^9 (Figure 4), a sign that this group is maintained in an active phase, an aspect strengthened by the activity of neutrophils.

Histological analysis—The samples represented by the maxillary incisors with the ligature, together with the related gum, were collected, fixed in 10% neutral buffered formalin, and demineralized in 5% nitric acid for 14 days. After decalcification, the specimens were dehydrated and embedded in paraffin. Sections with a thickness of 4 μm were obtained in the transverse plane. Sections were stained with hematoxylin and eosin (H&E) using standard protocols [26]. The sections were evaluated by light microscopy (4× magnification), and parameters such as the influx of inflammatory cells and the integrity of the alveolar bone and cement were monitored (Figures 5 and 6).
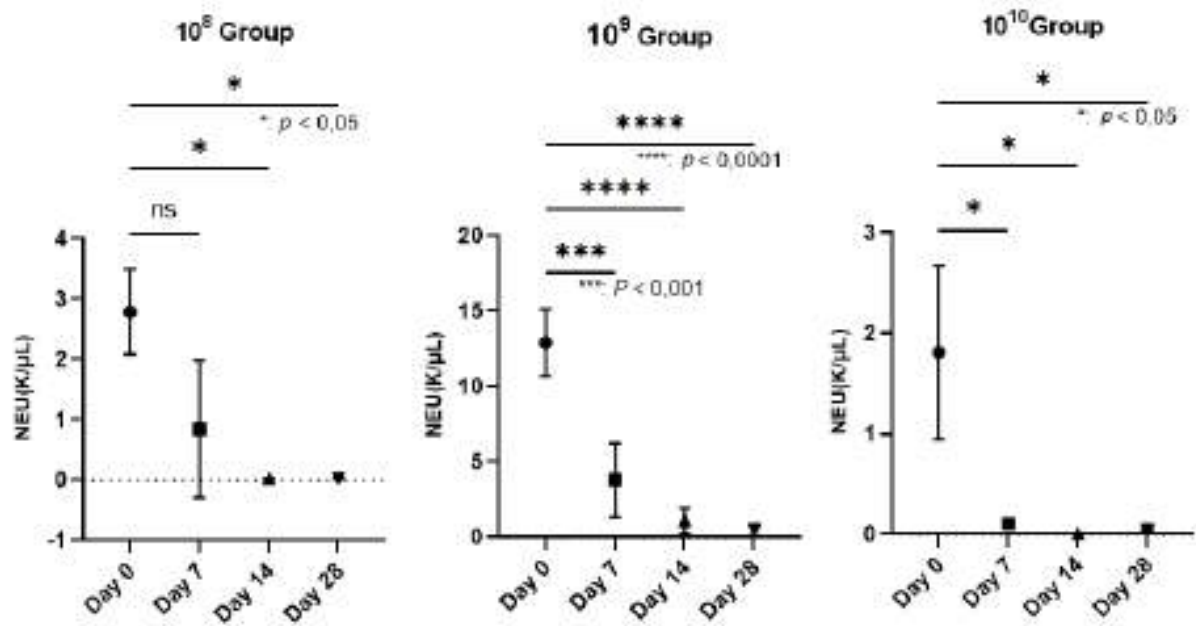
Figure 3. Reduction in the number of neutrophils (NEU) on the wall of the PD installation depending on the bacterial concentration used (In group 10^8, neutrophils decreased starting the 3rd week after contamination; $p < 0.05$). The most relevant decrease in neutrophils was observed in group 10^9, where, starting the second week, their number began to decrease more dramatically than in the case of group 10^8, registering increasingly lower values until the end of the study, when $p < 0.0001$. In group 10^{10}, the number of neutrophils decreased constantly during the study, with a p value < 0.05.
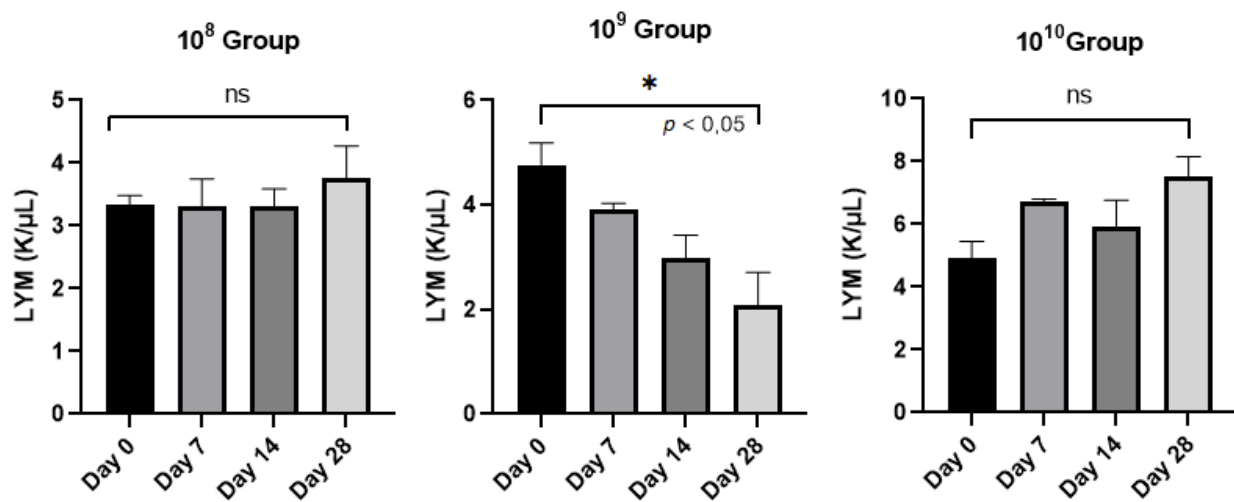

Figure 4. Evolution of the number of lymphocytes (LYM)/group analyzed from day 0 to day 28.

The microbiological examination consisted of taking samples from the gum and the ligatures. The samples were seeded in a liquid Schadler medium and incubated under anaerobic conditions for 24 h after each renewal of the ligatures. From the 24 h suspension, plates were inoculated with Shadler agar, as well as Columbia 5% ram blood and Columbia 7% ram blood. A 24 h reincubation of the plates followed; then, smears were made from the grown colonies to identify the bacterial strains used. From the first week after contamination, in the case of all groups, Gram(−) specific A.a coccobacilli, F.n Gram(−) bacilli, or S.o Gram(+) chains were identified in the smears, together with the oral microflora of rats represented by *Staphyococcus sciuri*, *Staphylococcus xylosus*, *Proteus mirabilis*, or *Enterococcus faecium*, with the analysis of the smears completed using a MaldiTof (Bruker MALDI Biotyper).
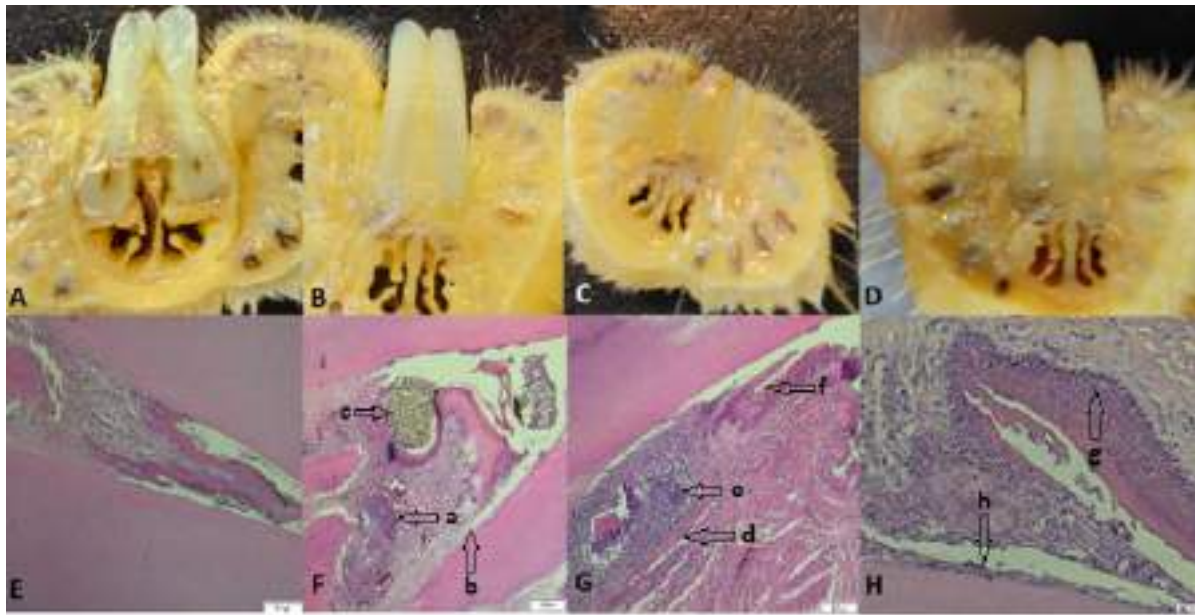
Figure 5. (**A–D**) Images with cross sections through the collected part; (**E**) the part collected from a control rat, uncontaminated and without ligature, showing intact alveolar bone and continuous cementum; (**F**) the part from a rat from group 10^8, which presents hypertrophy, granulation tissue (a) with nucleated cells that peel off, abundant neutrophils, coccobacilli, inflammation, hyperemia, hyperplasia of the gingival epithelium, and periodontal lysis (b), with a ligature thread present (c); (**G**) rat teeth from group 10^9 (granuloma) (d), alveolar bone lysis, pulp tissue with necrotic bone fragments surrounded by pyogranulomatous inflammation, neutrophilic infiltrate (e), abundant granulation tissue, bacteria (coccobacilli), and fodder in the space periodontally invaded with bacteria (f); (**H**) teeth of rats from group 10^{10} with hyperplasia (g), an intact alveolodental ligament, abundant granulation tissue, fewer inflammatory cells, bacteria in the alveolar sac, and anucleated desquamation cells on the alveolodental ligament area (h). Sections were stained with H&E. Original magnification: $4\times$; scale bars = 200 μm.
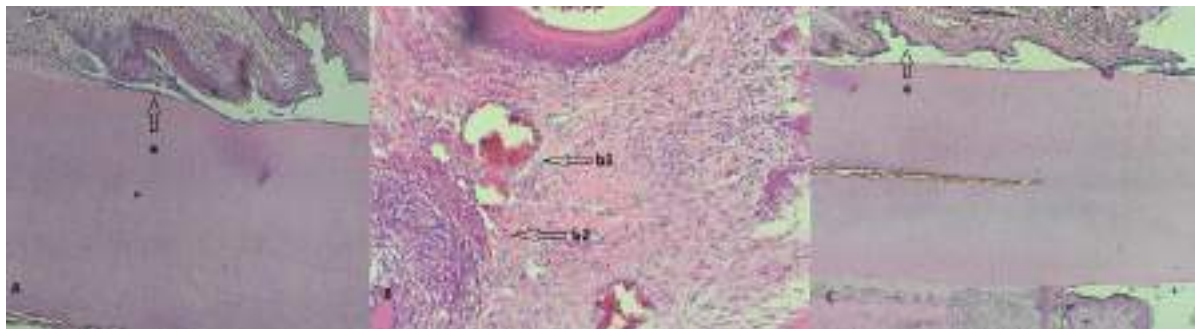

Figure 6. (**A**) Detail of a rat tooth from group 10^8 with a partially desquamated alveolodental ligament (a); (**B**) strong reaction of hyperemia (b1) and neutrophilic infiltrates (b2) in a rat from group 10^9; (**C**) overview highlighting the periodontal sac (c) of a rat from group 10^{10}.

4. Discussion

The term periodontitis is used to express the presence and multiplication of microorganisms at the level of the oral cavity—more precisely, at the level of the gum, ligament, and alveolar bone [27]. Incriminated in the development of PD are Gram(−) anaerobes, the most widespread of which, in the subgingival space, seem to be A.a, P.g, *Prevotella intermedia* (P.i), and T.f. Through an immunopathogenic mechanism, they are involved in the development of the disease from the beginning by multiplying, resulting in the

periodontal pocket. The body responds by forming the inflammatory infiltrate represented by macrophages and lymphocytes, which produce cytokines and biological mediators [28].

Dental plaque is a favorable environment for the multiplication of microorganisms and the formation of biofilms [29], so PD is associated with plaque, and although it has a wide etiology, the most studied causes are microbial and immunological [30,31]. In the oral environment, bacteria grow in complex polymicrobial associations, with more than 700 bacterial species living in the oral cavity [32]. Species of the genus *Streptococcus* are early colonizers of the mouth that actively recruit bacteria such as P.g through several genetic mechanisms [33], contributing to the general functional heterogeneity of the biofilm. This heterogeneity provides the biofilm new characteristics, such as easy adhesion to surfaces, metabolic co-operation whereby the waste product of one bacterial species serves as a food source for another [34], increased antibiotic resistance, and the ability of biofilms to evade the host's immune system. Recent research has shown that A.a, in associated with *Streptocoocus* spp., stimulates resistance to the host's innate immunity [35], generating imbalances in the normal flora of the oral cavity. This phenomenon is translated by the term dysbiosis, and as periodontitis develops, the oral microbiota changes from one consisting mainly of Gram(+) aerobes to a constant microbiota mainly comprising Gram(−) anaerobes [36], ultimately resulting in the clinical expression of the disease. Simultaneously, a succession of microbial complexes takes place, the first of which is the so-called "orange complex", which consists of anaerobic Gram(−) species, among which we find F.n [37,38]. F.n is a binder for other bacterial species responsible for PD development, i.e., strains belonging to the "red complex", which includes bacteria such as P.g, T.f, T.d, and, more recently, A.a [39]. In this sense, the objective of this study was to induce periodontitis through the oral contamination of rats with bacteria that are directly responsible for this condition in humans in order to better understand its pathogenesis and develop therapeutic schemes.

The analysis of periodontitis in a rat model provided remarkable insights into the pathogenesis of the disease, recapitulating the clinical or histological characteristics [40,41]. Rats resemble humans when developing periodontitis in terms of the composition of the dental plaque and the appearance of histopathological lesions specific to this disease. In rats, PD appears within a few weeks when induced by ligatures and in an even shorter period of 7–15 days when the pathogenic bacterial flora intervenes [42].

In most studies, placing a silk thread around the bundle of maxillary or mandibular premolars is reported to stimulate bacterial colonization and biofilm formation, resulting in apical epithelial migration and bone loss as observed in clinical settings [43]. In our study, we placed these ligatures with gingival retraction wire around the maxillary incisors for the advantage of easy access and injury of the gum to apply the ligatures contributed to the rapid establishment of PD, an aspect also mentioned by other researchers who associate traumatic injuries with the pathogenesis of PD induced by ligation in rodents [44]. A simple ligature without bacterial involvement does not cause significant bone loss in rats, as shown by Bezerra et al. [45], who concluded (in contrast to other researchers) that the accumulation of bacteria around the ligature thread plays an important role in PD induction and progression [46]. In light of these considerations with respect to PD induction, we chose the ligation model completed by oral contamination with three of the most representative bacteria for periodontitis. The clinical signs observed after the first week of contamination (bleeding when palpating the gums) suggested the onset of PD installation. A disadvantage of placing the ligature on the maxillary incisors is the loss of the ligatures within 4–5 days of application, even with the ligature in an "8" pattern [47,48], requiring renewal every week.

Biological mediators involved in periodontitis provide valuable information about host–microbial interactions and inflammation [49]. The diseased periodontal tissue constantly guides neutrophils and leukocytes [50] to the junctional epithelium that borders the oral microflora, causing the activation of immune cells such as lymphocytes. The latter trigger the release of prostaglandins, interleukin-1β (IL-1β), tumor necrosis factor-α (TNF-α), and IL-6, culminating in the triggering of osteoclastogenesis and bone destruction by direct stimulation of osteoclasts or by the release of enzymes for tissue destruction

by inflammatory cells [51]. Using the ligature-induced periodontitis model periodically impregnated with A.a, F.n, and S.o in rats, we addressed the host response at clinical, biological, and histological levels from the onset of the disease until the end of the 28-day experimental period, and our results provide evidence of PD installation and the fact that the disease was in full evolutionary process in the group in which the bacterial strains were tested at a concentration of 10^9.

From a histopathological point of view, the results indicate that the bacterially contaminated ligation pattern leads to progressive alveolar bone resorption, suggesting two distinct phases: an acute phase (in group 10^9) and a chronic phase (in the case of group 10^{10}). Molon et al. divided the process of ligation-induced periodontitis in rats into two successive processes, concluding that in the acute process of periodontitis, inflammatory cell infiltration was obvious and that alveolar bone resorption was rapid, whereas in the chronic phase, the number of infiltrating inflammatory cells decreased, and alveolar bone resorption slowed [47]. In the case of all the tested groups, different stages of periodontitis installation were observed, but the need to differentiate PD installation as a shoulder of ligature placement versus the bacterial action is imperative. Because bone resorption in the ligature model is dependent on the presence of oral micro-organisms [44], in our study, we observed the presence of bacteria in the periodontal sac or attached to the ligature wire, regardless of the concentration used. Clinical periodontitis is mainly an inflammatory disease caused by bacteria as the initiating factor. Through the formation of bacterial plaque, inflammatory cells infiltrate the local periodontal tissue, and the differentiation of osteoclasts occurs, resulting in alveolar bone resorption [52]. Similar to the traditional rat model of periodontitis, this model induced local periodontitis by simulating bacterial aggregation in the periodontal tissue, causing alveolar bone resorption [53]. Bone resorption occurred only in the case of concentrations of 10^9 and 10^{10}, complemented by a pyogranulomatous reaction specific to bacterial aggressiveness on the periodontal tissues, as mentioned by Bascones-Martínez in his research [28]. Comparing the histological effects produced by the three bacterial concentrations, we mention that the severity of the disease depends on the concentration in the sense of exacerbating its intensity, as suggested by Yuan et al. [54]. Therefore, for oral contamination over a period of 4 weeks, the bacterial action is necessary for a concentration of 10^9 or 10^{10} through the PD model thus created, and advanced bone loss can be expected in a relatively short time.

5. Conclusions

In summary, our findings obtained in rats provide experimental evidence that ligations impregnated in bacterial culture represented by A.a, F.n, and S.o induced obvious PD when concentrations of 10^9 and 10^{10} CFU/mL of each strain were used. Based on the presence of inflammatory infiltrate and bone resorption observed upon histopathological examination, complemented by the abundance of neutrophils in group 10^9, we recommend this model for the most effective induction of periodontitis in the shortest time.

References

1. Bhattarai, G.; Poudel, S.B.; Kook, S.-H.; Lee, J.-C. Resveratrol prevents alveolar bone loss in an experimental rat model of periodontitis. *Acta Biomater.* **2016**, *29*, 398–408. [CrossRef]
2. Okuda, K.; Kato, T.; Ishihara, K. Involvement of periodontopathic biofilm in vascular diseases. *Oral Dis.* **2004**, *10*, 5–12. [CrossRef]
3. Graves, D.T.; Jiang, Y.; Genco, C. Periodontal disease: Bacterial virulence factors, host response and impact on systemic health. *Curr. Opin. Infect. Dis.* **2000**, *13*, 227–232. [CrossRef]
4. Kobayashi, N.; Ishihara, K.; Sugihara, N.; Kusumoto, M.; Yakushiji, M.; Okuda, K. Colonization pattern of periodontal bacteria in Japanese children and their mothers. *J. Periodontal. Res.* **2008**, *43*, 156–161. [CrossRef]
5. Eke, P.I.; Dye, B.A.; Wei, L.; Slade, G.D.; Thornton-Evans, G.O.; Borgnakke, W.S.; Taylor, G.W.; Page, R.C.; Beck, J.D.; Genco, R.J. Update on Prevalence of Periodontitis in Adults in the United States: NHANES 2009 to 2012. *J. Periodontol.* **2015**, *86*, 611–622. [CrossRef]
6. Eke, P.I.; Borgnakke, W.S.; Genco, R.J. Recent epidemiologic trends in periodontitis in the USA. *Periodontology 2000* **2019**, *82*, 257–267. [CrossRef] [PubMed]
7. Raja, M.; Ummer, F.; Dhivakar, C.P. *Aggregatibacter actinomycetemcomitans*—A tooth killer? *J. Clin. Diagn. Res.* **2014**, *8*, ZE13–ZE16. [CrossRef] [PubMed]
8. Bucur, I.; Petrec, O.; Mărăcine, D.M.; Degi, J.; Fluerașu, L. Demonstration Of Clumping Factor Using A Screening Test In Staphylococci Isolated From Animals. *Sci. Work. Ser. C Vet. Med.* **2015**, *61*, 29–31.
9. Sălăvăstru, D.I.; Gherghiță, O.R. Considerations Regarding The Use Of Experimental Animal Models In Dental Medicine—A Literature Review. *Agrolife Sci. J.* **2020**, *9*.
10. Brennan, C.A.; Garrett, W.S. *Fusobacterium nucleatum*—Symbiont, opportunist and oncobacterium. *Nat. Rev. Microbiol.* **2019**, *17*, 156–166. [CrossRef] [PubMed]
11. Henderson, B.; Kaiser, F. Bacterial modulators of bone remodeling in the periodontal pocket. *Periodontology 2000* **2018**, *76*, 97–108. [CrossRef]
12. Fine, D.H.; Schreiner, H.; Velusamy, S.K. Aggregatibacter, a Low Abundance Pathobiont That Influences Biogeography, Microbial Dysbiosis, and Host Defense Capabilities in Periodontitis: The History of a Bug, and Localization of Disease. *Pathogens* **2020**, *9*, 179. [CrossRef]
13. DiRienzo, J.M. Breaking the Gingival Epithelial Barrier: Role of the *Aggregatibacter actinomycetemcomitans* Cytolethal Distending Toxin in Oral Infectious Disease. *Cells* **2014**, *3*, 476–499. [CrossRef]
14. Khzam, N.; Miranda, L.A.; Kujan, O.; Shearston, K.; Haubek, D. Prevalence of the JP2 genotype of *Aggregatibacter actinomycetemcomitans* in the world population: A systematic review. *Clin. Oral Investig.* **2022**, *26*, 2317–2334. [CrossRef]
15. Johansson, A. *Aggregatibacter actinomycetemcomitans* Leukotoxin: A Powerful Tool with Capacity to Cause Imbalance in the Host Inflammatory Response. *Toxins* **2011**, *3*, 242–259. [CrossRef] [PubMed]
16. Kelk, P.; Moghbel, N.S.; Hirschfeld, J.; Johansson, A. *Aggregatibacter actinomycetemcomitans* Leukotoxin Activates the NLRP3 Inflammasome and Cell-to-Cell Communication. *Pathogens* **2022**, *11*, 159. [CrossRef] [PubMed]
17. Kumar, P.; Griffen, A.; Barton, J.; Paster, B.; Moeschberger, M.; Leys, E. New Bacterial Species Associated with Chronic Periodontitis. *J. Dent. Res.* **2003**, *82*, 338–344. [CrossRef]
18. Asakawa, R.; Komatsuzawa, H.; Kawai, T.; Yamada, S.; Goncalves, R.B.; Izumi, S.; Fujiwara, T.; Nakano, Y.; Suzuki, N.; Uchida, Y.; et al. Outer membrane protein 100, a versatile virulence factor of *Actinobacillus actinomycetemcomitans*. *Mol. Microbiol.* **2003**, *50*, 1125–1139. [CrossRef]
19. Stacy, A.; Everett, J.; Jorth, P.; Trivedi, U.; Rumbaugh, K.P.; Whiteley, M. Bacterial fight-and-flight responses enhance virulence in a polymicrobial infection. *Proc. Natl. Acad. Sci. USA* **2014**, *111*, 7819–7824. [CrossRef] [PubMed]
20. Ozuna, H.; Snider, I.; Belibasakis, G.N.; Oscarsson, J.; Johansson, A.; Uriarte, S.M. *Aggregatibacter actinomycetemcomitans* and *Filifactor alocis*: Two exotoxin-producing oral pathogens. *Front. Oral Health* **2022**, *3*, 981343. [CrossRef]
21. Al-Ahmad, A.; Wunder, A.; Auschill, T.M.; Follo, M.; Braun, G.; Hellwig, E.; Arweiler, N.B. The in vivo dynamics of *Streptococcus* spp., *Actinomyces naeslundii*, *Fusobacterium nucleatum* and *Veillonella* spp. in dental plaque biofilm as analysed by five-colour multiplex fluorescence in situ hybridization. *J. Med. Microbiol.* **2007**, *56 Pt 5*, 681–687. [CrossRef]
22. Teles, R.; Teles, F.; Frias-Lopez, J.; Paster, B.; Haffajee, A. Lessons learned and unlearned in periodontal microbiology. *Periodontology 2000* **2013**, *62*, 95–162. [CrossRef] [PubMed]
23. Mahabady, S.; Tjokro, N.; Aharonian, S.; Zadeh, H.; Chen, C.; Allayee, H.; Sedghizadeh, P. The in vivo T helper type 17 and regulatory T cell immune responses to *Aggregatibacter actinomycetemcomitans*. *Mol. Oral Microbiol.* **2017**, *32*, 490–499. [CrossRef] [PubMed]

24. Hiyoshi, T.; Domon, H.; Maekawa, T.; Tamura, H.; Isono, T.; Hirayama, S.; Sasagawa, K.; Takizawa, F.; Tabeta, K.; Terao, Y. Neutrophil elastase aggravates periodontitis by disrupting gingival epithelial barrier via cleaving cell adhesion molecules. *Sci. Rep.* **2022**, *12*, 8159. [CrossRef] [PubMed]

25. Matthews, J.B.; Wright, H.J.; Roberts, A.; Cooper, P.R.; Chapple, I.L.C. Hyperactivity and reactivity of peripheral blood neutrophils in chronic periodontitis. *Clin. Exp. Immunol.* **2007**, *147*, 255–264. [CrossRef]

26. Leitão, R.; Ribeiro, R.; Chaves, H.; Rocha, F.; Lima, V.; Brito, G. Nitric oxide synthase inhibition prevents alveolar bone resorption in experimental periodontitis in rats. *J. Periodontol.* **2005**, *76*, 956–963. [CrossRef]

27. Mombelli, A.; Mombelli, A. Periodontitis as an infectious disease: Specific features and their implications. *Oral Dis.* **2003**, *9* (Suppl. 1), 6–10. [CrossRef]

28. Bascones-Martínez, A.; Figuero-Ruiz, E. Periodontal diseases as bacterial infection. *Med. Oral Patol. Oral Cir. Buccal* **2004**, *9*, 92–100. (In English and Spanish) [CrossRef]

29. Darveau, R.P.; Tanner, A.; Page, R.C. The microbial challenge in periodontitis. *Periodontology 2000* **1997**, *14*, 12–32. [CrossRef]

30. Marsh, P.D. Dental plaque: Biological significance of a biofilm and community life-style. *J. Clin. Periodontol.* **2005**, *32*, 7–15. [CrossRef]

31. Ten Cate, J.M. Biofilms, a new approach to the microbiology of dental plaque. *Odontology* **2006**, *94*, 1–9. [CrossRef]

32. Aas, J.A.; Paster, B.J.; Stokes, L.N.; Olsen, I.; Dewhirst, F.E. Defining the normal bacterial flora of the oral cavity. *J. Clin. Microbiol.* **2005**, *43*, 5721–5732. [CrossRef] [PubMed]

33. Kuboniwa, M.; Tribble, G.D.; James, C.E.; Kilic, A.O.; Tao, L.; Herzberg, M.C.; Shizukuishi, S.; Lamont, R.J. *Streptococcus gordonii* utilizes several distinct gene functions to recruit *Porphyromonas gingivalis* into a mixed community. *Mol. Microbiol.* **2006**, *60*, 121–139. [CrossRef]

34. Davey, M.E.; O'toole, G.A. Microbial biofilms: From ecology to molecular genetics. *Microbiol. Mol. Biol. Rev.* **2000**, *64*, 847–867. [CrossRef]

35. Ramsey, M.M.; Whiteley, M. Polymicrobial interactions stimulate resistance to host innate immunity through metabolite perception. *Proc. Natl. Acad. Sci. USA* **2009**, *106*, 1578–1583. [CrossRef] [PubMed]

36. Marsh, P.D. Microbial ecology of dental plaque and its significance in health and disease. *Adv. Dent. Res.* **1994**, *8*, 263–271. [CrossRef]

37. Socransky, S.S.; Haffajee, A.D.; Cugini, M.A.; Smith, C.; Kent, R.L., Jr. Microbial complexes in subgingival plaque. *J. Clin. Periodontol.* **1998**, *25*, 134–144. [CrossRef] [PubMed]

38. Socransky, S.S.; Haffajee, A.D. Periodontal microbial ecology. *Periodontology 2000* **2005**, *38*, 135–187. [CrossRef]

39. Åberg, C.H.; Kwamin, F.; Claesson, R.; Dahlén, G.; Johansson, A.; Haubek, D. Progression of attachment loss is strongly associated with presence of the JP2 genotype of *Aggregatibacter actinomycetemcomitans*: A prospective cohort study of a young adolescent population. *J. Clin. Periodontol.* **2014**, *41*, 232–241. [CrossRef]

40. De Aquino, S.G.; Abdollahi-Roodsaz, S.; Koenders, M.; Van De Loo, F.A.J.; Pruijn, G.J.M.; Marijnissen, R.J.; Walgreen, B.; Helsen, M.M.; van den Bersselaar, L.A.; de Molon, R.S.; et al. Periodontal pathogens directly promote autoimmune experimental arthritis by inducing a TLR2- and IL-1-driven Th17 response. *J. Immunol.* **2014**, *192*, 4103–4111. [CrossRef]

41. Klausen, B. Microbiological and immunological aspects of experimental periodontal disease in rats: A review article. *J. Periodontol.* **1991**, *62*, 59–73. [CrossRef] [PubMed]

42. Wong, R.L.; Hiyari, S.; Yaghsezian, A.; Davar, M.; Lin, Y.-L.; Galvan, M.; Tetradis, S.; Camargo, P.M.; Pirih, F.Q. Comparing the Healing Potential of Late-Stage Periodontitis and Peri-Implantitis. *J. Oral Implant.* **2017**, *43*, 437–445. [CrossRef]

43. Saadi-Thiers, K.; Huck, O.; Simonis, P.; Tilly, P.; Fabre, J.-E.; Tenenbaum, H.; Davideau, J.-L. Periodontal and systemic responses in various mice models of experimental periodontitis: Respective roles of inflammation duration and *Porphyromonas gingivalis* infection. *J. Periodontol.* **2013**, *84*, 396–406. [CrossRef] [PubMed]

44. Abe, T.; Hajishengallis, G. Optimization of the ligature-induced periodontitis model in mice. *J. Immunol. Methods* **2013**, *394*, 49–54. [CrossRef]

45. Bezerra, M.; Brito, G.; Ribeiro, R.; Rocha, F. Low-dose doxycycline prevents inflammatory bone resorption in rats. *Braz. J. Med. Biol. Res.* **2002**, *35*, 613–616. [CrossRef]

46. Matsuda, Y.; Kato, T.; Takahashi, N.; Nakajima, M.; Arimatsu, K.; Minagawa, T.; Sato, K.; Ohno, H.; Yamazaki, K. Ligature-induced periodontitis in mice induces elevated levels of circulating interleukin-6 but shows only weak effects on adipose and liver tissues. *J. Periodontal. Res.* **2016**, *51*, 639–646. [CrossRef]

47. De Molon, R.S.; Park, C.H.; Jin, Q.; Sugai, J.; Cirelli, J.A. Characterization of ligature-induced experimental periodontitis. *Microsc. Res. Tech.* **2018**, *81*, 1412–1421. [CrossRef]

48. Jeong-Hyon, K.; Bon-Hyuk, G.; Sang-Soo, N.; Yeon-Cheol, P. A review of rat models of periodontitis treated with natural extracts. *J. Tradit. Chin. Med. Sci.* **2020**, *7*, 95–103. [CrossRef]

49. Cavagni, J.; de Macedo, I.C.; Gaio, E.J.; Souza, A.; de Molon, R.S.; Cirelli, J.A.; Hoefel, A.L.; Kucharski, L.C.; Torres, I.L.D.S.; Rösing, C.K. Obesity and Hyperlipidemia Modulate Alveolar Bone Loss in Wistar Rats. *J. Periodontol.* **2016**, *87*, e9–e17. [CrossRef]

50. Darveau, R.P.; Marques, C.P.C.; Maor, Y.; de Andrade, M.S.; Rodrigues, V.P.; Benatti, B.B.; Tsuchida, S.; Satoh, M.; Takiwaki, M.; Wakabayashi, M.; et al. The oral microbial consortium's interaction with the periodontal innate defense system. *DNA Cell Biol.* **2009**, *28*, 389–395. [CrossRef]

51. Mundy, G.R. Inflammatory mediators and the destruction of bone. *J. Periodontal. Res.* **1991**, *26 Pt 2*, 213–217. [CrossRef] [PubMed]

52. Usui, M.; Onizuka, S.; Sato, T.; Kokabu, S.; Ariyoshi, W.; Nakashima, K. Mechanism of alveolar bone destruction in periodontitis—Periodontal bacteria and inflammation. *Jpn. Dent. Sci. Rev.* **2021**, *57*, 201–208. [CrossRef] [PubMed]

53. Marchesan, J.; Girnary, M.S.; Jing, L.; Miao, M.Z.; Zhang, S.; Sun, L.; Morelli, T.; Schoenfisch, M.H.; Inohara, N.; Offenbacher, S.; et al. An experimental murine model to study periodontitis. *Nat. Protoc.* **2018**, *13*, 2247–2267. [CrossRef] [PubMed]
54. Yuan, H.; Gupte, R.; Zelkha, S.; Amar, S. Receptor activator of nuclear factor kappa B ligand antagonists inhibit tissue inflammation and bone loss in experimental periodontitis. *J. Clin. Periodontol.* **2011**, *38*, 1029–1036. [CrossRef]

S.I. : 50TH ANNIVERSARY OF APPLIED PHYSICS

Laser engineered polymer thin films as drug delivery systems

A. Bonciu[1] · L. Cremer[2] · A. Calugaru[2] · E. Vlase[2] · C. Coman[2] · Alexandra Palla-Papavlu[1] · Dan Alin Cristian[3,4] · F. Grama[3,4]

Abstract

This study is focused on the fabrication of thin films of hydroxypropyl methylcellulose (HPMC) and ethyl cellulose (EC) polymer blends impregnated with captopril via matrix assisted pulsed laser evaporation (MAPLE) for the design of transdermal patches. The laser engineered polymer blend: captopril films are evaluated for physicochemical characteristics such as film morphology, chemistry of the films surface, drug content, and in vivo animal irritancy and skin sensitivity studies. The morphological investigation of the MAPLE fabricated coatings, i.e., by atomic force microscopy reveals that the morphology and topography of the polymer: drug films may be tuned by adjusting the HPMC: EC ratio in the MAPLE target. In addition, by tuning the HPMC: EC ratio in the as-deposited MAPLE films, it is possible to adjust the drug release profile. The Fourier-transform infrared spectroscopy investigation showed no interaction between captopril and the polymers (HPMC: EC) used. The skin irritation studies carried out on rabbits, showed no noticeable skin reactions, thus pointing out the compatibility of captopril with both the polymer blend and with the skin. In addition, no skin sensitization was noted among the guinea pigs that were challenged with the MAPLE fabricated transdermal patches. To sum up, the application of matrix-assisted pulsed laser evaporation for the fabrication of hydrophilic: hydrophobic polymer blends shows that there is great potential for the development of transdermal drug delivery system of captopril.

Keywords Captopril · Transdermal patches · Matrix-assisted pulsed laser evaporation · Laser · MAPLE · Hydroxypropyl methylcellulose · HPMC · Ethyl cellulose · EC · Drug delivery · Blends

1 Introduction

Drug delivery to patients for the treatment of acute or chronic diseases has been mostly accomplished using drug carriers like injectables, capsules, or tablets. Transdermal patches are alternative drug delivery systems, which are applied on the skin and are able to provide the controlled release of a drug, for the systemic treatment of the disease [1, 2]. They are designed to support the passage of drug substances from the surface of the skin, through its various layers and into the systemic circulation [3]. The advantages of the transdermal patches over its oral counterpart arise from the fact that they can offer a controlled release of the drug to the patient, enable a steady blood level profile, and a better patience compliance by avoiding hepatic first pass metabolism and effectiveness [4, 5]. Furthermore, the dosage form of transdermal patch is user friendly, convenient and offers multi-day dosing [6].

Transdermal patches are available on the pharmaceutics market since the 1980s, and are particularly important for the treatment of chronic diseases such as hypertension [7]. Hypertension is one of the most spread heart conditions, most commonly treated by oral medications, i.e., captopril (Catapres-TTS® (ALZA Corporation, Vacaville, CA, USA) [8]. Captopril is used in chronical treatment of hypertension and congestive heart failure as first agent, because of the absence of side effects in the majority of patients. The

✉ Alexandra Palla-Papavlu
alexandra.papavlu@inflpr.ro

✉ Dan Alin Cristian
dancristi@gmail.com; Daniel.cristian@umf.ro

1   National Institute for Lasers, Plasma, and Radiation Physics, Atomistilor 409, 077125 Magurele, Romania

2   "Cantacuzino" National Medico-Military Institute for Research and Development, Bucharest, Romania

3   "Carol Davila" University of Medicine and Pharmacy, Bucharest, Romania

4   General Surgery Department, Colțea Hospital, Bucharest, Romania

drug is an orally effective angiotensin I converting enzyme inhibitor [9]. However, long term therapy of hypertension by captopril on oral administration generally results in poor patient compliance due to the low bioavailability and short plasma half-life requiring increased frequency of drug administration [10].

The various properties of captopril are very suitable for a transdermal therapeutic system i.e., comparatively short elimination half-life and its oxidation rate in dermal homogenate is significantly lower than that in intestinal homogenate, low molecular weight (217.29 Da), low melting point (105–108 °C) and low daily therapeutic dose (50–75 mg) [9]. Captopril has a relatively short elimination half-life in plasma (1–3 h) and low oral bioavailability (60–75%). For these reasons, by applying this drug as a transdermal therapeutic system, dosing time intervals will be expanded [11]. However, to design efficient and cost-effective transdermal patches, all these possible benefits must be weighed against potential disadvantages. For example, there are some critical considerations to be taken into account for the optimization of a transdermal patch, such as its compatibility with the skin, and physical or chemical stability of the formulation and its components [12, 13]. Thus, material selection and fabrication techniques are crucial for the design of an efficient controlled drug release system based on transdermal patches.

The combination of hydrophilic:hydrophobic polymers are gaining increasing attention for their usage in controlled drug release systems. This is due to the possibility to tailor the drug release by changing the viscosity, substitution type and concentration of the hydrophilic polymer [14, 15].

Hydroxypropyl methylcellulose (HPMC): ethylcellulose (EC) blend was chosen for our approach, because it accrues both advantages of HPMC and EC. HPMC is frequently used due to the fact that is responsible for the formation, by hydration, of a diffusion and erosion-resistant gel layer which is able to control drug release [16]. EC is a non-toxic, stable, compressible, inert, hydrophobic polymer used for the fabrication of different drug release systems including tablets [17] or microcapsules [18]. Although there are numerous studies available on the realization of transdermal patches, there are still various questions to be answered and many parameters to be optimized. For example, rashes, local irritation or erythema could appear as a result of the drug, the adhesive, or excipients in the patch formulation. Moreover, the physicochemical properties of the drugs to be delivered are very important as only drugs with a lipophilic character can cross the stratum corneum, and ionic drugs cannot be delivered using transdermal route. In addition, transdermal drug delivery system cannot achieve high drug levels in blood/plasma [19, 20].

Thus, the aim of this study is focused on the realization of new proof-of-concept transdermal patches by using an alternative fabrication technology based on lasers, i.e., matrix assisted pulsed laser evaporation (MAPLE) [21–25]. Briefly, MAPLE is a thin film deposition technique similar to the pulsed laser deposition [26], with a different procedure for target fabrication. In PLD, the laser beam interacts with a target material, resulting in the formation of a plasma plume that is transporting the ablated species to a substrate placed parallel to the target. In MAPLE, the target consists in suspending the guest material in a solvent which is named matrix, and flash-freezing in liquid nitrogen the mixture resulting in a solid target. MAPLE has some advantages over the classical PLD, which arise mainly from the fact that in MAPLE, the matrix absorbs the laser radiation, there are no photochemical interactions between the matrix and the guest material, and ultimately, the guest material is collected, as a thin film onto the substrate. MAPLE has been already demonstrated for the successful deposition of polymer coatings [27, 28], polymer blends [29, 30], nanoparticles [31], and even polymer: carbon nanotube films [32].

The objective of the present work is to formulate matrix transdermal patches of captopril, to evaluate and establish their physico-chemical characteristics as well as their drug release profile, together with the skin irritancy and sensitization potential. With this research study we aim at advancing the optimization of transdermal therapeutic systems via novel laser-based approaches. In addition, this study could contribute to the understanding of laser-polymer-drug interactions and open new avenues for biomaterial development.

2 Materials and methods

2.1 Materials

Ethylcellulose (EC), i.e., the most insoluble cellulose derivative, and hydroxypropyl methylcellulose (HPMC) (hydrophilic polymer) are chosen as materials for the fabrication of thin films via matrix-assisted pulsed laser deposition (MAPLE). Captopril (Cp) is a well-established antihypertensive drug that is available in oral dosage form and could benefit from transdermal drug delivery. All materials are obtained from Sigma-Aldrich and used without further purification. The chemical formulas of ethylcellulose, hydroxypropyl methylcellulose, and captopril are shown in Fig. 1.

Double distilled water, toluene, and ethanol are also obtained from Sigma-Aldrich and used as matrices without further purification. The polymers are suspended in the compatible solvents (EC in toluene: ethanol 80:20 wt%, HPMC in distilled water, two different experiments) to 1 and 2 wt% solutions and then flash frozen in liquid nitrogen resulting in solid targets which are used in the MAPLE experiments.
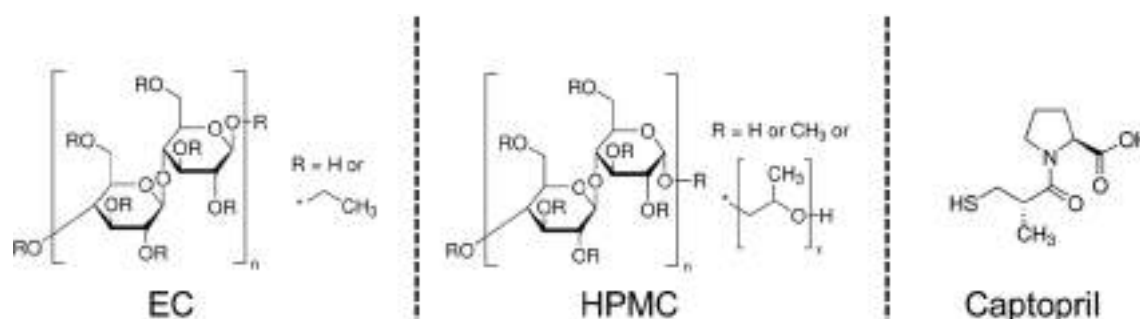
Fig. 1 Chemical structure of the materials used for laser processing

2.2 Preparation of patches via matrix assisted pulsed laser evaporation (MAPLE)

In this work, we aim at the fabrication of a proof-of-concept transdermal therapeutic system via matrix assisted pulsed laser evaporation. Here, the forth harmonic (266 nm laser wavelength) of a "Surelite II" pulsed Nd:YAG laser system (Continuum Company) is used to irradiate the frozen (polymer blend: drug): solvent target. The target is rotated with a motion feedthrough driven by a motor resulting in the laser beam describing a circle onto the sample to achieve uniform evaporation. The laser fluence is set at 500 mJ/cm^2. The polymer blend: drug thin film depositions are carried out in vacuum, at a background pressure ranging from 7×10^{-5} to 2×10^{-4} mbar, obtained with a Pfeiffer-Balzers TPU 170 turbomolecular pump (170 Ls^{-1}). During some depositions the pressure varied probably due to outgassing of the targets under vacuum. A scheme of the experimental setup is shown in Fig. 2 [32]. The number of pulses is varied between 96,000 and 100,000, resulting in polymer blend: drug films with thickness of around 500 nm thick. The substrates are kept at ambient temperature during the depositions and are placed at a distance of 4 cm from the frozen target. For the MAPLE experiments, two types of substrates are used: (1) double polished silicon substrates Si(100) cut into 1 cm^2 samples, which are transparent in the IR further and which are used for post-characterization; (2) flexible polyimide substrates which are further used for the in vivo tests.

All substrates used in both types of experiments are cleaned prior to any deposition. The substrates are ultrasonicated in successive baths of acetone and ethanol, followed by rinsing them several times in the ultrasonic bath with ultrapure water (0.2 μm filtered). They are finally dried in a nitrogen flow.
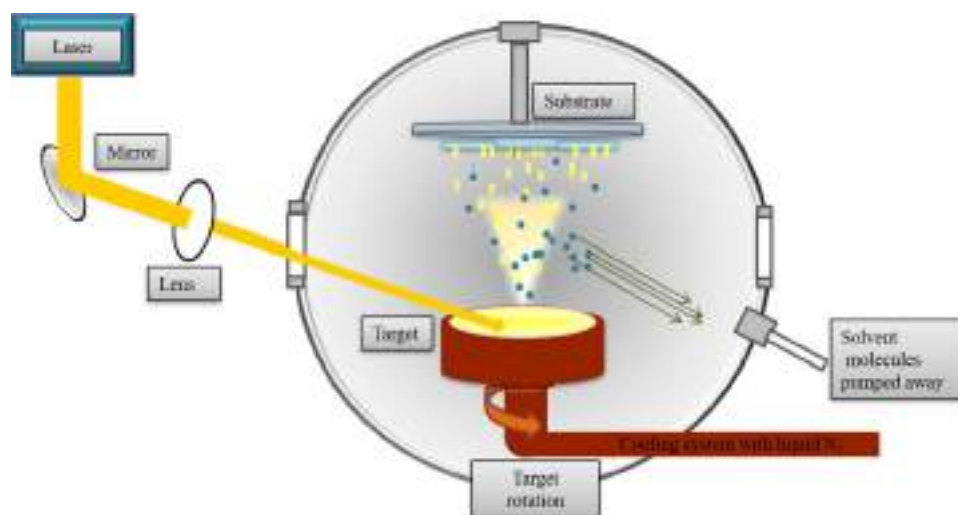
2.3 Animals

2.3.1 Ethics statement

This study on animals is carried out in compliance with the principles of ethics and in accordance with the provisions of EU Directive 63/2010 on compliance with the rules for the care, use, and protection of animals used for scientific purposes.

The study has been favorably evaluated by the Ethics Committee of the "Cantacuzino" National Medical-Military

Fig. 2 Scheme of the MAPLE experimental setup

Development Research Institute and approved by the national competent authority.

2.3.2 Animals

All animal experiments are conducted according to the International Standard ISO 10993-10:2010, biological evaluation of medical devices—part 10: tests for irritation and skin sensitization and made under Good Laboratory Practice (GLP) requirement.

Healthy, male New Zealand rabbits (weighing 2.2–2.5 kg, 6 months of age) and healthy adult male Dunkin-Hartley guinea pigs (weighing 300–500 g, 10–16 weeks of age) are provided by Băneasa Animal Facility area for rabbits and guinea pigs of "Cantacuzino" National Medical-Military Development Research Institute, Bucharest. All aspects related to animal housing and care are undertaken in accordance with the national and international regulations concerning animal testing. The breeding system is conventional, and the health monitoring is done according to the Federation of European Laboratory Animal Science Associations (FELASA) recommendations, all animals being negative for the specified pathogens. Throughout the study, the animals are kept under controlled conditions: artificial light 12 of 24 h, temperature of 18 °C $\pm$ 2°, relative humidity between 45 and 65% and they received standard pellets food (Cantacuzino Institute, Romania) and water ad libitum. The animals are inspected daily for health status. The rabbits are kept individually in $713 \times 716 \times 115$ mm stainless steel cages (Tecniplast spa, Italia) and the guinea pigs 5 animals per $612 \times 435 \times 216$ mm polycarbonate cages, (Tecniplast spa, Italia). Acclimation period is 7 days prior to the beginning of the experiment.

2.4 Evaluation of patches

2.4.1 Physical–chemical investigations

Given the multiple considerations and complexity in the design of a transdermal therapeutic system, we have been studying both the physical and chemical properties of the polymer blend and drug as thin films together with the compatibility of the laser engineered thin films with the skin.

Atomic force microscopy (AFM) measurements are carried out with an XE 100 AFM setup from Park Systems working in non-contact mode. Commercial silicon cantilevers are used (OMCL-AC240TS, Olympus cantilevers), with 70 kHz nominal resonance frequency and 2 N/m nominal force constant.

The as-deposited polymer blend: drug films morphology, as well as the root mean square roughness (RMS) on several different areas and dimensions, i.e., from 5 µm $\times$ 5 µm to 40 µm $\times$ 40 µm are determined.

In order to check for any chemical changes on the surface of the laser engineered thin films, the infrared spectra of the native molecules are measured and compared with the thin film spectra. Fourier transform infrared spectroscopy (FTIR) measurements are carried out with a Jasco FT/IR-6300 type A spectrometer in the range 400–4000 cm^{-1}. All spectra are obtained by absorption measurements, accumulating 128 scans, and CO_2/H_2O correction.

The wettability of the deposited thin films is investigated by measuring the contact angles with the sessile drop technique, by depositing a drop of liquid onto the film surface. The drop is imaged and the resulting contact angle is determined by drop shape image analysis calculation. The instrument used is a CAM101 optical system (KSV Instrument Ltd.). The contact angle measurements are carried out in open air, at a room temperature of 22 $\pm$ 2 °C by using water. The volume of the water droplets is 1.5 $\pm$ 0.2 µl. Three droplets are deposited at different regions of the same film. The contact angle is averaged over three measurements.

2.4.2 Drug release studies

The determination of the drug release rate is a very important study which gives an indication on the sustained release performance of the as-deposited MAPLE films together with the duration of the drug release.

To study the drug release profile of the as-deposited MAPLE polymer blend: drug films, they have been immersed in 100 mL phosphate-buffered saline solution (PBS, pH 7.4) at 37 °C. At pre-determined time intervals, 1 mL of solution is withdrawn and an equal amount of PBS is added (pH 7.4 at 37 °C). The Cp content within the extracted volume is analyzed with a Perkin-Elmer UV–Vis spectrophotometer by the absorbance at 200 nm [33]. All experiments are carried out in triplicate and the mean values are calculated. Further on, the data obtained is fitted with different models, i.e., Higuchi, Hixson–Crowell, Korsemeyer–Peppas, etc. in order to shed light on the mechanisms governing the captopril release kinetics from the MAPLE deposited films.

2.4.3 In vivo tests: skin irritancy

The first test carried out is the evaluation of the skin irritancy of the polymer blend: drug films obtained by MAPLE. The study is carried out according to the International Standard ISO 10993-10 biological evaluation of medical devices—part 10: tests for irritation and skin sensitization and was approved by the Ethics Committee of the Cantacuzino Institute.

To evaluate the skin irritancy, the MAPLE fabricated polymer: drug coatings are deposited onto polyimide substrates (2.5×2.5 cm each). The control substance is sodium lauryl
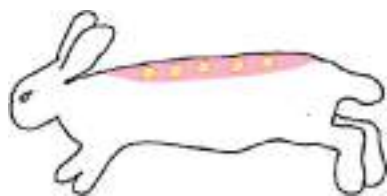
Fig. 3 Representative image of in vivo study displaying patches application process. (i) Shaving the rabbit hair on the back, (ii) patches applied in situ, (iii) patches removed from the back of a rabbit after 24, 48, 72 h

sulphate (SLS). The control substance is diluted to a final concentration of 5%wt in PBS. According to [34] SLS has an irritant potential, and concentrations between 2 and 5% may cause allergic reactions or sensitize the skin.

Three male albino rabbits are used for this study, 6 months old, 2200–2500 g each. 18 h prior to the experiments the fur of the rabbits is shaved to allow the application of the polymer blend: drug films. The MAPLE fabricated polymer blend: drug films are applied in three or five places paravertebrally on each side of every rabbit. Similarly, a control patch is applied either in three or five places of every rabbit paravertebrally. A scheme depicting the application process of the as-deposited MAPLE coatings is shown in Fig. 3.

The rabbits are scored according to the ISO, i.e., if the difference between the average of the MAPLE polymer blend: drug films and the control polymer blend: drug films is smaller or equal to 1, then the MAPLE patches are considered non-irritant.

2.4.4 In vivo tests: skin sensitization by Guinea Pig Maximization Test (GPMT)

The second test carried out is the evaluation of the skin sensitization by the Guinea Pig Maximization Test (GPMT) as a result of the application of the as-deposited MAPLE films. The study is conducted according to the International Standard ISO 10993-10: biological evaluation of medical devices—part 10: 2010—tests for irritation and skin sensitization.

The animals used are albino guinea pigs, males (15 animals in total) with weighs between 300 and 500 g. The animals are divided into two groups: a test group and a control group. Prior to each phase of the study, the animals are shaved in the areas where the test substances are applied.

The substances used in this test are: (1) Test sample—polymer film extract from the patches; (2) solvent – methanol; (3) diluent—extra virgin olive oil; and (4) Freund's complete adjuvant (FCA). The study consists of three phases: (1) induction stage 1 (day 0), (2) induction stage

2 (day 7), and (3) the challenge stage (day 21), which shall be described below.

In the intradermal injection phase, the skin of the animals from the control group is injected intradermally (as shown in Fig. 4) with a volume of (A) 0.1 mL of FCA, (B) solvent, (C) 0.1 mL mixture FCA with methanol 50%v/v. Similarly, the skin of the animals from the testing group is injected intradermally (as shown in Fig. 4) with a volume of (A) 0.1 mL of mixture FCA: solvent 50% v/v, (B) sample to test undiluted, (C) 0.1 mL mixture FCA: solvent 50%v/v with the sample to test undiluted 50% v/v.

7 days after the intradermal injection phase, in the induction phase, the test solution is applied on a cotton patch of approx. 8 cm^2 on the shaved skin of the animals in the test group. Similarly, the animal in the control group is treated the same, with solvent. The patches are held firmly in place for 48 h by wrapping the trunk of the animal with elastic bandages.

14 days after the induction phase, the animals are prepared for the challenge phase. A challenge dose is applied topically on the right side (which remained untreated during the induction application) to all the animals in the test group. The left side which had previously received induction applications, is unchallenged. All patches are held in contact with the skin for 24 h before removal.

The skin sites are evaluated using the scoring system for erythema and edema formation of Magnusson and Kligman (ISO 10993-10) [35] for each site challenged. Observations are made 24 and 48 h after initiation of the challenge application and the skin reactions are recorded (Table 1).
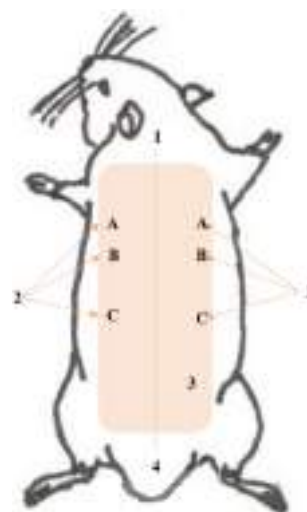

Fig. 4 Injection sites. 1: cranial end; 2: A, B, C, intradermic administration of 0.1 mL; 3: shaved interscapular region; 4: caudal end

Table 1 Classification after Magnusson and Kligman [35]

The reaction after removing patches grading scale	Grading scale
No visible change	0
Discrete or barely perceptible erythema	1
Moderate to severe erythema	2
Severe erythema and/or edema	3

3 Results and discussion

3.1 Morphological investigation of the fabricated patches

The aim of this work is the demonstration of a proof-of-concept transdermal patch fabricated via matrix-assisted pulsed laser evaporation (MAPLE) consisting of a polymer blend: drug for the controlled release of captopril. First, we focus on the morphological investigation of the polymer blend: drug films as-deposited by MAPLE and the potential influence of the surface morphology and topography on the drug release profile.

The first observation is that the hydrophilic/hydrophobic ratio modification within the MAPLE deposited thin films results in morphology and roughness changes. These changes are investigated by a detailed morphological evaluation of the MAPLE deposited thin films via atomic force microscopy (AFM) operating in non-contact mode. The polymer blend: drug AFM images taken on 40 µm × 40 µm areas are shown in Fig. 5 and the root-mean-square (RMS) values (representing the standard deviation of the surface heights) of the scanned surface topography, at the different scan areas are presented in Table 2. The AFM investigations reveal that the as-deposited polymer blend: drug films cover the entire substrate and are free of micrometric cracks. The polymer blend: drug films are dense, and they present micrometric and nanometric formations on the surface as well as small pores (between 70 and 200 nm). Additionally, 10% captopril-containing polymer blend films exhibit a subtly different morphology compared to 1% captopril-containing films, characterized by decreasing roughness values as drug

Table 2 RMS as calculated from the AFM for the HPMC: EC: Cp thin films

MAPLE coatings/ RMS (nm)	No Cp	Cp 1%	Cp 5%	Cp 10%
HPMC80:EC20	248	430	321	240
HPMC60:EC40	330	363	211	166
HPMC40:EC60	227	230	220	160
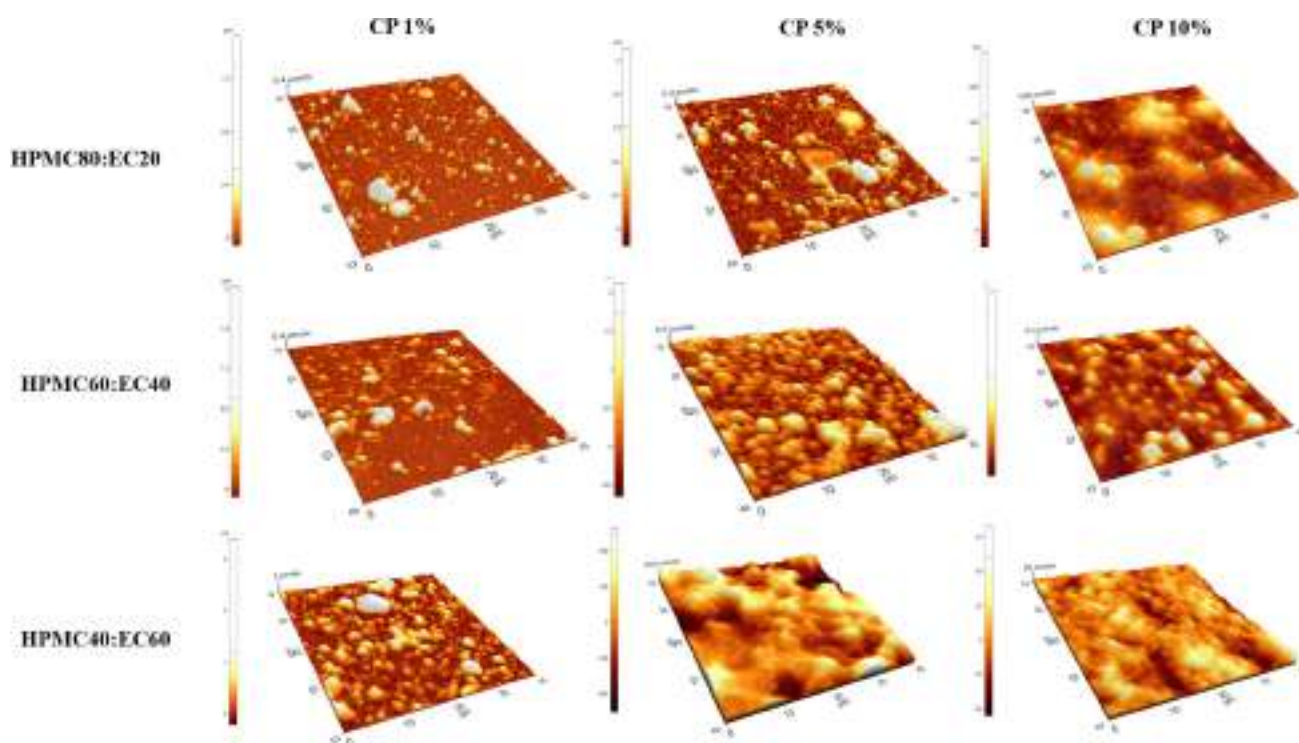
Fig. 5 3D Atomic force microscopy images taken on a 40 µm × 40 µm are of HPMC: EC: Cp thin films deposited by MAPLE

concentration increases, clearly indicating that surface morphology and microstructure can change depending on composition. Furthermore, higher amount of EC leads to films characterized by the presence of nano-domains of spherical form, usually called clusters. In the dynamic simulations, the amount and size of clusters formed during the MAPLE process are influenced by the polymer chain entanglement, which can vary depending on the polymer concentration in the solution. The higher the polymer concentration (or, the higher the entanglement), the larger the clusters form. A coating may become rougher as a result of the deposition of large clusters.

Nano-domains are due to the existence of aggregates or clusters of HPMC chains in the film-forming solution [36] and the hydrophobic interactions between the hydrophobic substituents of HPMC polymer induce the formation of these clusters [37]. For all mixing ratios within the HPMC: EC polymer blends, the films are continuous, with an increased surface structuring and RMS up to 430 nm. The corresponding AFM images also show distinct features for

the polymer blend: drug, with the surface RMS roughness results revealing an increased roughness with the increase of HPMC ratio in the HPMC:EC blend incorporating 1% captopril (Table 2). Thus, this is a clear indication that the surface morphology and microstructure changes with the polymer blend: drug composition. The granular structure, characteristic of pure HPMC, preserves when the percentage of captopril increases, leading also to smoother films (as for example HPMC40:EC60: Cp 10%).

In addition to the surface morphology and topography, the surface chemistry of the as-deposited polymer blend: drug films is also important for tailoring the drug release profile. Thus, we apply Fourier transform infrared spectroscopy (FTIR) to study the characteristic vibrations of the functional groups in the MAPLE-deposited films. The FTIR measurements of unprocessed HPMC, EC, and Cp together with the different polymer: drug films deposited by MAPLE are shown in Fig. 6. The HPMC spectra reveals both the broad spectra of the stretching vibration of O–H at 3446 cm^{-1} as well as the stretching of the C–O–C
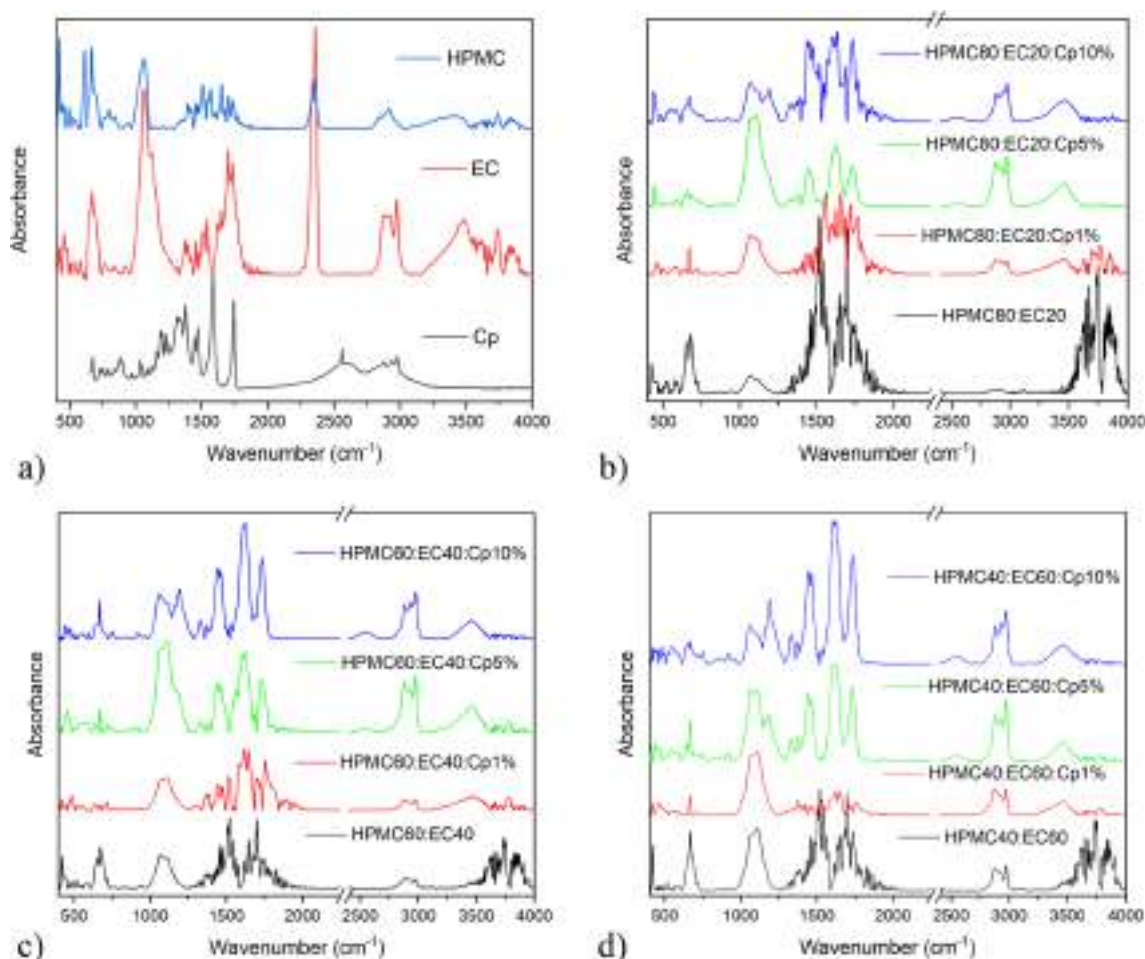

Fig. 6 FTIR spectra of different HPMC: EC: Cp films deposited by MAPLE

anhydroglucose ring at 1054 cm^{-1}, similar to those reported for HPMC [38]. The FTIR spectra of EC (see Fig. 6a) shows the characteristic peaks at 2974 cm^{-1} and 2869 cm^{-1} due to C–H stretching vibration peak. The –OH stretching vibration peak is observed at 3485 cm^{-1}. The peaks at 1091 cm^{-1}, and 1373 cm^{-1} correspond to C–O–C stretching and C–H bending respectively [39]. Furthermore, in the captopril powder spectra shown in Fig. 6a, the peaks at 2981 and 2949 cm^{-1} are assigned to the asymmetric CH$_3$ and CH$_2$ stretching vibration, whilst the peak at 2877 cm^{-1} is due to the symmetric CH$_3$ stretching mode. The peak at 2567 cm^{-1} corresponds to the SH stretching vibration, while the peaks at 1747 and 1591 cm^{-1} are assigned to the C=O stretching vibration of carboxylic acid and amide band, respectively. The peaks at 1469 cm^{-1} and 1385 cm^{-1} is due to the asymmetric and symmetric CH$_3$ bending vibrations, and the peak at 1333 cm^{-1} is assigned to the OH bending vibration. Finally, the peaks at 1228 cm^{-1} and 1200 cm^{-1} corresponded to the C–O and/or CN stretching vibrations [40–42]. The acquired spectra of the different ratios HPMC: EC films (i.e., 80:20, 60:40, and 40:60 respectively), shown in Fig. 6b–d, are similar to those reported in Ref. [43]. In the FTIR spectra of MAPLE-deposited HPMC:EC, the characteristic bands of HPMC and EC clearly appear.

For all the HPMC:EC films, the same bands may be seen in the spectra, although they are of different intensity, which may be attributable, at least in part, to the differences in the HPMC:EC film thickness.

The spectra recorded in Fig. 6 indicates that there is no significant change in the absorbance peaks of the mixture compared to individual polymers, therefore, it is suggested that no interaction occurred between the two polymers. Moreover, the IR spectra of the MAPLE deposited HPMC: EC: Cp films show that the polymer blend: drug films have not suffered any structural changes during MAPLE, and that there is no significant chemical modification between captopril and the two polymers used.

Furthermore, the wettability as well as the combined action between wettability and surface morphology of the polymer blend: drug films obtained by MAPLE is of major importance for the biocompatibility of a surface. The variation of the HPMC: EC: Cp films static contact angles with the modification of the drug loading is shown in Fig. 7. The contact angle of polymer blends decreases with the increase of the HPMC concentration and the decrease of the EC concentration. This tendency is attributed to the reduction of CH$_3$ groups from the film surface. Indeed, for pure ethyl cellulose, a contact angle of 84.5° has been observed previously [44] and the more hydrophobic groups there are in the polymeric chains, the films are unable to provide the hydrophilic property. The highest wettability values were obtained for films produced with increased EC amounts, respectively 40 and 60. It is possible to explain this result
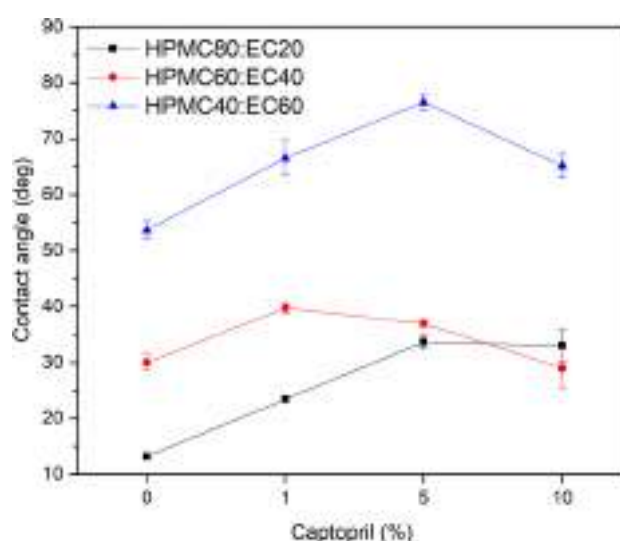

Fig. 7 Static contact angles measured on the HPMC: EC: Cp films deposited by MAPLE as function of concentration of captopril. The lines between points are guides to the eyes

by the greater granularity of the surfaces of these films (see Fig. 5). A decrease in wettability occurs as the granularity of the film surface increases. As the film's amount of contact with water decreases, different adhesion forces are generated, which are not strong enough to overcome the cohesion forces between water molecules. Furthermore, in these films, water access to EC hydroxylic groups is hampered due to the establishment of numerous hydrogen bonds between the cellulose chains. Thus, there is greater exposure of the axial direction of the glucopyranose ring, which is hydrophobic due to the C-H bonds between the pyranoside groups [45, 46]. Taking into account the classification of the contact angle, values between 0° and 90° indicate surfaces susceptible to wetting, all the polymer blends present a rather hydrophilic character. As a result of incorporating captopril into composites, the values of contact angles tended to increase, except for those containing 10% Cp. This variation in contact angle can be related to the surface morphology, specifically roughness, quite similar for the HMPC60:EC40:Cp10 and HMPC80:EC20:Cp10.

An important investigation carried out in this work is the study of the in vitro drug release profile of the as-fabricated MAPLE polymer blend: captopril films (Fig. 8a–c). The first observation we could make is that captopril release over 24 h from the as-fabricated MAPLE films increases with the increase of hydrophilic HPMC in the films. The HPMC80: EC20 and HPMC60: EC40 films as-deposited by MAPLE show a higher captopril release over 24 h (Fig. 8a, b) as compared to HPMC40:EC60, which show a slower release over 24 h (around 60%) (see Fig. 8c). Films with EC60 showed more prominent granularity (Fig. 5). The presence of HPMC between 60 and 80 in the film's composition, prevented
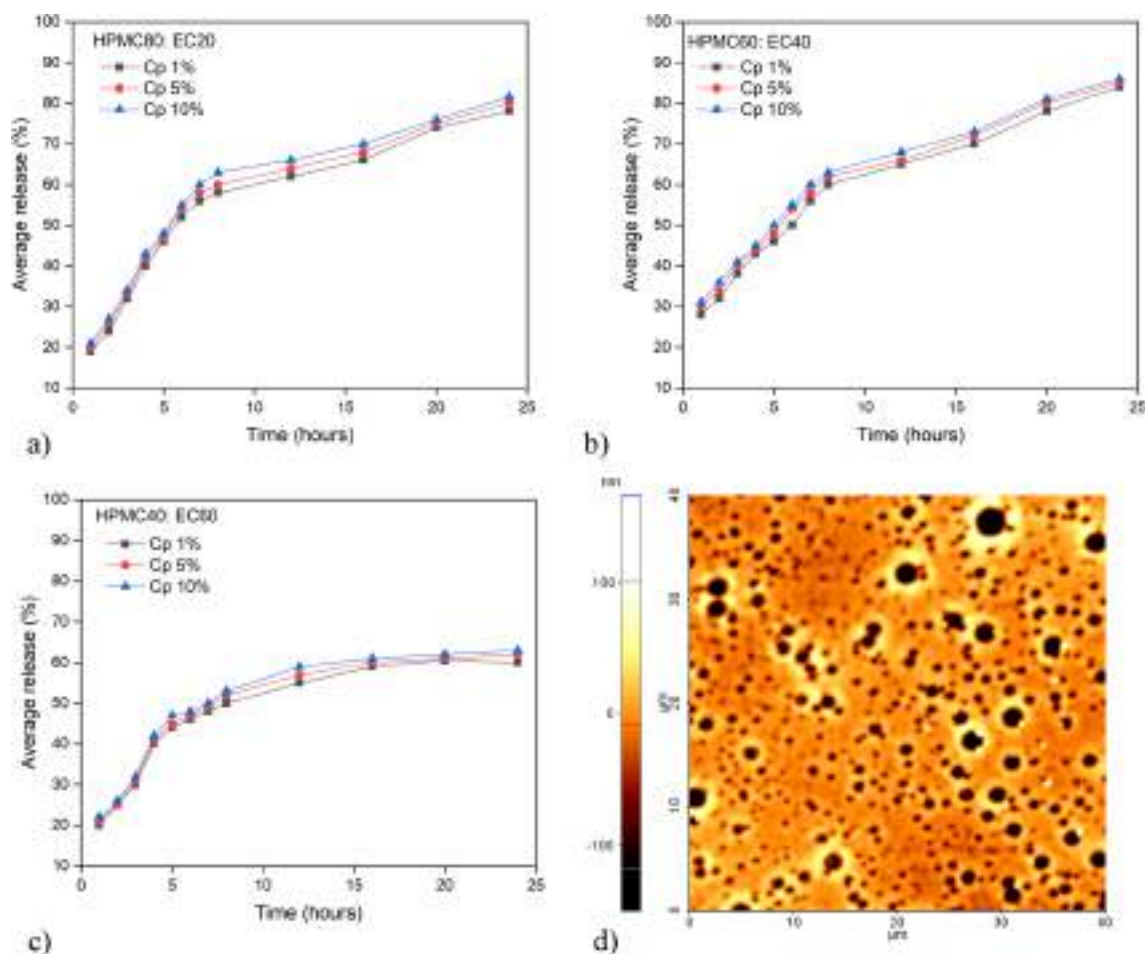
Fig. 8 **a–c** Average captopril release from different HPMC: EC films fabricated via MAPLE, **d** AFM image of HPMC60: EC40: Cp1 after 24 h of immersion in PBS

the formation of EC aggregates in larger dimensions and allowed the formation of layers. Furthermore, smaller diameters of the EC also contribute to a decrease in porosity due to the filling of empty spaces in the matrix. Upon contact with water, HPMC undergoes hydration, transitioning from a vitreous to an elastic state, resulting in the formation of a gel [46]. HPMC has a large amount of hydroxyl groups on its surface, which absorbs large amounts of molecules and disperse the matrix [47]. It has been found that EC in the HPMC matrix allows degradation in water to be reduced since cellulose is insoluble in water because of its crystallinity [48]. Furthermore, the hydrogen bonds formed by hydroxylic groups in the EC network and matrix are more robust and stable [49], reducing the degradation in the water of the films. Corroborating this, Larsson et al. [50] stated that structures composed of HPMC and EC suffer dissociation of EC and HPMC network, with the water entry into empty spaces. Thus, the hydrated HPMC will be diluted to lower concentrations and may untangle and diffuse out of the films.

The in vitro captopril release profile of all MAPLE fabricated patches shows an initial burst release, followed by a slow release of the drug. The initial burst release could be attributed to the release of captopril close to the surface of the films [51].

To better understand the mechanism of captopril release from the as-deposited HPMC: EC MAPLE films, the average percentage release of captopril is fitted into different models with the purpose of understanding the mechanism of drug diffusion from the patches. The models applied are compared by calculating the squared correlation coefficient (R^2) value. We found that the data follow the Korsemeyer–Peppas kinetic model [52], which describes the drug release from a polymer system equation.

The Korsmeyer–Peppas Eq. (1) is [52]:

$$M_t/M_\infty = k_{kp}t^n. \tag{1}$$

In Eq. (1), M_t represents the amount of drug released at time t, M_∞ represents the amount of drug released after ∞

period, k_{kp} is the Korsmeyer–Peppas release rate constant, whilst the value n characterizes the release mechanism of the drug, i.e., $n < 0.45$ the drug transport mechanism is Fickian diffusion, for $n = 1$, case II transport occurs leading to the zero-order release and for $0.45 < n < 1$ non-Fickian diffusion occurs.

The data obtained for captopril release from the HPMC: EC films obtained by MAPLE by applying the Korsmeyer–Peppas model is shown in Table 3.

As it can be observed from Table 3, the HPMC60: EC40: Cp10 together with HPMC40: EC60: Cp5 and HPMC40: EC60: Cp10 indicate the case II transport model. As it has been reported previously [53], this release mechanism occurred through the polymer dissolution controlled and polymeric chain expansion or polymer relaxation/swelling [53].

In contrast, the HPMC 80: EC20 films and HPMC60: EC40 with Cp1 and Cp5 films show a sustained release of captopril over 24 h, i.e., over 80, which is due to the diffusion mechanism, similar to the work reported in Refs. [51, 54]. The validity of this assumption is also based on the AFM image taken on a HPMC60: EC20: Cp1 sample after 24 h of Cp release in the PBS medium, shown in Fig. 8d. After 24 h of drug release in PBS, large pores can be seen on the surface of the HPMC60: EC40:Cp1 sample, which explain the enhanced drug release. The diffusion mechanism is based on the fact that the captopril transport from the HPMC:EC blend into the PBS medium is due to a concentration gradient. In particular, the difference in the concentration gradient leads to captopril release.

Thus, the MAPLE fabricated polymer blend: drug are efficient captopril release systems, which represent an advantage for the treatment of chronic conditions such as hypertension.

3.2 In vivo evaluation of the MAPLE fabricated transdermal patches

3.2.1 Skin irritation studies

The results for skin irritation studies are depicted in Table 4. From the results it has been observed that no erythema and edema were observed on any of the rabbits at the place of application of the test substance and control at 24, 48 and 72 h after inoculation (Fig. 9). In accordance with the International Standard ISO 10993-10, the requirements for testing are met if the final score of the difference between the test substance and the control substance is ≤ 1.0. The end result of this test was -1.76. Under the test conditions according to this study, the test substance is considered a non-irritating substance.

3.2.2 Guinea Pig Maximization Test (GPMT)

Following the skin sensitization test, none of the animals under study had any abnormal clinical signs during the 25 days of the entire test period. No sensitization was noted among the guinea pigs that were challenged with transdermal patch or the placebo patch. Erythema and edema were not observed after the challenge in this experiment. Thus, according to this study, the MAPLE fabricated patches are considered to have a non-sensitizing effect on the skin.

4 Conclusions

In this study, matrix-assisted pulsed laser evaporation (MAPLE) has been applied for the realization of polymer: drug blends for the controlled release of captopril. The polymer: drug thin films have been obtained by depositing

Table 3 Captopril release kinetics. The data is obtained by applying the Korsmeyer–Peppas model [52]

Sample	R^2	k_{kp}	n	Release mechanism
HPMC80: EC20: Cp1	0.98	27.82	0.33	Fickian diffusion
HPMC80: EC20: Cp5	0.98	29.29	0.32	Fickian diffusion
HPMC80: EC20: Cp10	0.97	30.42	0.31	Fickian diffusion
HPMC60: EC40: Cp1	0.99	26.40	0.36	Fickian diffusion
HPMC60: EC40: Cp5	0.99	28.34	0.34	Fickian diffusion
HPMC60: EC40: Cp10	0.00	0.85	1.03	Case II transport
HPMC40: EC60: Cp1	0.97	28.78	0.25	Fickian diffusion
HPMC40: EC60: Cp5	0.99	0.96	1.04	Case II transport
HPMC40: EC60: Cp10	0.99	0.85	1.02	Case II transport

Table 4 Results of examination of rabbits for test substance and control substance

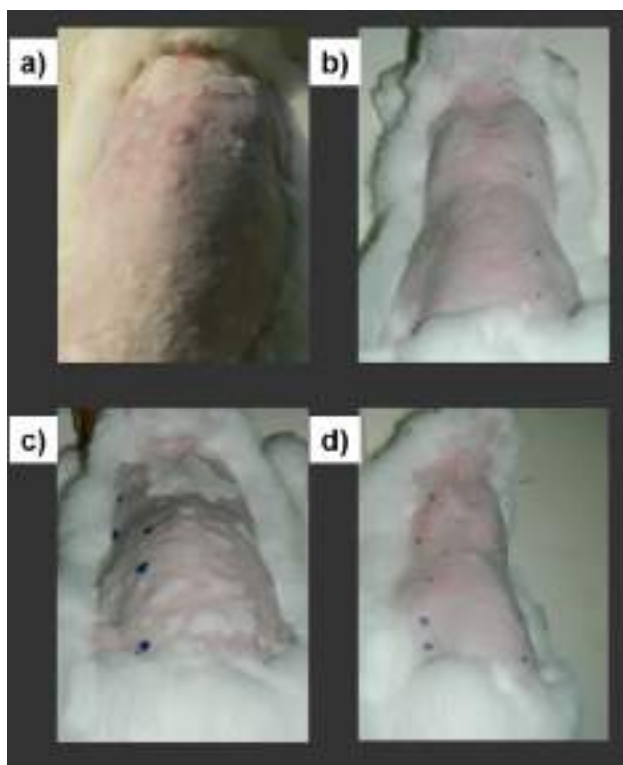| Rabbit	Test			Control		
	24 h	48 h	72 h	24 h	48 h	72 h
1	0	0	0	4	4	4
2	0	0	0	2	2	2
3	0	0	0	1	2	2
Total	0			23		
Average (total/13)	0			1.76		
Difference	-1.76					

Fig. 9 Rabbit skin **a** before the administration of the as-fabricated MAPLE patch and **b** 24 h, **c** 48 h, and **d** 72 h after the administration of the as-fabricated MAPLE patch

hydroxypropyl methylcellulose (HPMC): (EC) ethyl cellulose blends loaded with different captopril concentrations. The approach followed in this work is quite straight forward, i.e., polymer: drug blends can be directly deposited onto flexible supports by MAPLE without the need for prior surface functionalization or preparation of the surface.

Surface characterization of the resulting films via infrared spectroscopy, atomic force microscopy, and contact angle measurements, corroborated that HPMC: EC: Cp films were deposited without any chemical modifications of their structure. In addition, the HPMC: EC: Cp films as-deposited by MAPLE show a good potential for transdermal drug delivery. The skin irritation studies carried out on rabbits, showed no noticeable skin reactions, thus pointing out the compatibility of captopril with both the polymer blend and with the skin. Last, no skin sensitization was noted among the guinea pigs that were challenged with the MAPLE fabricated transdermal patches.

Therefore, this study has demonstrated that the polymer: drug films fabricated via MAPLE could be significant alternatives for the delivery of captopril. Although this study may be considered a "proof-of-concept" study, we can state that the investigations carried out herein could have applications in other studies, such as the fabrication of therapeutic systems with similar drugs.

Declarations

References

1. M.N. Pastore, Y.N. Kalia, M. Horstmann, M.S. Roberts, Br J Pharmacol. **172**(9), 2179–2209 (2015)
2. D. Bird, N.M. Ravindra, Med Devices Sens. **3**, e10069 (2020)
3. Y.Q. Yu, X. Yang, X.F. Wu, Y.B. Fan, Front. Bioeng. Biotechnol. **9**, 646554 (2021)
4. S. Korani, S. Bahrami, M. Korani, M. Banach, T.P. Johnston, A. Sahebkar, Lipids Health Dis. **18**(1), 193 (2019)
5. I. Singh, A.P. Morris, Int J Pharm Investig. **1**(1), 4–9 (2011)
6. T. Tanner, R. Marks, Skin Res. Technol. **14**, 249–260 (2008)
7. T. Unger, C. Borghi, F. Charchar, N.A. Khan, N.R. Poulter, D. Prabhakaran, A. Ramirez, M. Schlaich, G.S. Stergiou, M. Tomaszewski, R.D. Wainford, B. Williams, A.E. Schutt, Hypertension **75**, 1334–1357 (2020)
8. T.D. Giles, B.J. Materson, J.N. Cohn, J.B. Kostis, J. Clin. Hypertens. **11**, 611–614 (2009)
9. D.R. Gullick, W.J. Pugh, M.J. Ingram, P.A. Cox, G.P. Moss, Drug Dev. Ind. Pharm. **36**(8), 926–932 (2010)
10. D.A. Smith, K. Beaumont, T.S. Maurer, L. Di, J. Med. Chem. **61**(10), 4273–4282 (2018)
11. A. Ahad, M. Aqil, K. Kohli, Y. Sultana, M. Mujeeb, A. Ali, Asian J. Pharm. Sci. **5**, 276–288 (2010)
12. K.A. Walters, K.R. Brain, Dermatological formulation and transdermal systems, in *Dermatological and transdermal formulations*. ed. by K.A. Walters (Informa, New York, 2002), pp.319–400
13. S. Güngör, Y. Ozsoy, Ther. Deliv. **3**(9), 1101–1116 (2012)
14. E. Verhoeven, C. Vervaet, J.P. Remon, Eur. J. Pharm. Biopharm. **63**, 320–330 (2006)
15. R. Enayatifard, M. Saeedi, J. Akbari, Y. HaeriTabatabaee, Trop. J. Pharm Res. **8**(5), 425 (2009)
16. M.J. Vasques, B. Perez-Marcus, J.L. Gomez-Amora, R. Martinez-Pacheo, C. Souto, A. Concheiro, Drug Dev. Ind. Pharm. **18**, 1355–1375 (1992)
17. Y. Okuda, Y. Irisawa, K. Okimoto, T. Osawa, S. Yamashita, Int. J. Pharm. **423**(2), 351–359 (2012)
18. X.-Y. Shi, T.-W. Tan, Biomaterials **23**(23), 4469–4473 (2002)
19. A. Arunachalam, M. Karthikeyan, V.D. Kumar, M. Prathap, S. Sethuraman, S. Ashutoshkumar, S. Manidipa, Curr. Pharma Res. **1**(1), 70–81 (2010)
20. G. Raj, R. Raveendran, *Introduction to Basics of Pharmacology and Toxicology Volume 1: General and Molecular Pharmacology: Principles of Drug Action* (Springer Nature Singapore Pte Ltd., Singapore, 2019)
21. P.K. Wu, J. Fitzgerald, A. Pique, D.B. Chrisey, R.A. McGill, Mater. Res. Soc. Symp. Proc. **617**, J2.3.1-6 (2000)
22. J. Schou, Appl. Surf. Sci. **255**, 5191 (2009)

23. C. Constantinescu, A. Palla-Papavlu, A. Rotaru, P. Florian, F. Chelu, M. Icriverzi, A. Nedelcea, V. Dinca, A. Roseanu, M. Dinescu, Appl. Surf. Sci. **255**, 5491 (2009)

24. A.T. Sellinger, E.M. Leveugle, K. Gogick, L.V. Zhigilei, J.M. Fitz-Gerald, J. Vacuum Sci. Technol. A **24**, 1618 (2006)

25. Y. Wang, H. Jeong, M. Chowdhury, C.B. Arnold, R.D. Priestley, Polym. Cryst. **1**, e10021 (2018)

26. D.B. Chrisey, A. Piqué, R.A. McGill, J.S. Horwitz, B.R. Ringeisen, D.M. Bubb, P.K. Wu, Chem. Rev. **103**(2), 553 (2003)

27. N.L. Dumitrescu, M. Icriverzi, A. Bonciu, P. Florian, A. Moldovan, A. Roseanu, L. Rusen, V. Dinca, F. Grama, Int. J. Mol. Sci. **23**, 3988 (2022)

28. A. Palla-Papavlu, V. Dinca, M. Dinescu, F. Di Pietrantonio, D. Cannatà, M. Benetti, E. Verona, Appl. Phys. A **105**, 651–659 (2011)

29. R. Cristescu, A. Doraiswamy, T. Patz, G. Socol, S. Grigorescu, E. Axente, F. Sima, R.J. Narayan, D. Mihaiescu, A. Moldovan, I. Stamatin, I.N. Mihailescu, B. Chisholm, D.B. Chrisey, Appl. Surf. Sci. **253**, 7702 (2007)

30. I.A. Paun, V. Ion, A. Moldovan, M. Dinescu, Appl. Phys. Lett. **96**, 243702 (2010)

31. A.P. Caricato, V. Arima, M. Catalano, M. Cesaria, P.D. Cozzoli, M. Martino, A. Taurino, R. Rella, R. Scarfiello, T. Tunno, A. Zacheo, Appl. Surf. Sci. **302**, 92–98 (2014)

32. D.A. Cristian, F. Grama, R. Papagheorghe, S. Brajnicov, V. Ion, S. Vizireanu, A. Palla-Papavlu, M. Dinescu, Appl. Phys. A **125**, 424 (2019)

33. H.G. Brittain, H. Kadin, Pharm. Res. **7**, 1082–1085 (1990)

34. C.H. Lee, H.I. Maibach, Contact Dermatitis **33**(1), 1–7 (1995)

35. B. Magnusson, A.M. Kligman, J. Investig. Dermatol. **52**, 268–276 (1969)

36. A. Fahs, M. Brogly, S. Bistac, M. Schmitt, Carbohydr. Polym. **80**(1), 105–114 (2010)

37. N.A. Camino, O.E. Pérez, C. Carrera Sanchez, J.M. Rodriguez Patino, A.M.R. Pilosof, Food Hydrocolloids **23**(8), 2359–2368 (2009)

38. N.K. Anuar, W.T. Wui, D.K. Ghodgaonkar, M.N. Taib, J. Pharm. Biomed. Anal. **43**(2), 549–557 (2007)

39. M.K. Trivedi, A. Branton, D. Trivedi, G. Nayak, R.K. Mishra, S. Jana, J. Biomed. Mater. Res. **3**(6), 83–91 (2015)

40. S. Cavalu, S. CintaPinzaru, V. Chis, Rom. J. Biophys. **17**(3), 195–203 (2007)

41. H. Jancovics, C. Pettinari, F. Marchetti, E. Kamu, L. Nagy, S. Troyanov, L. Pellerito, J. Inorg. Biochem. **97**, 370–376 (2003)

42. A. Palla-Papavlu, L. Rusen, V. Dinca, M. Filipescu, T. Lippert, M. Dinescu, Appl. Surf. Sci. **302**, 87–91 (2014)

43. P.E. Luner, E. Oh, Colloids Surf. A **181**, 31 (2001)

44. L. Li, S. Roethel, V. Breedveld et al., Cellulose **20**, 3219–3226 (2013)

45. P.C. Faria-Tischer, C.A. Tischer, L. Heux et al., Mater. Sci. Eng. C Mater. Biol. Appl. **51**, 167–173 (2015)

46. T. Kiss, T. Alapi, G. Varga, C. Bartos, R. Ambrus, P. Szabo-Revesz, G. Katona, J. Pharm. Sci. **108**(8), 2552–2560 (2019)

47. M. Ci, J. Liu, S. Shang, Z. Jiang, P. Zhu, S. Sui, Fibers Polym. **21**, 2179–2185 (2020)

48. S. Belbekhouche, J. Bras, G. Siqueira, C. Chappey, L. Lebrun, B. Khelifi, S. Marais, A. Dufresne, Carbohydr. Polym. **83**, 1740–1748 (2011)

49. S. Van Nguyen, B.K. Lee, Cellulose **28**, 5693–5705 (2021)

50. M. Larsson, A. Johnsson, S. Gårdebjer, R. Bordes, A. Larsson, Mater. Des. **122**, 414–421 (2017)

51. H. Bera, Y.F. Abbasi, V. Gajbhiye, K.F. Liew, P. Kumar, P. Tambe, A.K. Azad, D. Cun, M. Yang, Mater. Sci. Eng. C **110**, 110628 (2020)

52. R.W. Korsmeyer, R. Gurny, E. Doelker, P. Buri, N.A. Peppas, Int. J. Pharm. **15**(1), 25–35 (1983)

53. A.K. Azad, S.M.A. Al-Mahmood, B. Chatterjee, W.M.A. Wan Sulaiman, T.M. Elsayed, A.A. Doolaanea, Pharmaceutics **12**, 219 (2020)

54. M.S. Latif, A.K. Azad, A. Nawaz, S.A. Rashid, M.H. Rahman, S.Y. Al Omar, S.G. Bungau, L. Aleya, M.M. Abdel-Daim, Polymers **13**, 3455 (2021)

Long-term treatment with chloroquine increases lifespan in middle-aged male mice possibly via autophagy modulation, proteasome inhibition and glycogen metabolism

Thorsten R. Doeppner[1,2,3,*], Cristin Coman[4,*], Daiana Burdusel[5,*], Diana-Larisa Ancuta[4,6], Ulf Brockmeier[7], Daniel Nicolae Pirici[5], Kuang Yaoyun[1], Dirk M. Hermann[7], Aurel Popa-Wagner[7,8]

[1]Department of Neurology, University Medical Center Göttingen, Göttingen 37075, Germany
[2]Research Institute for Health Sciences and Technologies (SABITA), Medipol University, Istanbul, Turkey
[3]Department of Anatomy and Cell Biology, Medical University of Varna, Varna, Bulgaria
[4]Cantacuzino National Medico-Military Institute for Research and Development, Bucharest 050096, Romania
[5]Department of Biochemistry, University of Medicine and Pharmacy Craiova, Craiova 200349, Romania
[6]Faculty of Veterinary Medicine, University of Agronomic Sciences and Veterinary Medicine of Bucharest, Bucharest, Romania
[7]Vascular Neurology and Dementia, Department of Neurology, University of Medicine Essen, Essen 45147, Germany
[8]Experimental Research Center for Normal and Pathological Aging, ARES, University of Medicine and Pharmacy Craiova, Craiova 200349, Romania
[*]Equal contribution

Correspondence to: Aurel Popa-Wagner, Dirk M. Hermann; **email:** aurel.popa@uk-essen.de, Dirk.hermann@uk-essen.de
Keywords: chloroquine, longevity, middle-aged mice, toxicity, autophagy, proteasome
Received: March 5, 2022 **Accepted:** April 28, 2022 **Published:** May 23, 2022

ABSTRACT

Previous studies have shown that the polyamine spermidine increased the maximum life span in *C. elegans* and the median life span in mice. Since spermidine increases autophagy, we asked if treatment with chloroquine, an inhibitor of autophagy, would shorten the lifespan of mice. Recently, chloroquine has intensively been discussed as a treatment option for COVID-19 patients. To rule out unfavorable long-term effects on longevity, we examined the effect of chronic treatment with chloroquine given in the drinking water on the lifespan and organ pathology of male middle-aged NMRI mice. We report that, surprisingly, daily treatment with chloroquine extended the median life span by 11.4% and the maximum life span of the middle-aged male NMRI mice by 11.8%. Subsequent experiments show that the chloroquine-induced lifespan elevation is associated with dose-dependent increase in LC3B-II, a marker of autophagosomes, in the liver and heart that was confirmed by transmission electron microscopy. Quite intriguingly, chloroquine treatment was also associated with a decrease in glycogenolysis in the liver suggesting a compensatory mechanism to provide energy to the cell. Accumulation of autophagosomes was paralleled by an inhibition of proteasome-dependent proteolysis in the liver and the heart as well as with decreased serum levels of insulin growth factor binding protein-3 (IGFBP3), a protein associated with longevity. We propose that inhibition of proteasome activity in conjunction with an increased number of autophagosomes and decreased levels of IGFBP3 might play a central role in lifespan extension by chloroquine in male NMRI mice.

INTRODUCTION

By the end of 2030 the number of people older than 60 will increase by 56% to reach 1.4 billion (WHO). However, the quality of life in the elderly depends heavily on their health conditions. Therefore, there is a need in finding treatments to enable aged people to live in good health to avoid the negative impact of poor health for society.

A popular method to increase lifespan and health conditions is calorie restriction (CR) both in lower organisms [1] and rodents [2, 3]. Thus, intermittent fasting at the beginning of adulthood induced lifespan expansion by 25% in *D. melanogaster* most likely by a mTOR-independent mechanism [1].

The effect of CR has been also studied in non-human primates whose physiology and life style are very similar to that of humans. One study conducted on Rhesus monkey (*Macaca mulatta*) at the University of Wisconsin reported a significant positive impact of CR on health, age-related survival [4], and all-cause survival [5], but the study conducted at the National Institute on Aging study detected no significant effect on longevity [6]. However, a direct comparison of longitudinal data from both studies has revealed differences in the source of the monkeys, feeding practices, diet composition, macronutrient composition and finally suggested that the age of onset of CR may be a critical factor that determines the extent of the beneficial effects of CR on health and longevity [7].

Recent studies involving energy metabolism and adipose tissue have provided novel insights into the possible mechanisms underlying longevity and health span. Indeed, nonshivering thermogenesis via enhanced mitochondrial uncoupling in the brown adipose tissue has been associated with increased longevity in CR animals and the dwarf mice [8, 9].

Many studies investigated the effects of CR-mimetics like resveratrol, a plant derivative with anti-oxidants and anti-inflammatory properties, on health- and lifespan in *S. cerevisiae*, *C. elegans* and *D. melanogaster.* In *C. elegans*, resveratrol did extend lifespan only under conditions of enhanced oxidative stress caused by high glucose concentrations in the culture medium [10]. In another study, treatment with resveratrol increased mean and maximum lifespan by delaying the onset of the "dying phase" [11].

In higher organisms, like mice, resveratrol treatment shifts the signaling pathways of middle-aged mice kept on a high-calorie diet towards that of mice on a standard diet and significantly increases their survival [12]. However, in other studies resveratrol given intraperitoneally to mice did not act as CR mimetic [13] suggesting that the effect of resveratrol on longevity in flies, worms or mice may vary from species to species. Further, resveratrol given as a food supplement to humans did not show positive results on the health status [14].

Inhibition of mTOR (target of rapamycin) signaling using rapamycin led to an extension of lifespan in *Caenorhabditis elegans* by 250% [15] and by 20% in *Drosophila melanogaster* [16]. In mice, treatment with rapamycin increased life expectancy by 10% in males and 18% in females [17]. Other beneficial effects of rapamycin include a dose-dependent decline in the liver degeneration in male mice, reduced number of atypical nuclei in the heart and tumors of the adrenal gland and improved tendon elasticity. Behaviourally, rapamycin delayed the age-related decline in spontaneous activity [17]. However, rapamycin treatment also led to a pronounced testicular tubular degeneration and cataracts in mice suggesting that time to start the treatment and the dosage should be carefully investigated [18].

In the clinic, rapamycin has been used as an immunosuppressant and through its anti-proliferative action, as a potential anticancer agent. However, long-term use as immunosuppressor may have side effects including gonadal dysfunction and infertility [19, 20], an effect that has been reported in aged male mice, too [18].

Another approach to extend life span is to enhance autophagy. Autophagy is a major pathway for the turnover of cell organelles and may play a pivotal role in health- and lifespan extension [21–24]. For example, long-term treatment of young and middle-aged mice with the autophagy enhancer spermidine led to an increased mean lifespan by 11% and extended longevity by 8% most likely by enhancing cardiac autophagy [25]. However, the effect of spermidine seems to be species-specific. For example, work done in our group has shown that in rats, autophagy enhancement by spermidine treatment increased the healthspan by attenuating neuro-inflammation, anxiety and the exploratory behavior, but not the maximum life span [26]. On this occasion, we asked if the autophagy inhibitor chloroquine (CQ), would shorten the lifespan of rodents. Contrary to our hypothesis, we observed an extension, not reduction of lifespan by 11.7% by CQ when given in drinking water to middle-aged male NMRI mice. We

therefore examined possible mechanisms underlying lifespan augmentation by chloroquine.

RESULTS

Treatment with chloroquine expanded the median and maximum lifespan in middle-aged male NMRI mice

Treatment was initiated at the age of 500 days and continued for 286 days. Macroscopically, the fur of the treated animals looked less ruffled as compared to controls (Figure 1A vs. 1B). The male mice fed with CQ significantly lived longer (786 days) than controls (689 days) ($P = 0.0002$), and the median lifespan was also significantly different between the two groups (Figure 1C). When the treatment was initiated, the body weights were similar. However, in the control mice gradually there was an age-related increase in the body weight that was prevented by the CQ treatment ($P = 0.0001$; t-test, two-tailed) between the weight of the control mice and the weight of CQ-treated animals between days 600–700 (Figure 1D). The volume of liquid intake was, on the average, significantly lower ($P = 0.002$; t-test, two-tailed) in the CQ-treated group (Figure 1E). However, the average amount of consumed food was not significantly different between the two groups (Figure 1F).
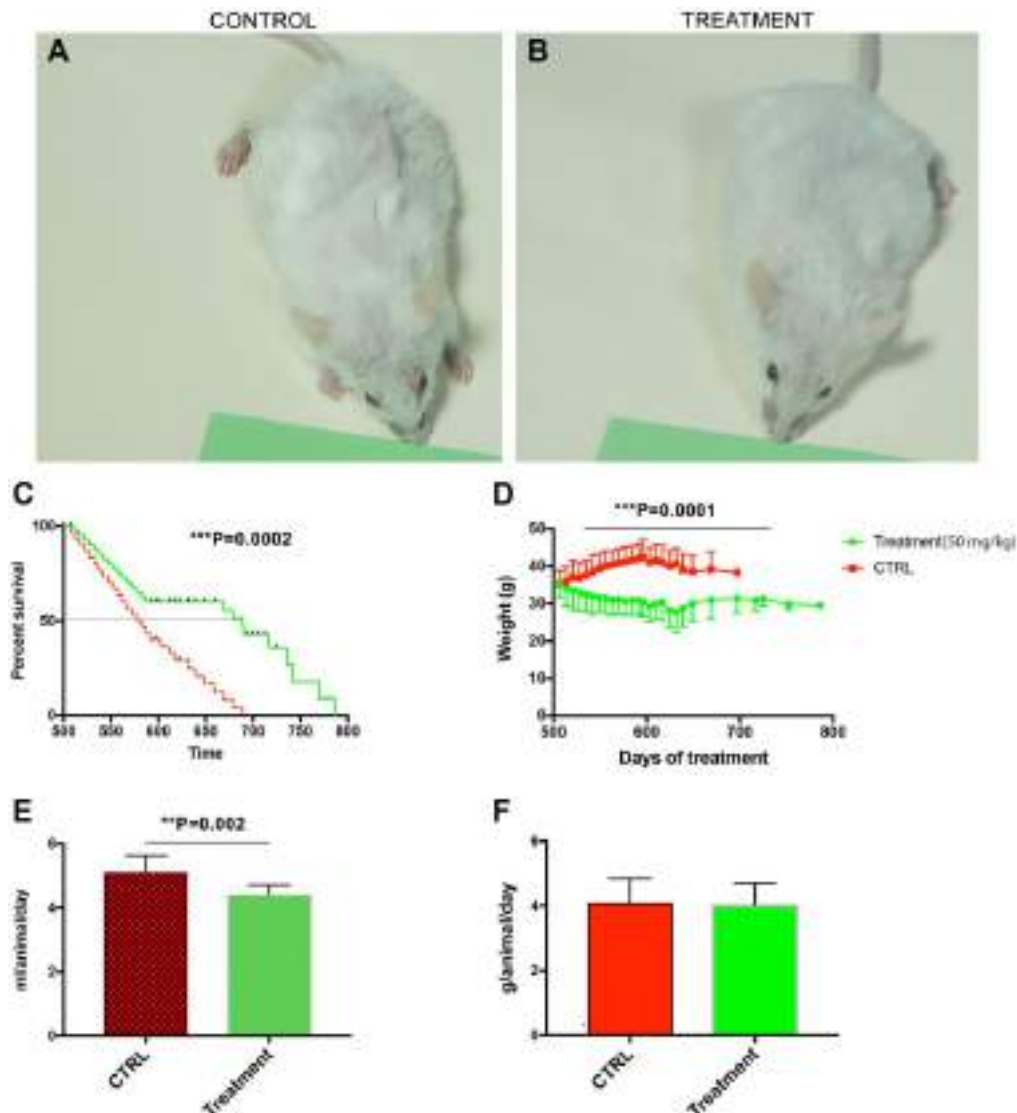

Figure 1. Treatment with chloroquine expanded the median and maximum lifespan in middle-aged male NMRI mice. Macroscopically, the fur of the treated animals looked less ruffled as compared to controls (**A** vs. **B**). The male mice fed with CQ significantly lived longer (786 days) than controls (689 days) and the median lifespan was also significantly different between the two groups (**C**). Long-term treatment with CQ (50 mg/kg) led to a gradual increase in the body weight of control animals that peaked at day 600 (t-test, two-tailed) (**D**). The volume of liquid intake was, on the average, significantly lower in the CQ-treated group (t-test, two-tailed) (**E**). However, the average amount of consumed food was not significantly different (**F**). Data are mean ± SD values. $N = 28$ for each group.

The lower dose of CQ did not cause significant pathological changes in the liver and the heart

On autopsy, one control and two of the treated mice presented with retroperitoneal cysts. One control and one of the treated animals had a retroperitoneal tumor masses. In treated animals, at higher doses (100- and 200 mg/kg), however, the most frequent and obvious histological changes occurred in the liver, and consisted in hydropic degeneration and hepatocyte necrosis, both indicators of hepatocyte toxicity and intense metabolic distress. The changes were visible mostly in portal areas and as they became more advanced, they spread through the lobule. Fibrosis and mononuclear inflammatory infiltrates were also present on occasion in portal spaces rather than with a central or intralobular distribution, and thus were not included in the stratification of liver pathology (Figure 2, upper panel).

In the heart, interstitial oedema, intercalate disks fragmentation, loss of myocardiocyte striations and even areal necrosis could be seen, more frequent and more intense with increasing treatment dosage (Figure 2, lower panel). However, overall, we noted that the dose of 50 mg/kg of CQ did not cause significant pathological changes in the liver and heart (Figure 2; Table 1).

CQ treatment caused an increase in the LC3-II/LC3-I ratio and p62 levels in the liver and heart

Chloroquine at 60 mg/kg has been shown to disturb autophagy in mice by inducing an autophagy-independent severe disorganization of the Golgi and endolysosomal systems, which might contribute to autophagosome-lysosome fusion impairment and degradation of intra-autophagosomal components by lysosomal hydrolases [27].

Physiologically, lysosomal turnover of autophagosome reflects starvation-induced autophagic activity and the structural proteins of autophagosomes are routinely used to assess the effect of drugs on autophagy in animal models. The microtubule-Associated Protein 1 Light Chain 3 (LC3) family of proteins required for phagocytic clearance are the major structural proteins of autophagosomal membranes and consists of three highly homologous members, MAP1LC3A (LC3A), MAP1LC3B(LC3B), and MAP1LC3C (LC3C) [28].

In our toxicity study, there was a progressive, significant increase in the LC3-II/LC3-I ratio in the liver (Figure 3A, 3B) [$F_{(3,8)} = 19.84$; $P = 0.0005$] and to a lesser extent in the heart (Figure 3D, 3E) [$F_{(3,8)} = 12.69$; $P = 0.0021$] homogenates with increasing chloroquine concentration in drinking water. Interestingly, CQ treatment significantly increased the expression of both LC3-I and LC3-II in the heart. However, there was a clear conversion of LC3-I to LC3-II in the liver of CQ-treated animals as compared to control animals.

p62 is a protein that interacts with autophagic substrates and delivers them to autophagosomes for degradation.
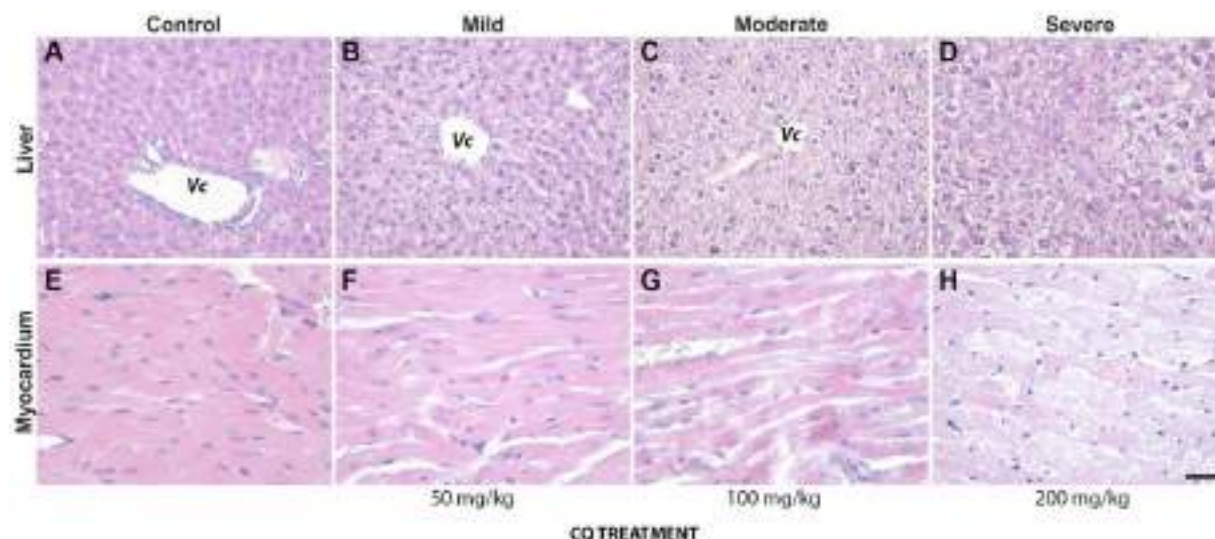

Figure 2. The lower dose of 50 mg/kg CQ did not cause significant pathological changes in the liver and the heart. (*upper panel*): Pathological changes in the liver of controls (**A**) and treatment (50 mg/kg) (**B–D**) consisted of hydropic degeneration and hepatocyte necrosis. The changes were visible mostly in portal areas and as they became more advanced, they spread through the lobule. Fibrosis and mononuclear inflammatory infiltrates were also present on occasion in portal spaces. (*lower panel*): In the heart of controls (**E**) and treatment (50 mg/kg) (**F–H**), interstitial oedema, intercalate disks fragmentation, loss of myocardiocyte striations and even areal necrosis could be seen, more frequent and more intense with increasing treatment dosage. Abbreviation: *Vc*, central vein. *N* = 10 for each group.

Table 1. Overall, we noted that the dose of 50 mg/kg of CQ did not cause significant pathological changes in the liver and heart.

Liver	50 mg/kg				100 mg/kg				200 mg/kg			
Pathological grading	GVD	PII	PF	HN	GVD	PII	PF	HN	GVD	PII	PF	HN
Mild (+)	1/10	0/10	1/10	2/10	3/10	2/10	0/10	2/10	3/10	3/10	2/7	5/10
Moderate (++)	3/10	1/10	0/10	1/10	4/10	0/10	0/10	1/10	2/10	1/10	0/7	5/10
Severe (+++)	1/10	0/10	0/10	1/10	3/10	0/10	0/10	0/10	2/10	0/10	0/7	0/10

Abbreviations: GVD: Granulovacuolar degeneration; PII: Portal inflammatory infiltrate; PF: Portal fibrosis HN: hepatocyte necrosis.

Heart	50 mg/kg		100 mg/kg		200 mg/kg	
Pathological grading	IO	LS	IO	LS	IO	LS
Mild (+)	6/10	4/10	4/10	1/10	6/10	4/10
Moderate (++)	1/10	1/10	3/10	3/10	5/10	2/10
Severe (+++)	0/10	0/10	1/10	1/10	2/10	1/10

Abbreviations: IO: interstitial oedema; LS: loss of striations. N = 10 for each group.

The increases in LC3-II were paralleled by an increase in the expression level of p62 in the liver (Figure 3C) [$F_{(3,8)}$ = 8.32; P = 0.0077] and heart (Figure 3F) [$F_{(3,8)}$ = 10.97; P = 0.0033] homogenates with increasing chloroquine concentration in drinking water.

LC3B immunohistochemistry

In the myocardium, the anti-LC3B antibody exhibited a very fine granular pattern in the cytoplasm of myocardiocytes. A strong immunostaining was visible
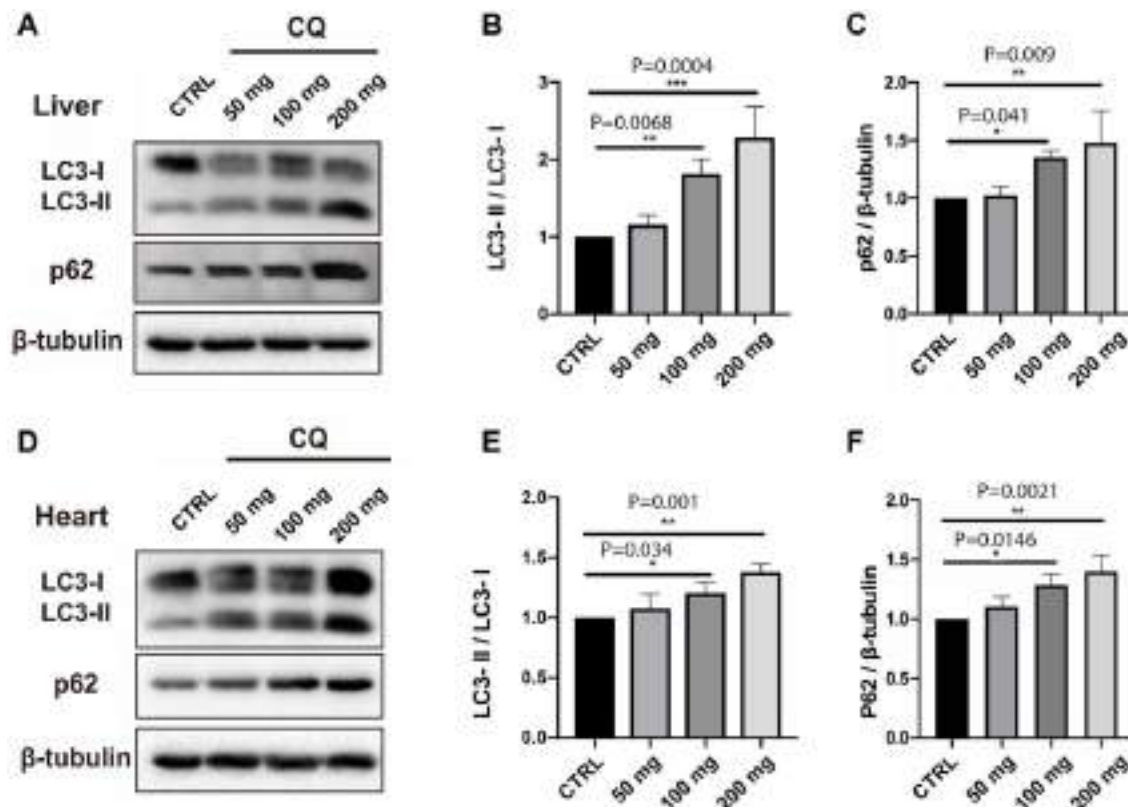

Figure 3. CQ treatment caused an increase in the LC3-II/LC3-I ratio and p62 levels in the liver and heart homogenates. In our toxicity study, there was a progressive, significant increase in the LC3-II/LC3-I ratio in the liver (**A**, **B**). The increase in the LC3-II/LC3-I ratio was paralleled by an increase in the expression level of p62 in the liver (**C**). The increase in the LC3-II/LC3-I ratio with increasing chloroquine concentration in drinking water was also significant, albeit less obvious in the heart homogenates (**D**, **E**). The increase in the LC3-II/LC3-I ratio was paralleled by an increase in the expression level of p62 in the heart (**F**) homogenates. Data are mean ± SD values. N = 5 for each group.

in the smooth muscle layer of both arterioles and venules from the parenchyma of treated animals (Figure 4B) as compared to controls (Figure 4A).

In the liver, LC3B immunostaining showed a diffuse granular pattern in the cytoplasm of hepatocytes, without a preferred disposition in the lobules. LC3B immunostaining was more intense in treated animals as compared to controls (Figure 4C vs. 4D). Enlarged images of LC3B immunostainings in hepatocytes of controls and treated animals are also shown (Figure 4E vs. 4F).

Electron microscopy

Four animals in each group were analyzed by EM. In the control group we could not see autophagosomes (Figure 5A–5D). Instead, there was a massive accumulation of glycogen granules in the liver cells (white arrowheads). Following CQ treatment, autophagosome-like structures that were encircled by double membranes containing portions of cytoplasmic organelles were detected (Figure 5E–5H; black arrowheads).

Higher doses of CQ attenuated proteasome activity in the liver and heart

There is an intimate linkage of proteostasis with the aging process and associated pathologies [29]. In addition, autophagy and proteostasis are interconnected [30]. We found that at a dose of 100 mg/kg and higher, proteasome activity was significantly reduced in the liver [F(3,45) = 63.2, $P < 0.0001$] (Figure 6A), whereas
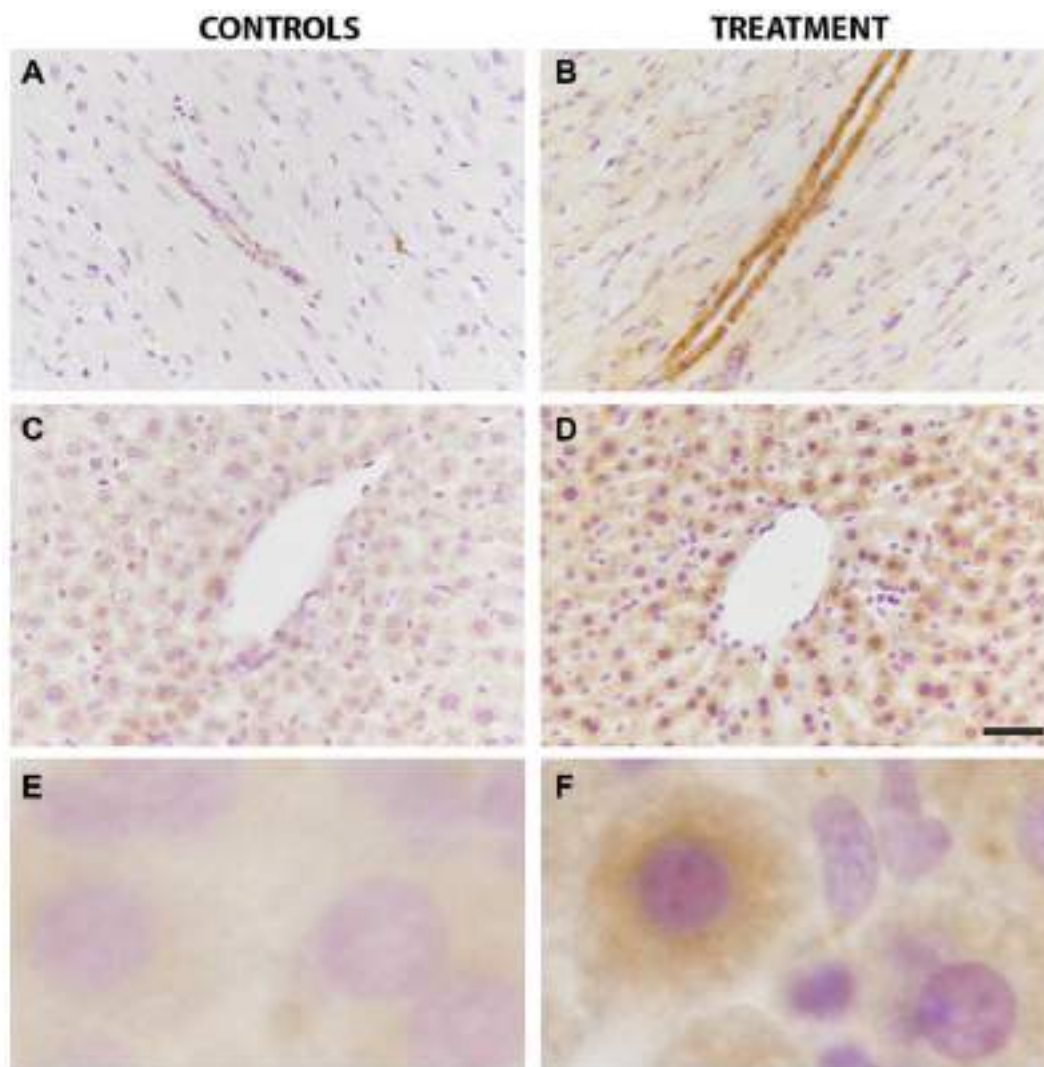

Figure 4. LC3B immunoreactivity in the liver and heart was increased by chloroquine treatment. In the heart tissue, a strong immunostaining was visible in the smooth muscle layer of both arterioles and venules from the parenchyma of treated animals as compared to controls (**A** vs **B**). In the liver, LC3B immunostaining showed a diffuse granular pattern in the cytoplasm of hepatocytes that was more intense in treated animals as compared to controls (**C** vs **D**). Enlarged images are shown for controls (**E**) and treatment (**F**). *N* = 10 for each group.

proteasomal activity in the heart was reduced only at the highest CQ dose of 200 mg/kg [F(3,45) = 24.24, $P < 0.0001$] (Figure 6B). Of note, treatment with 50 mg/kg did not reduce significantly the proteasomal activity in the liver and heart in the toxicity study.

Serum insulin growth factor binding protein 3 was decreased by chloroquine treatment

The IGF system plays an important role in regulating signal pathways involved in aging. By ELISA, we found that serum IGFBP3 was significantly decreased ($P = 0.0001$) in serum collected from animals treated with CQ for 3 months as compared to controls (Figure 7A). There was no statistically significant difference in serum IGF-1, IRS or GH levels of treated animals as compared to controls (Figure 7B–7D).

DISCUSSION

Living a longer, healthier life is at the focus of aging research. Recently, administration of an autophagy enhancer, spermidine, in drinking water to pre-aged male and female mice significantly prolonged median lifespan by ~10% [25]. However, as reported by us, the same drug given to middle-aged male rats may not extend lifespan but healthspan by attenuating neuro-inflammation and improving anxiety and exploratory behavior [26]. In this context, we asked if chloroquine, a drug which inhibits autophagy by disorganizing the Golgi complex and the endolysosomal system *in vitro*

and *in vivo* [27], would shorten the lifespan in middle-aged male mice. We report that, surprisingly, chloroquine administered in drinking water at a dose of 50 mg/kg extended the median lifespan of middle-aged NMRI male mice by 11.8% and the maximum life span by 11.4%.

Aging mice normally develop a ruffled fur [31]. Macroscopically, the fur of the treated mice looked smoother than the fur of controls. Further, the mice in the treatment group did lose, on the average, 27% of their weight at 90 days of treatment. However, with increasing time, the difference in weight became less noticeable possibly due to decreasing numbers of survivors.

Except for a report on retinopathy after long-term use (250 mg CQ daily, for seven years) in humans [32], studies on CQ organ toxicity in young rats given at a dose of 124 mg/kg over a period of 6 weeks, showed marked hydropic degeneration and necrosis in the liver and heart [33]. In our experiments, 50 mg/kg given in drinking water over 12 weeks did not cause significant pathological changes in the heart. In the liver, mononuclear infiltrates were present occasionally in portal spaces, especially at higher CQ concentrations of 100 and 200 mg/kg.

Microtubule-associated protein light chain 3 (LC3-II) is generated by the conjugation of cytosolic LC3-I to phosphatidylethanolamine (PE) on the surface of
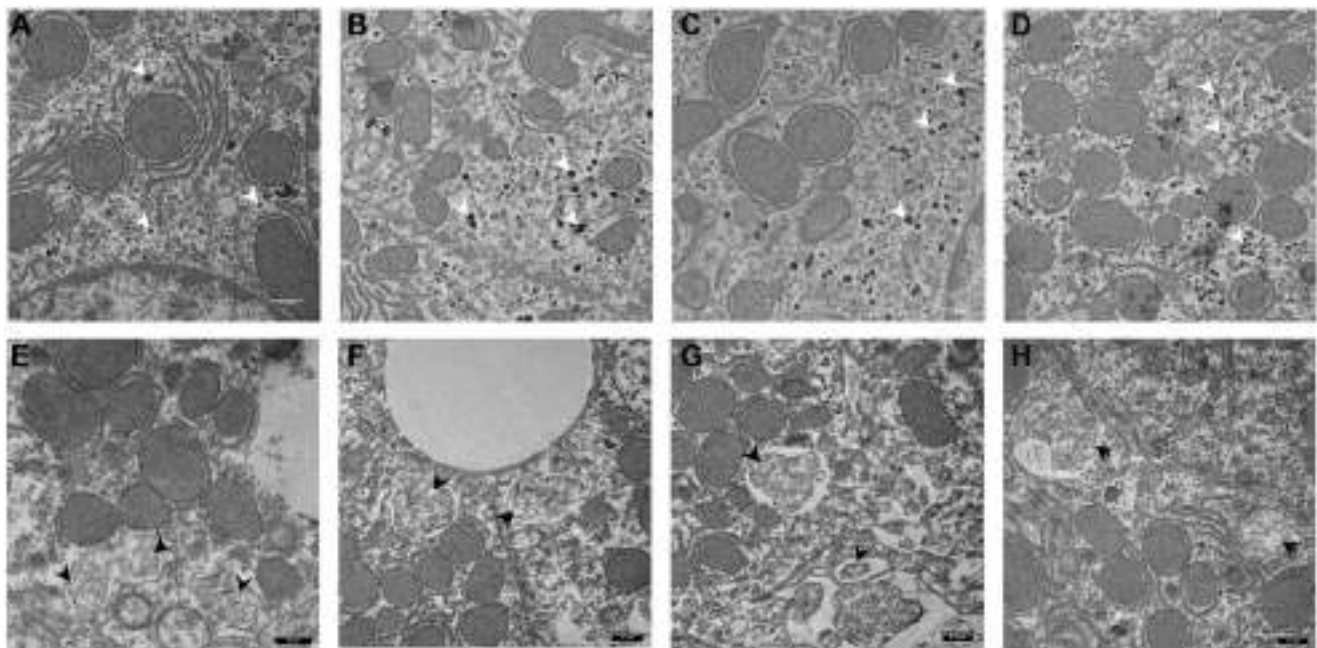

Figure 5. Electron microscopy images of autophagosomes in mouse liver. Control animal (**A–D**) vs. Chloroquine-treated animal (**E–H**). Highlighted are glycogen granules (white arrow) in controls and autophagosomes (black arrow) in the liver of treated animals. Scale bar, 0,5 µm. *N* = 3 for each group.

nascent autophagosomes and is widely used to monitor autophagy [34, 35]. When CQ is given intraperitoneally at a dose of 60 mg/kg, it mainly inhibits autophagy by impairing autophagosome fusion with lysosomes [27].

In our toxicity study, we found, by Western blotting, a dose-dependent increase in the levels of the autophagy marker LC3-I/II in the liver and to a lesser extent in the heart, suggesting that indeed, CQ disrupted autophagy by impairing autophagosome fusion with lysosomes which led to the accumulation of LC3-II on auto-phagosomes which is, at least in part, attributable to an impaired autophagic flux [36]. The accumulation of LC3B-I/II was also confirmed on liver and heart tissue sections.

Studies from other groups question the simple relationship between LC3-I and LC3-II. Thus, it was
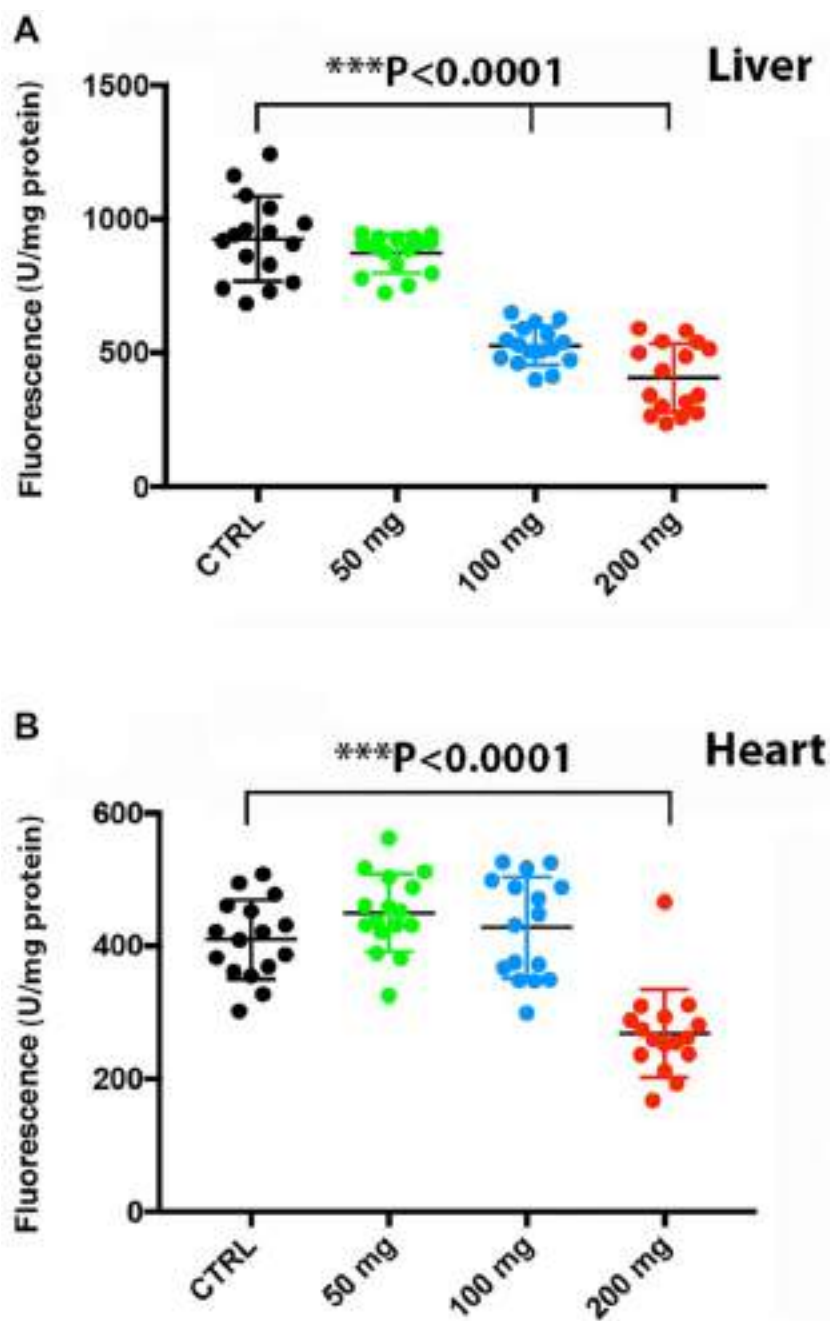

Figure 6. Higher doses of CQ attenuated proteasome activity in the liver and heart. Treatment with increasing doses of chloroquine significantly reduced proteasome activity in the liver at a dose of 100 mg/kg (**A**), whereas proteasomal activity in the heart was reduced only at 200 mg/kg (**B**). Data are given as arbitrary fluorescence units per mg protein as indicated in the materials and method section of the manuscript. *N* = 5 for each group.

found that autophagy inducing signals can stabilize LC3-I levels and subsequently increase LC3-II expression and increase autophagic flux, which means consistently induced autophagy may continue replenishment of LC3-II from the larger pool of LC3-I [37].

However, the increased LC3B immunoreactivity on liver and heart tissue could not be specifically attributed either to LC3B-I or LC3B-II because the antibody we have used did not distinguish between LC3B-I and LC3B-II. It should be noted that LC3B-positive puncta become larger and are prominent even with transient and incomplete inhibition of autophagosome biogenesis [35]. Moreover, CQ lipidation of LC3-I might not be related to autophagosome accumulation and highlights the need for greater understanding of the functional consequences of noncanonical autophagy [38].

TEM images reported by us also support the hypothesis that long-term treatment led to an accumulation of autophagosomes due to impaired autophagosome fusion with lysosomes.

Chloroquine has been shown to decrease proteolysis in human neuroblastoma SK-N-SH cells and in WT or Atg5−/− mouse embryonic fibroblasts [39]. Indeed, in our toxicity experiment, at higher doses of CQ, there was a decrease in the proteasome activity in the liver and heart tissue. Of note, the dose we have used for longevity studies did not change, after 60 days of treatment, the proteasome activity in the liver and heart. However, we cannot exclude that a longer treatment (9 months) might have reduced the proteasome activity in the liver and heart.

Regulation of proteasomal activity is a well characterized signaling pathway under both physiological and pathophysiological conditions [40]. A progressive decline in proteasome activity has been reported for the aging rat liver and heart suggesting either age-related changes in proteasome structure or increases in the level of oxidized and ubiquitinated proteins [41–43]. Although numerous reports indicate a decrease in proteasome activity during aging in animal models [44], new developments in the measurement of protein turnover indicate, except for the fat tissue,
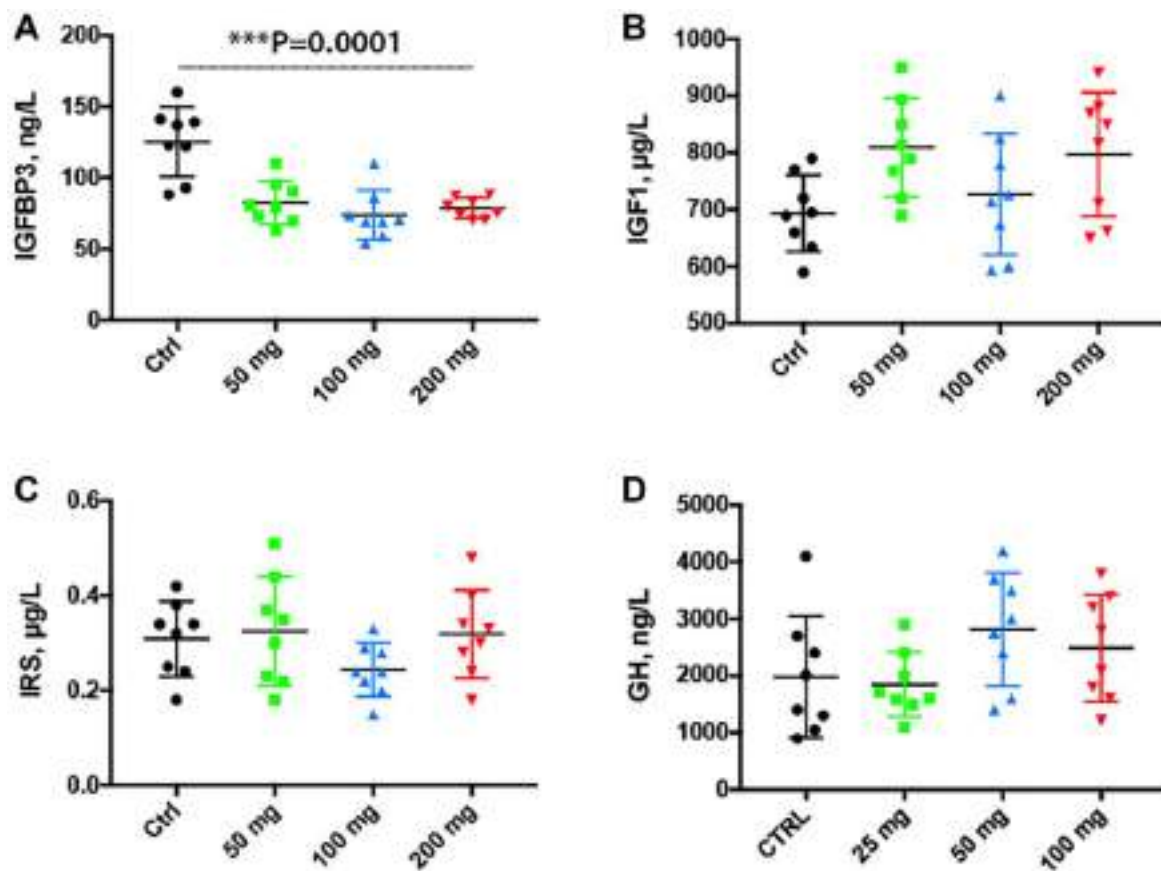

Figure 7. Serum insulin growth factor binding protein 3 was decreased by the chloroquine treatment. Treatment for 2 months with increasing doses of CQ did not cause significant changes in the body weight (**A**). Note that serum IGFBP3 was significantly decreased in serum collected from animals treated with CQ for 3 months (**B**). There was no statistically significant difference in the levels of serum IGF-1 and IRS of treated animals (**C**, **D**). Data are mean ± SD values. *N* = 15 for each group.

minimal changes in protein abundance in mouse tissues up to 26 months [45, 46].

The biological role of proteasomal activity, however, depends on cell and tissue conditions. As such, regulation of proteasome activity is a double-edged sword. Several studies have shown that proper proteasomal activity is essential for both cell cycle completion and cell survival [47]. In previous work, we have shown that proteasome inhibition was neuroprotective and was associated with increased post-stroke neurogenesis and angiogenesis that persisted at least for three months [48]. Herein, it is fair enough to assume that proteasomal inhibition may be in part responsible for the observed effects on longevity.

Growth hormone, insulin and the IGF (insulin-like growth factor) signaling pathway, all involved in the regulation of carbohydrate metabolism, play an important role in aging in animal models by activating multiple intracellular signaling cascades [49, 50]. Thus, inhibition of IGF signaling is thought to delay aging. However, the molecular mechanism underlying the modulation of lifespan by IGF signaling are still incompletely understood [51]. In our experiments, 2-months treatment with CQ lowered the levels of serum IGFBP3, a metabolic regulator that inhibits insulin-stimulated glucose uptake in murine models [52].

Autophagy mediates the degradation of cellular components in lysosomes and the resulting products are used for synthetic processes. The remaining, mostly fatty acids and to a lesser extent amino acids, are used to generate energy [53]. Accumulation of glycogen granules in controls suggests that CQ interferes with glycolysis. A similar observation has been reported in Zmpste24−/− mice, progeria mouse model [54]. A reduction in substrate availability of the components of the Krebs cycle following CQ treatment has been previously reported [55]. We hypothesize that the reduction in energy availability caused by the blockade of fusion of autophagosomes to the lysosomes, is compensated by an increased degradation of glycogen that could not be seen in the treated animals.

Previous studies have shown that *in vitro*, IGFBP3 is increased in aging human fibroblasts [56] and human umbilical endothelial cells from aged humans [57]. In animal studies, aging in rats has been associated with decreased levels of GH and IGFBP3 in liver and serum [58]. Therefore, one of the beneficial effects of the CQ treatment was indeed, to lower the levels of serum IGFBP3. However, the treatment did not significantly change the levels of serum GH, IGF1 and IRS.

CQ was originally discovered and used to prevent or treat malaria and amebiasis [59], and subsequently inflammatory diseases [60, 61]. CQ and its derivate hydroxychloroquine (HCQ) are FDA-approved drugs and are currently the principal compounds used in clinical trials aimed to treat tumors through autophagy inhibition [62].

Autophagy eliminates long-lived proteins, insoluble protein aggregates and even mitochondria, peroxisomes and bacteria whereas the ubiquitin–proteasome system (UPS) is responsible for the degradation of short-lived proteins and soluble misfolded proteins [63]. The UPS and autophagy are interconnected. Thus, inhibition of one system led to a compensatory upregulation of the other system in order to maintain cellular homeostasis [30, 64].

Furthermore, HCQ given *ip* to mice at a dose of 60 mg/kg induced an autophagy-independent severe disorganization of the Golgi and endo-lysosomal systems in kidney and intestinal cells calling for caution when interpreting results obtained by blocking autophagy with this drug [27]. Indeed, the action of CQ on the cell seems to be dose-dependent. Thus, treatment of Zmpste24−/− mice (a progeria mouse model with low DNA repair capacity) with CQ given in 0.9% saline twice per week at 3.5 mg/kg body weight for about 3 months, activates Ataxia telangiectasia mutated (ATM), a serine/threonine protein kinase, a key regulator of DNA damage response, promotes DNA damage clearance, ameliorates premature aging and extends lifespan by 19% [54]. However, the effect of CQ in the wild type mice has not been shown. Moreover, CQ treatment did not extend lifespan in Atm−/− mice. Therefore, we hypothesize that the initial target of CQ could be the proteasome system those inhibition could lead to the upregulation of LC3B-II on the autophagosomes.

CONCLUSION

Our results suggest that chloroquine extends the maximal lifespan of middle-aged mice possibly by disrupting autophagocytosis, decreasing proteolysis and increasing glycogen metabolism in the liver and heart in male NMRI mice. Systemically, we measured decreased levels of serum IGFPB3. Given the constancy of the body weight in CQ-treated animals might also imply that the effects of CQ in treated mice could be similar to caloric restriction or possibly through an effect on amino acid homeostasis. Indeed, a wide-scale comparative analysis of longevity genes and interventions indicates a quite ambiguous role of autophagy in the control of longevity [65]. Quite intriguingly, chloroquine treatment was also associated

with a decrease in glycogenolysis in the liver suggesting a compensatory mechanism to provide energy to the cell that supports the concept of "physiological hormesis" that might have been caused by CQ-induced mild stress in the liver [66]. Clearly, further studies are needed to explore the underlying mechanisms at several chloroquine doses and to extend the treatment to female mice and rats.

MATERIALS AND METHODS

Animals and treatment

Middle-aged (500 days old) NMRI (Naval Medical Research Institute) mice were kept on a 12-hour light/dark cycle at 23°C, having free access to standard food and water. The mice were randomly assigned to two groups: (1) control group ($N = 28$) and (2) treatment group ($N = 28$). Mice were treated with 50 mg/kg chloroquine (CQ; Sigma-Aldrich, Munich, Germany) dissolved in drinking water until death. The control group received water only. Survival was daily controlled. All studies on laboratory animals were performed in accordance with the Directive 2010/63/EU of the European Parliament and the Council of 22 September 2010 on the protection of animals used for scientific purposes with relevant acts and regulations. All protocols were approved by the local Animal Ethics Committee (#112-14112018), and all appropriate measures were taken to minimize pain and suffering.

Chloroquine toxicity, histology, immunohistochemistry and electron microscopy

For toxicity studies CQ (3-months old mice; 50, 100, and 200 mg/kg body weight; $N = 10$) was administered in the drinking water. Control animals ($N = 10$) received water without CQ. After 2 months of treatment, animals were anesthetized with a mix of xylazine/ketamine and blood was collected by cardiac puncture. After intra-cardiac perfusion with 4% paraformaldehyde (PFA) and dissection, the organs were fixed for 48 h in 4% PFA and processed for paraffin embedding. Four micrometer-thick sections were cut and collected on poly-lysine coated slides. A first series of slides were routinely stained with hematoxylin and eosin-stained for diagnostic purposes.

For immunohistochemistry, slides were deparaffinated and re-hydrated, processed for antigen retrieval by boiling in citrate buffer pH6, endogenous peroxidase blocked in 0.1% water peroxide and unspecific binding sites blocked with skimmed milk. The primary antibody was added overnight (rabbit anti-LC3B, monoclonal, clone 12K5, 1:10; Sigma-Aldrich), and the next day the

signal was detected with species-specific peroxidase-labelled polymer secondaries (Vector Laboratories) for 1 hour, then the sections were counterstained with hematoxylin and coverslipped. All sections have been imaged under a Nikon 90i microscope equipped with a plane-apochromat objectives and a Nikon DS-Ri2 16Mp CMOS camera.

We have assessed and graded histopathological changes in the liver and myocardium in all animal groups. For the liver, we have assessed the extent of hepatocyte hydropic degeneration and necrosis as absent (0), mild (+), moderate (++) or severe (+++). Also, using the same tier, we have evaluated interstitial myocardial oedema, loss of myocardiocyte striations and necrosis.

Electron microscopy

For transmission electron microscopy we treated 18-months old male mice with 50 mg/kg CQ for 2 months. Samples of liver from controls ($N = 4$) and treatment ($N = 4$) were fixed in 2.5% glutaraldehyde in 0.1 M PBS at 4°C overnight. The samples were subsequently post-fixed in 1% osmium tetroxide and further processed by standard procedures, including dehydration, infiltration and polymerization in araldite. Ultramicrotomy and transmission electron microscopy (TEM) was performed at the Electron Microscopy Unit (EMU) of the Imaging Center Essen (IMCES). Here, ultrathin sections with a diameter of 55 nm were generated using a Leica UC7 ultramicrotome and sections were collected on 200 mesh copper grids. After air drying, the samples were examined with a JEOL JEM-1400Plus, operating at 120 kV and equipped with a 4096 × 4096 pixels CMOS camera (TemCam-F416, TVIPS, Gauting, Germany).

Western blot analysis of the autophagosomal membrane protein LC3B

Tissue lysates from heart and liver and lung (25 µg protein/well) were treated with sample buffer (dithiothreitol, 0.1% SDS, 0.1 M Tris HCl; pH 7.0) and boiled for 5 min at 95°C before separation on 12% SDS-polyacrylamide gel electrophoresis gels. The samples were then transferred to polyvinylidene fluoride membranes (Merck Group, Darmstadt, Germany). The membranes were blocked in 5% milk diluted with Tris-buffered saline solution with 1% Tween-20 for 1 h at room temperature and probed with LC3BI/II (1:1000, Abcam, Cambridge, UK), p62 and ß-tubulin (1:1000, Abcam, Cambridge, UK) antibodies overnight followed by 1 h of incubation with a matched horseradish peroxidase-labeled secondary antibody. Immunoreactivity was detected using chemi-luminescence detection kit reagents and a Chemidoc

Station (Bio-Rad, Hercules, CA, USA). Western blots from three independent experiments were quantified using ImageJ software (version 1.41, National Institutes of Health). To enhance the visibility of bands, images were equally adjusted for contrast in Adobe Photoshop.

Analysis of proteasome activity

Liver and heart tissue were homogenized in a lysis buffer containing 100 mM Tris-HCl, 145 mM NaCl, 10 mM EDTA, and 0.5% Triton X-100 at pH 7.5 as previously described by us [27]. Chymotrypsin-like activity was evaluated by fluorescence in a reaction buffer consisting of 50 mM Tris, 20 mM KCl, 1 mM magnesium acetate, 2 mM dithiothreitol, 1 mM leupeptin (Sigma-Aldrich), 1 mM phenylmethylsulfonyl fluoride (PMSF; Merck) and Suc-Leu-Leu-Val-Tyr-AMC (Sigma-Aldrich; 50 μM) as a substrate. Proteasome activity was fluorimetrically measured at $\lambda_{exc.}$ 355 nm and at $\lambda_{em.}$ 460 nm and is given in arbitrary fluorescence units per mg protein. Protein concentrations were determined using the Bradford assay.

Blood biochemistry

Growth hormone (GH; Cloud-Clone Corp. Wuhan, China), insulin-like growth factor 1 (IGF-1; RayBio, Norcross, GA, USA), insulin-like growth factor binding protein-3 (IGFBP-3; RayBio, Norcross, GA, USA) and insulin receptor substrate-1 (IRS-1; Cloud-Clone Corp. Wuhan, China) were determined in serum of controls and treated animals by ELISA following the manufacturer's instructions.

Statistical analysis

The effect of treatment on body weight, liquid intake was done using unpaired two-tailed t tests. The main effect of treatment on longevity was analyzed using Mantel-Cox test (GraphPad Software, San Diego, CA, USA). Statistical analysis regarding ELISA, Western blot and proteasome activity involved a one-way ANOVA followed by Tukey's post-hoc test. Quantitative data were expressed as mean ± standard deviation (SD). $P < 0.05$ was regarded as statistically significant.

Availability of data and material

Data will be made available to qualified researchers upon request.

AUTHOR CONTRIBUTIONS

TRD, CC, KY, DB, UB performed the experiments. DNP assessed the pathology and contributed to the writing of the manuscript. TD and DMH contributed to the design of the experiments and to the writing of the manuscript. APW designed the experiments and wrote the manuscript.

CONFLICTS OF INTEREST

The authors declare no conflicts of interest related to this study.

REFERENCES

1. Catterson JH, Khericha M, Dyson MC, Vincent AJ, Callard R, Haveron SM, Rajasingam A, Ahmad M, Partridge L. Short-Term, Intermittent Fasting Induces Long-Lasting Gut Health and TOR-Independent Lifespan Extension. Curr Biol. 2018; 28:1714–24.e4. https://doi.org/10.1016/j.cub.2018.04.015 PMID:29779873

2. Madeo F, Carmona-Gutierrez D, Hofer SJ, Kroemer G. Caloric Restriction Mimetics against Age-Associated Disease: Targets, Mechanisms, and Therapeutic Potential. Cell Metab. 2019; 29:592–610. https://doi.org/10.1016/j.cmet.2019.01.018 PMID:30840912

3. Speakman JR, Mitchell SE, Mazidi M. Calories or protein? The effect of dietary restriction on lifespan in rodents is explained by calories alone. Exp Gerontol. 2016; 86:28–38. https://doi.org/10.1016/j.exger.2016.03.011 PMID:27006163

4. Colman RJ, Anderson RM, Johnson SC, Kastman EK, Kosmatka KJ, Beasley TM, Allison DB, Cruzen C, Simmons HA, Kemnitz JW, Weindruch R. Caloric restriction delays disease onset and mortality in rhesus monkeys. Science. 2009; 325:201–4. https://doi.org/10.1126/science.1173635 PMID:19590001

5. Colman RJ, Beasley TM, Kemnitz JW, Johnson SC, Weindruch R, Anderson RM. Caloric restriction

reduces age-related and all-cause mortality in rhesus monkeys. Nat Commun. 2014; 5:3557.
https://doi.org/10.1038/ncomms4557
PMID:24691430

6. Mattison JA, Roth GS, Beasley TM, Tilmont EM, Handy AM, Herbert RL, Longo DL, Allison DB, Young JE, Bryant M, Barnard D, Ward WF, Qi W, et al. Impact of caloric restriction on health and survival in rhesus monkeys from the NIA study. Nature. 2012; 489:318–21.
https://doi.org/10.1038/nature11432
PMID:22932268

7. Mattison JA, Colman RJ, Beasley TM, Allison DB, Kemnitz JW, Roth GS, Ingram DK, Weindruch R, de Cabo R, Anderson RM. Caloric restriction improves health and survival of rhesus monkeys. Nat Commun. 2017; 8:14063.
https://doi.org/10.1038/ncomms14063
PMID:28094793

8. Bruss MD, Khambatta CF, Ruby MA, Aggarwal I, Hellerstein MK. Calorie restriction increases fatty acid synthesis and whole body fat oxidation rates. Am J Physiol Endocrinol Metab. 2010; 298:E108–16.
https://doi.org/10.1152/ajpendo.00524.2009
PMID:19887594

9. Brown-Borg HM, Borg KE, Meliska CJ, Bartke A. Dwarf mice and the ageing process. Nature. 1996; 384:33.
https://doi.org/10.1038/384033a0
PMID:8900272

10. Chen W, Rezaizadehnajafi L, Wink M. Influence of resveratrol on oxidative stress resistance and life span in Caenorhabditis elegans. J Pharm Pharmacol. 2013; 65:682–8.
https://doi.org/10.1111/jphp.12023
PMID:23600385

11. Gruber J, Tang SY, Halliwell B. Evidence for a trade-off between survival and fitness caused by resveratrol treatment of Caenorhabditis elegans. Ann N Y Acad Sci. 2007; 1100:530–42.
https://doi.org/10.1196/annals.1395.059
PMID:17460219

12. Baur JA, Pearson KJ, Price NL, Jamieson HA, Lerin C, Kalra A, Prabhu VV, Allard JS, Lopez-Lluch G, Lewis K, Pistell PJ, Poosala S, Becker KG, et al. Resveratrol improves health and survival of mice on a high-calorie diet. Nature. 2006; 444:337–42.
https://doi.org/10.1038/nature05354
PMID:17086191

13. Pallauf K, Chin D, Günther I, Birringer M, Lüersen K, Schultheiß G, Vieten S, Krauß J, Bracher F, Danylec N, Soukup ST, Kulling SE, Rimbach G. Resveratrol,

lunularin and dihydroresveratrol do not act as caloric restriction mimetics when administered intraperitoneally in mice. Sci Rep. 2019; 9:4445.
https://doi.org/10.1038/s41598-019-41050-2
PMID:30872769

14. van der Made SM, Plat J, Mensink RP. Resveratrol does not influence metabolic risk markers related to cardiovascular health in overweight and slightly obese subjects: a randomized, placebo-controlled crossover trial. PLoS One. 2015; 10:e0118393.
https://doi.org/10.1371/journal.pone.0118393
PMID:25790328

15. Vellai T, Takacs-Vellai K, Zhang Y, Kovacs AL, Orosz L, Müller F. Genetics: influence of TOR kinase on lifespan in C. elegans. Nature. 2003; 426:620.
https://doi.org/10.1038/426620a
PMID:14668850

16. Kapahi P, Zid BM, Harper T, Koslover D, Sapin V, Benzer S. Regulation of lifespan in Drosophila by modulation of genes in the TOR signaling pathway. Curr Biol. 2004; 14:885–90.
https://doi.org/10.1016/j.cub.2004.03.059
PMID:15186745

17. Miller RA, Harrison DE, Astle CM, Baur JA, Boyd AR, de Cabo R, Fernandez E, Flurkey K, Javors MA, Nelson JF, Orihuela CJ, Pletcher S, Sharp ZD, et al. Rapamycin, but not resveratrol or simvastatin, extends life span of genetically heterogeneous mice. J Gerontol A Biol Sci Med Sci. 2011; 66:191–201.
https://doi.org/10.1093/gerona/glq178
PMID:20974732

18. Wilkinson JE, Burmeister L, Brooks SV, Chan CC, Friedline S, Harrison DE, Hejtmancik JF, Nadon N, Strong R, Wood LK, Woodward MA, Miller RA. Rapamycin slows aging in mice. Aging Cell. 2012; 11:675–82.
https://doi.org/10.1111/j.1474-9726.2012.00832.x
PMID:22587563

19. Rovira J, Diekmann F, Ramírez-Bajo MJ, Bañón-Maneus E, Moya-Rull D, Campistol JM. Sirolimus-associated testicular toxicity: detrimental but reversible. Transplantation. 2012; 93:874–9.
https://doi.org/10.1097/TP.0b013e31824bf1f0
PMID:22357177

20. Boobes Y, Bernieh B, Saadi H, Raafat Al Hakim M, Abouchacra S. Gonadal dysfunction and infertility in kidney transplant patients receiving sirolimus. Int Urol Nephrol. 2010; 42:493–8.
https://doi.org/10.1007/s11255-009-9644-8
PMID:19774480

21. Rubinstein AD, Eisenstein M, Ber Y, Bialik S, Kimchi A. The autophagy protein Atg12 associates with

antiapoptotic Bcl-2 family members to promote mitochondrial apoptosis. Mol Cell. 2011; 44:698–709.
https://doi.org/10.1016/j.molcel.2011.10.014
PMID:22152474

22. Madeo F, Zimmermann A, Maiuri MC, Kroemer G. Essential role for autophagy in life span extension. J Clin Invest. 2015; 125:85–93.
https://doi.org/10.1172/JCI73946
PMID:25654554

23. Madeo F, Eisenberg T, Pietrocola F, Kroemer G. Spermidine in health and disease. Science. 2018; 359:eaan2788.
https://doi.org/10.1126/science.aan2788
PMID:29371440

24. Lin X, Han L, Weng J, Wang K, Chen T. Rapamycin inhibits proliferation and induces autophagy in human neuroblastoma cells. Biosci Rep. 2018; 38:BSR20181822.
https://doi.org/10.1042/BSR20181822
PMID:30393233

25. Eisenberg T, Abdellatif M, Schroeder S, Primessnig U, Stekovic S, Pendl T, Harger A, Schipke J, Zimmermann A, Schmidt A, Tong M, Ruckenstuhl C, Dammbrueck C, et al. Cardioprotection and lifespan extension by the natural polyamine spermidine. Nat Med. 2016; 22:1428–38.
https://doi.org/10.1038/nm.4222
PMID:27841876

26. Filfan M, Olaru A, Udristoiu I, Margaritescu C, Petcu E, Hermann DM, Popa-Wagner A. Long-term treatment with spermidine increases health span of middle-aged Sprague-Dawley male rats. Geroscience. 2020; 42:937–49.
https://doi.org/10.1007/s11357-020-00173-5
PMID:32285289

27. Mauthe M, Orhon I, Rocchi C, Zhou X, Luhr M, Hijlkema KJ, Coppes RP, Engedal N, Mari M, Reggiori F. Chloroquine inhibits autophagic flux by decreasing autophagosome-lysosome fusion. Autophagy. 2018; 14:1435–55.
https://doi.org/10.1080/15548627.2018.1474314
PMID:29940786

28. Yoshii SR, Mizushima N. Monitoring and Measuring Autophagy. Int J Mol Sci. 2017; 18:E1865.
https://doi.org/10.3390/ijms18091865
PMID:28846632

29. Klaips CL, Jayaraj GG, Hartl FU. Pathways of cellular proteostasis in aging and disease. J Cell Biol. 2018; 217:51–63.
https://doi.org/10.1083/jcb.201709072
PMID:29127110

30. Kocaturk NM, Gozuacik D. Crosstalk Between Mammalian Autophagy and the Ubiquitin-Proteasome System. Front Cell Dev Biol. 2018; 6:128.
https://doi.org/10.3389/fcell.2018.00128
PMID:30333975

31. Toth LA. Identifying and Implementing Endpoints for Geriatric Mice. Comp Med. 2018; 68:439–51.
https://doi.org/10.30802/AALAS-CM-18-000022
PMID:30486919

32. Kazi MS, Saurabh K, Rishi P, Rishi E. Delayed onset chloroquine retinopathy presenting 10 years after long-term usage of chloroquine. Middle East Afr J Ophthalmol. 2013; 20:89–91.
https://doi.org/10.4103/0974-9233.106404
PMID:23580861

33. El Shishtawy MA, Hassan KH, Ramzy R, Berri F, Mortada M, Nasreddine S, Ezzedine M. Comparative toxicity study of chloroquine and hydroxychloroquine on adult albino rats. Eur Sci J. 2015; 1:399–407.

34. McLeland CB, Rodriguez J, Stern ST. Autophagy monitoring assay: qualitative analysis of MAP LC3-I to II conversion by immunoblot. Methods Mol Biol. 2011; 697:199–206.
https://doi.org/10.1007/978-1-60327-198-1_21
PMID:21116969

35. Runwal G, Stamatakou E, Siddiqi FH, Puri C, Zhu Y, Rubinsztein DC. LC3-positive structures are prominent in autophagy-deficient cells. Sci Rep. 2019; 9:10147.
https://doi.org/10.1038/s41598-019-46657-z
PMID:31300716

36. González-Rodríguez A, Mayoral R, Agra N, Valdecantos MP, Pardo V, Miquilena-Colina ME, Vargas-Castrillón J, Lo Iacono O, Corazzari M, Fimia GM, Piacentini M, Muntané J, Boscá L, et al. Impaired autophagic flux is associated with increased endoplasmic reticulum stress during the development of NAFLD. Cell Death Dis. 2014; 5:e1179.
https://doi.org/10.1038/cddis.2014.162
PMID:24743734

37. Jia R, Bonifacino JS. Negative regulation of autophagy by UBA6-BIRC6-mediated ubiquitination of LC3. Elife. 2019; 8:e50034.
https://doi.org/10.7554/eLife.50034
PMID:31692446

38. Jacquin E, Leclerc-Mercier S, Judon C, Blanchard E, Fraitag S, Florey O. Pharmacological modulators of autophagy activate a parallel noncanonical pathway driving unconventional LC3 lipidation. Autophagy. 2017; 13:854–67.
https://doi.org/10.1080/15548627.2017.1287653
PMID:28296541

39. Myeku N, Figueiredo-Pereira ME. Dynamics of the degradation of ubiquitinated proteins by proteasomes and autophagy: association with sequestosome 1/p62. J Biol Chem. 2011; 286:22426–40.
https://doi.org/10.1074/jbc.M110.149252
PMID:21536669

40. VerPlank JJS, Lokireddy S, Zhao J, Goldberg AL. 26S Proteasomes are rapidly activated by diverse hormones and physiological states that raise cAMP and cause Rpn6 phosphorylation. Proc Natl Acad Sci U S A. 2019; 116:4228–37.
https://doi.org/10.1073/pnas.1809254116
PMID:30782827

41. Conconi M, Szweda LI, Levine RL, Stadtman ER, Friguet B. Age-related decline of rat liver multicatalytic proteinase activity and protection from oxidative inactivation by heat-shock protein 90. Arch Biochem Biophys. 1996; 331:232–40.
https://doi.org/10.1006/abbi.1996.0303
PMID:8660703

42. Bulteau AL, Szweda LI, Friguet B. Age-dependent declines in proteasome activity in the heart. Arch Biochem Biophys. 2002; 397:298–304.
https://doi.org/10.1006/abbi.2001.2663
PMID:11795886

43. Husom AD, Peters EA, Kolling EA, Fugere NA, Thompson LV, Ferrington DA. Altered proteasome function and subunit composition in aged muscle. Arch Biochem Biophys. 2004; 421:67–76.
https://doi.org/10.1016/j.abb.2003.10.010
PMID:14678786

44. Walther DM, Mann M. Accurate quantification of more than 4000 mouse tissue proteins reveals minimal proteome changes during aging. Mol Cell Proteomics. 2011; 10:M110.004523.
https://doi.org/10.1074/mcp.M110.004523
PMID:21048193

45. Yu Q, Xiao H, Jedrychowski MP, Schweppe DK, Navarrete-Perea J, Knott J, Rogers J, Chouchani ET, Gygi SP. Sample multiplexing for targeted pathway proteomics in aging mice. Proc Natl Acad Sci U S A. 2020; 117:9723–32.
https://doi.org/10.1073/pnas.1919410117
PMID:32332170

46. Kito Y, Matsumoto M, Hatano A, Takami T, Oshikawa K, Matsumoto A, Nakayama KI. Cell cycle-dependent localization of the proteasome to chromatin. Sci Rep. 2020; 10:5801.
https://doi.org/10.1038/s41598-020-62697-2
PMID:32242037

47. Roeten MSF, Cloos J, Jansen G. Positioning of proteasome inhibitors in therapy of solid malignancies. Cancer Chemother Pharmacol. 2018; 81:227–43.
https://doi.org/10.1007/s00280-017-3489-0
PMID:29184971

48. Doeppner TR, Kaltwasser B, Kuckelkorn U, Henkelein P, Bretschneider E, Kilic E, Hermann DM. Systemic Proteasome Inhibition Induces Sustained Post-stroke Neurological Recovery and Neuroprotection via Mechanisms Involving Reversal of Peripheral Immunosuppression and Preservation of Blood-Brain-Barrier Integrity. Mol Neurobiol. 2016; 53:6332–41.
https://doi.org/10.1007/s12035-015-9533-3
PMID:26572637

49. Brown-Borg HM, Bartke A. GH and IGF1: roles in energy metabolism of long-living GH mutant mice. J Gerontol A Biol Sci Med Sci. 2012; 67:652–60.
https://doi.org/10.1093/gerona/gls086
PMID:22466316

50. Kim KS, Kim MS, Seu YB, Chung HY, Kim JH, Kim JR. Regulation of replicative senescence by insulin-like growth factor-binding protein 3 in human umbilical vein endothelial cells. Aging Cell. 2007; 6:535–45.
https://doi.org/10.1111/j.1474-9726.2007.00315.x
PMID:17635417

51. Junnila RK, List EO, Berryman DE, Murrey JW, Kopchick JJ. The GH/IGF-1 axis in ageing and longevity. Nat Rev Endocrinol. 2013; 9:366–76.
https://doi.org/10.1038/nrendo.2013.67
PMID:23591370

52. Yamada PM, Mehta HH, Hwang D, Roos KP, Hevener AL, Lee KW. Evidence of a role for insulin-like growth factor binding protein (IGFBP)-3 in metabolic regulation. Endocrinology. 2010; 151:5741–50.
https://doi.org/10.1210/en.2010-0672
PMID:20926583

53. Singh R, Cuervo AM. Autophagy in the cellular energetic balance. Cell Metab. 2011; 13:495–504.
https://doi.org/10.1016/j.cmet.2011.04.004
PMID:21531332

54. Qian M, Liu Z, Peng L, Tang X, Meng F, Ao Y, Zhou M, Wang M, Cao X, Qin B, Wang Z, Zhou Z, Wang G, et al. Boosting ATM activity alleviates aging and extends lifespan in a mouse model of progeria. Elife. 2018; 7:e34836.
https://doi.org/10.7554/eLife.34836
PMID:29717979

55. Redmann M, Benavides GA, Berryhill TF, Wani WY, Ouyang X, Johnson MS, Ravi S, Barnes S, Darley-Usmar VM, Zhang J. Inhibition of autophagy with bafilomycin and chloroquine decreases mitochondrial

quality and bioenergetic function in primary neurons. Redox Biol. 2017; 11:73–81.
https://doi.org/10.1016/j.redox.2016.11.004
PMID:27889640

56. Kim SS, Lee CK. Growth signaling and longevity in mouse models. BMB Rep. 2019; 52:70–85.
https://doi.org/10.5483/BMBRep.2019.52.1.299
PMID:30545442

57. Li P, Sun X, Cai G, Chen X. Insulin-like Growth Factor System and Aging. J Aging Sci. 2017; 5:1.
https://doi.org/10.4172/2329-8847.1000171

58. Velasco B, Cacicedo L, Escalada J, Lopez-Fernandez J, Sanchez-Franco F. Growth hormone gene expression and secretion in aging rats is age dependent and not age-associated weight increase related. Endocrinology. 1998; 139:1314–20.
https://doi.org/10.1210/endo.139.3.5779
PMID:9492067

59. Rainsford KD, Parke AL, Clifford-Rashotte M, Kean WF. Therapy and pharmacological properties of hydroxychloroquine and chloroquine in treatment of systemic lupus erythematosus, rheumatoid arthritis and related diseases. Inflammopharmacology. 2015; 23:231–69.
https://doi.org/10.1007/s10787-015-0239-y
PMID:26246395

60. O'Neill PM, Bray PG, Hawley SR, Ward SA, Park BK. 4-Aminoquinolines--past, present, and future: a chemical perspective. Pharmacol Ther. 1998; 77:29–58.
https://doi.org/10.1016/s0163-7258(97)00084-3
PMID:9500158

61. Al-Bari MA. Chloroquine analogues in drug discovery: new directions of uses, mechanisms of actions and toxic manifestations from malaria to multifarious diseases. J Antimicrob Chemother. 2015; 70:1608–21.
https://doi.org/10.1093/jac/dkv018
PMID:25693996

62. McAfee Q, Zhang Z, Samanta A, Levi SM, Ma XH, Piao S, Lynch JP, Uehara T, Sepulveda AR, Davis LE, Winkler JD, Amaravadi RK. Autophagy inhibitor Lys05 has single-agent antitumor activity and reproduces the phenotype of a genetic autophagy deficiency. Proc Natl Acad Sci U S A. 2012; 109:8253–8.
https://doi.org/10.1073/pnas.1118193109
PMID:22566612

63. Demishtein A, Fraiberg M, Berko D, Tirosh B, Elazar Z, Navon A. SQSTM1/p62-mediated autophagy compensates for loss of proteasome polyubiquitin recruiting capacity. Autophagy. 2017; 13:1697–708.
https://doi.org/10.1080/15548627.2017.1356549
PMID:28792301

64. Fan T, Huang Z, Wang W, Zhang B, Xu Y, Mao Z, Chen L, Hu H, Geng Q. Proteasome inhibition promotes autophagy and protects from endoplasmic reticulum stress in rat alveolar macrophages exposed to hypoxia-reoxygenation injury. J Cell Physiol. 2018; 233:6748–58.
https://doi.org/10.1002/jcp.26516
PMID:29741768

65. Yanai H, Budovsky A, Barzilay T, Tacutu R, Fraifeld VE. Wide-scale comparative analysis of longevity genes and interventions. Aging Cell. 2017; 16:1267–75.
https://doi.org/10.1111/acel.12659
PMID:28836369

66. Rattan SIS. Physiological hormesis and hormetins in biogerontology. Current Opinion in Toxicology. 2022; 29:19–24.
https://doi.org/10.1016/j.cotox.2022.01.001

Copper Bead Therapy in Severe Bone Infection: A Rabbit Tibial Model

Carmen C. Surdu-Bob[1]   Ene Vlase[2]   Florica Barbuceanu[3]   Danut Turcu[4]   Mariana Coman[5]
Marius Badulescu[1]   Mariana Oporanu[6]   Cristin Coman[2]

[1] Low Temperature Plasma Laboratory, National Institute for Lasers, Plasma and Radiation Physics, Magurele, Romania
[2] Unit of Animal Experimentation "Cantacuzino" National Institute for Medico-Military Research and Development, Bucharest, Romania
[3] Department of Morphopathology, Institute for Diagnosis and Animal Health, Bucharest, Romania
[4] "Spiru Haret" University, Veterinary Medicine Faculty, Bucharest, Romania
[5] Department of Radiology, Marie Sklodowska Curie Children's Hospital, Bucharest, Romania
[6] ROMVAC Company S.A., Jud. Ilfov, Bucharest, Romania

Address for correspondence Carmen C. Surdu-Bob, Low Temperature Plasma Laboratory, National Institute for Lasers, Plasma and Radiation Physics, MG-36, 077125, Magurele, Romania (e-mail: cristina.surdubob@plasmacoatings.ro).

Abstract

Objective   We investigated the benefits of a local preventive therapy based on copper beads against severe bone infection using a rabbit open tibial fracture model.

Materials and Methods   Cotton mesh balls soaked in a very high concentration of *Staphylococcus aureus* ATCC 6538 culture were inoculated in drilled holes of the tibiae of treated and control groups. The treated group was also implanted with small copper beads simultaneously, as prevention therapy.

Results   Survival rate in the treated group was 67% compared with 25% in the control group (difference 40%, for a 95% confidence interval: 40%, 93.4%). The few remaining animals in the control group had bone lesions which developed into osteomyelitis, while the tibiae of treated group had clear signs of reparatory processes. Sixty days after inoculation, signs of local-only toxicity were observed in healthy tibia of a separate non-infected control group. Drawbacks of copper toxicity were weighed against the threat of septicaemia and also against prolonged use of powerful systemic antibiotic medications in severe bone contamination.

Cinical Significance   It was found that the proposed therapy prevented septicaemia and the spread of infection, and it also induced reparatory processes. The findings of this study may be relevant in antisepsis of open fractures in less appropriate medical settings (such as military camps or remote locations), as well as in severe bone infections.

Keywords
► osteomyelitis
► septicaemia
► bone infection
► rabbit
► copper bead

Introduction

Bone infection is a real concern, with major possible outcomes such as osteomyelitis and even septicaemia. Effective therapies of bone infection are still open issues, as debridement of open fracture and strong antibiotic therapy are not always satisfactory.[1,2]

Local antibiotic therapy used in conjunction with systemic antibiotics emerged in the hope of better infection

prevention control and treatment of bone fractures.[3,4] In terms of both effectiveness and toxicity, local antibiotic delivery systems were found to have higher potential than high-dose oral or injectable antibiotics.[5,6] Therefore, several materials and methods are being tested for local delivery: antibiotic-impregnated materials[3,7,8] (polymethyl methacrylate, ceramic, bone cement or biodegradable beads, cancellous bone, nanotubes, nanoparticles, etc.) and bone fixation elements either made of antibacterial alloys[9] or coated with hydroxyapatite or with copper, silver or a combination of copper and silver.[10–12]

We investigated the efficiency of a local therapy based on small copper beads. High-precision local inoculation in affected small bone areas, minimal bone damage (spherical shape, no fixation needed), preservation of inoculation position (beads diameter much larger than local blood vessels), and efficient, antibacterial action are the main assets of the proposed therapy.

Copper toxicity may be of concern, as very high concentrations of copper induce cytotoxicity.[12–14]. Nevertheless, this stands true for antibiotic medications also. As in the case of antibiotic drugs, the dose of copper ions released by copper-containing materials can be controlled, and the benefit to risk ratio can be maximized. A method to control copper ion release is by using beads made of a metal mixture that contains copper in a desired quantity, for example, titanium + 10% copper. Another method is to coat titanium beads with a layer of copper of a thickness calculated so that the film is 'consumed' within a certain period while in contact with biological tissue.

The aim of this work was to study the efficacy of copper beads against severe bone contamination, where outcomes such as septicaemia or osteomyelitis are otherwise common. To assess their preventive role, copper beads were inserted into the bone immediately after inoculation of bacteria. A very high concentration of bacterial suspension was inoculated into rabbit tibiae and the health of control rabbit group was assessed against that of copper beads treatment rabbit group.

Another less known but very important asset of copper is induction of bone regeneration[15,16] when used in sub-toxic levels. The main pathways are stimulation of proliferation and osteogenic differentiation of stem cells. We have also observed here formation of new bone tissue as a result of copper presence.

Preliminary studies of copper toxicity were also undertaken in the present work.

Materials and Methods

Materials
Copper and silver spherical particles (beads) were synthesized in our laboratory[17] and were 0.5 mm in diameter.

Metal ion release of our copper and silver beads was studied individually and also simultaneously by inductively coupled plasma mass spectrometry (ICP-MS) (Elan DRC-e, Perkin Elmer, SCIEX, Connecticut, United States). Liquid samples for ICP-MS ion release studies were prepared by keeping 0.5 mm-diameter copper and silver metal beads in contact with 10 mL physiological saline solution (0.9% NaCl) per sample for 7 and 20 days, respectively.

In Vitro Study
An in vitro study was designed to compare the antimicrobial effectiveness of the copper and silver beads used separately and also together against the ATCC 6538 strain of S. aureus. For this purpose, copper and silver beads were immersed in S. aureus suspension of 5×10^6 colony forming unit (CFU)/mL concentration. Each sample contained 200 μL of S. aureus culture and 20 beads made of silver, copper or 10 silver and 10 copper respectively. Contact intervals varied from 20 to 40 minutes. After each contact time had elapsed, the particles were removed and the samples were diluted down to 10^{-6} and cultured on agar plates using the standard technique. After 24 hours, the number of colonies were counted and CFU calculated accordingly. The measurements were made in triplicate.

In Vivo Study

Infection Model
Animal Ethics Committee of our institute, in accordance with the European Union (EU) Directive 2010/63/EU, approved the animal protocol used.

Thirty-three male and female New Zealand rabbits of 2,300 g average weight were involved in this study. They were divided into four groups, as shown in ►Table 1.

The rabbits were anaesthetized using 35 mg/kg ketamine + 7 mg/kg xylazine. The proximal third of the left tibia was

Table 1 Total number of rabbits involved in each group, the number of rabbits that died of septicaemia and the number of rabbits euthanatized to be studied at the specified time intervals

Rabbit group	Initial no. of rabbits	Septicaemia, no. of dead rabbits	Euthanasia, 30 days after inoculation	Euthanasia, 60 days after inoculation	Euthanasia, 90 days after inoculation
Healthy group	3	0	1	1	1
Toxicity group—treatment beads only	6	0	2	2	2
Control group (infected, untreated)	12	9	1	0	2
Treated group (infected, treated)	12	4	2	3	3

prepared for surgical intervention with local shaving and betadine disinfection.

Two 1.1 mm-diameter drill holes were made into the mediolateral part of the tibia, the first being made at 5 mm distance from the femorotibial articulation and the second approximately 10 mm more distal from the first. In the control and treated group rabbits, a cotton mesh ball previously sterilized under ultraviolet radiation and soaked in the *S. aureus* suspension was inserted into each drill hole using a pointed tweezer as described previously.[4] A 0.2-mL aliquot of *S. aureus* ATCC 6538 suspension of 10^8 CFU/mL concentration was used for inoculation into each rabbit tibia. The cotton mesh balls were used to provide substrate for bacterial attachment and increase the chance of infection.

The rabbits were contained in individual cages with computer-controlled humidity (45–65%) and temperature (16–21°C). Water and food were available *ad libitum*. Skin adhesive (Surgi Bond, SMI AG, Belgium) and aluminium spray (AluSpray, NeogenVet, France) were used for closing the wound and lesion protection respectively.

Treatment

Treated group rabbits were inoculated with two silver and four copper beads in each of the two drilled holes per rabbit, just after insertion of cotton mesh balls.

Animal Monitoring

General and local clinical observation were performed daily for 90 days. Radiological investigations were undertaken every 2 weeks and diagnosis was given by three independent specialists in radiology. Presence of lesions such as periosteal deformation, bone architecture deformation, soft tissue deformation, enlargement of bone shaft and bone neoformation was noted.

Haematological analysis of blood taken from the marginal vein of the ear was performed monthly in all animals using a Pro CYTE IDDEX instrument. Standard haematology and thrombocyte counts were monitored throughout the 90 days investigation period.

Bacteriological and histological analyses of inoculation sites of the tibiae were performed on the same day, after euthanasia, after random selection of rabbits from each group. Microbiological evaluation was focused on identifica-tion of inoculated *S. aureus* strain by biopsy of the haema-togenous bone marrow and also of the mesh used as foreign body.

►**Table 1** presents the initial number of rabbits in each group and the schedule used for euthanasia.

Statistical Analysis

Haematology and weight gain data were reported as mean ± standard deviation. Statistical differences of the first two parameters were analysed with unpaired Student *t*-test and *p*-values smaller than 0.05 were considered significant. Weight gain data were analysed with one-way analysis of variance followed by post-hoc analysis to determine which were the differing groups. For that, the Tukey–Kramer var-iant was used to accommodate the differing number of samples. Radiological data consisting of percentages of ani-mals presenting a certain lesion in each group were analysed using the Mann–Whitney U test.

Results

Material Characterization

The 0.5-mm diameter beads used in this work were chosen to be sufficiently large so that free circulation through the bone is not possible. In ►**Fig. 1**, images of the beads are presented. A typical scanning electron microscopy image showing a very good sphericity is also given in the figure. X-ray photoelectron spectroscopy analysis of the beads revealed that the surface contained only the stable form of copper oxide.

►**Table 2** presents the number of ions released in phy-siological saline solution by our treatment (experiment done in triplicate) consisting of four copper and two silver beads for two time intervals, 7 days and 20 days, respectively. The copper ion count of four copper beads is also given for comparison purposes.

### *In Vitro* Antibacterial Effectiveness

The study of microbial inactivation effectiveness of copper, silver and copper mixed with silver materials provided infor-mation on their relative antibacterial power. As observed in ►**Fig. 2**, the use of copper and silver beads simultaneously had a greater antibacterial effect than each metal alone.

Fig. 1 Scanning electron microscopy image of a copper particle (**A**). Photographic images of copper (**B**) and silver (**C**) spherical particles.

Table 2 The results of copper ion release in saline solution analysis by copper beads used alone and also in combination with silver beads

Sample	Four copper beads in 10 mL physiological saline solution		Four copper + 2 silver beads in 10 mL physiological saline solution	
Contact time	7 days	20 days	7 days	20 days
Concentration of copper ions (ppm = mg/L]	0.820 ± 0.08	1.055 ± 0.10	1.466 ± 0.14	1.974 ± 0.19
Concentration of silver ions (ppm = mg/L]	–	–	0.009 ± 0.00	0.021 ± 0.00
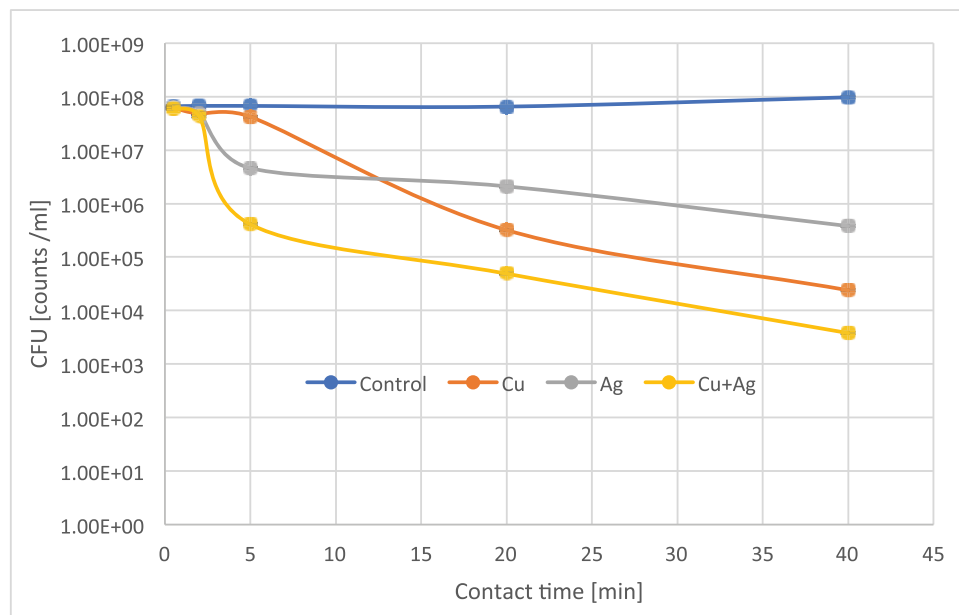
Fig. 2 Time-dependent antimicrobial effect induced by copper, silver and copper-and-silver beads against *Staphylococcus aureus*.

In Vivo Assessment

General Features

A series of rabbits died of septicaemia within the first 3 days after inoculation of the high concentration *S. aureus* solution (as shown in ►**Table 1**). Survival rate in the treated group was 67% compared with 25% in the control group (difference 40%, for a 95% confidence interval 40%, 93.4%). On necropsy investigation, it was found that septicaemia affected their vital organs. These results suggest a fast and effective antibacterial action of the therapy against severe infection where foreign bodies were not removed during treatment.

The haematological data analyses revealed very few significant ($p < 0.05$) differences in blood counts between control and treated rabbits. Such counts either fell inside the normality interval or were transient.

Body temperature had a similar behaviour (►**Fig. 3**). Although significant differences compared with the temperature before surgery were found, they were still within normal limits (38.5–39.5°C).

Abscesses were observed clinically, within the soft tissue on day 7 and remained visible until the 28th day in three out of eight rabbits in the treated group and in one out of six in the toxicity group of rabbits.

Body weight gain showed between-groups and also within-group variation (►**Fig. 4**). During the first 28 days after inoculation, the weight of infected animals (both treated and control groups) was significantly lower than that of non-infected rabbits.

Treated group rabbits gained weight slightly faster than the rabbits in the other groups and reached the weight of healthy rabbits in the third month of experiment.

Microbiological assessment of the tibiae at inoculation site as well as that of extracted mesh failed to identify the causative pathogen in most cases. No bacteria could be found on harvested samples, as if they were sterile. Nevertheless, progression of infection was clearly observed by clinical, radiological and histological investigations.

Radiological Features

Radiology imaging of the bone inoculation area taken on the 30th day after bacterial inoculation and thereafter showed bone modifications of both control and treated groups, with clear evidence of higher severity lesions in the control group.

While tibiae of control rabbits had signs of localized prominent swelling of increasing density, treated tibiae had an almost flat surface throughout the investigation period, without any bone proliferation (►**Fig. 5**).
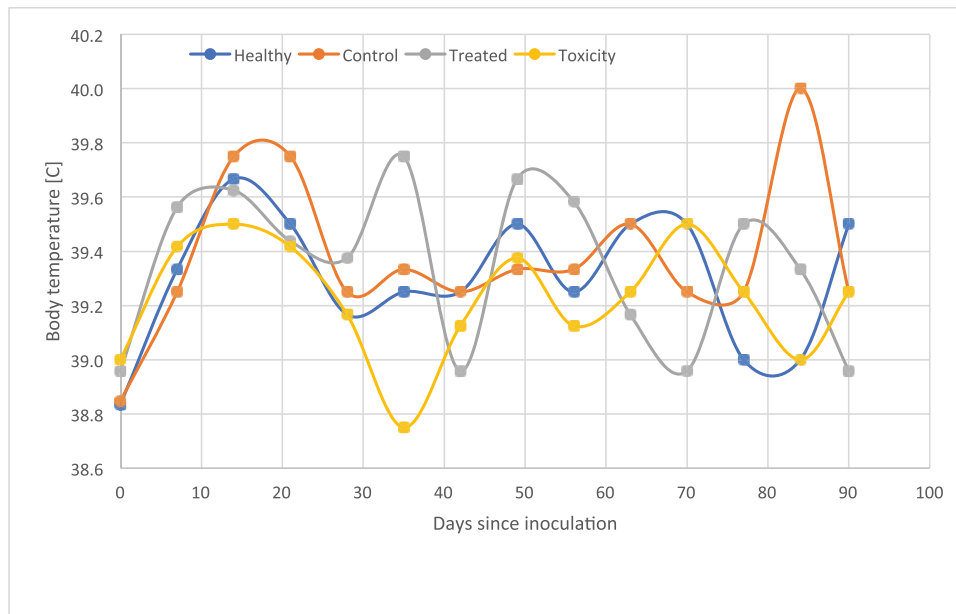
Fig. 3 Variation in body temperature of rabbits with time. The values represent average values of rabbits in the same group.
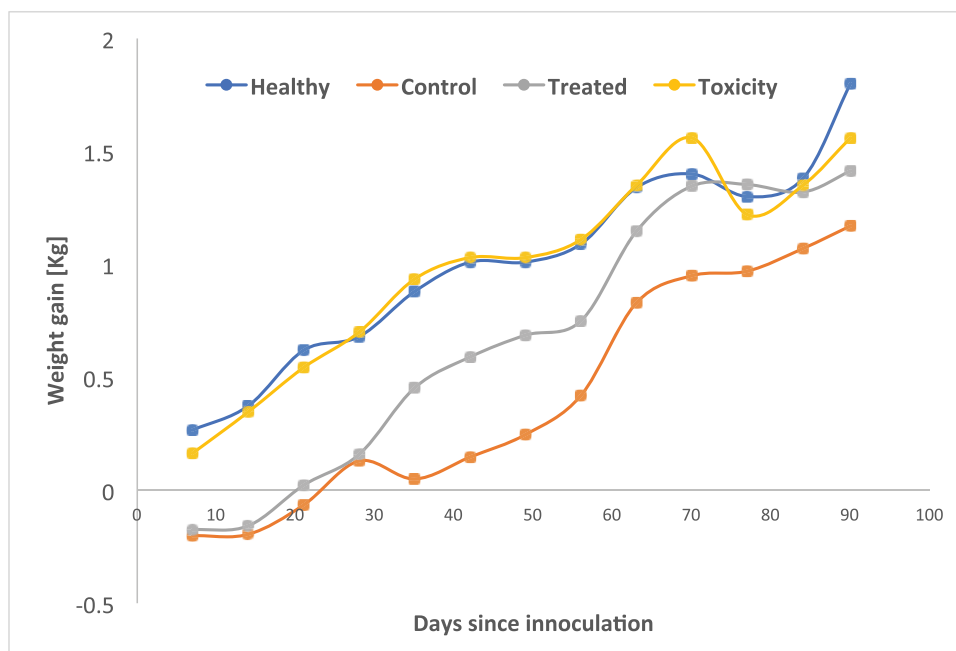

Fig. 4 Variation in weight gain (difference between the initial weight and that at the measurement time) with time. The values represent average values of rabbits in the same group.

In the control group tibiae, bone architecture was deformed (this includes periosteum and bone shaft), suggesting development of osteomyelitis. Bone deformation extended to the epiphyseal level. The treated group rabbits did not present such lesions.

Micromorphological Features
Histological assessment of experimental tibiae revealed a good outcome of treated tibiae compared with control, the results being in agreement with radiology.

Osteoblasts at different developmental stages as well as hyperaemia and haemorrhagic micro-spots were the main features found by histology at the inoculation site.

In ►**Fig. 6**, interrupted black arrows indicate osteoblasts with incipient, limited activity while solid black arrows point at higher density osteoblasts with intense reparatory activity. Treated tibiae presented a higher density of osteoblasts in Haversian canals than the control at the same time point. While osteogenic reparatory activity was the main feature observed in the tibiae of treated rabbits on the 90th day
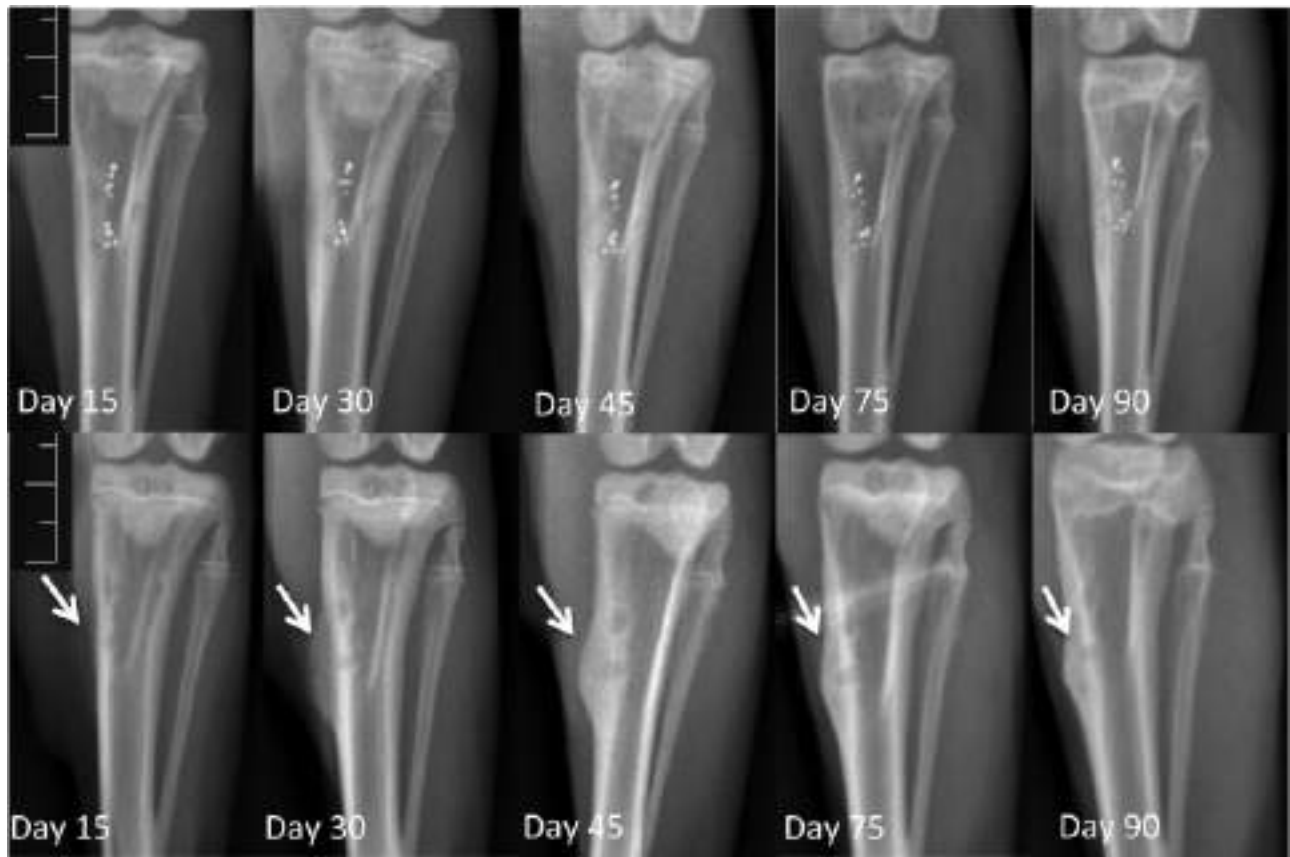
Fig. 5 Radiological images showing the left hind tibia of treated (upper row) and control rabbits (lower row) at different points in time over a monitoring period of 90 days. Treatment beads are also visible (upper row). White arrows indicate bone architecture modifications.
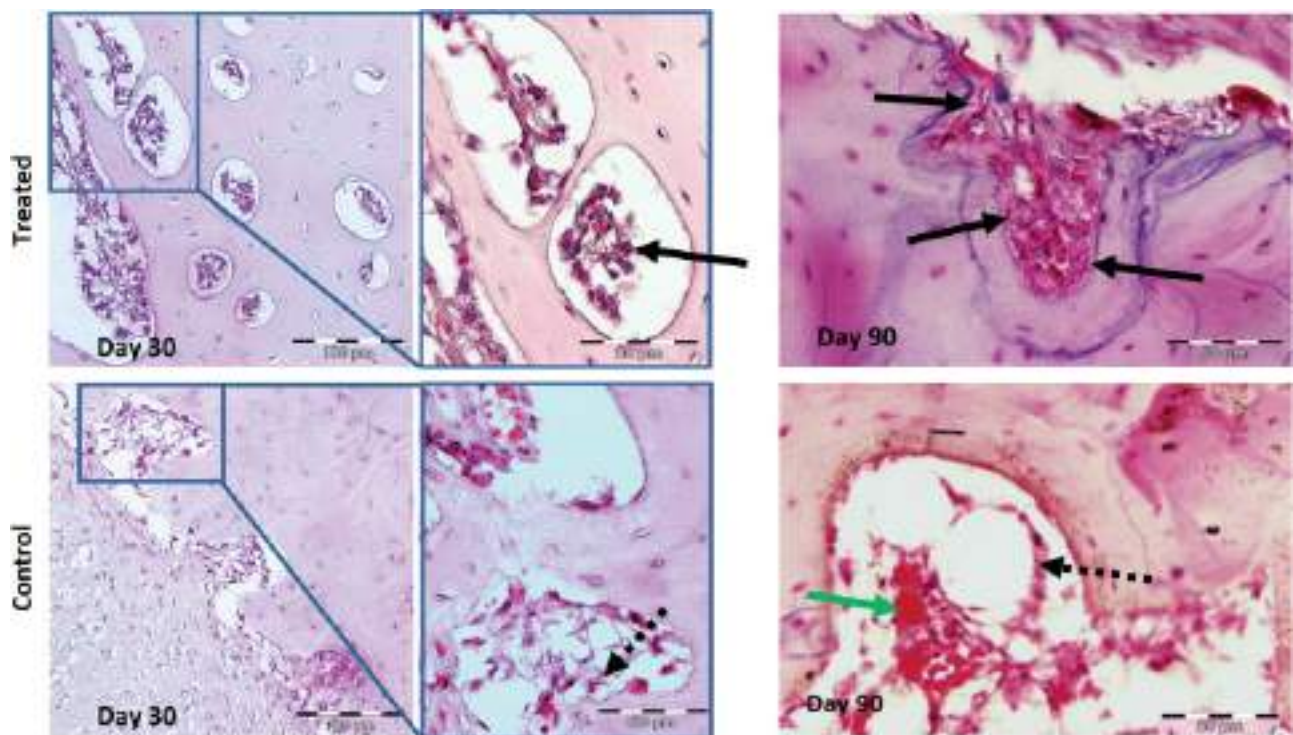
Fig. 6 Histological images of bone compact of bead treated (first raw) and control (second raw) rabbit tibia, 30 and 90 days after inoculation respectively. Reparatory activity of osteoblasts within Haversian canals with intense activity are evidenced by solid black arrows while incipient, limited activity by interrupted black arrow (Masson trichrome staining, x200); Inset x400. Green arrow indicates hyperaemia and haemorrhage.
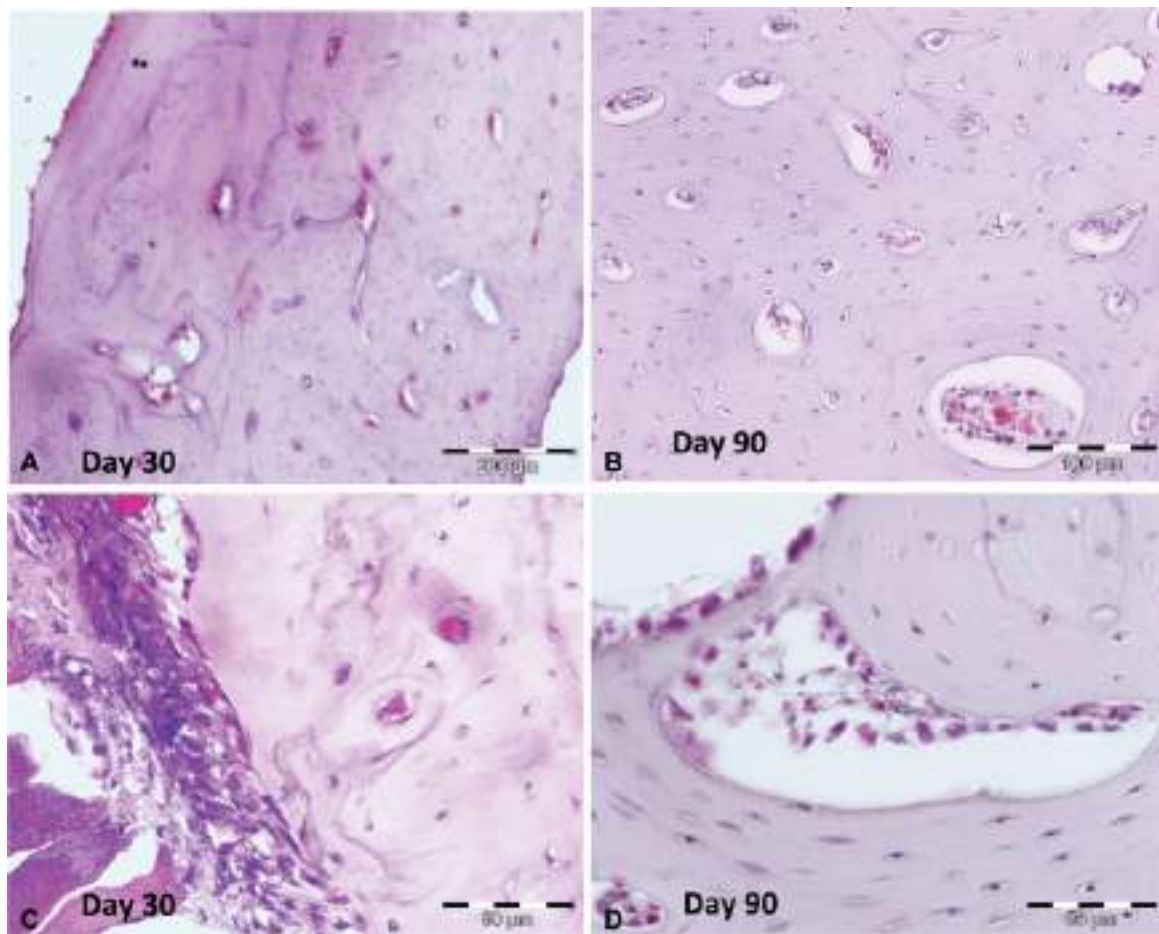
Fig. 7 Histological images of copper and silver beads inoculated site of bone in healthy rabbits (toxicity group rabbits) at two time points. Increased cellular activity towards regeneration observed throughout experiment in bone compact (**A**) and (**B**); periosteum (**C**) and endosteum (**D**).

following treatment, hyperaemia and haemorrhagic infiltrations dominated cellular activity of control tibia, as also shown in ►**Fig. 6**.

Signs of intense reparatory processes were found in the rabbits of toxicity group by histological investigation starting with day 30 onwards. They were expressed by increased cellular regenerative activity within Haversian canals, endosteum and periosteum (►**Fig. 7**).

Beads Treatment: Toxicity

While our experiment was focused on the efficacy of copper and silver particles, some issues about toxicity were also investigated.

Copper is stored in the liver, bile or blood plasma.[18] No signs of copper toxicity were observed on clinical, haematological and necropsy investigation of treated group rabbits in our experiment. Some histological signs of local toxicity expressed by dilatation of Haversian canals, osteolytic processes in the compact bone, excess mineralization and medullar reactivity with haemorrhage and increased cellularity were found in the toxicity group rabbits, 60 days after inoculation of beads (►**Fig. 8**). Nevertheless, these lesions did not influence the general state of health of rabbits for the length and parameters used in our experiment.

Discussion

Copper, as most metals, forms a stable copper oxide layer on its surface in the ambient air.[19] Copper ion release from copper oxide surfaces also takes place, although at a smaller rate than pure copper.[20] To enhance copper ion release of our particles via galvanic corrosion, silver particles were used in conjunction with the copper ones. Copper is the anodic member of the galvanic couple and it is therefore preferentially corroded.

Our semiquantitative results showed an expected achievement: copper ion release almost doubles in the presence of silver metal. This fact makes the copper–silver mixture treatment more effective than copper alone, as ion release profile correlates with antimicrobial efficacy. Similar results were published by others.[21] This is relevant in high bacterial load infected bone where a rapid antibacterial effect is essential for avoiding septicaemia or osteomyelitis.

The copper and silver beads improved survival of infected rabbits by reducing the incidence of septicaemia. The copper and silver beads offered protection against the otherwise lethal dose of high-concentration bacterial suspension. Moreover, none of the surviving rabbits in the bead-treated
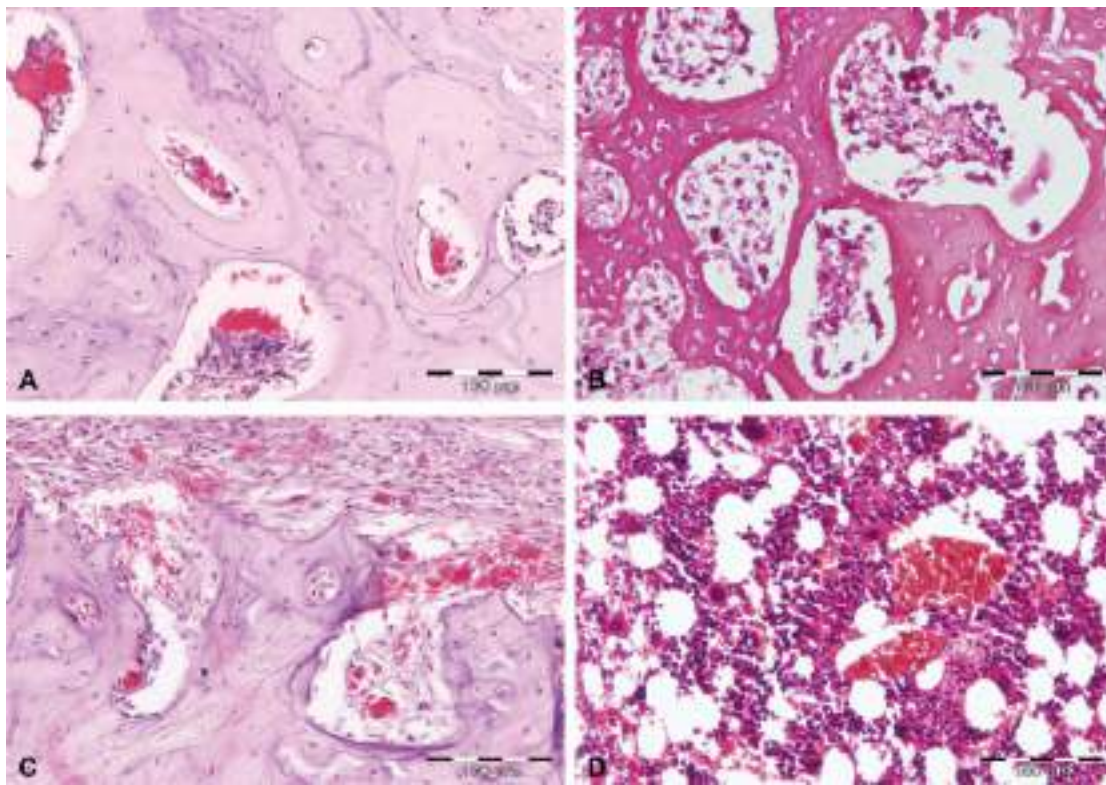
Fig. 8 Evidence of toxicity in the tibia of toxicity group rabbits. (**A**) Osteon thickening suggesting mineralization in excess of cortical bone and microtrombosis within Haversian canals; (**B**) cortical bone with dilatations of Haversian canals and osteolytic processes; (**C**) periosteal and subperiosteal haemorrhagic infiltrations inside Haversian canals; (**D**) medular reactivity, haemorrhage and megakaryocytes.

group developed any specific radiographical signs of osteo-myelitis. To increase copper ion release above that of copper alone, silver beads were used together with the copper ones, as a combined treatment.

The lack of any sign of migration of inoculated treatment beads within the bone during the 90 days suggests that this treatment is local and controllable, in contrast to nanoparticles which penetrate into blood vessels and are transported throughout the body.[22]

Body weight loss, observed on the first week after operation, was observed for bacteria-inoculated rabbits only. Weight loss is associated with the presence of bacteria in the bone, as also found by other investgators.[23]

Microbiological assessment of the samples harvested from inoculation site did not reveal the presence of *S. aureus*, not even in the control rabbit group. Nevertheless, clear signs of infection were observed on clinical and radiological investigations. This phenomenon is also encountered in clinical practice, as presented by Arciola and colleagues.[24] The explanation given by these authors is that biofilm-forming bacteria do not form colonies on agar, causing wrong diagnostic results in implant-associated infections. Molecular diagnostic methods are also mentioned by these authors to be more sensitive. This is also the reason why no microbiological data can be given here.

In agreement with radiology, in the treated group, histological analysis revealed clear evidence of reparatory processes on all investigation days at the level of cortex and medulla

expressed by the presence of conjunctive tissue, osteoblasts and newly formed bone. Control tibiae showed local osteolytic processes, high cellular reactivity, enlarged Haversian canals and bone neoformation, typical signs of osteomyelitis.[25,26] These data suggest that copper–silver bead treatment had a positive effect on the just-infected bone by playing a double role, namely that of pathogen annihilator as well as osteogenic promotor. The main result of our experiment is prevention of septicaemia and osteomyelitis in spite of the high-concentration bacterial suspension inoculated. The rapid release of copper ions was most probably the key factor of investigated treatment, as bacteria may have been killed before attachment to bone or foreign body.

Regarding toxicity in rabbits, risk levels of copper are not known.[14]

Copper is stored in the liver, bile or blood plasma.[18] Muller and colleagues reported evidence of adaptation of liver cells to high copper levels in healthy organisms.[27] Blood results in our experiment were within normal limits in all rabbits and did not suggest the necessity for supplementary biochemical investigations targeting the liver.

Within certain limits, the presence of excess copper is not expected to be toxic. As an example, intrauterine devices used for contraception are made of copper and were clinically approved to be worn for several decades.[28]

In strong antibiotic therapy applied to fight bone-related infections, important side effects such as hyperkalaemia and renal failure are real concerns.[29] The proposed local copper

bead therapy against severe infection prevented septicaemia and the spread of infection without affecting internal organs. Moreover, this therapeutic design allows removal of beads in a further surgical intervention to eliminate the risk of copper toxicity.

This treatment is relevant in severe cases of infection where the risk of septicaemia is high and also in the absence of appropriate medical settings where proper wound management is not possible. Once the threat of septicaemia and osteomyelitis are passed and aseptic surgical conditions are available, a second intervention may be programmed for beads removal. Although signs of local toxicity started to appear on day 60, it should also be noted that no further increase in toxicity was found on day 90. Moreover, toxicity was only local, no other organ or general health state being affected within the observation interval. In contrast, it is widely known that current practice for preventive treatment of bone infection which involves long-term antibiotic medications (either systemic or locally administered) has important toxic effects.[29]

In less severe cases, or where further surgeries are excluded, a lower copper ion dose may be administered by using beads made of copper alloys with biocompatible materials (such as titanium or gold). Such beads may be designed to remain in the body for months, years and even for life.

In terms of body weight gain, toxic levels of copper were reported to induce weight loss in *in vivo* tests.[30] The fact that no significant differences in weight between the toxicity group and the healthy group were registered in our study may indicate that, for the period and dose used, copper was below toxic level. Furthermore, it induced reparatory processes. Copper-induced reparatory processes were previously reported, also.[31]

Conclusions

It was found that local copper and silver bead therapy of severely contaminated bone prevented septicaemia and development of bone infection in New Zealand rabbits. The rapid antibacterial effect of the treatment inoculated simultaneously with bacteria is a promising solution in the management of severe infections and in less appropriate medical settings. Thus, the copper bead treatment may weigh more in terms of associated risks such as septicaemia and osteomyelitis.

Under inappropriate medical settings (such as battlefield camps and remote sites), proper wound management with removal of debris may not be available (our model contained cotton mesh which was not removed during treatment). Moreover, reparatory processes induced by copper beads is an added benefit of the treatment.

Blood counts, body temperature and microbiological investigation were not helpful in monitoring the state of infection. Body weight loss was correlated to the presence of infection, while weight gain was fast and could reflect progress in treated rabbits.

The work may serve as foundation for further studies on optimization of therapeutic doses and comparisons with antibiotic therapy.

References
1 Jennison T, McNally M, Pandit H. Prevention of infection in external fixator pin sites. Acta Biomater 2014;10(02):595–603
2 O'Brien CL, Menon M, Jomha NM. Controversies in the management of open fractures. Open Orthop J 2014;8:178–184
3 Niikura T, Lee SY, Iwakura T, Sakai Y, Kuroda R, Kurosaka M. Antibiotic-impregnated calcium phosphate cement as part of a comprehensive treatment for patients with established orthopaedic infection. J Orthop Sci 2016;21(04):539–545

4 Surdu-Bob CC, Coman C, Barbuceanu F, Turcu D, Bercaru N, Badulescu M. The influence of foreign body surface area on the outcome of chronic osteomyelitis. Med Eng Phys 2016;38:870–876

5 Gogia JS, Meehan JP, Di Cesare PE, Jamali AA. Local antibiotic therapy in osteomyelitis. Semin Plast Surg 2009;23(02):100–107

6 Tuleubaev B, Saginova D, Abiyev T, Davletbaev M, Koshanova A. Local antibiotic therapy of osteomyelitis using nonabsorbable implant (review) [article in Russian]. Georgian Med News 2016; 255: 21–26

7 Anagnostakos K, Schröder K. Antibiotic-impregnated bone grafts in orthopaedic and trauma surgery: a systematic review of the literature. Int J Biomater 2012;2012:538061

8 Wang X, Cheng F, Liu J, et al. Biocomposites of copper-containing mesoporous bioactive glass and nanofibrillated cellulose: biocompatibility and angiogenic promotion in chronic wound healing application. Acta Biomater 2016;46:286–298

9 Shirai T, Tsuchiya H, Shimizu T, Ohtani K, Zen Y, Tomita K. Prevention of pin tract infection with titanium-copper alloys. J Biomed Mater Res B Appl Biomater 2009;91(01):373–380

10 Ionita D, Ungureanu C, Demetrescu I. Electrochemical and antibacterial performance of CoCrMo alloy coated with hydroxyapatite or silver nanoparticles. J Mater Eng Perform 2013;22(11):3584–3591

11 Kizuki T, Matsushita T, Kokubo T. Antibacterial and bioactive calcium titanate layers formed on Ti metal and its alloys. J Mater Sci Mater Med 2014;25(07):1737–1746

12 Mauerer A, Lange B, Welsch GH, et al. Release of Cu2+ from a copper-filled TiO2 coating in a rabbit model for total knee arthroplasty. J Mater Sci Mater Med 2014;25(03):813–821

13 Tolerable Upper Intake Levels for Vitamins and Minerals. European Food Safety Authority European Commission, 2006; ISBN: 92-9199-014-0

14 Mineral Tolerance of Animals. Washington: The National Academies Press; 2005

15 Dollwet HH, Sorenson JR. Roles of copper in bone maintenance and healing. Biol Trace Elem Res 1988;18:39–48

16 Prinz C, Elhensheri M, Rychly J, Neumann HG. Antimicrobial and bone-forming activity of a copper coated implant in a rabbit model. J Biomater Appl 2017;32(02):139–149

17 Surdu-Bob CC, Badulescu M. Synthesis of metal spheres obtained in an anodic arc plasma in high vacuum. Paper presented at: Joint Conference of the 7th MC & WG Meetings. COST ACTION P21 2009; Bucharest

18 Zatulovskaia YA, Ilyechova EY, Puchkova LV. The features of copper metabolism in the rat liver during development. PLoS One 2015; 10(10):e0140797

19 Platzman I, Brener R, Haick H, Tannenbaum R. Oxidation of polycrystalline copper thin films at ambient conditions. J Phys Chem C 2008;112(04):1101–1108

20 Hans M, Erbe A, Mathews S, Chen Y, Solioz M, Mücklich F. Role of copper oxides in contact killing of bacteria. Langmuir 2013;29 (52):16160–16166

21 Hans M, Támara JC, Mathews S, et al. Laser cladding of stainless steel with a copper–silver alloy to generate surfaces of high antimicrobial activity. Appl Surf Sci 2014;320(00):195–199

22 Hofmann-Amtenbrink M, Grainger DW, Hofmann H. Nanoparticles in medicine: current challenges facing inorganic nanoparticle toxicity assessments and standardizations. Nanomedicine (Lond) 2015;11(07):1689–1694

23 Nijhof MW, Stallmann HP, Vogely HC, et al. Prevention of infection with tobramycin-containing bone cement or systemic cefazolin in an animal model. J Biomed Mater Res 2000;52(04):709–715

24 Arciola CR, Campoccia D, Ehrlich GD, Montanaro L. Biofilm-based implant infections in orthopaedics. In: Donelli G, ed. Biofilm-Based Healthcare-Associated Infections. Vol I. Switzerland: Springer International Publishing; 2015:38

25 Cassat JE, Hammer ND, Campbell JP, et al. A secreted bacterial protease tailors the Staphylococcus aureus virulence repertoire to modulate bone remodeling during osteomyelitis. Cell Host Microbe 2013;13(06):759–772

26 Chai H, Guo L, Wang X, et al. Antibacterial effect of 317L stainless steel contained copper in prevention of implant-related infection in vitro and in vivo. J Mater Sci Mater Med 2011;22(11): 2525–2535

27 Muller P, van Bakel H, van de Sluis B, Holstege F, Wijmenga C, Klomp LW. Gene expression profiling of liver cells after copper overload in vivo and in vitro reveals new copper-regulated genes. J Biol Inorg Chem 2007;12(04):495–507

28 Wu JP, Pickle S. Extended use of the intrauterine device: a literature review and recommendations for clinical practice. Contraception 2014;89(06):495–503

29 Fíca A, Lamas C, Olivares F, et al. Cotrimoxazole in bone-related infections: toxicity and clinical and economic impact [article in Spanish]. Rev Chilena Infectol 2015;32(06):609–617

30 Oyewo EO, Don-Pedro KN. Acute toxicity and induced weight changes in laboratory tests with Mn and Cu against Tilapia guineensis (Dumeril) and Tympanotonus fuscatus (Linne). J Environ Biol 2006;27(2, Suppl):327–334

31 Ren L, Yang K, Guo L, Chai HW. Preliminary study of anti-infective function of a copper-bearing stainless steel. Mater Sci Eng C 2012; 32(05):1204–1209